CONTRIBUTIONS TO THE ECONOMICS OF CLIMATE CHANGE MITIGATION

Dissertation
submitted to the Faculty of Economics,
Business Administration and Information Technology
of the University of Zurich

to obtain the degree of
Doktorin der Wirtschaftswissenschaften, Dr. oec.
(corresponds to Doctor of Philosophy, PhD)

presented by

Anca Claudia Pana
from Romania

approved in October 2015 at the request of

Prof. Dr. Marc Chesney
Prof. Dr. Salvatore di Falco
Prof. Dr. Olivier Bahn

The Faculty of Economics, Business Administration and Information Technology of the University of Zurich hereby authorizes the printing of this dissertation, without indicating an opinion of the views expressed in the work.

Zurich, 21.10.2015

Chairman of the Doctoral Board: Prof. Dr. Steven Ongena

Contents

List of Figures

List of Tables

Acknowledgements

This PhD thesis is attributed to a single author, but PhD studies can be better seen as a long and twisted voyage, whereby one benefits from the companionship of many fellow travelers. Although not exclusive, the list of people mentioned below tries to shed light on the main pillars that have sustained this PhD thesis.

My first thoughts go to my PhD supervisor, Prof. Dr. Marc Chesney, whom I am especially admiring for not following the mainstream topics that are usually highly regarded in finance. Instead, Prof. Chesney gave me the opportunity and inspiration to focus on topics related to environmental finance and economics, which are of high current relevance for both the academic and 'real' world. From Prof. Chesney I learned not only how to lead research, but also how to teach and explain complex matters first to myself and then to others.

Together with Prof. Chesney, I consider Prof. Dr. Olivier Bahn to be my PhD thesis 'father'. He was my inspiration for leading research in a way that insists on logic, accuracy, and non-redundancy. Prof. Bahn has also sharpened my research skills with his persistence to succeed and lively humor.

In the second part of my PhD studies, I had the pleasure to meet Prof. Dr. Salvatore di Falco. I consider his love for meaningful research and passion in speech to be the best motivation for work. I will try to keep his enthusiasm and kindness in mind for whenever I will feel discouraged with my work or otherwise.

Writing a PhD thesis is luckily something that one does not undertake alone. During the five years at the Department of Banking and Finance, I was very lucky to share office space, lunch/coffee/cake brakes, and stories with Sabine Elmiger, Jakub Rojcek, Nikola Vasilievic, Bruno Troja, Felix Fattinger, Jonathan Gheyssens, Jakob Stroemberg, Ethem Guney, Kathrin De Greiff, and Lena Hoernlein.

Some precious people succeeded in making Zurich a warm and lovely home for me. Remaining sane during these five years is due to Eva Jakubcaninova, Naike Beggiato, Christian Gattringer, Amin Mazloumian and Antonio Rampoldi. Although not physically present all the time, my family has always been there for me. I would not be here without the love and laughter shared with Daniela and Laura Pana.

Leaving the sweetest to the end, the constant traveler by my side in this journey and main accomplice is my beloved Stefano Balietti. He is the person I would like to be like and always be with.

Any errors in this thesis are mine.

Chapter 1

Introduction

Climate change is one of the most serious environmental challenges that humankind has ever faced (Stern, 2006). Its main contributing factor is the accumulation of greenhouse gas (GHG) emissions from anthropogenic sources, which have been steadily increasing since the Industrial Revolution due to population and economic growth. In 2012, the average increase in global land and ocean temperature reached about 0.82 °C compared to pre-industrial levels. The natural system is sensitive to changes in climate. Since the 1850s there is an unequivocal decrease in the amounts of snow and ice, and a significant rise in sea level due to higher temperatures. Other observed consequences of climate change include: modifications in hydrological systems impacting the quality and quantity of water resources; shifts in geographic ranges, seasonal activities, migration patterns, and abundances of many species; negative net impacts on crop yields (IPCC, 2014).

Dealing with climate change requires vast reductions in emissions – also known as *mitigation* – in the near future. Otherwise, in a business-as-usual scenario, continued GHG emissions would cause further increases in average temperature and changes in the climate system, increasing the likelihood of sizable damages on human and natural systems (IPCC, 2014).

Tackling the climate change problem is vastly challenging. Some key points are discussed below. First, the climate issue is an inter-temporal one. Emitted GHGs have lifespans ranging from centuries to millennia. As such, undertaking current mitigation actions would impose costs in the present (e.g. from divesting from fossil-intensive industries and investing into low-carbon ones), while benefits would be felt far ahead in the future (once GHG concentrations are reduced). This time gap between costs and benefits is likely to create incentives to postpone timely action, at least until sizable damages occur, raising dangers for future generations (Keller et al., 2007; Nordhaus, 2008).

Second, climate change can be viewed as a *common good* problem (Millard-Ball, 2012). Earth's atmosphere is shared by all living beings on our planet, and all benefit from it. However, living beings, and especially humans, tend to be organized in clusters, such as regions, states, and unions of states, with sometimes diverging interests. Reducing emissions unilaterally would accrue all costs to the party undertaking the action, but bring benefits to all. This creates free-riding incentives diluting the motivation to start unilateral mitigation actions.

Third, several questions arise regarding the distribution of mitigation duties across countries and the right to develop economically. Past contributions to climate change can be mainly attributed

to developed countries which, in their way up the progress ladder, have relied intensively on the combustion of fossil fuels. If mitigation actions are undertaken, should efforts be proportional to past emissions? How to involve in the mitigation agenda the high-growth economies, such as China and India, which have contributed little in the past, but whose emissions are escalating in the present? Could a stable and safe GHG concentration level be reached without the participation of the least developed countries, that have not contributed significantly to climate change, but will be the ones to suffer the most from it?

Reaching international agreements on climate change mitigation is subject to a common understanding of these key issues and, thus far, individual interests have often proved to be diverging. Despite the pressing climate change problem, little progress can be observed so far in terms of emission reductions.

Tackling the climate change problem appears to be a strenuous challenge indeed. It brings consequences at various social, political, and geo-physical levels, and it requires concentrated efforts from multiple scientific fields. This thesis aims to contribute to the climate change mitigation debate from an economics and finance perspective. With a collection of three independent research articles, different both in their specific focus and in the methodology used, this thesis can only touch upon a reduced number of points related to the vast topic of climate change mitigation. The first paper studies the optimal way to combine mitigation, adaptation, and geoengineering as approaches to deal with climate change. The remaining two papers focus on two mitigation mechanisms already in place: a cap-and-trade system implemented in Europe and a program to reduce emissions from deforestation in developing countries. The analysis aims to point to the weaknesses and possible ways of improvement in these human designed mechanisms. The three papers that constitute this thesis are summarized below. The first two papers of this thesis have been published in 2015. For copyright reasons, their final (published) version appears in the Appendix; Chapters 2 and 3 include an intermediary (before final revisions, but without major changes) version.

Chapter 2 presents the first study, which is entitled 'Is there Room for Geoengineering in the Optimal Climate Policy Mix?'. It represents a joint work with Olivier Bahn, Marc Chesney, Jonathan Gheyssens and Reto Knutti, and is published in the journal of 'Environmental Science and Policy' 2015. With the help of an integrated assessment model, we analyse in a dynamic setting the optimal mix of policies to deal with climate change. Accounting for the possible strengths and weaknesses of mitigation, adaptation, and geoengineering, we study which strategy should be implemented and when, if decisions were taken at the global level. We find that the optimal strategy to deal with climate change is mitigation, i.e. the reduction in GHG emissions, through a fast transition from a carbon-intensive to a low-carbon economy. Due to the already high levels of GHG concentrations, adaptation is used to reduce damages from temperature increases. When the magnitude and persistence of geoengineering side-effects are low, this strategy is also employed to control temperature levels.

In Chapter 3, we focus on a specific mitigation project: Reducing Emissions from Deforestation and Forest Degradation (known as REDD+). This paper is entitled 'Baseline Choice and Performance Implications for REDD'; it is a joint work with Jonathan Gheyssens and published in the journal of 'Environmental Economics and Policy' 2015. REDD projects target reductions in emissions from deforestation in tropical countries, where deforestation is a major contributor to total GHG emissions. A typical cause of deforestation is the use of land for agriculture and cattle ranching. Preventing forest owners in tropical countries to deforest would alter their revenue flow. REDD projects offer financial compensation for reduced deforestation, and are designed as international contracts in which funds are directed from developed to developing countries. A key element of the incentive structure is the *baseline*, i.e. the threshold against

which reductions in emissions from deforestation are computed and payments are made. In this paper, we study different alternatives for setting the baseline and indicate which ones are more likely to achieve the REDD goals. The methodology consists in solving (analytically and numerically) a dynamic optimization problem.

Finally, in Chapter 4, I focus on a different existing mitigation strategy, namely the market for emission allowances in Europe (the so-called European Union Emissions Trading System, EU ETS). This study is entitled 'Who is driving the volatility of the CO_2 permit price? Evidence from EU ETS Phase I'. I focus on the allowance price formation process and investigate whether the trading activity of different market players has correlated significantly with the large movements observed in permit prices during Phase I. The empirical analysis shows that, depending on the sector of primary business activity, the trading activity of market players tended to correlate differently with volatility. The paper discusses possible explanations for the observed diverging trading behaviour. Although, generally, the trading activity - volatility relation is found to be positive, I show that many players remained mostly inactive during Phase I and a large share of them tended to trade mostly when volatility levels were low. This finding suggests that, at times of frequent information arrivals, when prices tended to move more pronouncedly, some market participants avoided to adjust their permit positions according to the newly disclosed information. The paper discusses how these findings might indicate a lack of market efficiency.

Summing up, this thesis is dedicated to the study of different aspects of climate change mitigation. It tries to emphasize that a timely reduction in GHG emissions is necessary in order to avoid sizable damages from climate change. Although little progress is observed in terms of mitigation programs at the global level, some regional projects are already in place, such as the cap-and-trade scheme in Europe or the programs targeting reduced emissions from deforestation in tropical countries. This thesis tries to underpin specific design improvements for these existing mitigation approaches. Although this thesis' contribution might be considered modest in relation to the vast aspects that the climate change problem entails, the analysis tried to reach depth in the few areas it has focused on. I believe that only a continued discussion and dedicated research from representatives of all backgrounds can lead to a deeper understanding of how to successfully tackle the pressing climate change problem.

Chapter 2

Is there room for geoengineering in the optimal climate policy mix?

Joint work with Olivier Bahn, Marc Chesney, Reto Knutti, and Jonathan Gheyssens.

Abstract

We investigate geoengineering as a possible substitute for mitigation and adaptation measures to reduce damages from climate change. With the help of an integrated assessment model, we distinguish between the effects of solar radiation management (SRM) on atmospheric temperature levels and its side-effects on the environment. We account for the uncertainty in the magnitude of side-effects and their persistency over time, and show that this geoengineering option lacks robustness. The optimal climate portfolio represents a mix between mitigation, adaptation, and SRM, and no strategy fully substitutes the others. We then analyse the welfare consequences of basing the SRM decision on wrong assumptions about side-effects, and show that total output losses are considerable and increase with the error horizon. This reinforces the need to balance the climate portfolio in favour of mitigation.

Keywords: Climate change; Climate policy mix; Adaptation; Mitigation; Geoengineering

2.1 Introduction

Climate change is one of the most serious challenges faced by humankind. One of its contributing factors is the anthropogenic greenhouse gas (hereafter GHG) emissions that impact the radiation budget and atmospheric temperature levels (Pinker et al., 2005). The projected temperature increase for the end of the century falls in the range 1.4 - 5.8 °C above pre-industrial levels[1] (Andreae et al., 2005; Stainforth et al., 2005), posing important risks for the wellbeing of many managed and natural ecosystems. Avoiding climate change is challenging since its cause is endogenous, the consequences entail uncertainty both in magnitude and in timing of occurrence, and solutions to it would require a thorough modification in the organisation of human activities.

Solutions for dealing with climate change enter three main categories: mitigation, adaptation, and climate geoengineering (Bellamy et al., 2013). International agreements and scientific opinion support actions that achieve reductions in GHG emissions - mitigation - attempting to curb the increasing trend in atmospheric GHG concentrations. Despite its direct impact on temperature levels, its technical feasibility, and its ethical appeal, several factors limit the implementation of mitigation: (i) the strong inertia in the carbon cycle leads to a gap between the required large present costs (investments in clean technologies) and future benefits (lower GHG concentrations) (Keller et al., 2007; Nordhaus, 2008); (ii) the decades to millennia long lifespan of GHG render mitigation ineffective in case of sudden climate change damages; (iii) the atmosphere is a common good and unilateral actions are discouraged by the potential existence of free riders (Millard-Ball, 2012).

An alternative for dealing with climate change is adaptation, the development of strategies that effectively reduce the impacts of climate change (Tol, 2005; Adger et al., 2007; Klein et al., 2007). Adaptation covers a large array of sectors, and can be 'proactive' or 'reactive' (de Bruin, 2011). While proactive adaptation is directed towards infrastructure and medium- to long-term economic transformations (Agrawala et al., 2011), reactive adaptation can be deployed almost instantaneously to mitigate unforeseen or underestimated damages. Several features distinguish adaptation from mitigation: (i) adaptation actions can be implemented unilaterally, giving full control of the benefits to the countries developing them; (ii) adaptation measures are expected to exhibit a fast implementation - fast benefits feature, avoiding deadlocks due to discounting preferences. However, with uncertainty surrounding the magnitude of climate change effects and the vulnerability of environmental equilibria, assessing the effectiveness of adaptation proves to be challenging and might limit investments in adaptation (de Bruin and Dellink, 2011).

Given the increasing risk of an unmanageable temperature path and the current mitigation and adaptation deadlock, new proposals suggest to rely on geoengineering for dealing with the climate change problem (Keith, 2000; Crutzen, 2006; Brovkin et al., 2009). Geoengineering solutions correspond to deliberate modifications of the climate system in order to alleviate climate change impacts (Keith, 2000; Caldeira et al., 2013). One may distinguish between two main techniques, namely Carbon Dioxide Removal (CDR) and Solar Radiation Management (SRM).

In this paper, we focus on an SRM approach that targets the reduction of incoming solar radiation by injection of sulphur in the stratosphere, believed to be one of the most efficient geoengineering strategies to reduce global temperature (Nordhaus, 2001; Wigley, 2006; Shepherd, 2009). Its premise is the ability to keep temperature levels artificially low, instead of reducing GHG emissions. SRM presents several advantages: (i) it involves low implementation

[1]The recent IPCC report notes that the most likely increase in temperature by 2100 will reach a level above 3 °C (Edenhofer et al., 2014).

costs (Crutzen, 2006; Robock et al., 2009); (ii) in case of rapid climate changes (when climate tipping points are reached), with rare but catastrophic impacts, SRM could act as a quick and effective temperature 'backstop' (Crutzen, 2006; Barrett, 2008); (iii) it can be implemented either unilaterally or cooperatively (Barrett, 2008; Blackstock et al., 2009).

However, SRM brings along important risks, as it may produce unintended consequences and harmful side effects (Victor, 2008). A comprehensive summary is given in Barrett et al. (2014). Injecting sulphur particles into the upper atmosphere is expected to cause polar ozone depletion (Crutzen, 2006; Tilmes et al., 2008; Solomon et al., 2009), acid deposition at the poles (Kravitz et al., 2009), alter ecosystems (Stanhill and Cohen, 2001; Adams et al., 2003; Rasch et al., 2008), and trigger regional imbalances (e.g., in the patterns of surface temperature, radiation, and the hydrological cycle; Trenberth and Dai, 2007; Bala et al., 2008; Brovkin et al., 2009; Kravitz et al., 2013; Niemeier et al., 2013; Schaller et al., 2013; Huneeus et al., 2014). Simulations of sulphate injection predict disruptions in the Asian and African summer monsoons (Robock et al., 2008). Stratospheric aerosol loading impacts the ratio of direct to diffuse light, with consequences for terrestrial and marine photosynthesis and for technologies relying on direct light (Rasch et al., 2008; Vaughan and Lenton, 2011).

Furthermore, SRM achieves only an 'artificial' reduction in temperature levels. With a continued increase in GHG concentrations, the injection of aerosols would need to raise proportionally, and a disruption would lead to a significant jump in temperatures at the corresponding concentration level (Brasseur and Roeckner, 2005; Brovkin et al., 2009; Jones et al., 2013) with probable dire consequences. Additionally, SRM will not be able to counteract other negative consequences coming from high GHG concentrations, such as ocean acidification (Orr et al., 2005; Doney et al., 2009), CO_2 fertilisation of land plants, and other biogeochemical modifications (Ban-Weiss and Caldeira, 2010). Finally, with a lack of assessment of SRM impacts on the whole (natural and human) system, there remains the possibility for unexpected consequences – unknown unknowns (Kravitz et al., 2009; Vaughan and Lenton, 2011). The uncertainty is reinforced by the fact that expected consequences of SRM (both positive and negative) are estimated by comparison with natural volcanic eruptions, which are an imperfect analog to continuous anthropogenic stratospheric forcing (Robock et al., 2013). Finally, there are important societal and political dimensions to geoengineering (Markusson et al., 2013; Macnaghten and Szerszynski, 2013; Wright et al., 2014).

Given these important caveats, support for geoengineering measures has been inconclusive so far. Crutzen (2006), Wigley (2006), Carlin (2007), and Bickel (2013) advocate additional research on geoengineering before a robust recommendation could be formulated. More recent studies focus on modelling decision-making in the context of multiple sources of risk. Gramstad and Tjotta (2010) propose an integrated assessment model (hereafter IAM) that allows for parametric uncertainty in the impact of SRM on radiative forcing. They find that SRM passes the cost-benefit test under all scenarios, but admit that other factors (such as the risk of SRM interruptions) could lead to the rejection of such projects. Goes et al. (2011) use an IAM where the total damage from climate change is a function of a rate-dependent temperature component, and account for the failure to sustain aerosol forcing and for the subsequent unraveling of drastic climate changes. In such a case, SRM is found to be an economically inefficient strategy. Bickel and Agrawal (2012) rely on the model of Goes et al. (2011) and show that under modified assumptions some totally different conclusions regarding the use of SRM can be found.

In this paper, we assess the optimal mix of policies to deal effectively with climate change. Our methodology relies on the Ada-BaHaMa integrated assessment model (Bahn et al., 2012), which allows for mitigation and adaptation actions, and enriches it by explicitly considering an SRM strategy. In a cost-benefit framework, we model in a stylised manner the interactions between

the climate and the economic systems. We distinguish between the different effects of SRM on atmospheric temperature levels and on natural and socio-economic systems. While the *desired* effects of SRM on radiative forcing can be estimated with a considerable degree of confidence (Crutzen, 2006), the magnitude of *undesired* side-effects of sulfur injection remains a significant unknown. We focus on this second uncertainty source, and unlike previous IAMs that consider SRM side-effects to be constant over time (Goes et al., 2011; Bickel and Agrawal, 2012), we model side-effects as a time-varying and persistent process with a stochastic component.

Our original contribution consists in assessing, within an integrated assessment framework, the optimal policy mix when different strategies are available (mitigation, proactive and reactive adaptation, and SRM). We focus on the possible interactions and substitutions between the different policies, while accounting for the possible variability in the downside risks of SRM. We show that the optimal strategy for dealing with climate change involves the joint use of mitigation, adaptation, and geoengineering. While mitigation and adaptation are optimally employed in the vast majority of analysed scenarios, SRM passes a cost-benefit test only when its side-effects are low. We contribute to the geoengineering debate by underlying that SRM should not be seen as the ultimate solution to climate change; large reductions in emissions are necessary even in the optimistic SRM side-effect scenarios. Moreover, small deviations from expected side-effects can potentially cause large welfare losses, and further reduce the use of SRM.

The reminder of the paper is structured as follows. Section 2.2 details our dynamic IAM and its calibration. Sections 2.3 and 2.4 provide numerical results and analyse specific uncertainties related to SRM. Section 2.5 concludes.

2.2 Modelling approach

In this section we briefly review the original Ada-BaHaMa model (Bahn et al., 2012) and detail the new modelling features: (i) the introduction of SRM as an instrument to control temperature increase and (ii) a separate accounting of proactive and reactive adaptation.

2.2.1 Welfare maximisation

We consider a global decision maker that maximises total social welfare (W) given by the sequence of future discounted utility from per capita consumption (c). The welfare criterion is given by:

$$W = \sum_{n=0}^{14} \Delta t R(t_0 + n\Delta t) L(t_0 + n\Delta t) U(c(t_0 + n\Delta t)) \tag{2.1}$$

We assume a constant relative risk aversion (CRRA) utility function, with $U(c(t)) = \frac{c(t)^{1-\mu}-1}{1-\mu}$, where $1/\mu$ is the elasticity of intertemporal substitution, per capita consumption is given by $c(t) = \frac{C(t)}{L(t)}$, C is the total consumption, L is the population size at time t, n is the number of decades passed since t_0, and Δt is the decision time step. R represents the time preference discount factor, with $R(t_0 + n\Delta t) = e^{-r(n-1)\Delta t}$ and r the yearly rate of time preference. We perform the optimisation for fifteen time periods of one decade each, for the time horizon spanning over the years 2005 and 2155, with $t_0 = 2005$, $n \in [0, 14]$, and $\Delta t = 10$ years.

The population size is calibrated on the 2007 version of DICE, hereafter DICE2007,[2] and evolves according to the following dynamics:

$$L(t) = L(t_0)e^{\frac{g}{dg}\left(1-e^{-\frac{dg}{n-1}}\right)} \tag{2.2}$$

where $L(t_0)$ is the initial (2005) population size, g is the initial growth rate of the population, and dg is the rate of decrease for the growth rate of population.

Consumption comes from an optimised share of production (Y). The Ada-BaHaMa distinguishes between two types of economy: a 'carbon' economy (our present economy, indexed 1) where production is realised with a high level of fossil fuels, and a 'low-carbon' economy (indexed 2, for instance a hydrogen economy) with small GHG contributions.[3] After consumption, the remaining share of production is used: (i) to invest in the production capital of the carbon and low-carbon economies (I_1, I_2) and in the proactive adaptation capital (I_3); (ii) to spend for reactive adaptation (S_3) and SRM measures (S_4); and (iii) to pay for energy costs, where p_{E_1} and p_{E_2} are energy prices per unit of emission, E_1 and E_2 the emission levels, and ϕ_1 and ϕ_2 the energy efficiency in the carbon-intensive and low-carbon economies, respectively. The presence of damages (D) from climate change and SRM side-effects reduces the available production such that:

$$\begin{aligned}(1-D(t))Y(t) &= C(t)+I_1(t)+I_2(t)+I_3(t)+S_3(t)+S_4(t)\\ &\quad +p_{E_1}(t)\phi_1(t)E_1(t)+p_{E_2}(t)\phi_2(t)E_2(t)\end{aligned} \tag{2.3}$$

Production occurs in the two economies according to an extended Cobb-Douglas production function in three inputs: capital (K), labor (L), and energy (measured through GHG emission level E):

$$\begin{aligned}Y(t) &= A_1(t)K_1(t)^{\alpha_1}(\phi_1(t)E_1(t))^{\theta_1(t)}L_1(t)^{1-\alpha_1-\theta_1(t)}\\ &\quad +A_2(t)K_2(t)^{\alpha_2}(\phi_2(t)E_2(t))^{\theta_2(t)}L_2(t)^{1-\alpha_2-\theta_2(t)}\end{aligned} \tag{2.4}$$

where for each economy i ($i = 1, 2$): A_i is the total factor productivity, α_i the elasticity of output with respect to capital K_i, ϕ_i the energy efficiency and θ_i the elasticity of output with respect to emissions. Capital stock in each economy evolves according to the choice of investment (I_i) and a depreciation rate δ_{K_i} through a standard relationship:

$$K_i(t+\Delta t) = I_i(t)\Delta t + (1-\delta_{K_i})^{\Delta t}K_i(t) \tag{2.5}$$

The same dynamics apply for proactive adaptation capital (K_3). Total labor (L) is divided between the two economies:

$$L(t) = L_1(t) + L_2(t) \tag{2.6}$$

The optimal policy consists in choosing at each time period the investment levels (I_1, I_2, I_3), the spending (S_3, S_4), the emissions (E_1, E_2), and the labor allocation (L_1, L_2).

[2] See: http://www.econ.yale.edu/ nordhaus/DICE2007.htm.

[3] We calibrate a baseline scenario—in which only the carbon economy is producing—to match as closely as possible production, concentration, and temperature trajectories of the DICE2007 baseline. Production in the low-carbon economy is more energy efficient, but also more costly, than in the carbon economy. Without distinguishing among specific technologies, we rely on the MERGE model (Manne and Richels, 2005) for its calibration.

2.2.2 Climate dynamics in the presence of SRM

GHG stocks evolve according to the dynamic equations of the DICE model (Nordhaus, 2008) that distinguishes between three reservoirs: (i) an atmospheric one (M_{AT}), (ii) a quickly mixing one in the upper oceans and the biosphere (M_{UP}), and (iii) a slowly mixing deep-ocean reservoir (M_{LO}) which acts as a long-term sink.

$$M_{AT}(t+\Delta t) = \Delta t(E_1(t)+E_2(t)) + \psi_{11}M_{AT}(t) + \psi_{21}M_{UP}(t) \tag{2.7}$$
$$M_{UP}(t+\Delta t) = \psi_{12}M_{AT}(t) + \psi_{22}M_{UP}(t) + \psi_{32}M_{LO}(t) \tag{2.8}$$
$$M_{LO}(t+\Delta t) = \psi_{23}M_{UP}(t) + \psi_{33}M_{LO}(t) \tag{2.9}$$

where $\psi_{i,j}$ are calibration parameters.

We extend the original Ada-BaHaMa to account for a solar radiation management (SRM) strategy that increases the albedo effect through sulfur injection in the lower stratosphere. The sulphate aerosols formed increase the stratospheric reflection of shortwave radiation back to space (Stenchikov et al., 1998), reducing the radiative forcing from an increase in CO_2 concentrations:

$$F(t) = \eta log_2\left(\frac{M_{AT}(t)}{M_{AT}(1750)}\right) + F_{EX}(t) - F_{GE}(t) \tag{2.10}$$

where $\eta = 3.7$ W m^{-2} is the radiative forcing for a doubling of atmospheric CO_2 concentrations, F_{EX} the exogenous radiative forcing term, and F_{GE} is the radiative forcing created by the sulphates.

The radiative forcing from SRM depends on the amount of sulfur injected, the size of the particles, and the location of injection (Vaughan and Lenton, 2011). Sulfur injection simulations show that at high injection rates (above 40 Tg S) the efficacy on radiative forcing levels off (English et al., 2012). However, for smaller injection rates, a linear relation approximates well the impact of sulfur injected on radiative forcing.[4] We follow Crutzen (2006) and allow for a linear relation:

$$F_{GE}(t) = \omega G(t) \tag{2.11}$$

where ω is the effectiveness factor of SRM, and G the yearly amount of sulfur injected in the stratosphere measured in tetragrams of sulfur (Tg S). Based on the observations from the volcanic eruption of Mount Pinatubo (June 1991), Crutzen (2006) finds ω to have a value of approximately 0.75 W m^{-2} per Tg S.

The link between the increase in atmospheric CO_2 concentrations and temperature increase is captured by the impact of radiative forcing on temperature. As in Ada-BaHaMa, we follow the DICE model to compute the increase in earth's mean surface temperature (T_{AT}) and in the average temperature of the deep oceans (T_{LO}) from pre-industrial levels:

$$T_{AT}(t+\Delta t) = T_{AT}(t) + \xi_1\left[F(t+\Delta t) - \xi_2 T_{AT}(t) - \xi_3\left(T_{AT}(t) - T_{LO}(t)\right)\right] \tag{2.12}$$
$$T_{LO}(t+\Delta t) = T_{LO}(t) + \xi_4\left(T_{AT}(t) - T_{LO}(t)\right) \tag{2.13}$$

where ξ_j $(j = 1, 2, 3, 4)$ are calibration parameters.

[4] In our simulations, the optimal amount of sulfur injected never exceeds 15 Tg S per annum.

2.2.3 Climate change damages and SRM side-effects

Ada-BaHaMa follows the approach used in MERGE (Manne and Richels, 2005) to link climate change damages and their economic impacts. Here, we additionally account for negative externalities from sulfur injection. Total yearly damages (D) on production come from atmospheric temperature increase ($D_{T_{AT}}$) and side-effects from sulfur injection (D_{GE}):

$$D(t) = D_{T_{AT}}(t) + D_{GE}(t) \tag{2.14}$$

2.2.3.1 Climate change damages and adaptation

The increase in temperature (T_{AT}) from pre-industrial levels entails damages that can be alleviated through adaptation (AD):

$$D_{T_{AT}}(t) = \mathrm{AD}(t) \left(\frac{T_{AT}(t) - T_d}{cat_T - T_d} \right)^2 \tag{2.15}$$

where T_d is the temperature deviation (from pre-industrial level) at which damages start to occur, while cat_T represents the 'catastrophic' temperature level at which the entire production would be wiped out. To have a comparable basis with the current literature on IAM with adaptation, T_d and cat_T are calibrated to replicate the damage intensity in DICE; see Bahn et al. (2012).

We distinguish between reactive (flow) and proactive (stock) adaptation, similar to Bosello et al. (2010) and Agrawala et al. (2011). We model the effectiveness of the two adaptation strategies in reducing climate change damages as follows:

$$\mathrm{AD}(t) = 1 - \alpha_{\mathrm{AD}_p}(t) \frac{K_3(t)}{K_{3\max}(t)} - \alpha_{\mathrm{AD}_r}(t) \frac{S_3(t)}{S_{3\max}(t)} \tag{2.16}$$

where α_{AD_p} (respectively, α_{AD_r}) is the maximum proactive (resp. reactive) adaptation effectiveness, K_3 (resp. S_3) the amount of proactive adaptation capital (resp. reactive adaptation spending), $K_{3\max}$ (resp. $S_{3\max}$)[5] the maximum amount of adaptation capital (resp. spending) that would ensure the optimal effectiveness of the proactive (resp. reactive) adaptation measures. Like $K_{3\max}$ in our original model, $S_{3\max}$ is modelled as an increasing function of the temperature level:

$$S_{3\max}(t) = \beta_{\mathrm{AD}_r} \left(\frac{T_{AT}(t)}{T_d} \right)^{\gamma_{\mathrm{AD}_r}} \tag{2.17}$$

where β_{AD_r} and γ_{AD_r} are calibration parameters.

The two options are assumed to be complementary, in that the implementation of one enhances the effectiveness of the other. On the one hand, reactive adaptation requires the existence of some infrastructure; for instance, the deployment of new crops (better suited to new climatic condition) possibly requires that tests have been conducted beforehand (pro-actively) in R&D facilities. On the other hand, since investments in (proactive) adaptation are initiated much earlier than their first use, they are based on expectations and can result in inadequate solutions when damages start to occur. Reactive adaptation can marginally modify the solution to ensure

[5] We impose $K_3(t) \leq K_{3\max}(t)$ and $S_3(t) \leq S_{3\max}(t)$ at all time periods.

maximum effectiveness. Adaptation effectiveness is modelled as follows:

$$\alpha_{\mathrm{AD}_p}(t) = (\overline{\alpha_{\mathrm{AD}_p}} - \underline{\alpha_{\mathrm{AD}_p}}) \left(\gamma_1 \frac{K_3(t)}{K_{3max}(t)} + \gamma_2 \frac{S_3(t)}{S_{3max}(t)} \right) + \underline{\alpha_{\mathrm{AD}_p}} \quad (2.18)$$

$$\alpha_{\mathrm{AD}_r}(t) = (\overline{\alpha_{\mathrm{AD}_r}} - \underline{\alpha_{\mathrm{AD}_r}}) \left(\gamma_1 \frac{S_3(t)}{S_{3max}(t)} + \gamma_2 \frac{K_3(t)}{K_{3max}(t)} \right) + \underline{\alpha_{\mathrm{AD}_r}} \quad (2.19)$$

where $\underline{\alpha_{\mathrm{AD}_p}}$ and $\overline{\alpha_{\mathrm{AD}_p}}$ (resp., $\underline{\alpha_{\mathrm{AD}_r}}$ and $\overline{\alpha_{\mathrm{AD}_r}}$) are the minimum and maximum effectiveness values for proactive (resp., reactive) adaptation, and γ_1, γ_2 calibration parameters ($\gamma_1 > \gamma_2$, $\gamma_1 + \gamma_2 = 1$). We model adaptation effectiveness such that in particular: (i) the absence of one adaptation strategy does not make the other ineffective, but reduces its potential; and (ii) only maximum capital level ($K_3(t) = K_{3max}(t)$) and spending ($S_3(t) = S_{3max}(t)$) ensure maximum effectiveness.

Calibration of the adaptation strategies follows the AD-DICE approach (de Bruin et al., 2009), accounting for the additional reactive adaptation option and its complementarity with proactive adaptation. The calibration of $K_{3\mathrm{max}}$ and $S_{3\mathrm{max}}$ relies on World Bank estimates (Margulis and Narain, 2009). However, we assume that reactive adaptation is 50% more costly than proactive adaptation to achieve its maximum potential.[6] The calibration of the effectiveness parameters α_{AD_p} and α_{AD_r} reflects stylised assumptions about the reactive-proactive relationship. First, we assume that reactive adaptation is slightly more efficient than proactive adaptation, as 'last-minute' strategies are easier to adjust to observed damages. This assumption is coherent with Agrawala et al. (2011), where reactive adaptation offsets on average 27% of gross damages and proactive adaptation only 21%. Our calibration is very close, with 25% for reactive adaptation ($\overline{\alpha_{\mathrm{AD}_r}}$) and 22% for proactive ($\overline{\alpha_{\mathrm{AD}_p}}$). Second, the maximum effectiveness of total adaptation cannot be higher than 0.5. This is coherent with Nordhaus and Boyer (2000) where total adaptation potential is 0.48 (compared to 0.47 in our calibration). And third, the difference between minimum and maximum effectiveness for the two strategies is chosen to be relatively small, which implies that proactive and reactive adaptation options are only weakly complementary, similar to Agrawala et al. (2011).

2.2.3.2 SRM measures and side-effects

SRM implementation is expected to be inexpensive and fast (Barrett, 2008). Following Moreno-Cruz and Keith (2013), we allow for linear SRM implementation costs (S_4), proportional to the yearly amount of sulfur injected in the atmosphere (G):

$$S_4(t) = p_{GE}(t)G(t) \quad (2.20)$$

where p_{GE} refers to the cost of injecting one tetragram of sulfur. Following Crutzen (2006), we consider $p_{GE} = \$25$ billion per Tg S annually.

Despite the low implementation costs, SRM is believed to bring along important risks. A comprehensive, but not exhaustive, list of expected sulfur injection side-effects has been presented in the introduction. In particular, injecting large amounts of sulfur in the upper atmosphere may have potentially disruptive effects on weather patterns and the water cycle (Ramanathan et al., 2001; Brovkin et al., 2009). Additional damages are expected in case sulfur particles

[6] Indeed, deployment of last minute strategies should incur organisational costs much higher than under a long-planned strategy. Besides, compared to proactive adaptation, reactive adaptation should bear some of the infrastructure and deployment costs upfront, which induces large overhead.

enter the troposphere and add to the sulfur concentration in soil (Crutzen, 2006). Though we are beginning to form a better image of the possible side-effects from sulfur injection, the exact type and magnitude of side-effects are still to be quantified (Robock et al., 2013).

We model the magnitude of SRM side-effects (D_{GE}) following the approach of Goes et al. (2011), where sulfur injection damages depend on an intensity factor ($\alpha_{GE} \in [0, 1]$) and the radiative forcing created by SRM (F_{GE}), normalised by the radiative forcing for a doubling of atmospheric CO_2 concentrations (η). However, unlike previous IAMs that consider SRM side-effects (parameter α_{GE}) to be constant over time (Goes et al., 2011; Bickel and Agrawal, 2012), we model side-effects as a time-varying and persistent process. Modifying the radiative forcing through sulphate injection is expected to impact different Earth system processes, whose consequences will be felt for periods beyond the lifetime of sulphates in the stratosphere (Brovkin et al., 2009; Vaughan and Lenton, 2011). Therefore, we account for persistency in damages and allow the intensity factor (α_{GE}) to vary over time:

$$D_{GE}(t + \Delta t) = \lambda D_{GE}(t) + \alpha_{GE}(t + \Delta t)\frac{F_{GE}(t + \Delta t)}{\eta} AD_{GE}(t) \tag{2.21}$$

where λ (< 1) is a constant depreciation rate,[7] α_{GE} a time-varying random process, F_{GE} the radiative forcing created through SRM, η the radiative forcing for a doubling of atmospheric CO_2 concentrations, and $AD_{GE} \in [0, 1]$ a parameter describing the effectiveness of adaptation to damages from sulfur injection. Eq. (2.21) accounts only for 'direct' effects (such as changes in the water cycle); 'indirect' effects (such as ocean acidification) are addressed in Section 2.4. Moreover, the decision maker could possibly reduce the SRM side-effects through adaptation measures, in a similar manner to the adaptation to damages from temperature increase (see Eq. (2.15)). However, the research on this issue is in its infancy, and the costs of reducing the highly uncertain SRM damages are still to be estimated. For simplification, we consider that no adaptation measures are available for side-effects from sulfur injection, i.e. $AD_{GE}(t) = 1, \forall t$. Thus, we disregard both benefits and costs of such adaptation, and we focus instead on a large range of values for SRM side-effects.

Considering the multitude of systems that SRM impacts and the likely existence of complex feedback loops, we consider its short- and long-term disturbances to be unpredictable and to evolve in a possibly non-monotonic manner.[8] While some of the responses to stratospheric sulfur are believed to be fast (e.g., precipitation), others would come with longer time scales (e.g., oceanic responses) (MacMynowski et al., 2011a,b; Robock et al., 2013). We therefore rely on a binomial tree representation in order to model the possible evolution of (monetary) side-effects over time (α_{GE}). This approach allows us to capture the uncertainty in the size of side-effects and the possible variability in effects due to interactions between different components of the Earth system. The binomial representation assumes that at each moment of time, side-effects can either increase or decrease compared to the previous state, such that:

[7] Given the lack of evidence on the strength of the persistency of SRM side-effects, we run a sensitivity analysis for λ, with $\lambda \in \{0, 0.25, 0.5, 0.75, 1\}$.

[8] This time-varying representation of SRM side-effects is motivated by the view that ecosystems present dynamic and non-linear resilience to shocks and perturbations (Holling, 1973; Gunderson, 2003). Complex socio-ecological systems can have a highly optimised tolerance to a certain set of disturbances (Carlson and Doyle, 2002; Janssen et al., 2007), but they would suffer if the disturbances evolve or change outside of their optimised tolerance zone, causing them to move to new equilibria.

$$\alpha_{GE}(t) \begin{cases} \rightarrow \alpha_{GE}(t+\Delta t) = (1+u)\,\alpha_{GE}(t) \\ \rightarrow \alpha_{GE}(t+\Delta t) = (1-d)\,\alpha_{GE}(t) \end{cases}$$

with u the percentage increase, and d the percentage decrease.

The parameter α_{GE} refers to percentage losses in world GDP (Y) due to side-effects from geoengineering, when the radiative forcing created through sulfur injections equals the radiative forcing for a doubling of atmospheric CO_2 concentrations ($F_{GE} = \eta$). To capture all possible (from highly optimistic to very pessimistic) side-effect scenarios, we allow parameter α_{GE} to take values between 0 - 100% of world GDP. We define three levels of side-effects: an initial level $\alpha_{GE}(t_0)$, and two boundary values for the final period T defining a minimum ($\underline{\alpha_{GE}} = 0$) and a maximum level ($\overline{\alpha_{GE}} = 1$). Similarly to Goes et al. (2011), we run different scenarios in which the initial size of side-effects ($\alpha_{GE}(t_0)$) takes values in the range $[0, 0.1]$,[9] where the upper limit of the initial damages – from an SRM radiative forcing equal to the radiative forcing for a doubling of atmospheric CO_2 concentrations – of 10% would correspond to output losses from an increase in temperature of about 5.2 °C .

Parameter u is calibrated to link $\alpha_{GE}(t_0)$ to $\overline{\alpha_{GE}}$ in a monotonically increasing path over 15 decades (until 2155): $\overline{\alpha_{GE}} = \alpha_{GE}(t_0) \cdot (1+u)^{15}$. Similarly, a monotonically decreasing path is obtained for $\underline{\alpha_{GE}} = \alpha_{GE}(t_0) \cdot (1+d)^{15}$. Based on the binomial representation, for each initial $\alpha_{GE}(t_0)$ we obtain 32,768 ($= 2^{15}$) different scenarios. The optimisation is realised under perfect foresight regarding each of the distinctive α_{GE} scenarios.

2.3 Optimal policy mix

2.3.1 Selected scenarios for SRM side-effects

In this section, we show what are the optimal decisions regarding investments and spendings for production and climate measures, and the impact on temperature levels and atmospheric GHG stocks, when different climate policy portfolios are available. Namely, we consider three available portfolios: (i) mitigation only; (ii) mitigation and adaptation; (iii) mitigation, adaptation, and SRM.

The net benefits of the SRM strategy depend on the uncertain side-effects entailed by sulfur injection; as detailed in Section 2.2.3.2. To illustrate the optimal decisions when the SRM option is available, we hereby choose three scenarios for SRM side-effects. Section 2.3.2 reports on optimal decisions over the entire distribution of possible damages.

Following Goes et al. (2011), we first choose a constant path for SRM side-effects, entitled hereafter *mild* scenario. With our calibration, SRM is optimally employed in at least one decade over the horizon 2005-2155 if the constant side-effects are at maximum 0.15% of total output ($\alpha_{GE}(t) = 0.015$, $\forall t$). Additionally, we consider two illustrative cases, where the side-effect paths are time-varying. The first scenario refers to *strong* damages, where α_{GE} increases monotonically from $\alpha_{GE}(t_0) = 0.015$ to $\alpha_{GE}(2155) = \overline{\alpha_{GE}}$. It corresponds to the upper edge

[9] Goes et al. (2011) consider constant $\alpha_{GE} \in \{0, 0.01, 0.02, 0.03, 0.05\}$.

of the distribution (of all possible paths for side-effects starting at 0.015) when all forecasted impacts would be triggered (e.g., ozone depletion, unfavourable change in precipitation patterns, warming of the tropical tropopause) and the total magnitude would be amplified by cross-interactions. The second scenario refers to *weak* damages, where α_{GE} decreases monotonically from $\alpha_{GE}(t_0) = 0.015$ to $\alpha_{GE}(2155) = \underline{\alpha_{GE}}$. It corresponds to the lower edge of the distribution when sulfur injection has only modest side-effects. Tackling the climate change problem at its root requires mitigation, which corresponds in our model to a transition from the carbon economy to the low-carbon one. Fig. 2.1 illustrates the optimal capital accumulation in the two economies. In the mitigation-only scenario, there is a clear transition between the two

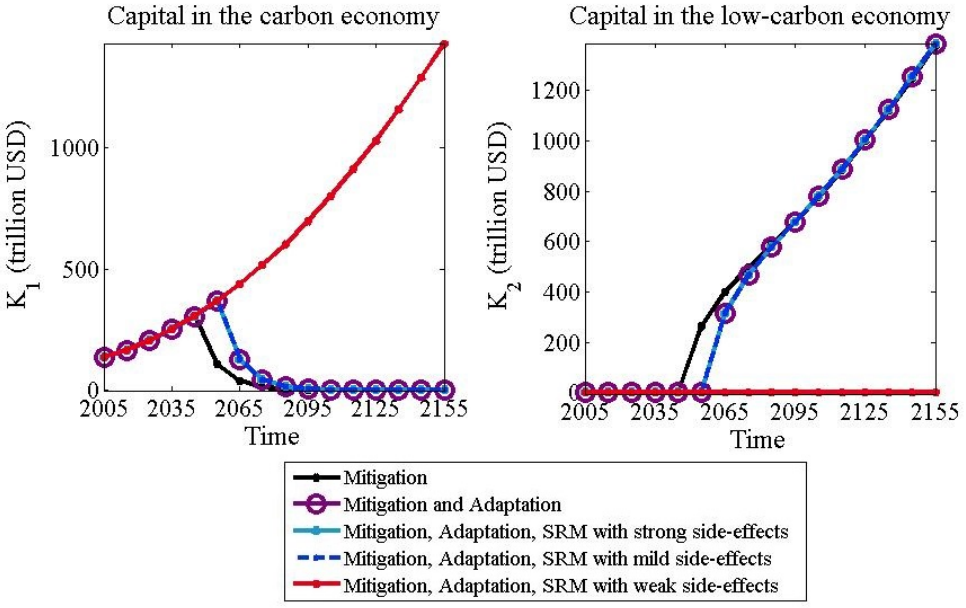

Fig. 2.1: Capital accumulation in the carbon and low-carbon economies.

economies: the carbon-intensive capital is rapidly phased out after 2055 and completely replaced by the low-carbon capital before the end of the century. When adaptation is also available as a policy tool (mitigation and adaptation portfolio), this transition does take place, but starts one decade later. The SRM option has contrasted implications: under mild and strong side-effects, the transition takes place similarly to the mitigation-adaptation portfolio, whereas the transition never occurs under weak side-effects. In agreement with Barrett (2008), our results indicate thus that there is no incentive to curb GHG emissions if SRM is available and its side-effects are benign.

Fig. 2.2 captures adaptation and SRM decisions. When its side-effects are weak, SRM is the main instrument to address climate change. It is used after 2045 (substituting for mitigation efforts), together with low proactive adaptation efforts (after 2095). When its side-effects are mild, SRM is only used (for two only decades 2065 - 2085) as a complement to adaptation and mitigation strategies. SRM is not used when its side-effects are strong. Concerning adaptation, we note that: (i) the accumulation of proactive adaptation capital starts before spending on reactive adaptation; and (ii) the decreasing trend in adaptation towards the end of the horizon reflects the stabilisation of temperature (see Fig. 2.3) reached through SRM and/or mitigation. An interesting aspect is the relative dynamics of reactive adaptation and SRM, as they share the advantages of rapid implementation and immediate reduction of damages. The weight given to either measure depends on the magnitude of sulfur damages: (i) in case of strong side-effects, between the two, only adaptation is used; (ii) for mild and weak side-effects, both measures

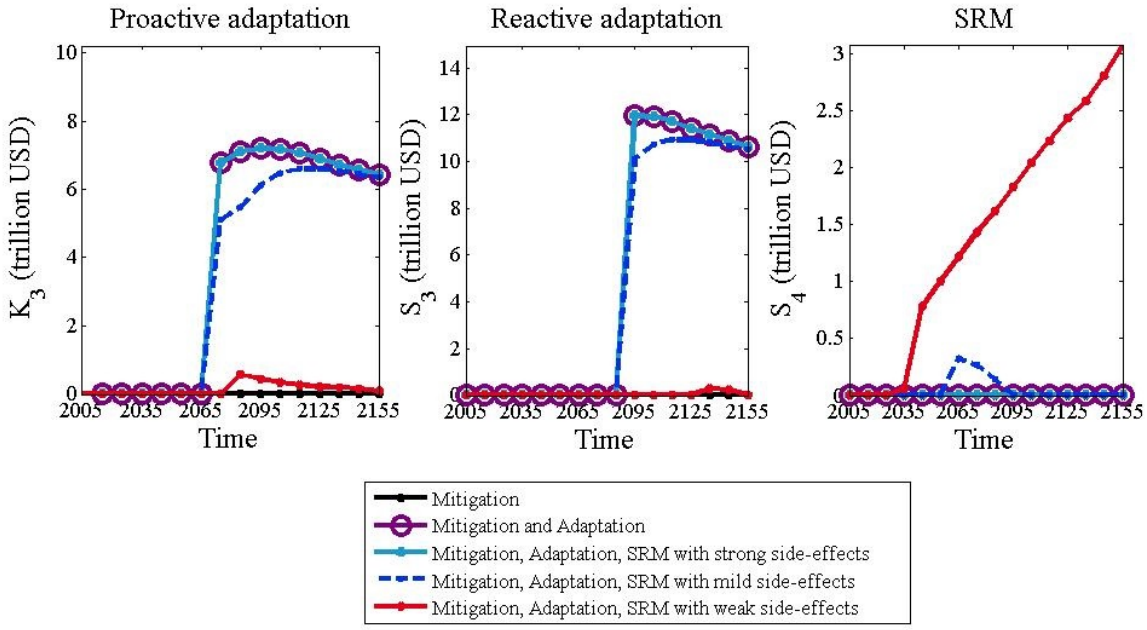

Fig. 2.2: Capital accumulation in proactive adaptation, and decade spending with reactive adaptation and SRM.

enter the policy portfolio, with more weight given to SRM when its side-effects are lower. This results from the limited effectiveness of reactive adaptation. Fig. 2.3 reveals that temperature is

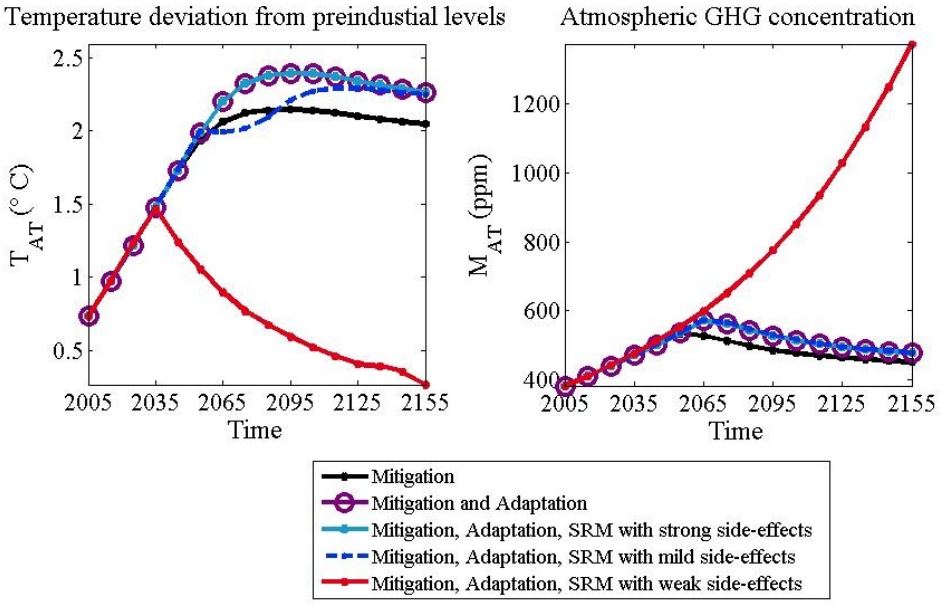

Fig. 2.3: Atmospheric temperature and GHG concentrations.

kept below the 2 °C threshold proposed by the Copenhagen Accord only when SRM side-effects are weak. This is achieved at the expense of: (i) a large deployment of SRM; and (ii) high GHG concentrations, due to the absence of any mitigation. In the other scenarios, concentrations and then temperature decrease slowly with the transition to the low-carbon economy. When SRM side-effects are mild, the use of SRM for two decades (2065-2085) reduces the temperature deviation for this period below the mitigation-only scenario; as SRM is stopped in 2085, the

temperature level begins to increase and converges to the weak side-effects path, reflecting the accumulation of GHGs in the atmosphere. The use of adaptation (in the 'mitigation and adaptation', and 'mitigation, adaptation, and SRM with strong side-effects' portfolios) reduces the damages from climate change, postponing the transition to the clean economy and resulting in higher temperature increases than the mitigation-only portfolio.

Imposing the 2 °C limit yields an earlier implementation of mitigation and/or SRM. In our parametrisation, with strong side-effects, investments in mitigation are advanced by two decades (2035); with weak side-effects, SRM remains predominant and is implemented from 2035 on. To reduce climate change damages, adaptation is still used with a similar timing (compared to the unconstrained temperature cases) but requires less funding.

2.3.2 Distributional analysis for SRM side-effects

In this section, we examine policy decisions for all side-effect scenarios from the binomial tree representation. We allow for seven different initial side-effect levels from SRM, i.e. $\alpha_{GE}(t_0) \in \{0.001, 0.01, 0.02, 0.03, 0.04, 0.05, 0.1\}$. For each $\alpha_{GE}(t_0)$, 32,768 different paths describing the evolution of side-effects over time are obtained; see Section 2.2.3.2.

We analyse first the frequency with which the different climate policies (mitigation, reactive and proactive adaptation, and SRM) are used. The frequency indicator is computed as the number of scenarios in which the policy is employed in at least one decade over the horizon 2005-2155, divided by the total number of scenarios corresponding to each $\alpha_{GE}(t_0)$. However, the frequency indicator tells nothing regarding the probability associated with the different α_{GE} paths.

Fig. 2.4 illustrates that the optimal policy portfolio depends on the initial value of SRM damages ($\alpha_{GE}(t_0)$). Namely, the use of SRM is strongly dependent on the initial SRM side-effects, such that SRM is implemented in at least one decade in almost 100% of the scenarios when $\alpha_{GE}(t_0)$ is 0.1%, declining abruptly as $\alpha_{GE}(t_0)$ increases, to the point that SRM is employed in about 11% of the scenarios when $\alpha_{GE}(t_0)$ is 10%. Despite the availability of the inexpensive SRM

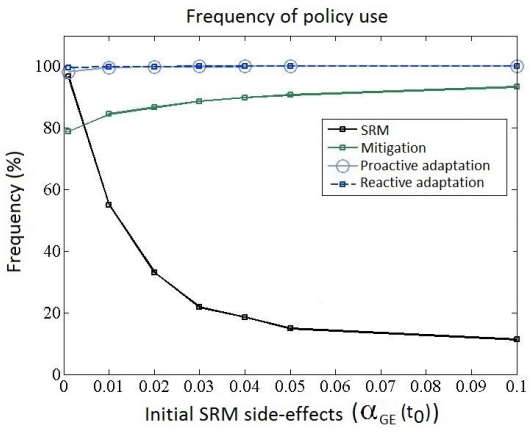

Fig. 2.4: Policy frequency different $\alpha_{GE}(t_0)$ (at $\lambda = 0.5$).

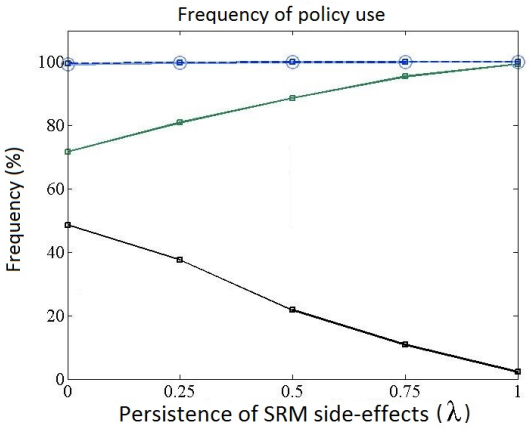

Fig. 2.5: Policy frequency different λ (at $\alpha_{GE}(t_0) = 0.03$).

option, mitigation and adaptation strategies are an important part of the optimal climate policy portfolio. Proactive and reactive adaptation strategies are employed in all scenarios,

independent of the SRM side-effects. The use of mitigation increases from about 80% when initial side-effects are low, to 93% of the scenarios when $\alpha_{GE} = 0.1$.

The SRM strategy occupies the smallest share of total investments and spendings among the different policies; see Fig. 2.B.2 in the Appendix. Its share decreases to a negligible level as side-effects increase and SRM is less employed. Moving from the carbon-intensive to the low-carbon technology requires investments that sum up to about 70% of the budget, with less variability as SRM side-effects increase and SRM is consequently less used. Investments in proactive adaptation and spendings with reactive adaptation are stable on average, being little influenced by sulfur injection side-effects and SRM decisions.

Another parameter that strongly influences the use of SRM is the persistency of SRM side-effects over time (parameter λ). Fig. 2.5 illustrates that for moderate initial SRM damages ($\alpha_{GE}(t_0) = 0.03$), SRM is used mostly as a complement to mitigation and adaptation even when side-effects from sulfur injection are active only during the implementation period ($\lambda = 0$). The SRM option becomes quickly unattractive as the persistency of side-effects increases. Moreover, at higher persistency levels, the implementation of SRM is postponed towards the end of the decision horizon. The start of mitigation and adaptation policies is not impacted on average by SRM side-effects persistency; see Fig. 2.B.4 in the Appendix.

Due to the uncertainty related to the initial side-effects value and the persistency of damages over time, the variability in SRM use is very large, and therefore the SRM option does not constitute a robust climate policy. Even in the optimistic SRM side-effects scenarios, SRM will play the role of a (rather modest) complement to adaptation and mitigation, and rarely a substitute, as highlighted also by the breakdown of total investments and spendings.

2.4 Indirect and unexpected SRM side-effects

The previous section indicates that SRM should be used when its side-effects are low and their persistency is limited. Here, we discuss additional concerns with SRM and analyse the adjustments in the optimal policy mix.

Failure to continue with SRM
An important concern with SRM is the potential damage that would be caused by a failure to sustain the sulfur injection (Robock et al., 2009; Goes et al., 2011). We analyse, in the case of weak side-effects, the consequences of SRM interruption (e.g., following a technical breakdown) from 2105. Our results confirm that temperature increases rapidly after the SRM failure, and that the benefits to be gained from mitigation are then limited due to the inertia in the climate system. Moreover, we find that proactive and reactive adaptation play an important role immediately after the SRM interruption, partly reducing the damages from the sudden increase in temperature; see Fig. 2.B.5 in the Appendix.

GHG concentrations
Our model accounts for direct SRM side-effects, but scientists point also to indirect side-effects such as ocean acidification (Orr et al., 2005). This arises from high CO_2 concentrations in the absence of mitigation. Damages to ocean ecosystems may occur starting with CO_2 concentration levels of 450 ppm (Cao and Caldeira, 2008). In our distributional analysis, no scenario is consistent with such a level, and, in fact, no scenario keeps concentration levels below 550 ppm. The percentage of scenarios that reach concentration levels in the range [550, 650] ppm strongly depends on the initial SRM side-effects: only 6% of the scenarios when $\alpha_{GE}(t_0) = 0.001$, and

about 92% of scenarios when $\alpha_{GE}(t_0) = 0.1$ (Fig. 2.B.3c in Appendix). Moreover, low initial side-effects levels are associated also with longer periods during which high concentrations are maintained (Fig. 2.B.3d). Finally, the average concentration level (and its right skewness) is much higher for low α_{GE} levels when SRM is widely used and mitigation efforts are scarce (Fig. 2.B.3a, b).

When constraining for instance concentration levels to 550 ppm (in the case of $\alpha_{GE}(t_0) = 0.03$, where average MAT was 530 ppm), the use of SRM is reduced from 21.79% to 19.45% of all scenarios, while the use of mitigation is increased from 88.68% to 100%. Adaptation continues to be used in all scenarios.

Wrong assumptions about side-effects

Finally, the most important concern with SRM is probably that the type and magnitude of side-effects remain largely unknown. Up to now, the optimal policy mix was evaluated under perfect foresight, assuming that the side-effects were known along each scenario. Here, we study the consequences of incurring a different (random) side-effect path than the one presumed. First, we compute following Eq. (2.21) the *presumed* SRM damages ($D_{GE}(t, s)$) that translate into output losses, where s is given by each SRM side-effects path from the binomial representation. Next, we compute *unexpected* output losses ($D_{GE}(t, s')$) that would arise if a different side-effect path s' occurs. More precisely, we replace in Eq. (2.21) $\alpha_{GE}(t)$ by a factor chosen randomly from the possible side-effect paths, while keeping the same levels for sulfur injection. Forming wrong assumptions regarding the side-effects should only last for short periods. Indeed, although the earth system presents some inertia, the magnitude of side-effects is ex-post identifiable via decreases in production. However, it might take several decades until true realisations are identified. As an illustration, we consider an error horizon of one to three decades and compare output losses[10] under known (presumed) and random (unexpected) side-effect paths. Fig. 2.6 reveals that output losses double on average when the side-effect path has a different outcome than the one assumed, even for a ten-year horizon. With a twenty to thirty-year horizon, the variance and right skewness of output losses increases further on average, indicating that extreme losses have a higher chance of occurrence. The output loss is higher in the case of larger initial SRM side-effects, indicating that when SRM implementation is optimal in only few of the possible α_{GE} paths, misestimating the damages can be very punitive; see Fig. 2.B.6 in the Appendix. Besides estimating welfare losses, we study the adjustments to the optimal policy mix after observing the true damages. As an example, we examine the (extreme) case where side-effects were assumed to be weak, but turn out to be strong. With (presumed) weak side-effects, SRM is first implemented in 2065 at the expense of any mitigation efforts. But suppose that after three decades the policy maker realises that side-effects are actually strong. We simulate this situation by running the model from 2065 on with the true α_{GE} values, keeping all investment and spending decisions blocked for the error horizon (2065-2085). The policy maker reacts by stopping all SRM activities from 2095 on. A quick transition to the low-carbon economy takes place, but cannot prevent a temperature increase to almost 3 °C. To alleviate some of the climate damages, adaptation (especially reactive) is extensively used; see Fig. 2.B.7 in the Appendix. Overall, deviating during the error horizon from the optimal policy in case of strong side-effects results in lower consumption levels for the remaining horizon.

[10]For each scenario $s \in [1, 32768]$, we compute the sum of presumed damages as: $SD_{GE} = \sum_{t=t_{GE}}^{t_{GE}+h\Delta t} D_{GE}(t, s)$, where t_{GE} is the first period of SRM implementation in scenario s and $h \in \{1, 2, 3\}$ decades of SRM implementation. Unexpected damages are computed as: $\frac{1}{5000} \sum_{i=1}^{5000} \sum_{t=t_{GE}}^{t_{GE}+h\Delta t} D_{GE}(t, s'_i)$, where $\alpha_{SE}(t, s'_i)$ is randomly selected from the initial side-effect distribution over 5000 simulations.

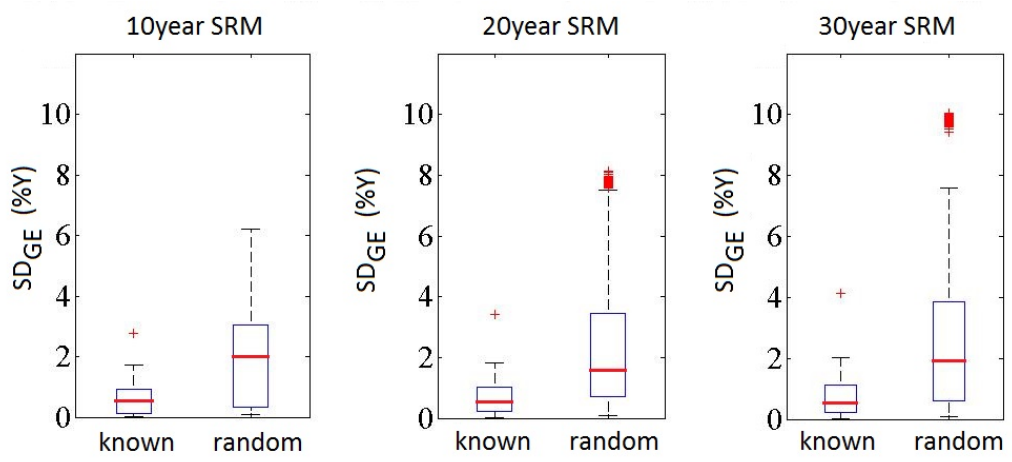

Fig. 2.6: Distribution of output losses under known and random SRM damages for different error horizons ($SD_{GE} = \sum_{t_{GE}}^{t_{GE}+h\Delta t} D_{GE}(t)$, $\alpha_{GE}(t_0) = 0.03$, $\lambda = 0.5$).

Note: The figure captures the distributional characteristics of the average yearly GDP losses due to environmental side-effects of sulfur injection, for two cases: (i) under perfect foresight, when the realisations of the α_{SE} path are known, and (ii) when the realisation of the α_{SE} is random and differs from the assumed one. The three panels refer to three different geoengineering implementation horizons, of one, two, and three decades respectively. Results refer to averages over 10,000 simulations.

2.5 Conclusions

This paper extends the Ada-BaHaMa model with an explicit representation of reactive adaptation and geoengineering (SRM). Reactive adaptation is modelled as a flow, and allows for its benefits to be internalized once with its costs, representing a climate policy that may avoid problems with discounting preferences. Reactive adaptation complements proactive adaptation, and its modelling gives a richer representation of possible adaptation strategies. SRM is a potential alternative to traditional climate strategies, and we distinguish between its (desired) effects on temperature levels and its (undesired and uncertain) side-effects on the environment. To the best of our knowledge, this is the first paper to assess, within an integrated assessment framework, the optimal policy mix when mitigation, proactive and reactive adaptation, and SRM strategies are available. We focus on the possible interactions and substitutions between the different policies, while accounting for the possible variability and persistency in the side-effects of SRM.

Our analysis reveals that the climate portfolio should give primary weight to mitigation and adaptation. With large predominance, SRM takes the role of a complement to mitigation and adaptation, and rarely a substitute, revealing that SRM will not provide the easy way out of the climate problem, replacing mitigation. The use of SRM is strongly dependent on the magnitude of its side-effects and their persistency through time. Due to the uncertainty related to these two features, the variability in SRM use is very large, leading us to conclude that the SRM option lacks robustness.

An extensive use of SRM brings additional concerns. One is the potential damage caused by a failure to continue with sulfur injection. Another one consists in indirect side-effects, such as ocean acidification. We investigate also possible welfare losses due to incorrect assumptions about SRM side-effects. Our analysis shows that output losses rise considerably when side-effects are different than presumed, even for short error horizons. Besides, longer horizons are

more costly, with extreme losses having a higher chance of occurrence. Accounting for these additional concerns reduces the use of SRM.

Although adaptation postpones the start of mitigation, it plays a vital role in reducing damages from sudden and sharp temperature increases in case the SRM option is unanticipatedly stopped (e.g., in case of technical breakdown or if side-effects prove to be sizeable compared to expectations). This particular feature highlights the importance of accounting for adaptation in the climate policy portfolio, especially when analysing the mitigation - SRM trade-off.

In our cost-benefit approach, despite the predominant role of mitigation, we note that investments in the low-carbon economy start after 2055 at the earliest. However, when following a cost-effectiveness approach to limit temperature increase to 2 °C, climate policies are implemented 20 years earlier. Meeting the agreed 2 °C temperature target would thus require earlier actions at the global level.

Our analysis could be improved along the following lines. First, our model assumes exogenous technological progress. With an endogenous formulation, one might expect that (R&D) investments in low-carbon technologies start earlier to get 'on-time' the needed technologies for mitigation. Second, being derived in a cost-benefit framework, our results (and in particular the timing of mitigation) critically depend on the magnitude of the estimated climate change damages, calibrated in our model on DICE and AD-DICE. Recent papers (Stern, 2013; Pindyck, 2013) signal possible underestimations of climate change damages in the DICE-like integrated assessment models; further research could help address these issues. Third, the deployment of SRM depends on various unknowns, such as the type and magnitude of side-effects, and the process governing their variability through time. The calibration of all involved parameters in our model will benefit from revisions reflecting scientific advances. Finally, our model assumes the existence of a well-functioning international cooperation for undertaking mitigation and SRM at a global level. Future research could improve our understanding of the two policies by accounting for differentiated geographical impacts and investigating strategic country behaviour.

Appendix Chapter 2

2.A Parameter values

The following three tables present the calibration values of the model parameters. We calibrated a baseline scenario – in which production is obtained only with the carbon-intensive technology – to match as closely as possible production, GHG concentrations, temperature trajectories, and population dynamics of the DICE2007 model (Nordhaus, 2007). Without distinguishing between specific technologies, the carbon-intensive and low-carbon economies are calibrated based on the MERGE model (Manne and Richels, 2005). Calibration of the adaptation strategies follows the AD-DICE approach (de Bruin et al., 2009), accounting for the additional reactive adaptation option and its complementarity with proactive adaptation. The calibration of $K_{3\max}$ and $S_{3\max}$ relies on World Bank estimates (Margulis and Narain, 2009).

Table 2.A.1: Calibration parameters.

Parameter	Value/Dynamics	Definition
Time and preference		
t	$\in [2005, 2155]$	Time period
t_0	2005	Initial time period
n	$\in [0, 14]$	Decades passed since t_0
Δt	10 years	Decision time step
r	0.015	Yearly rate of time preference
μ	2	$1/\mu$ is the elasticity of intertemporal substitution for CRRA utility
Energy		
Carbon economy		
p_{E_1}	0.425	Energy price per unit of emissions
$\phi_1(0)$	0.65	Energy efficiency at t_0
$\phi_1(t)$	$\phi_1(0)(e^{\upsilon_{\phi_1}\kappa_{\phi_1}})/e^{\upsilon_{\phi_1}}$	Energy efficiency at t
υ_{ϕ_1}	$-g_{\phi_1}(0)/dg_{\phi_1}$	
κ_{ϕ_1}	$exp(-dg_{\phi_1}(n+1))$	
$g_{\phi_1}(0)$	0.2	Growth rate of energy efficiency at t_0
dg_{ϕ_1}	0.3	Rate of decrease for growth rate of energy efficiency
Low-carbon economy		
p_{E_2}	0.55	Energy price per unit of emissions
$\phi_2(0)$	10	Initial value for energy efficiency
$\phi_2(t)$	$\phi_2(0)(e^{\upsilon_{\phi_2}\kappa_{\phi_2}})/e^{\upsilon_{\phi_2}}$	Energy efficiency at t
υ_{ϕ_2}	$-g_{\phi_2}(0)/dg_{\phi_2}$	
κ_{ϕ_2}	$exp(-dg_{\phi_2}(n+1))$	
$g_{\phi_2}(0)$	0.8	Growth rate of energy efficiency at t_0
dg_{ϕ_2}	0.01	Rate of decrease for growth rate of energy efficiency

Parameter	Value/Dynamics	Definition
Production		
Y	$A(t)\{K_1(t)^{\alpha_1}(\phi_1(t)E_1(t))^{\theta_1(t)}L_1(t)^{1-\alpha_1-\theta_1(t)}+$ $K_2(t)^{\alpha_2}(\phi_2(t)E_2(t))^{\theta_2(t)}L_2(t)^{1-\alpha_2-\theta_2(t)}\}$	Cobb-Douglas production
$A(t)$	$A(t-1)/(1-gA_0e^{-(dgA)n})$	Total factor productivity (TFP)
$A(0)$	0.039	Initial value for TFP
$gA0$	0.11	Initial value for growth rate of TFP
dgA	0.005	Rate of decrease for growth rate of TFP
α_i	0.3	Capital elasticity in production function
$\theta_i(0)$	0.05	Initial value for energy elasticity in production function
$g_{\theta_i}(0)$	-0.0116	Initial value for growth rate of energy elasticity
dg_{θ_i}	0.008	Rate of decrease for growth rate of energy elasticity
$\theta_i(t)$	$\theta_i(0)(e^{\upsilon_{\theta_i}\kappa_{\theta_i}})/e^{\upsilon_{\theta_i}}$	Energy elasticity in production function
υ_{θ_i}	$g_{\theta_1}(0)/dg_{\theta_1}$	
κ_{θ_i}	$e^{-dg_{\theta_i}(n+1)}$	
i	$\in \{1,2\}$	Index 1 denotes the carbon-intensive technology Index 2 denotes the low-carbon technology
Capital accumulation		
$K_1(t_0)$	137	Initial carbon-intensive technology capital (billion USD)
$K_2(t_0)$	0.0137	Initial low-carbon technology capital (billion USD)
$K_3(t_0)$	0	Initial proactive adaptation capital (billion USD)
δ_{K_1}	0.1	Annual carbon capital depreciation rate
δ_{K_2}	0.1	Annual low-carbon capital depreciation rate
δ_{K_3}	0.1	Annual proactive adaptation capital depreciation rate
Labor		
$L(t)$	$L_0e^{\frac{g}{dg}\left(1-e^{-\frac{dg}{n-1}}\right)}$	World population at t
L_0	6,409	2005 world population (millions)
g	0.08	Initial value for growth rate of population
dg	0.3	Rate of decrease for growth rate of population
GHG Stocks		
$M_{AT}(t+\Delta t)$	$\Delta t(E_1(t)+E_2(t))+\psi_{11}M_{AT}(t)+\psi_{21}M_{UP}(t)$	GHG concentrations in the atmosphere
$M_{UP}(t+\Delta t)$	$\psi_{12}M_{AT}(t)+\psi_{22}M_{UP}(t)+\psi_{32}M_{LO}(t)$	GHG concentrations in the upper strata
$M_{LO}(t+\Delta t)$	$\psi_{23}M_{UP}(t)+\psi_{33}M_{LO}(t)$	GHG concentrations in the lower strata
$M_{AT}(t_0)$	808.8	Concentration in atmosphere 2005 (GtC)
$M_{UP}(t_0)$	1,255	Concentration in upper strata 2005 (GtC)
$M_{LO}(t_0)$	18,365	Concentration in lower strata 2005 (GtC)
ψ_{11}	0.810712	Carbon cycle transition matrix
ψ_{12}	0.189288	Carbon cycle transition matrix
ψ_{21}	0.097213	Carbon cycle transition matrix
ψ_{22}	0.852787	Carbon cycle transition matrix
ψ_{23}	0.05	Carbon cycle transition matrix
ψ_{32}	0.003119	Carbon cycle transition matrix
ψ_{33}	0.996881	Carbon cycle transition matrix
Radiative forcing		
$F(t)$	$\eta log_2\left(\frac{M_{AT}(t)}{M_{AT}(1750)}\right)+F_{EX}(t)-F_{GE}(t)$	Total radiative forcing (Wm^{-2})
η	3.7	Radiative forcing from a doubling of M_{AT} (Wm^{-2})
$M_{AT}(1750)$	596.4	Concentration in atmosphere 1750 (GtC)
$F_{EX}(2000)$	-0.06	Estimate of 2000 forcing of non-CO_2 GHG
$F_{EX}(2100)$	0.30	Estimate of 2100 forcing of non-CO_2 GHG
$F_{GE}(t)$	$\omega G(t)$	Radiative forcing created by sulphates
ω	0.75	Effectiveness factor of sulfur injection

Parameter	Value/Dynamics	Definition
Temperature increase		
$T_{AT}(t+\Delta t)$	$T_{AT}(t)+\xi_1[F(t+\Delta t)-\xi_2 T_{AT}(t)-\xi_3\left(T_{AT}(t)-T_{LO}(t)\right)]$	Increase in earth's mean surface temperature
$T_{LO}(t+\Delta t)$	$T_{LO}(t)+\xi_4\left(T_{AT}(t)-T_{LO}(t)\right)$	Increase in deep ocean's mean surface temperature
ξ_1	0.22	Climate-equation coefficient for upper level
ξ_2	1.27	Climate-equation coefficient
ξ_3	0.30	Transfer coefficient upper to lower stratum
ξ_4	0.05	Transfer coefficient for lower level
T_d	0.106	Temp level at which damages start to occur
cat_T	16	Catastrophic temperature increase
Adaptation		
$AD(t)$	$1-\alpha_{\mathrm{AD}_p}(t)\frac{K_3(t)}{K_{3\max}(t)}-\alpha_{\mathrm{AD}_r}(t)\frac{S_3(t)}{S_{3\max}(t)}$	Total adaptation effectiveness
$\alpha_{\mathrm{AD}_p}(t)$	$(\overline{\alpha_{\mathrm{AD}_p}}-\underline{\alpha_{\mathrm{AD}_p}})\left(\gamma_1\frac{K_3(t)}{K_{3max}(t)}+\gamma_2\frac{S_3(t)}{S_{3max}(t)}\right)+\underline{\alpha_{\mathrm{AD}_p}}$	Proactive adaptation effectiveness
$\alpha_{\mathrm{AD}_r}(t)$	$(\overline{\alpha_{\mathrm{AD}_r}}-\underline{\alpha_{\mathrm{AD}_r}})\left(\gamma_1\frac{S_3(t)}{S_{3max}(t)}+\gamma_2\frac{K_3(t)}{K_{3max}(t)}\right)+\underline{\alpha_{\mathrm{AD}_r}}$	Reactive adaptation effectiveness
$\overline{\alpha_{\mathrm{AD}_p}}$	0.22	Max marginal proactive adaptation efficiency
$\overline{\alpha_{\mathrm{AD}_r}}$	0.25	Max marginal reactive adaptation efficiency
$\underline{\alpha_{\mathrm{AD}_p}}$	0.20	Min marginal proactive adaptation efficiency
$\underline{\alpha_{\mathrm{AD}_r}}$	0.23	Min marginal reactive adaptation efficiency
γ_1	0.67	Learning effect parameter
γ_2	0.33	Complementarity parameter
$K_{3\max}(t)$	$\beta_{\mathrm{AD}_p}\left(\frac{T_{AT}(t)}{T_d}\right)^{\gamma_{\mathrm{AD}_p}}$	Max K_3 to ensure optimal effectiveness of proactive
$S_{3\max}(t)$	$\beta_{\mathrm{AD}_r}\left(\frac{T_{AT}(t)}{T_d}\right)^{\gamma_{\mathrm{AD}_r}}$	Max S_3 to ensure optimal effectiveness of reactive
β_{AD_p}	0.0138	Scale value
β_{AD_r}	0.0021	Scale value
γ_{AD_p}	2.0081	Power value
γ_{AD_r}	2.0400	Power value
Geoengineering		
$S_4(t)$	$p_{GE}(t)G(t)$	Annual spending with SRM
$p_{GE}(t)$	25	Cost of injecting one tetragram sulfur (billion USD)
$D_{GE}(t+\Delta t)$	$\lambda D_{GE}(t)+\alpha_{GE}(t+\Delta t)\frac{F_{GE}(t+\Delta t)}{\eta}AD_{GE}(t)$	Side-effects from SRM (% Y)
λ	$\in\{0;0.25;0.50;0.75;1\}$	Persistency parameter of SRM side-effects
$AD_{GE}(t)$	1	Effectiveness of adaptation to SRM side-effects
$\alpha_{GE}(t_0)$	$\in[0,1]$	Initial value of SRM side-effects
$\alpha^u_{GE}(t+\Delta t)$	$(1+u)\alpha_{GE}(t)$	Upward move in SRM side-effects
$\alpha^d_{GE}(t+\Delta t)$	$(1+d)\alpha_{GE}(t)$	Downward move in SRM side-effects
$\overline{\alpha_{GE}}$	1	Max SRM side-effects in 2155
$\underline{\alpha_{GE}}$	0	Min SRM side-effects in 2155
u	$\sqrt[15]{\frac{\overline{\alpha_{GE}}}{\alpha_{GE}(t_0)}}-1$	Percentage increase in SRM side-effects
d	$\sqrt[15]{\frac{\underline{\alpha_{GE}}}{\alpha_{GE}(t_0)}}-1$	Percentage decrease in SRM side-effects

2.B Distributional analysis of SRM side-effects: supporting results

2.B.1 Start of the climate policy implementation

This paragraph discusses the optimal start of each climate policy (mitigation, proactive and reactive adaptation, SRM) implementation. Fig. 2.B.1 displays the distributions of policy initiation (first year the policy is implemented) over each of the $\alpha_{GE}(t_0)$ scenarios. While the implementation of mitigation and adaptation presents on average no dependency to SRM side-effect magnitudes, the start of the SRM strategy is highly sensitive to the initial α_{GE}.

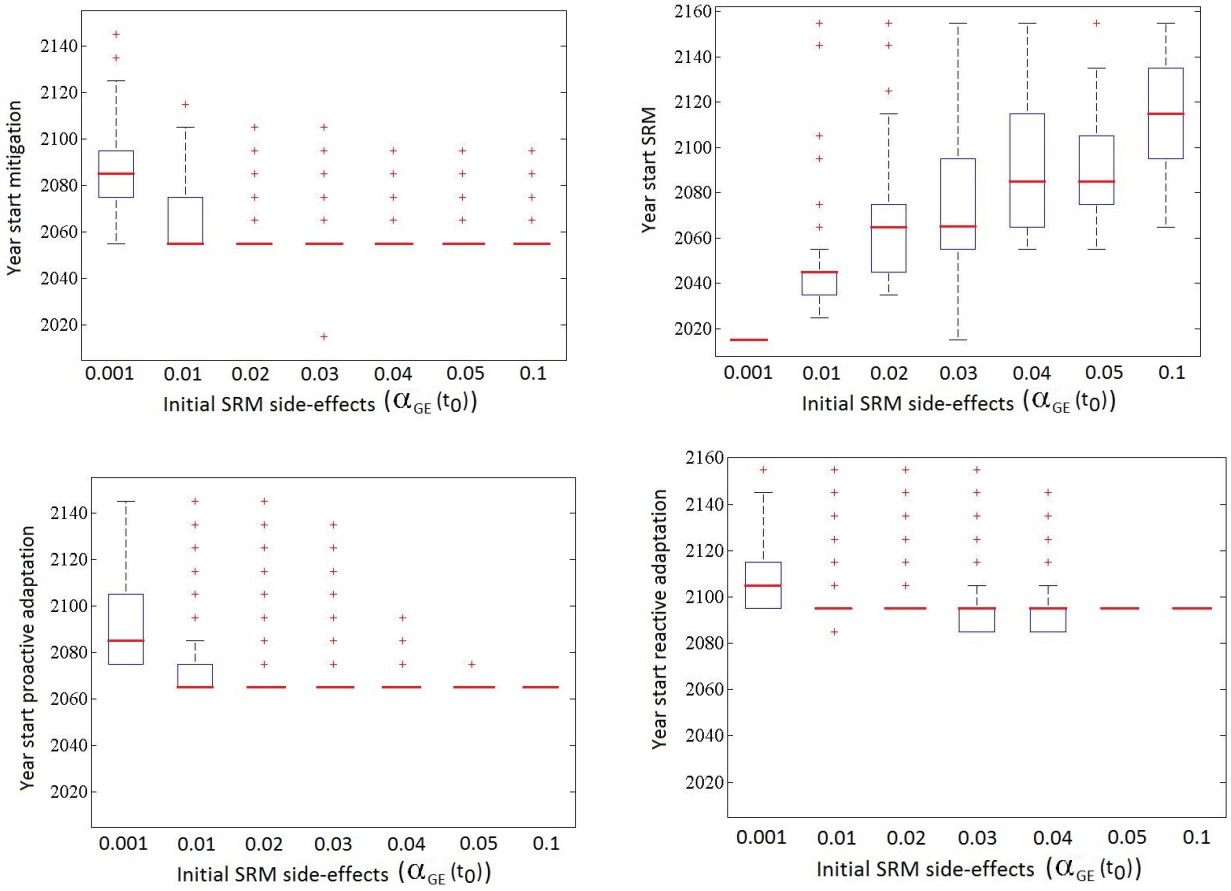

Fig. 2.B.1: Year when policy implementation starts across different $\alpha_{GE}(t_0)$.

2.B.2 Budget allocation between investments and spendings

In this section, we analyse how is the budget optimally divided between investments (in the carbon and low-carbon economies and proactive adaptation) and spendings (with reactive adaptation and SRM). We are interested in underlying not only the relative monetary requirements of different climate policies, but also how these vary with respect to initial SRM side-effects. For this purpose, we define in Eq. (2.B.1) an indicator of total discounted investments and spendings (IS):

$$IS = \sum_{n=0}^{14} e^{-rn\Delta t}\Delta t[I_1(t_0+n\Delta t) + I_2(t_0+n\Delta t) + I_3(t_0+n\Delta t) + S_3(t_0+n\Delta t) + S_4(t_0+n\Delta t)] \quad (2.B.1)$$

with $t_0 = 2005$, $n \in [0, 14]$, and $\Delta t = 10$ years. IS captures total investments and spendings over the 2005 - 2155 horizon. Fig. 2.B.2 displays the distribution of total investments/spendings for each policy, depending on the initial SRM side-effects ($\alpha_{GE}(t_0)$).

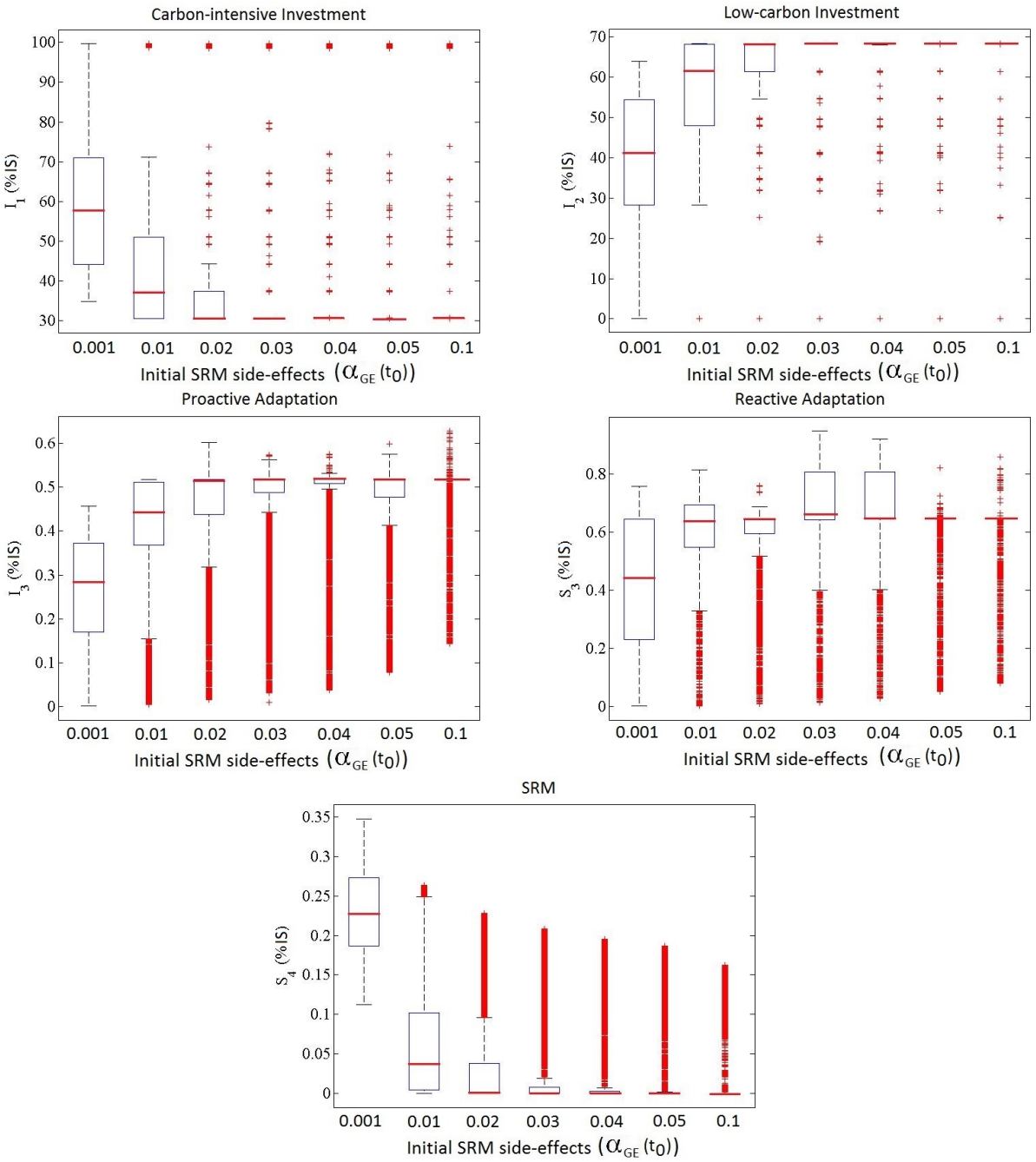

Fig. 2.B.2: Budget division across different $\alpha_{GE}(t_0)$.

Fig. 2.B.2 reveals that the investment/spendings budget is primarily distributed between the carbon and low-carbon technologies. When the initial SRM side-effects are low ($\alpha_{GE}(t_0) = 0.001$), investments in the carbon-economy predominate; as $\alpha_{GE}(t_0)$ increases, most investments are directed towards the low-carbon economy. The SRM strategy occupies the smallest share of total investments and spendings among the different policies, and this share decreases to a negligible level as side-effects increase.

2.B.3 Atmospheric GHG concentrations

Fig. 2.B.3 captures different aspects regarding the distribution of GHG concentrations attained for different levels of initial SRM side-effects. Panels a) and b) illustrate average and maximum GHG concentrations, respectively. Panel c) shows the percentage breakdown of scenarios that attain GHG concentration levels below and above 650 ppm. Panel d) illustrates how many decades (out of 15) are GHG concentrations kept above 550 ppm.

The percentage of scenarios that reach concentration levels in the range [550, 650] ppm strongly depends on the initial SRM side-effects: only 6% of the scenarios when $\alpha_{GE}(t_0) = 0.001$, and about 92% of scenarios when $\alpha_{GE}(t_0) = 0.1$ (Fig. 2.B.3c in Appendix). Moreover, low initial side-effects levels are associated also with longer periods during which high concentrations are maintained (Fig. 2.B.3d). Finally, the average concentration level (and its right skewness) is much higher for low α_{GE} levels when SRM is widely used and mitigation efforts are scarce (Fig. 2.B.3a, b).

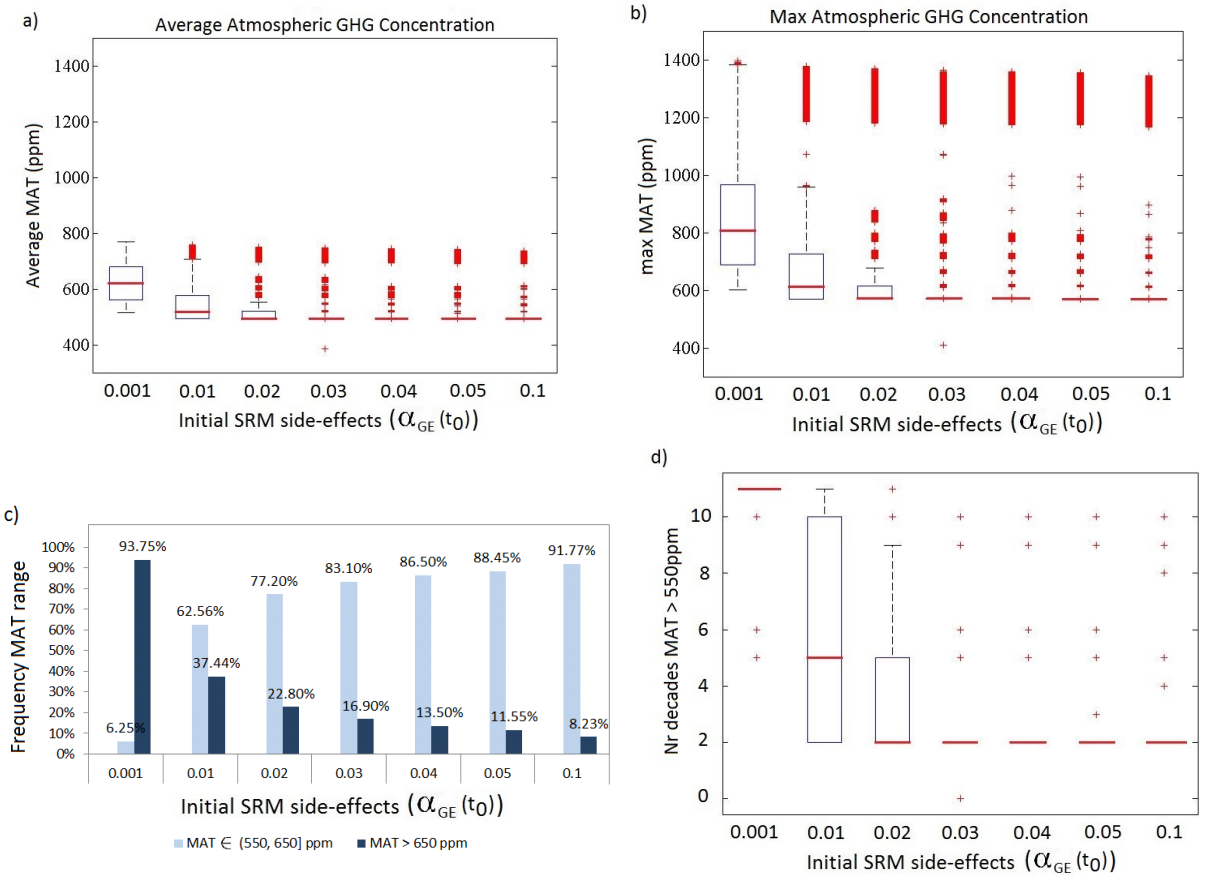

Fig. 2.B.3: GHG concentrations across different $\alpha_{GE}(t_0)$.

2.B.4 Sensitivity to the persistency of SRM side-effects

The use of SRM is subject not only to the initial level of side-effects, but also to the persistency of damages over time (parameter λ). Fig. 2.B.4 illustrates the distribution of years when different climate policies are initiated, depending on the persistency of SRM side-effects.

Fig. 2.B.4 shows that on average the start of the mitigation and adaptation strategies is robust to the persistency of the SRM side-effects. However, the start of the SRM implementation strongly depends on the persistency parameter: higher persistency postpones the start of sulphur injection.

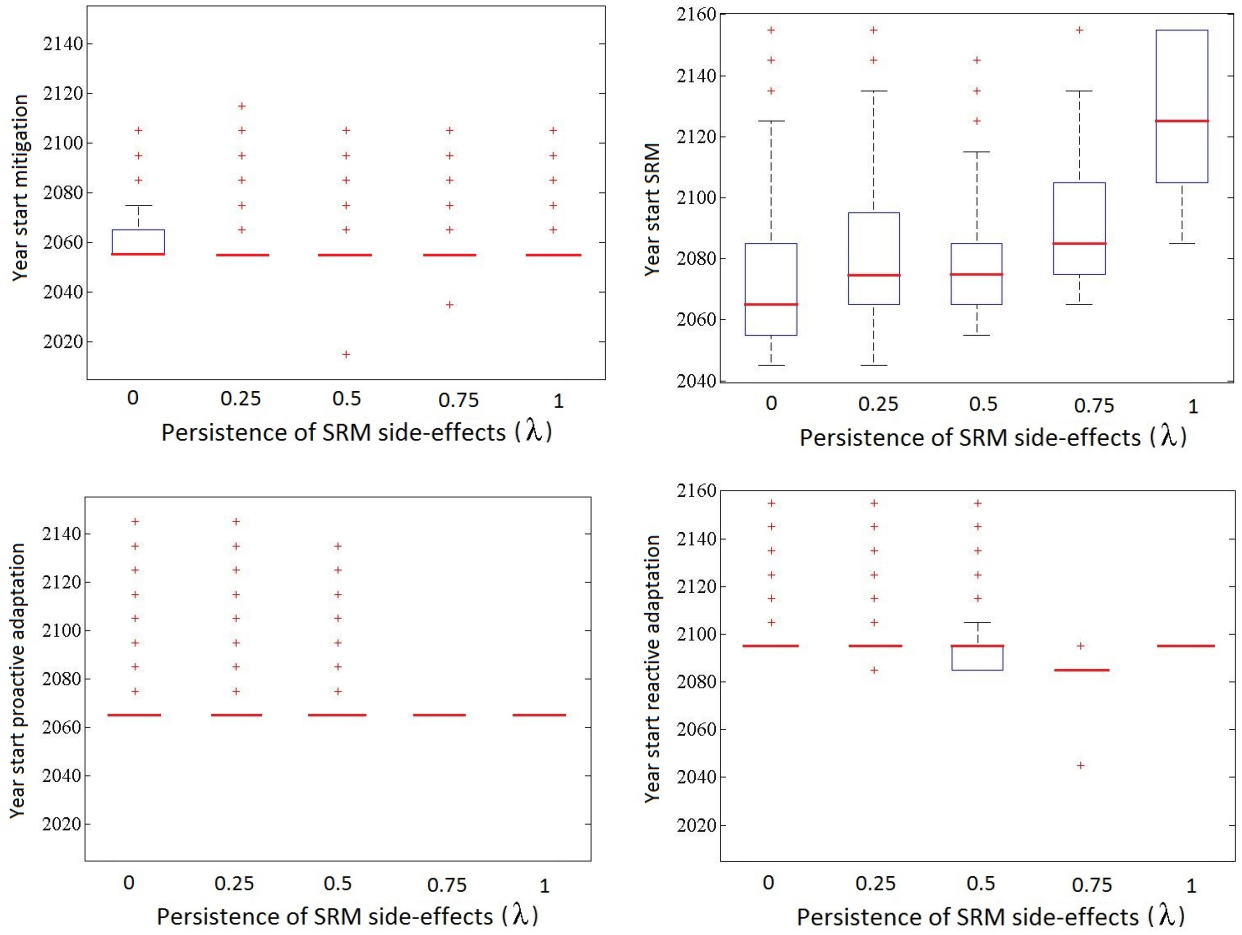

Fig. 2.B.4: Year when policy implementation starts across different λ (at $\alpha_{GE}(t_0) = 0.03$).

2.B.5 Failure to continue with SRM

Fig. 2.B.5 shows the evolution of capital, spendings, temperature deviation, and GHG concentrations in two scenarios. In the first one (SRM (2065 - 2155) in black), SRM is implemented and continued as long as it is optimal. In the second one, (SRM (stopped 2105) in blue) SRM is no longer available after 2105, and the decision maker need to adjust all the decisions after this period.

Fig. 2.B.5 reveals that after SRM is stopped, a quick transition from the carbon-intensive to the low-carbon economy takes place. Proactive and reactive adaptation strategies are quickly implemented to reduce damages from the temperature increase. Due to inertia in the climate system, the abrupt emission reduction (following the rapid transition to the low-carbon economy) translates only slowly into GHG concentration reduction. The deviation in atmospheric temperature increases very fast, reaching 3.5 °C by 2155.

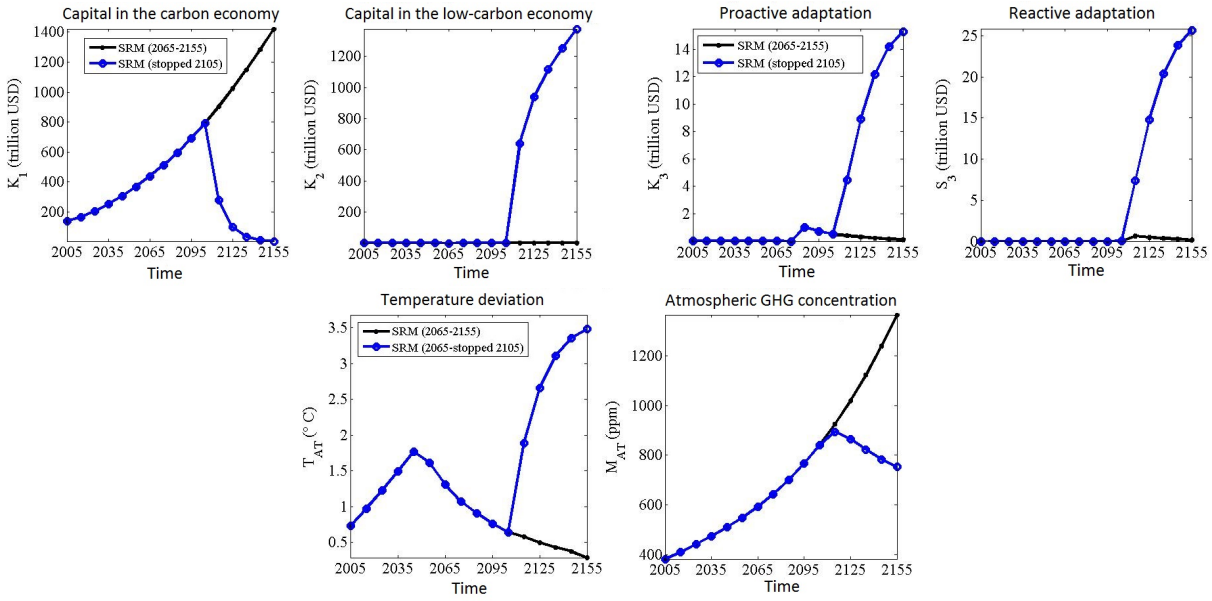

Fig. 2.B.5: Changes in policy, temperature, and GHG concentrations after failure to continue with SRM ($\alpha_{GE}(t_0) = 0.03$, $\alpha_{GE}(2155) = 0$, $\lambda = 0.5$).

2.B.6 Unexpected SRM side-effects

Fig. 2.B.6 compares the sum of output losses under known (presumed) and random (unexpected) SRM side-effects. Losses double on average when the side-effect path has a different outcome than the one assumed. The loss is higher in the case of larger initial SRM side-effects.

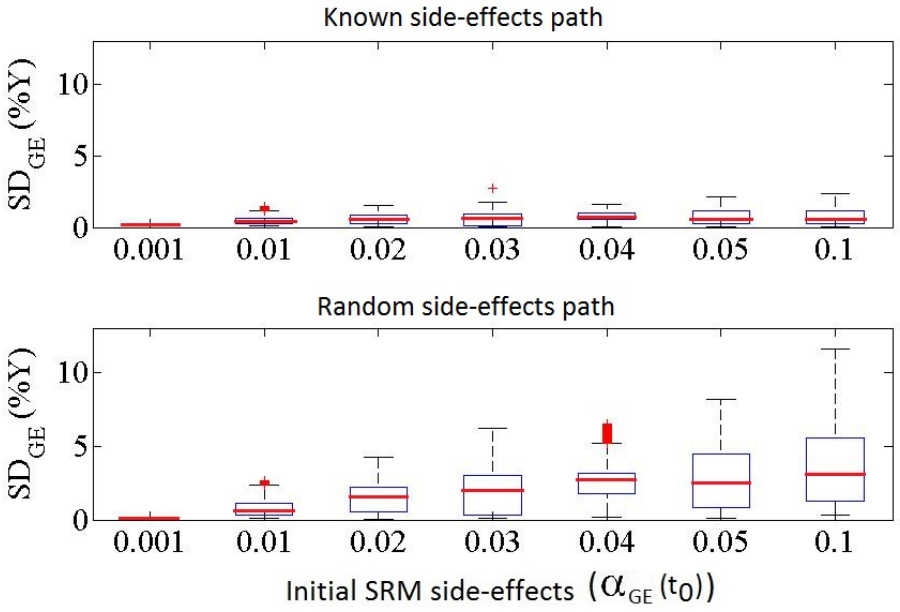

Fig. 2.B.6: Expected vs. unexpected SRM damages across different $\alpha_{GE}(t_0)$ ($\lambda = 0.5$).

Fig. 2.B.7 shows the evolution of capital, spendings, temperature deviation, and GHG concentrations in the three scenarios described in Table 2.B.1. Fig. 2.B.7 reveals that as the decision maker realizes that SRM side-effects are much larger than initially estimated, all SRM activities are stopped, and a quick transition from the carbon-intensive to the low-carbon economy takes place. Proactive and reactive adaptation strategies are immediately implemented to reduce

the damages caused by the large and sudden increase in temperature. GHG concentrations start a slow decline with the transition to the low-carbon economy.

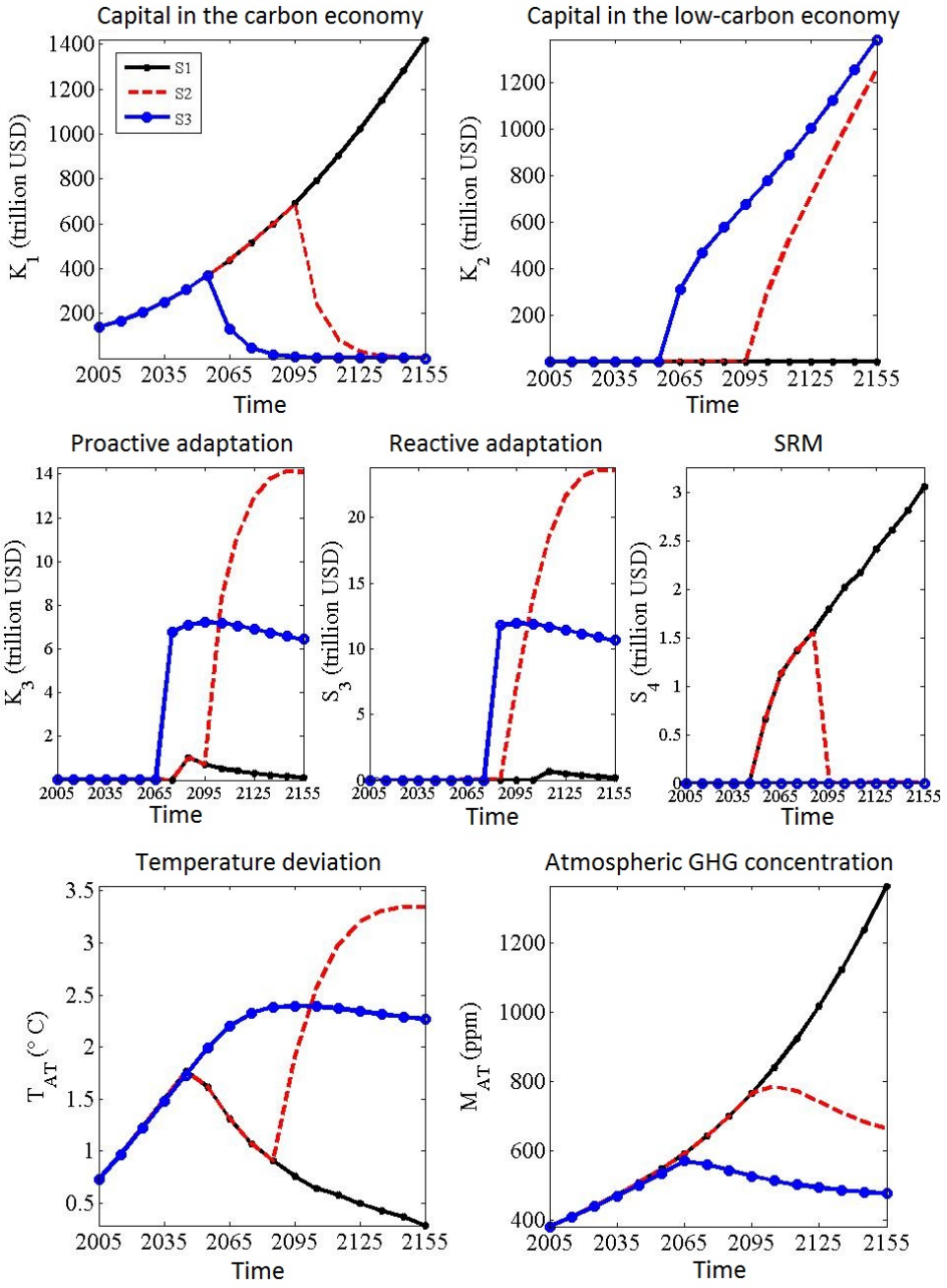

Fig. 2.B.7: Changes in policy, temperature, and GHG concentration after unexpected SRM side-effects ($\alpha_{GE}(t_0) = 0.03$, $\lambda = 0.5$).

Table 2.B.1: Analysed expected and unexpected SRM side-effects scenarios.

Scenario	Explanation	Assumed SRM side-effects	Realised SRM side-effects
S1	Known best-case scenario	$\alpha_{GE}(t_0) = 0.03$ $\alpha_{GE}(2155) = 0.001$	$\alpha_{GE}(t_0) = 0.03$ $\alpha_{GE}(2155) = 0.001$
S2	Unexpected scenario	$\alpha_{GE}(t_0) = 0.03$ $\alpha_{GE}(2155) = 0.001$	$\alpha_{GE}(t_0) = 0.03$ $\alpha_{GE}(2155) = 1$
S3	Known worst-case scenario	$\alpha_{GE}(t_0) = 0.03$ $\alpha_{GE}(2155) = 1$	$\alpha_{GE}(t_0) = 0.03$ $\alpha_{GE}(2155) = 1$

Chapter 3

Baseline choice and performance implications for REDD

Joint work with Jonathan Gheyssens.

Abstract

Reducing Emissions from Deforestation and forest Degradation (REDD) projects are being designed and implemented across tropical countries, intending to curb the contribution of deforestation to global greenhouse gas emissions. An important aspect of REDD implementation is choosing the deforestation *baseline* against which reductions are measured. We solve a dynamic model of land conversion from forest to agriculture in the presence of a voluntary REDD scheme, and assess the impact of four baseline types on REDD performance. We show that none of the analysed baselines dominates the others in all key performance aspects, and that the final baseline choice will need to maximise the trade-off between the different goals of REDD. We argue that the current proposal of rewarding reductions in emissions below the historical average could be improved by using a forward-looking baseline; this is shown to better account for the opportunity costs faced by landowners and to result in higher emission reductions. Moreover, we advocate the switch from a single-threshold baseline to a corridor methodology, which would provide continued incentives for reduced deforestation, even during periods of high opportunity costs. We finally show how the selection of certain baseline attributes, such as corridor bandwidth and symmetry, can enhance overall performance.

Keywords: Deforestation; REDD; Baselines; Effectiveness and Efficiency.

3.1 Introduction

Emissions from deforestation and forest degradation rank as the second largest source of carbon dioxide in the atmosphere after fossil fuel combustion, contributing about 12% of global anthropogenic emissions (van der Werf et al., 2009). Programs targeting the Reduction of Emissions from Deforestation and forest Degradation (REDD and REDD+)[1] have emerged as potential instruments for stabilising atmospheric CO_2 concentrations and mitigating climate change.

REDD programs target forest preservation in tropical areas, where deforestation is the largest contributor to total greenhouse gas (GHG) emissions (van der Werf et al., 2009). Here, the major drivers of deforestation have often been identified as timbering, land conversion to agriculture, cattle ranching, and the establishment of new settlements (Pfaff et al., 2013). Restricting deforestation would limit the development of such land use activities and alter the revenue flow of landowners. To compensate for the foregone income from deforestation, REDD schemes offer financial rewards for forest conservation.

REDD programs aim to achieve *additionality*, i.e. payments are intended to reward reductions in emissions from deforestation below business-as-usual levels. However, these counterfactual deforestation rates, which would occur in the absence of the policy, are not observable and, therefore, highly challenging to assess. Thus, REDD payments are linked to reductions below estimations of the business-as-usual, so-called *baselines* or *reference levels*.

The reward system of REDD can be financed through the creation of special funds or be designed as a market mechanism (Palmer, 2010; Corbera and Schroeder, 2011). In the second case, reducing deforestation below a reference level generates credits eligible for sale on various carbon markets. International emitters[2] that are above their compliance level and short of CO_2 permits might find reducing emissions internally to be expensive (Diaz et al., 2011) and could benefit from the comparative affordability of REDD permits (Kindermann et al., 2008; Stern, 2008). Despite this economic advantage, REDD projects remain complex to implement and prone to failure. Various aspects appear problematic: the measurement of reductions in emissions below business-as-usual levels; raising sufficient funds for implementation or establishing a link with (immature) carbon markets; the risk that forest loss will be postponed in time (lack of permanence) or transferred to unregulated areas (leakage); the existence of clear property rights that would rule out false permit claims from encroachers (Angelsen, 2008a).

The success of REDD is critically sensitive to the incentive structure promoted by the schemes (Griscom et al., 2009; Cattaneo et al., 2010; Busch et al., 2012). A central aspect is the establishment of the baseline against which reductions in deforestation are measured and financial rewards are granted. However, setting the baseline is not a straightforward task. First of all, to encourage participation and ensure significant reductions in GHG emissions, the baseline design would need to ensure that REDD rewards cover the various opportunity costs of deforestation (Irawan et al., 2013). In the same time, the selected baseline should achieve emission reductions in a cost-efficient manner, avoiding that payments greatly exceed opportunity costs and result in windfall profits for landowners (Busch et al., 2012), instead of being used for reducing deforestation elsewhere. As well, flooding the carbon markets with REDD credits in large supply would drive the emission allowance price down and possibly reduce the effectiveness of the already weak markets (Doupé, 2014, WP).

[1] While REDD gives priority to forest preservation, REDD+ targets additionally the sustainable management of forests and the enhancement of carbon stocks.

[2] These emitters could be found among the European polluting companies who are regulated by the EU ETS and need to comply with emission reduction targets.

REDD programs allow candidate countries to prepare their own proposals of baseline computation, and submit them for approval by a team of experts, together with supporting evidence (UNFCCC, 2011, Decision 12/CP.117). Several organisations have emerged with the goal of assisting countries in participating successfully in REDD programs, by offering technical, legal, and financial support. Among them, notable actors are the Forest Carbon Partnership Facility, the Amazon Fund, the UN-REDD program, Norway's International Climate and Forest Initiative (NICFI), and the German REDD Early Movers Program. So far, the existing REDD initiatives supported by these organisations have endorsed the decision of the UNFCCC to compute reference levels based on past deforestation rates, adjusted to account for country circumstances[3] (UNFCCC, 2009, Decision 4/CP.15). The decision to opt for historical reference levels is motivated by the desire to ensure transparency and credibility (The German REDD Early Movers Program, 2014). In order to account for national circumstances, historical averages can be adjusted upwards for countries with historically low deforestation rates and high remaining forest areas; downward adjustments are prescribed to countries with clear decreasing trends in deforestation (FCPF Carbon Fund, 2013).

Despite its recognised advantages, the historical baseline lacks the ability to reflect future drivers of deforestation. Moreover, provided as an average, it neglects the variability observed in deforestation rates, coming from fluctuating economic conditions. The historical baseline might, therefore, fail to account properly for the true opportunity costs that landowners face. Trying to address these issues, several baseline methodologies have been proposed; for an overview see Huettner et al. (2009) and Griscom et al. (2009). The contribution of our paper is to provide further insights into how to choose the most robust baseline methodology.

Our paper joins the stream of literature dedicated to the optimal contract design of REDD schemes (Huettner et al., 2009; Busch et al., 2009, 2011; Sathaye et al., 2011). We compare the impacts of four different baseline methodologies on REDD success. We focus on two of the most popular baseline categories: a retrospective baseline reflecting the historical average deforestation, and a model-implied baseline that proxies the business-as-usual deforestation path. We also analyse the so-called *fixed corridor* approach, which replaces the unique threshold level with an upper and a lower bound. In addition, we propose a new baseline type, the variable corridor approach, which aims to gather the strong points of the model-implied and the corridor baselines.

Our analysis relies on several steps. First, we show how to model land use decisions in the presence of REDD in a dynamic setting. In a second step, we rank baselines according to different performance indicators: (i) a measure of forest preservation (effectiveness), (ii) an indicator of the marginal cost of this preservation per hectare (efficiency), and (iii) a measure of changes in the total income of the landowner (change in welfare). The economic analysis is further put into perspective through a qualitative evaluation, accounting for environmental, technical, and social concerns with REDD. Finally, the paper explores different possibilities to improve the performance of each baseline category.

Previous research on REDD design overlooked the inter-temporality dimension in forest decisions (Huettner et al., 2009; Busch et al., 2009, 2011). Huettner et al. (2009) ran a survey to qualitatively compare three types of retrospective baselines, based on the historical deforestation rate, with a forward-looking baseline. We extend the types of baselines analysed beyond those considered in Huettner et al. (2009) and focus on the economic incentives generated by each baseline. Busch et al. (2009) approach the ranking of different baselines via a one-period partial equilibrium model at the country level. They show that an effective national baseline

[3]We thank an anonymous referee for the input.

simultaneously provides incentives to reduce deforestation in areas of high rates and ensures the continuation with low deforestation practices in areas of low previous forest loss. Busch et al. (2011) extend this approach by introducing different levels of annual REDD financing, either through funds or access to a dedicated market. They highlight the importance of designing baselines that minimise leakage to unregulated areas and are generous enough to guarantee the participation of both countries with high or low deforestation rates. Cattaneo et al. (2010) use a static partial equilibrium model to compare five different baseline designs from an equity perspective. They show that the crediting schemes considered obtain similar reductions in deforestation, but differ greatly in terms of cost-efficiency and two measures of equity.

The highly dynamic nature of land use practices has been studied in numerous papers and benefits from a large variety of models; for a review see Verburg et al. (2004). However, only a few papers deal explicitly with dynamic land use changes in the presence of REDD, and none of them tests for different baseline methodologies (Ollivier, 2012; Lu and Liu, 2013; Vitel et al., 2013; Mosnier et al., 2014). We attempt to fill this gap by analysing our selected baselines with a dynamic land use model. The dynamic model helps us illustrate the optimal deforestation decisions at several points in time, and show how land owners choose to take part in REDD depending on the time-varying opportunity costs for deforestation. Anticipating our results, with the help of the dynamic approach we are able to demonstrate that some baseline methodologies offer continued incentives to keep deforestation below business-as-usual levels, while others achieve only temporary effectiveness. This finding is key for understanding how we could potentially solve non-permanence issues with REDD and can only be grasped in a dynamic setting.

Another important decision concerning REDD implementation is the choice of the administrative level at which emission reductions are calculated and payments are made. While the accounting of emission reductions and the management of REDD payments is most likely to take place at the national level, land use decisions are usually taken at the subnational (regional or household) level. This reinforces the need to understand the incentives received by the local landowners (Angelsen, 2010; Busch et al., 2012). Our model describes the decisions of a single landowner who optimises over the rate of deforestation as he or she expands agriculture activities. The single-agent approach is in line with the literature on optimal forest extraction (Angelsen, 2007) and with a new literature trend arguing that REDD will face the same issues as traditional integrated conservation and development projects (ICDPs), since it will have to account for incentives at the community and individual levels (Blom et al., 2010). It is not intended to suggest that the complexity of implementing REDD projects can be summarised into a single-player model; nonetheless, we believe that our approach is relevant for highlighting the behavioral changes at the micro level, which can then be used to inform national or jurisdictional policy decisions.

The choice of the administrative level for REDD is expected to impact the effectiveness in reducing deforestation. Implementing REDD at the site-level, and then aggregating results at a larger (national) scale, may give way to leakage of deforestation to other areas (Busch et al., 2012), and raises questions regarding the organisation of carbon payments at the local level[4]. However, the estimation of reference levels is more likely to reflect the business-as-usual deforestation path if set at the household level, since jurisdictions at lower scales may have better information regarding the specific drivers of deforestation in the area (Busch et al., 2012). Potential policies for avoiding leakage include: (i) the monitoring of deforestation rates at the national level; and (ii) the setting of penalties for deforestation rates that exceed the estimated business-as-usual level, coming from beneficiaries of REDD payments elsewhere. In

[4]We are thankful to an anonymous reviewer for raising this important point.

this paper, we adopt the view that REDD should focus on providing incentives for reduced deforestation at the local level, while ensuring national monitoring.

Our analysis reaches several conclusions that we hold relevant for the design of forest carbon policies. First, solving for the optimal deforestation rate under a REDD regime, we show that baseline choice impacts REDD performance at multiple economic, social, and environmental levels. None of the considered baselines can fulfil all REDD criteria simultaneously, and baseline choice needs to maximise the trade-off between the different goals. We argue that the widespread current practice of rewarding emissions below the historical deforestation average could be improved by implementing a forward-looking baseline that would better account for the opportunity costs faced by landowners and would result in higher emission reductions. Moreover, we advocate the switch from a single-threshold baseline approach to a corridor methodology; this reduces losses from estimation errors and provides continued incentives for reduced deforestation, even during periods of high opportunity costs.

The rest of the paper is organised as follows. Section 3.2 introduces our methodology and the main assumptions of the dynamic model. In Section 3.3 a numerical application is performed and the robustness of our results is tested. Section 3.4 concludes on the policy implications of our results and the link with broader issues of REDD implementation.

3.2 Methodology

3.2.1 Model setting

In our model, the owner of a large area of forested land decides if, when and to what extent to exploit the forest for agricultural activities. To limit his or her deforestation, the owner is offered the possibility to take part in a REDD program that grants carbon permits each time the deforestation rate is below a pre-specified threshold. We model the voluntary participation in REDD along the approach of Busch et al. (2009, 2011), where the owner can "opt in" as long as he considers this to his or her advantage.[5] In our model, reforestation options are not accounted for; this assumes that costs for switching back from cropland to forest (together with the forgone discounted cash-flows from agriculture) are large enough to render the reforestation option unattractive.

The landowner's revenues are a trade-off between the net income from land exploitation and REDD rewards. The more the owner deforests, the higher the incomes from selling timber and subsequently using land for agricultural activities, and the lower the number of received REDD permits. Alternatively, lower deforestation (below the defined baseline level) results in smaller incomes from agriculture and timbering, but higher REDD revenues. We choose an approach similar to Busch et al. (2009), where the owner's revenues from land exploitation are modelled as a unique composite commodity, representing both the harvesting value of timber and a perpetual discounted flow of agricultural activities on the land.[6]

The owner maximises the sum of total discounted profits, taking into account the parameters that define the decision environment: the state of the forest, the dynamics of composite commodity and REDD permit prices, and the specified deforestation baseline. In our model, the

[5] In the paper of Busch et al. (2009, 2011) the owner will "opt in" if the REDD revenues are higher than the agricultural rental price and "opt out" otherwise.

[6] Reducing the complexity of the harvesting function, which is not central for comparing the reference levels, allows us to focus on the dynamic choice between maintaining the forest cover and harvesting.

prices of the composite commodity ($P^{cc}(t)$) and of the REDD permit ($P^R(t)$) are exogenous and follow deterministic dynamics:[7]

$$dP^{cc}(t) = \delta P^{cc}(t)dt \tag{3.1}$$
$$dP^R(t) = \gamma P^R(t)dt \tag{3.2}$$

where δ and γ represent the respective growth rates of the two price processes. Being a composite price, $P^{cc}(t)$ is a simplification of the actual commodity flow generated from harvesting one hectare of forest and using the area for perpetual agricultural activities, which could be modelled as follows:

$$P^{cc}(t) = P_h(t) + \int_t^{\infty} A(s)e^{-\psi s}ds \tag{3.3}$$

$P_h(t)$ represents the one-time timber harvest selling price, while $A(t)$ are the annual monetary flows from agricultural activities after land conversion. Land exploitation involves various operational costs that we model with the help of a quadratic function:

$$C(t) = a_1 d(t) + a_2 d(t)^2 \tag{3.4}$$

where $d(t)$ is the amount of forest converted to agriculture at time t. We assume the parameters of the cost function (a_1, a_2) to be constant. This stylised representation is in line with the classical approach of von Thünen (1826): when land is abundant and homogeneous, the agriculture expansion frontier depends on the cost of accessing new forest patches, which are further away from the initial location and thus costlier to exploit (Angelsen, 1999).

The offsetting scheme proposed by REDD imposes no liability: the owner is rewarded if the deforestation is below a certain reference level, but does not have to pay penalties in case this limit is exceeded (Griscom et al., 2009; Huettner et al., 2009; Joanneum Research Institute, 2006). The owner's revenues from REDD ($RR(t)$) can be described by a step function:

$$RR(t) = P^R(t)(dB - d(t))^+ \tag{3.5}$$

where $P^R(t)$ is the REDD permit price at time t, dB the baseline level, and $d(t)$ the actual deforestation at t. REDD cash flows are zero for deforestation rates above the baseline, i.e. $(dB - d(t))^+ = 0$ if $d(t) \geq dB$. REDD programs define reference levels (dB) in terms of tonnes of CO_2 equivalent per year. To simplify the presentation of results, we convert reference levels into hectares of avoided deforestation, as described in Section 3.2.3. Unlike in the traditional dynamic setting, we enforce a very loose constraint on the total owned patch of forest at $t(0)$ $\left(\bar{F}(0)\right)$. However, we impose a time window $[0, T]$ during which the optimisation occurs. While $\bar{F}(0)$ is not infinite, we consider its value so large that forest depletion is not likely;[8] we allow for a positive terminal stock at period T. However, future REDD schemes may have an explicit time frame[9] (Parker et al., 2008), which compels us to consider the time constraint as the most binding for the landowner.

[7]Using deterministic processes simplifies the solution to the model, but leaves outside of the scope of our analysis the role and influence of risk on the optimal land allocation decision. Under the hypothesis of a risk neutral landowner, the presence of risk would have no specific effects. However, in presence of risk aversion, the decision between preservation and deforestation will be significantly impacted by the relative volatility of the two prices and would favour the strategy giving the smallest cash flow variability.

[8]We consider this setting to be in line with the reality of many land owners' decision processes in tropical countries. In Latin America, ownership rights tend to be concentrated in the hands of a few proprietors (Brockett, 1990; Borras Jr et al., 2012).

[9]This time frame is expected to be aligned with the phases of the EU ETS or the successor of the Kyoto protocol.

We first solve the model for the business-as-usual case (the benchmark when no REDD project is in place), and then for four REDD crediting baselines: historical, model-implied, and two types of corridor. We proceed now with the presentation of each methodology, and then assess the incentives for avoiding deforestation observed in each case.

3.2.2 Baseline alternatives

3.2.2.1 Business-as-usual scenario (without REDD)

The *business-as-usual* (BaU) scenario illustrates the deforestation trend in the absence of REDD or other forest conservation projects. Here, the land brings only timbering and agriculture benefits, as reflected in the net cash flow ($\pi(\cdot)$) at time t:

$$\pi(d(t)) = P^{cc}(t)d(t) - \left(a_1 d(t) + a_2 d(t)^2\right) \tag{3.6}$$

where $P^{cc}(t)$ is the composite commodity price, $d(t)$ the deforestation rate, and a_1 and a_2 are the parameters of the cost function. The optimal control problem can be described as a maximisation over the deforestation rate of the total discounted net revenues resulting from land exploitation:

$$\max_{(d(t))_{t\in[0,T]}} \left\{ \int_0^T e^{-rt}\pi(d(t))dt \right\} \tag{3.7}$$

where r is the discount rate and T marks the end of the decision horizon. The variation in the stock of forested land is given by the following dynamics:

$$\dot{F} = -d(t) \tag{3.8}$$

where F is the stock of forest and $\dot{F}$ represents its variation between consecutive periods. We follow the solution approach of Chiang (1992) for determining the optimal deforestation path; see Appendix 1. The rate of deforestation at each moment of time is recursively linked to the initial deforestation level:

$$d(t) = d(0)e^{rt} + \frac{P^{cc}(0)(e^{\delta t} - e^{rt}) - a_1(1 - e^{rt})}{2a_2} \tag{3.9}$$

Reflecting the optimal deforestation path in the business-as-usual scenario, we denote $d(t) = d_{BaU}(t)$; it will be used below for computing the REDD rewards in the model-implied and the variable corridor scenarios.

3.2.2.2 Historical baseline

Most proposals include the historical average deforestation rate in the computation of the crediting baseline.[10] This comes as a recognition of the fact that average past deforestation, although an imperfect measure, is one of the best predictors at hand for short-to-medium term deforestation (Angelsen et al., 2009). We thus start the analysis of the deforestation behaviour under REDD with a simple historical baseline, where the REDD threshold is flat and equal to the average past deforestation rate. This baseline type is a simplification of what has been proposed by Brazil (Parker et al., 2008).

[10] Out of the 6 baseline methodologies studied by Griscom et al. (2009), 5 rely partially or totally on historical reference levels.

The merit of the historical baseline consists of its fair simplicity of computation and implementation, as well as its appeal to land owners who need to get used to new operation rules. The baseline has received support also for its ability to reflect local deforestation trends and avoid the one-measure-for-all caveats.

The historical reference level faces, however, a number of limitations, starting with the fact that many countries do not hold accurate data records of past deforestation (Guariguata et al., 2008). Second, an imperfect predictor of future deforestation has high chances of undermining the additionality principle and of distorting country participation, especially if one considers the specific forest transition stage[11] of each country (Angelsen, 2007). Forest-rich states with low past deforestation, but which expect increasing trends, might decide to stay out of REDD if the programs are based on historical baselines. On the other hand, nations with large past deforestation rates and scarce remaining forests would gladly join, since rewards based on historical averages would be generous relative to the required additional efforts (Angelsen, 2008a).

In the presence of REDD with a historical baseline, cash flows are generated by two counterbalancing activities, i.e. forest exploitation and REDD:

$$\pi(d(t)) = P^{cc}(t)d(t) - \left(a_1 d(t) + a_2 d(t)^2\right) + P^R(t)\left(dB - d(t)\right)^+ \tag{3.10}$$

As captured in Eq. (3.10), the landowner's profits are determined by the sales of the composite commodity, less the operational costs; additionally, REDD revenues are eligible for deforestation rates below the historical threshold (dB).

3.2.2.3 Model-implied baseline

An alternative to the retrospective historical baseline is the prospective method[12] that incorporates projections of future deforestation trends. The *model-implied* baseline relies on a time-varying level reflecting predicted deforestation paths under the *business-as-usual* scenario. Here, the landowner is rewarded for deforesting less than in the absence of the REDD program. If the forecasting is accurate, it enforces additionality, since only actual efforts would be rewarded. However, the model-implied baseline is not exempt from criticism that stems primarily from the baseline's vulnerability to forecasting errors and the reliance on model assumptions.

We incorporate the specificity of the model-implied baseline into the revenue function, accounting for the fact that the reference level ($dB(t)$) can fluctuate across time according to the projections of the model used:

$$\pi(d(t)) = P^{cc}(t)d(t) - \left(a_1 d(t) + a_2 d(t)^2\right) + P^R(t)\left(dB(t) - d(t)\right)^+ \tag{3.11}$$

Compared to the methodology of the historical baseline (Eq. (3.10)), the key difference in the model-implied approach is the modification of the baseline level from a static threshold (dB) to a dynamic one ($dB(t)$). In our model, $dB(t)$ is chosen to match the estimated deforestation

[11] According to Angelsen (2007), "*The FT describes a sequence where a forested region goes through four stages: (1) initially high forest cover and low deforestation, (2) accelerating and high deforestation, (3) slow-down of deforestation and forest cover stabilisation, and (4) a period of reforestation.*"

[12] According to Huettner et al. (2009), prospective (forward-looking) methods attempt to model land use change taking into account the various market drivers. The forecasting can be done by using either analytical, regression or simulation models.

pattern of the BaU scenario, such that:

$$dB(t) = d_{BaU}(t) \quad \forall t \in [0, T] \tag{3.12}$$

where $d_{BaU}(t)$ is the optimal deforestation in the business-as-usual scenario.

3.2.2.4 Fixed corridor

The corridor approach has been first proposed by Schlamadinger et al. (2005), and then reformulated jointly in 2006 by the Joanneum Research Institute, the Union of Concerned Scientists, the Woods Hole Research Center, and the Instituto de Pesquisa Ambiental da Amazonia (Griscom et al., 2009). This methodology modifies the historical baseline approach, by replacing the fixed threshold with a corridor whose bounds are computed as levels below and above the average past deforestation rate.

In this paper we analyse the so-called *corridor 2* methodology,[13] whereby the possible deforestation range is divided into three regions: (1) deforestation levels above the upper boundary do not receive any REDD payments; (2) rates below the lower boundary are entirely eligible for REDD permits, as they would under a fixed-baseline scheme; (3) deforestation levels within the corridor are discounted proportionally to the distance from the upper boundary, such that rewards are larger when deforestation approaches the lower bound, up to full payments if this lower bound is reached, and conversely, rewards are smaller for deforestation rates close to the upper bound, down to no payment if the upper bound is reached.

The corridor approach attempts to address an important feature of deforestation, namely its frequent fluctuations over time. Movements are usually caused by shifts in key market parameters, such as commodity prices, interest rates, or climate impacts (Joanneum Research Institute (2006)). The corridor reward system admits that avoiding deforestation in boom years implies higher opportunity costs, and is, therefore, more difficult to sustain than conservation efforts in years of medium to low timber and agriculture prices. With the corridor system, the landowner is encouraged to keep deforestation rates close to the average historical level, and is rewarded (although modestly) even if slightly above it. The corridor could also be useful when measurement errors hinder the estimation of the historical baseline. The corridor creates an "error" band around the threshold, advantageous in absence of incomplete information about past deforestation rates. In the words of Joanneum Research Institute (2006), the "corridor approach reduces the risk of missing a single-level target".

With the corridor approach for REDD, the shape of the profit function reflects the design of the reward program:

$$\pi(d(t)) = P^{cc}(t)d(t) - (a_1 d(t) + a_2 d(t)^2) + P^R(t)\omega \left(dB^U - d(t)\right)^+ \tag{3.13}$$

where $dB^L = (1-x)dB$ and $dB^U = (1+x)dB$ represent the lower and upper bounds of the corridor, respectively, dB is the historical deforestation rate, and x the corridor width. $\omega \in [0, 1]$ is the weight (discount factor) imposed by the corridor. In Eq. (3.13) the third term represents the income generated by the REDD project. The weighting system works as follows:

$$\omega = 1 - \frac{(d(t) - dB^L)^+}{dB^U - dB^L} = \begin{cases} 1 - \frac{d(t) - dB^L}{dB^U - dB^L} & \text{, if d(t)} > dB^L \\ 1 & \text{, if d(t)} \leq dB^L \end{cases}$$

[13] The *Corridor 1* method proposes that deforestation rates within the corridor accrue credits that would only be eligible for sale once emissions go below the lower boundary of the corridor (Joanneum Research Institute, 2006).

If the deforestation rate lies within the corridor ($d(t) \in (dB^L, dB^U)$), a linear weighting procedure is activated: on one hand, fewer permits will be received than the difference between the deforestation rate and the upper boundary ($\omega < 1$). On the other hand, deforestation rates below the lower boundary are rewarded full permits ($\omega = 1$). The last term in the REDD income, $(dB^U - d(t))^+$, ensures that rewards are received only for deforestation rates below the upper bound of the corridor.

3.2.2.5 Variable corridor

Similar to the difference between the static historical baseline and its dynamic model-implied counterpart, we suggest to modify the fixed corridor baseline by giving it a dynamic feature. The *variable* corridor replaces the constant lower and upper corridor bounds with time-varying levels, established below and above the deforestation rate of the dynamic business-as-usual scenario. To the best of our knowledge, this is the first time this baseline approach is proposed.

The variable corridor aims at bringing together the strong points of both the model-implied and the fixed corridor baselines. First, linking corridor bounds to the business-as-usual deforestation trend is expected to offer not only a dynamic but also a forward-looking perspective on deforestation paths, more likely to ensure additionality. Second, the corridor reward system should be able to better deal with estimation errors of the business-as-usual deforestation, and account for periodic fluctuations in deforestation levels, similarly to the fixed corridor. The revenue function follows the methodology of the fixed corridor, but introduces dynamic corridor bounds:

$$\pi(d(t)) = P^{cc}(t)d(t) - (a_1 d(t) + a_2 d(t)^2) + P^R(t)\omega(t)\left(dB^U(t) - d(t)\right)^+ \tag{3.14}$$

where the weighting factor is time-varying due to the dynamic corridor bounds, with $\omega(t) = 1 - \frac{(d(t)-dB^L(t))^+}{dB^U(t)-dB^L(t)}$, $dB^L(t) = (1-x)dB(t)$, $dB^U(t) = (1+x)dB(t)$, $dB(t) = d_{BaU}(t)$, and x the corridor width.

Summing up, in this paper we analyse four different REDD scenarios, namely two static and two dynamic, allowing for either a single-threshold or a corridor approach. While the static baselines are based on historical estimations of the deforestation rate, and are therefore retrospective, the dynamic baseline types are based on estimations of future deforestation trends, and are prospective. We denote the single-threshold approaches as H the historical and MI the model-implied. The fixed and variable corridors are labeled Cf and Cv hereafter. To summarise, the REDD revenues ($RR(t)$) offered to the landowner for each baseline methodology are the following:

Table 3.1: REDD revenues under different baseline methodologies.

	Single-threshold	Corridor
Static	$RR^H(t) = P^R(t)\,(dB - d(t))^+$	$RR^{Cf}(t) = P^R(t)\omega\left(dB^U - d(t)\right)^+$
Dynamic	$RR^{MI}(t) = P^R(t)\,(dB(t) - d(t))^+$	$RR^{Cv}(t) = P^R(t)\omega(t)\left(dB^U(t) - d(t)\right)^+$

H stands for historical baseline, MI for model-implied, Cf for fixed corridor, and Cv for variable corridor.

We solve for the optimal deforestation path under the business-as-usual scenario and the four different baselines.[14] We tackle the non-linearity in the profit function with the help of a numerical approach; see Appendix 2.

3.2.3 Model calibration

Our model is general enough to accommodate the characteristics of many regions where REDD could be implemented. For the numerical application, we take here the view of a forest owner from Peru. As the sensitivity analysis shows, the results are robust and generalizable to different regions of the world; see Appendix 3.D.

Peru is an important REDD candidate in terms of forest resources[15] and market volume.[16] The annual deforestation rate for 1990 - 2005 is estimated at 0.14%, remaining at low levels relative to its neighbouring countries (FAO, 2005). However, more recent estimates show that during 2000 - 2010 deforestation rates experienced an increasing trend,[17] which is predicted to persist in the near future mainly due to cropland expansion in the Andes (Wassenaar et al., 2007). Several local projects developing REDD credits are currently in implementation phase in Peru[18] (Hajek et al., 2011; Entenmann and Schmitt, 2013).

The list of parameters used for model fitting and their sources are presented in Table 3.2. In our model, the average deforestation rate obtained in the business-as-usual scenario is about 200 ha/year. We allow the historical baseline level (dB) to vary in a large interval (between 1 ha and 500 ha per annum), in order to cover a broad spectrum of scenarios. While REDD credits are granted in terms of tons of CO_2 reduced per year, we present our results in terms of hectares of avoided deforestation. We convert the deforested area into tons of carbon emitted with the help of a parameter (Ω), whose value for Peru can be found in the OSIRIS model for the above and below ground biomass carbon and for soil carbon (Busch et al., 2009). Another converter (ψ) transforms the quantity of tons of carbon emitted into tons of CO_2 emitted (Assante, 2011).

With the help of the parameter λ we express the price of the composite commodity from Eur/m^3 into Eur/ha, relying on the IPCC Good Practice Guide LULUCF (Penman et al., 2003). The initial price of the commodity ($P^{cc}(0)$) and its growth rate (δ) are computed for the Peruvian market from the Annual Review and Assessment of the World Timber Situation (ITTO, 2010). We use the State of the Forest Carbon Markets 2011 (Diaz et al., 2011) to set the initial REDD permit price ($P^R(0)$) and its growth rate. In our calibration, the growth rate of the REDD permit price is above the growth rate of the composite commodity price ($\delta > \gamma$). As a robustness check, we ran the analysis allowing for the opposite relationship ($\delta \leq \gamma$). This change impacts the amount of avoided deforestation, but does not modify the ranking of the baselines.

The chosen level for the discount rate (r) is 2%, placing it slightly lower than the growth rates of the composite commodity and the permit prices; we make here the assumption that forest exploitation and REDD bring higher financial benefits than saving at the discount rate. In

[14] The analytical results can be provided by the authors upon request.

[15] With about 68 million hectares of tropical forest covering nearly 53% of its territory, Peru is fourth in the global ranking, after Brazil, the Democratic Republic of Congo, and Indonesia. About 89% of the total classifies as primary forest (FAO, 2010).

[16] According to Diaz et al. (2011), the Peruvian and Brazilian Amazon dominate the forest carbon market, with Latin America accountable for about 60% of the 2010 total primary market volume.

[17] The annual change in forest area was -0.22% for 2005-2010 (FAO, 2010).

[18] Hajek et al. (2011) compare 12 local REDD+ projects in south-eastern Peru, five of which were at feasibility and seven at early implementation stage at the time of writing.

reality, discount rates in developing countries take usually larger values and vary over time (see the Appendix). Nonetheless, the sensitivity analysis shows that the ranking of baselines is consistent across different values of the discount rate ($r \in [0, 0.1]$).

Finally, for the calibration of the production cost, we adapt the cost function of Angelsen (1996), calibrating it to data from Verissimo et al. (1992) for the Amazonian forest.

Table 3.2: Calibration parameters for the numerical solution.

Note: The table captures values used for the calibration of the model parameters. S.A. stands for values used in the sensitivity analysis.

Parameter	Explanation	Value	Source
$P^{cc}(0)$	Composite commodity price	500 Eur/m^3	ITTO (2010)
δ	Growth rate of $P^{cc}(t)$	2.3% p.a. S.A. [0, 0.04] p.a.	ITTO (2010)
λ	Eur/m^3 to Eur/ha	158 m^3/ha	Penman et al. (2003)
$P^R(0)$	REDD permit price	5 Eur/tCO_2	Diaz et al. (2011)
γ	Growth rate of $P^R(t)$	2.5% p.a. S.A. [0, 0.04] p.a.	Diaz et al. (2011)
Ω	ha to tC emitted	179 tC/ha S.A. [50, 200] tC/ha	Busch et al. (2009)
ψ	tC to tCO_2	3.67 tCO_2/tC	Assante (2011)
a_1	Cost parameter 1	3.3198 Eur/ha	Angelsen (1996), Verissimo et al. (1992)
a_2	Cost parameter 2	798.0811 Eur/ha^2	Angelsen (1996), Verissimo et al. (1992)
r	Discount rate	2% p.a. S.A. [0, 0.01] p.a.	-
dB	Historical baseline	200 ha p.a. S.A. [1, 500] ha p.a.	-
dB^U	Corridor upper boundary	$(1 + x)$dB ha	-
dB^L	Corridor lower boundary	$(1 - x)$dB ha	-
x_0	Initial corridor width	0.1	-
x	Corridor width	[0.1, 0.9]	-
T	Time horizon	100 years	-

3.2.4 Performance indicators

We evaluate the performance of REDD programs under different baseline methodologies with the help of three indicators, in line with the *3E Criteria* proposed by Stern (2008).[19] The performance measures we consider are: effectiveness, landowner's welfare, and efficiency, as detailed in Table 3.3. First, the effectiveness indicator E_1 measures the avoided deforestation, and the inherent saved emissions. It quantifies the difference between the deforested area of the business-as-usual (no REDD) and the different baseline scenarios for REDD, being therefore a measure of additionality. Second, we measure the financial co-benefits of REDD with the help of the E_2 indicator, which quantifies the percentage change in landowner's income due to joining REDD. Finally, the efficiency indicator E_3 provides an estimate of the average cost of forest preservation per hectare of avoided deforestation. It divides the total received REDD revenues by the number of hectares of forest saved under each baseline type compared to the business-as-usual scenario. Here, the cost of each baseline scheme reflects realised (additional) savings in emissions.

[19] Stern (2008) suggests the evaluation of REDD design proposals with the help of three criteria: effectiveness, efficiency, and equity and co-benefits.

Table 3.3: Performance indicators of baseline scenarios.

Note: Three measures of REDD performance under different baselines are computed. d(t) is the deforested area, $\pi(t)$ the total income from land, RR(t) the REDD revenue at time t, and $i \in$ {H, MI, Cf, Cv}; BaU business-as-usual, H historical, MI model-implied, Cf fixed corridor, Cv variable corridor.

Indicator	Definition	Formula
1. Effectiveness (E_1)	Avoided deforestation from BaU (%)	$E_1^i = \frac{S_{Tot}^{BaU} - S_{Tot}^i}{S_{Tot}^{BaU}}$ $S_{Tot}^i = \int_0^T d^i(t)dt$
2. Land owner's welfare (E_2)	Change in income from BaU (%)	$E_2^i = \frac{\Pi_{Tot}^i - \Pi_{Tot}^{BaU}}{\Pi_{Tot}^{BaU}}$ $\Pi_{Tot} = \int_0^T e^{-rt}\pi(d^i(t))dt$
3. Efficiency (E_3)	Average cost of avoiding 1 ha of deforestation from BaU (Eur/ha)	$E_3^i = \frac{SRR^i}{S_{Tot}^{BaU} - S_{Tot}^i}$ $SRR^i = \int_0^T e^{-rt}RR^i(t)dt$

3.3 Results

This section presents the optimal deforestation paths for the business-as-usual and the four REDD baseline approaches, and discusses the implications for baseline choice. The beginning of Section 3.3.1 ranks the baselines according to their performance. Then, we explain the differences in performance based on the structure of the financial incentives offered by each baseline methodology. At the end of the section, we check the robustness of the baseline ranking to changes in key parameters. Section 3.3.2 relaxes the initial assumptions regarding corridor wideness and symmetry, and underlines possible design adjustments to increase baseline performance. Section 3.3.3 extends the analysis of baseline performance to technical, social, and environmental aspects of REDD.

3.3.1 A first comparison

We solve for the optimal deforestation paths under the business-as-usual and the four REDD baselines; see Fig. 3.1. With our calibration, under each baseline scheme the optimal deforestation path is increasing in time, as agricultural activities become more attractive due to rising composite commodity prices. We compare the performance of the baseline methodologies based on the indicators introduced in Section 3.2.4. Table 3.4 shows that the baselines differ in their performance, with each indicator revealing a new ranking of baselines.

First, we compare the baselines in terms of the ability to reduce deforestation. Fig. 3.1 is illustrative for the effectiveness of REDD. In all baseline scenarios, the area of deforested land remains lower or equal to the business-as-usual case; over the aggregated time horizon, REDD programs are effective in reducing deforestation.[20] However, the reduction in deforestation does not hold at all moments of time for the static baselines: our dynamic model shows that keeping reference levels constant while the opportunity costs of deforestation increase, will determine the forest owner to opt out of the REDD project and follow the business-as-usual path. This sheds light on the limited effectiveness of the static baselines, as opposed to the prospective ones that offer continued incentives for reducing deforestation. We argue that, with their temporary effectiveness, static baselines face higher non-permanence risks than dynamic

[20]For a more detailed illustration of deforestation paths for each period, see Fig. 3.B.3 in Appendix 3.B.

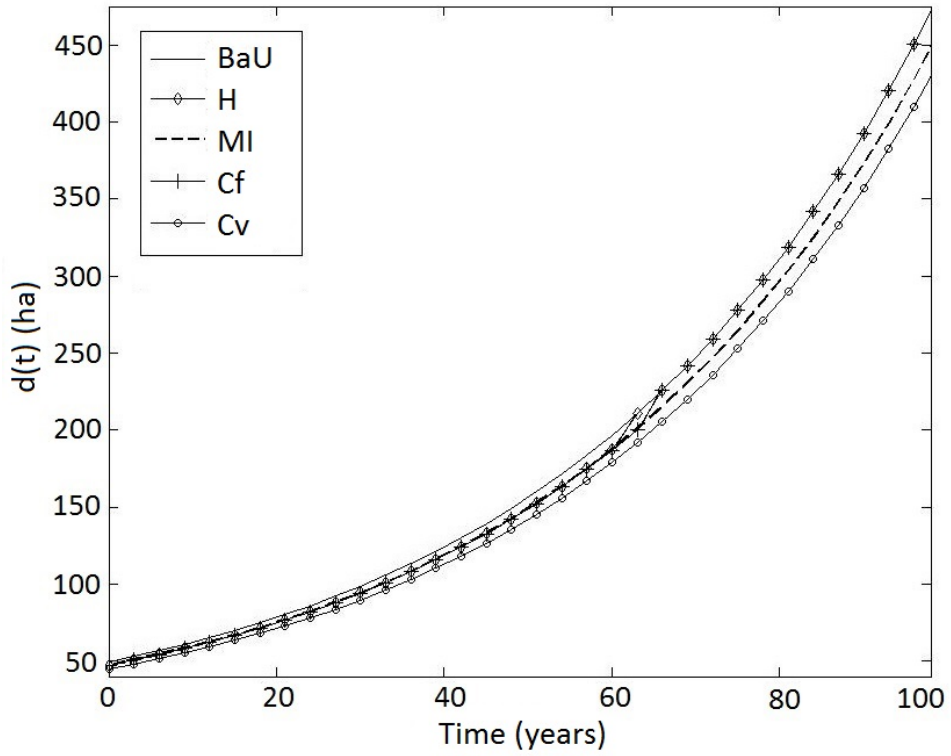

Fig. 3.1: Optimal deforestation paths under BaU and different REDD baselines.

Note: H stands for historical baseline, MI for model-implied, H for historical, Cf for fixed corridor, and Cv for variable corridor. The historical deforestation rate (dB) is 200 ha/year. Corridor width is $x = 0.1$.

baselines. Analysing the E_1 indicator, we indeed observe that the variable corridor achieves the best results, and it is followed at quite some distance by the model-implied baseline. The fixed corridor and the historical baseline lag far behind in terms of effectiveness.

Second, imposing no liabilities for deforestation rates above the baseline, all scenarios have a positive impact on landowner's welfare compared to the business-as-usual case (E_2). The increase in welfare across all baselines points to the ability of REDD to foster the voluntary opting-in of candidate countries, and alleviates some of the concerns with the need of additional enforcement measures. In particular, the static baselines prove to be more generous: the fixed corridor is the most attractive for the landowner, followed closely by the historical baseline. The remaining two baselines achieve only modest changes in welfare, with the model-implied baseline being the last ranked.

Third, in terms of cost-efficiency (E_3), the prospective baselines strongly outperform the static ones: the model-implied baseline is the top performer, with the variable corridor in second position. The historical and fixed corridor baselines require almost twenty times higher costs than MI.

Table 3.4: Indicators of REDD performance under different baselines.

Baseline	Effectiveness E_1 (%)	Welfare E_2 (%)	Efficiency E_3 (Eur/ha)
H	1.54	2.26	73,096.66
MI	4.77	0.23	4,680.18
Cf	1.76	2.76	78,043.75
Cv	9.08	0.92	9,318.13

3.3.1.1 The incentive structure of the baselines

In order to understand what drives the difference in baseline performance, we compare the incentive structure of the four baseline methodologies. To ease the comparison, we explicit the REDD revenues at different ranges of the deforestation rate; see Table 3.5. In particular, within the corridor we define the deforestation rate in terms of the reference level (dB, $dB(t)$), the corridor width (x), and a variable y, with $y \in (0, x)$, such that:

(1) When $d(t) \in (dB^L, dB]$, we define $d(t) = (1 - x + y)dB$ for the Cf case, and $d(t) = (1 - x + y)dB(t)$ for Cv;

(2) When $d(t) \in (dB, dB^U)$, $d(t) = (1+y)dB$ for the Cf case, and $d(t) = (1+y)dB(t)$ for Cv, with $dB(t) = d_{BaU}(t)$.

Table 3.5: REDD revenues (RR(t)) according to the range of the deforestation rate.

Static baselines

	$d(t) \in [0, dB^L]$	$d(t) \in (dB^L, dB]$	$d(t) \in (dB, dB^U)$	$d(t) \geq dB^U$
H	$P^R(t)(dB - d(t))$	$P^R(t)(x - y)dB$	0	0
Cf	$P^R(t)((1 + x)dB - d(t))$	$P^R(t)\left(2(x - y) + \frac{y^2}{2x}\right)dB$	$P^R(t)\frac{(x-y)^2}{2x}dB$	0

Dynamic baselines

	$d(t) \in [0, dB(t)^L]$	$d(t) \in (dB(t)^L, dB(t)]$	$d(t) \in (dB(t), dB(t)^U)$	$d(t) \geq dB(t)^U$
MI	$P^R(t)(dB(t) - d(t))$	$P^R(t)(x - y)dB(t)$	0	0
Cv	$P^R(t)((1 + x)dB(t) - d(t))$	$P^R(t)\left(2(x - y) + \frac{y^2}{2x}\right)dB(t)$	$P^R(t)\frac{(x-y)^2}{2x}dB(t)$	0

To account for possible misestimations in the BaU deforestation path and to increase participation rates, the corridor approaches reward landowners for choosing deforestation rates below an upper corridor bound, which is set above the corresponding single threshold ($dB^U = (1+x)dB$, $dB^U(t) = (1 + x)dB(t)$, with $x > 0$). We observe from Table 3.5 that by design, for the same deforestation rate, a corridor approach always gives larger or equal financial incentives to participate in REDD than the corresponding single-threshold approach. For all $t \in [0, T]$:

$$RR^H(t) \leq RR^{Cf}(t) \tag{3.15}$$

$$RR^{MI}(t) \leq RR^{Cv}(t) \tag{3.16}$$

The ranking of REDD payments influences the effectiveness of the baselines. Larger REDD revenues decrease the opportunity costs of deforestation, bringing stronger incentives to take part in REDD and keep deforestation below the baseline. Any decrease in deforestation will inevitably take place below $d_{BaU}(t)$.[21] It follows that relations (3.15) and (3.16) hold also for effectiveness with unchanged signs:

$$E_1^H \leq E_1^{Cf} \tag{3.17}$$
$$E_1^{MI} \leq E_1^{Cv} \tag{3.18}$$

Finally, we analyse the impact of higher REDD revenues on efficiency. Our efficiency indicator (E_3) is defined as a measure of total REDD revenues divided by the hectares of reduced deforestation below the business-as-usual. Therefore, an increase in REDD revenues will have a double (yet opposed) impact on efficiency. First, higher RR(t) lead to lower efficiency (higher E_3). Second, higher RR(t) raise effectiveness (avoided deforestation), increasing efficiency (lower E_3). As can be observed from Table 3.4, the effect on welfare dominates the effect on effectiveness[22]. It follows that the single-threshold approaches, with lower welfare increases, are more efficient than the corresponding corridor approaches, with higher welfare increases. That is:

$$E_3^H \leq E_3^{Cf} \tag{3.19}$$
$$E_3^{MI} \leq E_3^{Cv} \tag{3.20}$$

Summing up, we have shown that the corridor approaches dominate the corresponding single-threshold approaches in terms of effectiveness and welfare increase, but lag behind in terms of efficiency. If sufficient REDD funding is available, which remains to be seen, we argue that REDD promoters should opt for the corridor approach instead of the single-threshold one, in order to achieve the needed reductions in emissions.

3.3.1.2 Sensitivity analysis

REDD initiatives are currently being designed in a plethora of tropical countries, with several projects being already in implementation phase (Angelsen, 2010). In particular, Norway — through its International Climate and Forest Initiative (NICFI) — contributes to different multi- and bilateral REDD initiatives in several countries, including Brazil, Democratic Republic of Congo, Guyana, Indonesia, and Tanzania. The countries are distinct in terms of forest types, stages in the forest transition, and national forestry policies, apart from large diversity in the economic, social, and political contexts. To reach the REDD goals, NICFI recognises the need to design projects that account for national and sub-national differences (NIFCI, 2011).

To be able to generalise our findings outside the region of Peru, we test the robustness of our results across different settings. We focus on several key calibration parameters, describing the forest type (the carbon content Ω), the crediting threshold of the static baselines (dB), the time preference of the forest owner (the discount rate r), and the variables describing the opportunity costs of deforestation and the received REDD financial incentives (the growth rates of the composite commodity (δ) and REDD permit prices (γ)). The detailed analysis can be found in Appendix 3.D.

[21] $d(t)$ is bounded from above by $d_{BaU}(t)$, due to extraction cost constraints.
[22] For the full demonstration, see Appendix 3.C.

We find that the ranking of baselines is robust to different settings. The variable corridor continues to be the most effective in reducing deforestation. The fixed corridor offers the highest increase in welfare from BaU. The model-implied baseline is the most efficient, having the lowest costs per hectare of avoided deforestation. The sensitivity analysis underlines the importance of understanding the benefits of the variable corridor approach, whose performance can outpace significantly the other baselines, depending on the characteristics of the region where REDD is being implemented.

3.3.2 Corridor bandwidth and symmetry

When large uncertainties surround the business-as-usual deforestation rate, or high variability in opportunity costs is to be expected, one might be tempted to advocate a corridor approach with a larger bandwidth, such that a broader range of deforestation rates would be accounted for in the REDD payments. The corridor bandwidth should in this case be carefully chosen, to provide effective incentives for forest protection and, at the same time, achieve cost-efficiency.

With this motivation, we test the sensitivity of baseline performance to two key adjustments to the corridor methodology, namely corridor wideness and symmetry. We allow for increasing bandwidths ($x \in [0.1, 0.9]$) that reflect different reward magnitudes granted for reducing deforestation. Additionally, we check the variation in performance when allowing for asymmetric corridors. Namely, we consider both an upward- and a downward-biased corridor. For the variable corridor, bounds are set such that:

(1) In the upward-biased case, $dB^L(t) = (1 - x_0)dB(t)$ and $dB^U(t) = (1 + x)dB(t)$;

(2) In the downward-biased case, $dB^L(t) = (1 - x)dB(t)$ and $dB^U(t) = (1 + x_0)dB(t)$.

where $dB(t) = d_{BaU}(t)$, $x \in [0.1, 0.9]$ and x_0 is fixed, with $x_0 = 0.1$. The same applies for the fixed corridor, but $dB(t)$ is replaced as usually by the constant dB. On the one side, the upward-biased corridor approach raises the upper bound of the corridor, leading to an extension of the range of deforestation rates eligible for REDD revenues. This type of asymmetric corridor is in line with the proposal of Schlamadinger et al. (2005) who suggest setting the upper bound of the corridor so high that it minimises the probability that the deforestation rate will exceed this limit. On the contrary, the downward-biased approach takes down the lower bound of the corridor, imposing therefore heavier discounts on REDD rewards for deforestation rates in the range $(dB^L, dB]$ (resp. $(dB^L(t), dB(t)]$) for the fixed (resp. variable) corridor.

Fig. 3.2 displays the performance results of the variable corridor. The change in the performance of the fixed corridor follows a similar pattern; see Fig. 3.E.1 in Appendix 3.E. First, some effectiveness is always achieved ($E_1 > 0$), for all corridor bandwidths and all symmetry alternatives. Fig. 3.2 shows that, as bandwidth increases, effectiveness is higher for the upward-biased corridors, but decreasing for symmetric and downward-biased corridors. Second, increasing the corridor bandwidth achieves higher welfare improvements for the symmetric and upward-biased corridor approaches. Downward-biased corridors exhibit decreasing welfare for wider corridors. Third, cost-efficiency decreases for symmetric and upward-biased corridors, and improves slightly for the downward-biased when increasing the corridor width.

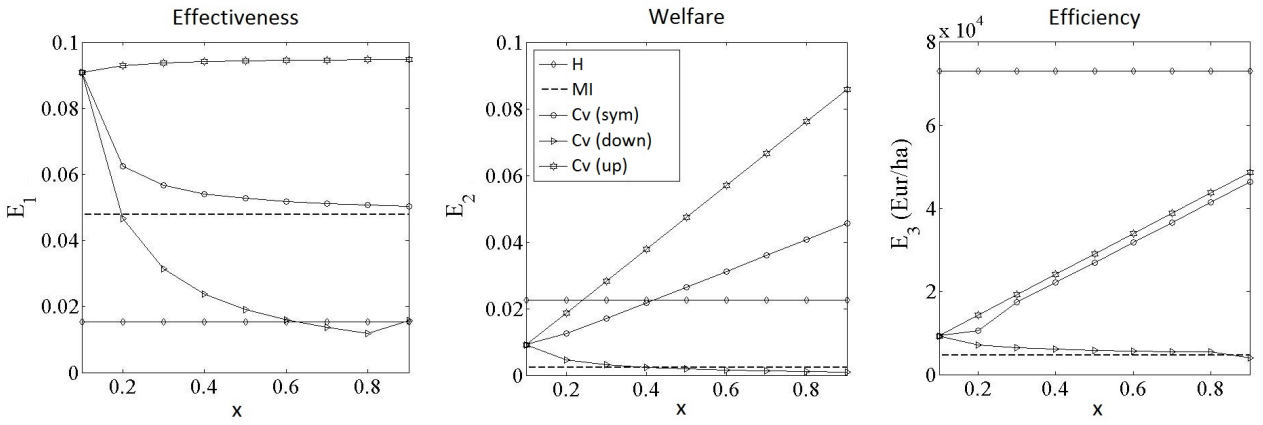

Fig. 3.2: Performance of the variable corridor at different corridor widths.

Note: The figure captures the performance of the variable corridor across different corridor bandwidths. The performance is compared to the historical and the model-implied baselines. Considered corridors are symmetric (*sym*), upward (*up*), and downward-biased (*down*).

3.3.2.1 The incentive structure of (a)symmetric corridors

The three symmetry scenarios provide distinct financial incentives, causing differences in performance. The upward-biased corridor is by design the most generous one, followed by the symmetric, and then the downward-biased corridor, i.e. $RR^{up}(t) \geq RR^{sym}(t) \geq RR^{down}(t)$ for all bandwidths[23]. Moreover, an increase in the corridor bandwidth (x) impacts the REDD revenues differently, depending on the symmetry assumption. The overall impact of an increase in bandwidth is twofold: (i) a linear impact on the number of REDD credits received for keeping deforestation rates below the upper corridor bound, i.e. on $n = dB^U(t) - d(t)$, and (ii) a non-linear impact on the weight ($\omega(t)$) provided by the corridor; see Table 3.6.

Table 3.6: Sensitivity of REDD revenues to corridor bandwidth and deforestation rate in the case of the variable corridor.

Note: Table captures the sign of the partial derivatives of REDD revenues ($RR(t)$) with respect to corridor width (x) and deforestation rate ($d(t)$) across different symmetry scenarios for the variable corridor, where $RR(t) = P^R(t)\omega(t)n$, with optimal $d(t) \in (dB^L(t), dB)$. The optimal deforestation rate stays within the corridor, i.e. $d(t) \in (dB^L(t), dB(t))$. $n = dB^U(t) - d(t)$ is the number of REDD credits awarded, $\omega(t) = 1 - (d(t) - dB^L(t))/(dB^U(t) - dB^L(t))$ is the weight imposed by the corridor approach, and the lower and upper bounds of the corridor $(dB^L(t), dB^U(t))$ vary across the three corridor symmetry assumptions. The computations are detailed in Appendix 3.E.

Symmetry	Linear impact on REDD credits $\frac{\partial n}{\partial x}$	Non-linear impact on weight $\frac{\partial \omega(t)}{\partial x}$	Overall impact on REDD revenues $\frac{\partial RR(t)}{\partial x}$	Second order impact on REDD revenues $\frac{\partial^2 RR(t)}{\partial x \partial d(t)}$
Upward-biased	+	+	+	−
Symmetric	+	−	+	+
Downward-biased	0	−	−	+

The upward-biased approach achieves increasing welfare at larger corridor widths. With an increase in x, both the number of REDD credits received and the weight provided by the upward corridor increase. As captured in Fig. 3.2, welfare and effectiveness change in the same direction when x increases, but the large increase in welfare obtained at wider corridors is

[23]For the demonstration, see Table 3.E.1 in Appendix 3.E.

accompanied by only modest improvements in effectiveness that have the tendency to flatten out as x increases. The stronger financial motivation has a diminishing effect on forest protection.

Downward-biased corridors exhibit negative partial derivatives with respect to x, showing that here welfare improvements from BaU are lower for wider corridors. Larger bandwidths decrease welfare and, as expected, effectiveness.

The symmetric corridor approach achieves higher welfare but lower effectiveness as bandwidth increases. The overall positive impact on welfare follows, as usually, from the fact that its REDD revenues are increasing in the corridor bandwidth. However, although the total impact is positive, the linear and non-linear effects have opposite signs (Table 3.6). As bandwidth increases, the landowner benefits on the one hand by receiving more REDD credits (higher n), but loses on the other hand from stronger discounts imposed by the weighting factor (lower $\omega(t)$). The impact on effectiveness is confirmed when analysing the joint sensitivity of REDD revenues to the deforestation rate and corridor bandwidth; see column 4 in Table 3.6. The increase in profits due to an increase in x is higher at larger $d(t)$, as indicated by the positive second order partial derivatives. At larger corridor bandwidths, it benefits the landowner to increase $d(t)$, and therefore reduce effectiveness.

Summing up, with a lack of confidence in the estimates of the business-as-usual deforestation, or with anticipated high seasonality in deforestation rates, wider corridors might need to be accommodated, in a way that forest protection is still incentivised. Our results show that increasing the corridor bandwidth ensures a higher effectiveness of reducing deforestation only in the upward-biased corridor design, and is counter-beneficial for symmetric and downward-biased cases. Both fixed and variable corridors benefit most from having an upward-biased corridor reward system of moderate bandwidth ($x = 0.4, 0.5$), which guarantees strong effectiveness and welfare results, at low efficiency losses.

3.3.3 Extended criteria for baseline evaluation

Our analysis thus far has highlighted three baseline alternatives with strong performance results: the model-implied (MI), the upward-biased fixed corridor (Cf(up)), and the upward-biased variable corridor (C(up)), with each baseline alternative performing best in a different area.

Although the three performance indicators considered so far capture the most important economic aspects of the alternative baselines, other factors play an equally important role in the REDD implementation process. In order to achieve a more holistic understanding of the baseline characteristics, we complement the economic evaluation with a multi-tier analysis focusing on the environmental, technical, and social performance of the baselines. Based on the study of Huettner et al. (2009), we select five new criteria whose fulfilment can be easily evaluated for our baselines, namely: easiness of implementation, low data requirements, accounting for business cycles, accounting for opportunity costs, and endorsing reduced losses from estimation errors.

The fulfilment of these additional qualitative factors cannot however be quantified in the same manner as our three initial economic indicators. For this reason, we proceed by giving each baseline type a score[24] representing a rough estimation of how well it is expected to fulfil the

[24]The score allocated to each baseline takes values from 1 to 4 (4 is the number of baselines considered for comparison: historical, model-implied, upward-biased fixed corridor, and upward-biased variable corridor), such that, for each indicator, a score of 4 is awarded to the baseline believed to be most likely to fulfil the criterion, and a score of 1 to the baseline least likely.

performance criteria relative to the other baselines. The scores awarded to each baseline for the three initial indicators and the new qualitative aspects are presented in Fig. 3.3. While

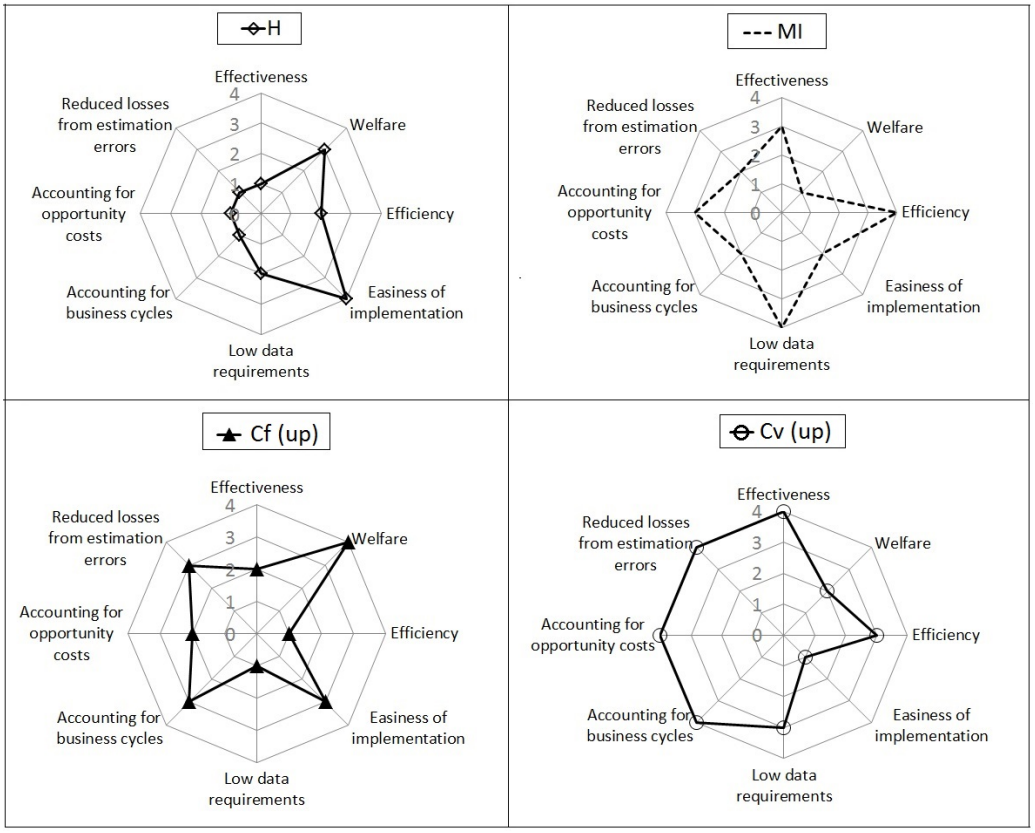

Fig. 3.3: Integrated performance of baseline approaches.

the economic analysis (based on E_1, E_2, and E_3) favoured each of the baselines for a different criterion, the integrative analysis sets the four baselines further apart, highlighting stronger differences.

One of the new criteria reveals a strong point of the historical baseline (H). REDD projects, especially in their initial phase, need to be designed as contracts with few and clear requirements in order to encourage the participation of diverse parties and create momentum for the development of such forest protection initiatives worldwide. The historical baseline is likely to benefit from the highest ease of implementation among the considered methodologies. If data availability is not an issue, policy makers will be required low efforts for baseline computation and landowners will be provided with contract guidelines they can easily relate to. Together with the fact that historical deforestation rates have some predictive power for short- to medium-term deforestation (Angelsen et al., 2009), the ease of implementation explains why current REDD initiatives have opted to rely on the historical baseline for computing reductions in deforestation.

The model-implied (MI) baseline provides rewards for reductions below the estimated counterfactual deforestation, accounting for future opportunity costs. Its computation does not rely on the availability of data records of past deforestation; instead, it requires information regarding current agricultural prices and estimations of the future trend in prices. We argue that the MI has comparatively less data restrictions than all the other baseline methodologies. Moreover, if the estimation of the BaU deforestation path is truthful, the implementation of REDD with the MI baselines favours additionality. Fig. 3.3 reminds us that this baseline stands out in terms

of the cost-efficiency criterion, as highlighted in Section 3.3.1. This can be a strong point in favour of the MI baseline, especially if future REDD rewards will be linked with compliance carbon markets.

The upward-biased fixed corridor (Cf(up)) modifies the historical baseline by replacing the single-threshold with a corridor. Section 3.3.2 showed that selecting an upward-biased corridor can improve its effectiveness and welfare performance. Indeed, the upward-biased corridor approach is the most attractive for the landowner from a welfare perspective. Despite large financial transfers, the effectiveness of the Cf(up) remains limited and its efficiency performance poor.

Overall, the integrative analysis appears to give highest support to the variable corridor approach. The upward-biased variable corridor (Cv(up)) is the most effective in reducing deforestation below business-as-usual levels; see again Section 3.3.1. Being a prospective method, based on expectations regarding the future movement of timber and agriculture prices, as well as REDD permit prices, the Cv(up) has a better ability to reflect the opportunity costs faced by the landowner. Additionally, the corridor design brings two advantages. First, the scheme offers REDD compensation also for deforestation rates that come close to the time-varying baseline, even if not strictly below it; this accommodates possible future business cycles and ensures (modest) positive REDD revenues should the economy be expanding (when opportunity costs are high). Second, replacing the single-threshold by a corridor approach, and introducing the weighting system for deforestation rates inside the corridor, the baseline has the ability to reduce losses due to misestimation of the BaU baseline (Joanneum Research Institute, 2006).

Summing up, designing a baseline methodology that achieves all REDD goals simultaneously proves to be highly challenging. Indeed, the analysed baselines exhibit strong attributes in different areas. For its ability to enhance environmental and economic performance, we consider the upward-biased variable corridor to be the best candidate for achieving the most important REDD goals.

Two delicate issues require further thought. The first one touches on the issue of additionality. REDD aims to reward reductions in deforestation below business-as-usual levels. One limitation of our analysis is that it is placed in a deterministic setting, where the business-as-usual deforestation path is known. However, in reality many variables of the decision environment are in fact stochastic, such as commodity and REDD prices, and asymmetries in information might lay between REDD promoters (who evaluate emission reductions) and forest owners (who benefit from REDD payments). This surrounds the estimation of the business-as-usual deforestation path with large uncertainties. REDD projects implemented based on misspecified business-as-usual deforestation levels can provide undesired incentives to forest owners: if the reference level is set (considerably) below the business-as-usual, the participation rate in REDD will be low; in the opposite case, windfall profits will be distributed to forest owners and the REDD rewards will not accurately reflect reductions in emissions. In both cases, the high probability of setting reference levels with error casts doubt on the effectiveness and efficiency of REDD. Implementing REDD in an uncertain environment might reveal other types of differences between the prospective and static baselines.

The second key issue concerns permanence. With REDD, the issue of permanence has a different dimension than on compliance carbon markets, like the EU ETS. There, being restricted to emit less than a pre-specified cap, regulated companies continue with the same business activity, but are given incentives to switch to a more efficient production process.[25] Being costly, the

[25]This refers to relying on less emission intensive sources of energy, like renewables or the more common switch from coal to gas for the generation of electricity.

switch is likely not to be reverted, and emission reductions could remain 'permanent'. The situation is not analogous to REDD, where the landowners cannot continue with their current occupation (deforesting for expanding agriculture), but need to stop the expansion if they want to receive payments (they cannot make the cutting down of trees less emission-intensive). REDD payments are offered on a per-period basis, being linked with deforestation flows instead of the remaining forest stocks. Thus, temporary reductions in deforestation can be reverted in later periods, questioning the long-term success of REDD. We argue that payments should instead be contingent on the emissions of the entire owned land parcel, such that all land uses are covered by the regulation umbrella, and more efficient operations are incentivised, similar to the mechanism of the cap-and-trade systems. However, this takes us away from the original REDD concept, and future research could further investigate this topic.

3.4 Conclusions

REDD programs target reductions in emissions from deforestation below business-as-usual levels. A key issue of REDD is the establishment of baselines, against which reductions in deforestation are measured. This paper assesses the performance of the most frequently proposed baselines: historical, model-implied, and fixed corridor. Additionally, we introduce a new baseline type – the variable corridor.

We solve for the optimal deforestation path in a dynamic setting where REDD projects are available. One of our main findings is that baseline choice has a significant impact on land use behaviour. Land owners choose different deforestation paths when incentivised by distinctive baseline methodologies. We believe this point is key for implementing effective REDD programs.

We first evaluate the selected baselines based on three economic indicators that describe the effectiveness, welfare increases, and cost-efficiency of reducing deforestation. We find that each indicator points to a different baseline as the best performer. Our analysis shows that a preference for strong effectiveness recommends the variable corridor. The fixed corridor provides the highest increase in landowner's welfare above business-as-usual. Efficiency reasons advocate the model-implied baseline.

We then discuss additional environmental, social, and technical aspects important for REDD implementation and the establishment of baselines. This analysis highlights stronger differences among the baselines, and reveals that the prospective variable corridor achieves the best trade-off among the economic and environmental REDD goals. Moreover, this performance can be boosted by setting the upper bound of the corridor (asymetrically) high above the estimated business-as-usual deforestation.

We conclude that the current widespread use of the historical baseline is no longer well motivated. Much stronger effectiveness and efficiency could be achieved with the use of a forward-looking baseline. Additionally, the currently used single-threshold methodology is also not optimal; replacing the single-threshold approach with a corridor formed around the estimated business-as-usual deforestation rate has higher potential of accounting for real opportunity costs and offering continued incentives for reduced deforestation. Our results offer potential insights for other emission regulation policies, such as EU ETS. There, regulated companies are allocated emission allowances based on their emissions' history, similar to the historical baseline in REDD. Based on our analysis, we expect the EU ETS to benefit also in terms of effectiveness and efficiency from replacing its historical cap with a forward-looking corridor approach. This

could potentially address some of the permit overallocation problems, which have persisted since the opening of the EU ETS.

Some additional concerns remain. This paper assumes that REDD funding is achieved through a market-based mechanism. In comparison to voluntary funds, international carbon markets can mobilise much larger amounts of money and favour cost-efficient emission reductions (Angelsen, 2008b). However, the weak carbon markets we face nowadays, characterised by low liquidity and permit overallocation, will most probably have difficulties in handling additional amounts of permits coming from the forestry sector. Therefore, when selecting the most appropriate baseline type, one might postpone the implementation of the most effective one in order to avoid collapses in permit prices until the stabilisation of the carbon market.

A robust understanding of the deforestation process would require an improved description of the different stakeholders involved in REDD implementation. As Griscom et al. (2009) point out, the selection of reference levels will be based not only on technical and economic considerations, but also on political negotiations among participating countries. REDD projects implemented at the national level will motivate countries to take a strategic position at the negotiation table and try to influence the establishment of crediting levels in their favour. Under these conditions, the adjusted deforestation decision will result in emission reductions of other magnitudes than the ones presented in this study, and might as well reveal a different ranking of baseline approaches. Future research, based on dynamic decision models with multiple players defending contrasting interests, could be relevant for this issue.

Appendix Chapter 3

3.A The optimal deforestation path in the business-as-usual scenario

When no REDD program is in place, the net revenue of the landowner at time t is given by:

$$\pi(d(t)) = P^{cc}(t)d(t) - (a_1 d(t) + a_2 d(t)^2) \tag{3.A.1}$$

The optimal control problem can be described as follows:

$$\max_{(d(t))_{t\in[0,T]}} \int_0^T e^{-rt}\pi(d(t))dt \tag{3.A.2}$$

$$\text{such that:} \quad \dot{F} = -d(t) \tag{3.A.3}$$

$$F(0) = F_0 \tag{3.A.4}$$

We build the current-value Hamiltonian as:

$$H^c = \pi(d(t)) - \mu d(t) \tag{3.A.5}$$

The equations of motion follow immediately:

$$\frac{\partial H^c}{\partial d(t)} : \pi'(d(t)) - \mu = 0 \tag{3.A.6}$$

$$-\frac{\partial H^c}{\partial F} + r\mu = \dot{\mu} \tag{3.A.7}$$

$$\dot{F} = -d(t) \tag{3.A.8}$$

The partial derivative of the Hamiltonian with respect to the forest stock is zero $\left(\frac{\partial H^c}{\partial F} = 0\right)$. We obtain from Eq. (3.A.7) that:

$$\dot{\mu} = r\mu \Rightarrow d\mu = \mu r dt \Rightarrow \mu(t) = \mu(0)e^{rt} \tag{3.A.9}$$

From Eq. (3.A.6) we know that $\pi'(d(t)) = \mu(t)$, which holds for all $t \in [0, T]$. It follows that $\pi'(d(0)) = \mu(0)$. Introducing this result in Eq. (3.A.9), we obtain that:

$$\pi'(d(t)) = \pi'(d(0))e^{rt} \tag{3.A.10}$$

We explicit Eq. (3.A.10) with the help of the profit function given in Eq. (3.A.1). After some simplifications, the optimal deforestation rate at time t is given by:

$$d(t) = d(0)e^{rt} + \frac{P^{cc}(0)(e^{\delta t} - e^{rt}) - a_1(1 - e^{rt})}{2a_2} \tag{3.A.11}$$

The optimal deforestation at time t depends on the initial deforestation rate ($d(0)$), the discount rate (r), the initial price of the composite commodity ($P^{cc}(0)$) and its growth function (δ), and the parameters of the cost function (a_1, a_2). In order to define the optimal deforestation path, the last element that needs to be defined is the initial deforestation rate ($d(0)$). We iterate over a large grid of possible values and choose the initial deforestation that maximises total profits.

3.B The optimal deforestation path under REDD

The simultaneous presence of REDD rewards for lower-than-baseline and absence of penalties for higher-than-baseline deforestation levels brings discontinuities to the profit function. The resulting non-smoothness in the objective function impedes the application of standard optimisation methods. To overcome this difficulty, we develop a solution approach based on regime switches. This method allows for a break in the continuity of the deforestation path, which would otherwise be forced under the standard Hamiltonian procedure. A smooth deforestation path would not be able to guarantee optimality in the context of a non-smooth objective function. Here, we allow the landowner to decide at each moment of time whether to deforest below or above the reference level, i.e. he makes his choice between a *REDD regime* (hereafter Regime 1) and a *BaU regime* akin to business-as-usual (hereafter Regime 2).

One observation is key for solving the optimisation problem: in the absence of stochasticities, the decision regarding deforestation levels at each moment of time can be taken from the beginning for all future periods. While it could be

possible in theory that the landowner switches between regimes multiple times, in practice the dynamic requirement at equilibrium ensures smooth evolution for the deforestation path within each regime and limited shifts between regimes over the entire horizon. We begin by explaining the solution approach for the historical and the model-implied cases. Since it requires an additional modification, we present the solution to the corridor scenario at the end of this section.

For the historical and the model-implied baselines, the landowner chooses low deforestation rates and stays in Regime 1 as long as the total benefits from REDD and forest exploitation below the reference level remain higher that the total benefits from forest exploitation above the reference level. Depending on the values of the parameters, the regime switch can occur either from the beginning, somewhere during the lifetime of the maximisation period, or never at all. Formally, the optimisation procedure can be described as follows:

$$\max_{d(t)|t\in[0,T]} \left\{ \int_0^{\tau} e^{-rt}\pi^{R_1}(d(t))dt + \int_{\tau}^{T} e^{-rt}\pi^{R_2}(d(t))dt \right\} \tag{3.B.1}$$

with R_1 and R_2 standing for Regime 1 and Regime 2, respectively. τ is the switching time from Regime 1 to Regime 2:

$$\tau = \inf\{t \geq 0 | d(t) \geq dB\} \tag{3.B.2}$$

We adapt the solution method of Chiang (1992) to allow for regime switches. The current-value Hamiltonian is defined as:

$$H^c = \begin{cases} H^{R_1} = \pi^{R_1}(d(t)) - \mu_1(t)d(t) & \text{, if } t \in [0,\tau) \\ H^{R_2} = \pi^{R_2}(d(t)) - \mu_2(t)d(t) & \text{, if } t \in [\tau,T] \end{cases} \tag{3.B.3}$$

It is important to underline that if Regime 1 occurs in our parametrisation, it will precede Regime 2, due to the different profit dynamics of the two activities. On the one hand, the landowner can gain from intensifying forest exploitation, as long as his inflows do not exceed operating costs. In time, his revenues rise due to the increasing price of the composite commodity. On the other hand, even if revenues from REDD increase due to rising permit prices, these profits are limited, since the deforestation rate is bounded from above by the reference level and from below by zero (we do not allow for reforestation). Therefore, even if initially marginal benefits with REDD could be higher than BaU marginal benefits, this advantage would decrease over time. As a consequence, remaining in Regime 1 could become suboptimal at a certain moment of time (τ), after which the landowner will move to Regime 2. Fig. 3.B.1 captures dominant profits

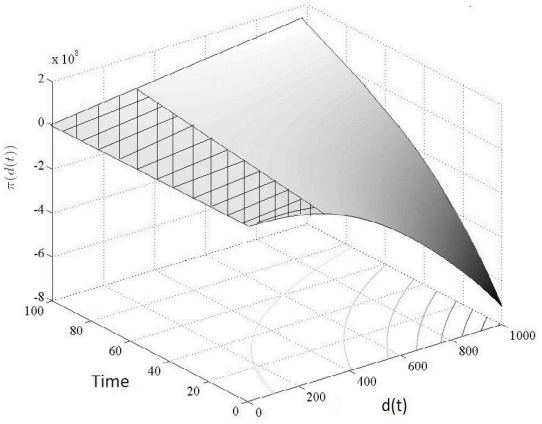

Fig. 3.B.1: Land use revenues.

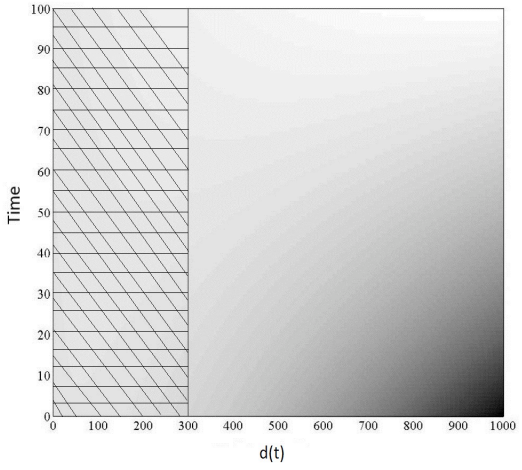

Fig. 3.B.2: Land use revenues (view from top).

of either REDD or BaU regimes at different deforestation rates. The hashed-area area represents cases where taking part in the REDD project is optimal, while the grey area symbolises regions where the BaU scenario is optimal. Within each section of the graph, lighter colours stand for higher profit values. As long as the deforestation rate is below the fixed baseline, the optimal regime to choose is the REDD one; see Fig. 3.B.2. This holds for initial time periods. As time passes, the overall optimum is to be found in the BaU regime. The two figures show that if a regime switch does occur at some moment of time, this switch is expected to take place one time only, as the dominance alternation takes place only once. Moreover, Fig. 3.B.1 shows that the REDD regime should precede the BaU, since for later periods of time profits are increasing in the deforestation rate and the landowner will be better off opting for the BaU regime. The solution for the optimal deforestation path is given by:

$$d(t) = \begin{cases} d(0)e^{rt} + \frac{P^{cc}(0)(e^{\delta t}-e^{rt}) - a_1(1-e^{rt}) - P^R(0)(e^{\gamma t}-e^{rt})}{2a_2}) & \text{, if } t \in [0,\tau) \\ d(\tau)e^{rt} + \frac{P^{cc}(\tau)(e^{\delta t}-e^{rt}) - a_1(1-e^{rt})}{2a_2} & \text{, if } t \in [\tau,T] \end{cases} \tag{3.B.4}$$

Considering the lack of continuity at τ, we solve the landowner's maximisation using a numerical search algorithm that combines all possible combinations of Regime 1 and Regime 2 paths at different switching points[26]. We select the combined path that yields the highest profits.

In the case of the corridor scenarios, the profit function is non-smooth at two points, i.e. at the boundaries of the corridor (dB^U and dB^L for the fixed; $dB^U(t)$ and $dB^L(t)$ for the variable); the landowner will be able to switch between three different regimes. Depending on the relationship between initial parameter values, he will choose an optimal deforested area that satisfies:

$$d(t) = \begin{cases} d(0)e^{rt} + \frac{P^{cc}(0)\left(e^{\delta t}-e^{rt}\right)-a_1\left(1-e^{rt}\right)-P^R(0)\left(e^{\gamma t}-e^{rt}\right)}{2a_2}) & \text{, if } t \in [0,\tau_1) \\ d(\tau_1)e^{rt}\frac{a_2-\frac{P^R(\tau_1)}{dB^U-dB^L}}{a_2-\frac{P^R(\tau_1)e^{\gamma t}}{dB^U-dB^L}} + \frac{P^{cc}(\tau_1)\left(e^{\delta t}-e^{rt}\right)-a_1(1-e^{rt})-P^R(\tau_1)\left(e^{\gamma t}-e^{rt}\right)\left(1+\frac{dB^U+dB^L}{dB^U-dB^L}\right)}{2\left(a_2-\frac{P^R(\tau_1)e^{\gamma t}}{dB^U-dB^L}\right)} & \text{, if } t \in [\tau_1,\tau_2) \\ d(\tau_2)e^{rt} + \frac{P^{cc}(\tau_2)\left(e^{\delta t}-e^{rt}\right)-a_1\left(1-e^{rt}\right)}{2a_2} & \text{, if } t \in [\tau_2,T] \end{cases} \quad \text{(3.B.5)}$$

in the fixed corridor case. For the variable corridor, the optimal deforestation rate will take the same form, with $dB^U(t)$ and $dB^L(t)$ replacing dB^U and dB^L, respectively. In our setting, the order of the switching times ($0 \leq \tau_1 \leq \tau_2 \leq T$) is due to the combination of two characteristics of our model. First, the benefits of taking part in REDD decrease over time: for later periods, net revenues from land exploitation outpace REDD revenues due to higher composite commodity prices and larger deforestation rates. Second, REDD gains get marginally smaller as the deforestation level gets closer to the upper corridor boundary until it eventually fades away for rates above the corridor. Therefore, the motivation to stay in REDD decreases over time, but at different paces within each interval. The landowner's optimisation problem accounts for three possible regimes:

$$\max_{d(t)|t\in[0,T]} \left\{ \int_0^{\tau_1} e^{-rt}\pi^{R_1}(d(t))dt + \int_{\tau_1}^{\tau_2} e^{-rt}\pi^{R_2}(d(t))dt + \int_{\tau_2}^{T} e^{-rt}\pi^{R_3}(d(t))dt \right\} \quad \text{(3.B.6)}$$

To determine the optimal regime switching times (τ_1 and τ_2), we first define optimal paths within each regime for all possible combinations of switching times. We then use a numerical search algorithm that selects the combination of the three paths yielding the highest profits.

Fig. 3.B.3 captures the optimal deforestation path for the business-as-usual and the four REDD baseline methodologies. The large box on the left-hand side refers to the entire deforestation path, reproducing the results in Fig. 3.1. To better understand the differences in optimal deforestation for each baseline, we detail in the other boxes on the right-hand side the deforestation path for sub-periods of 25 years each.

[26] We allow for all possible switching points in the range $[0, T]$

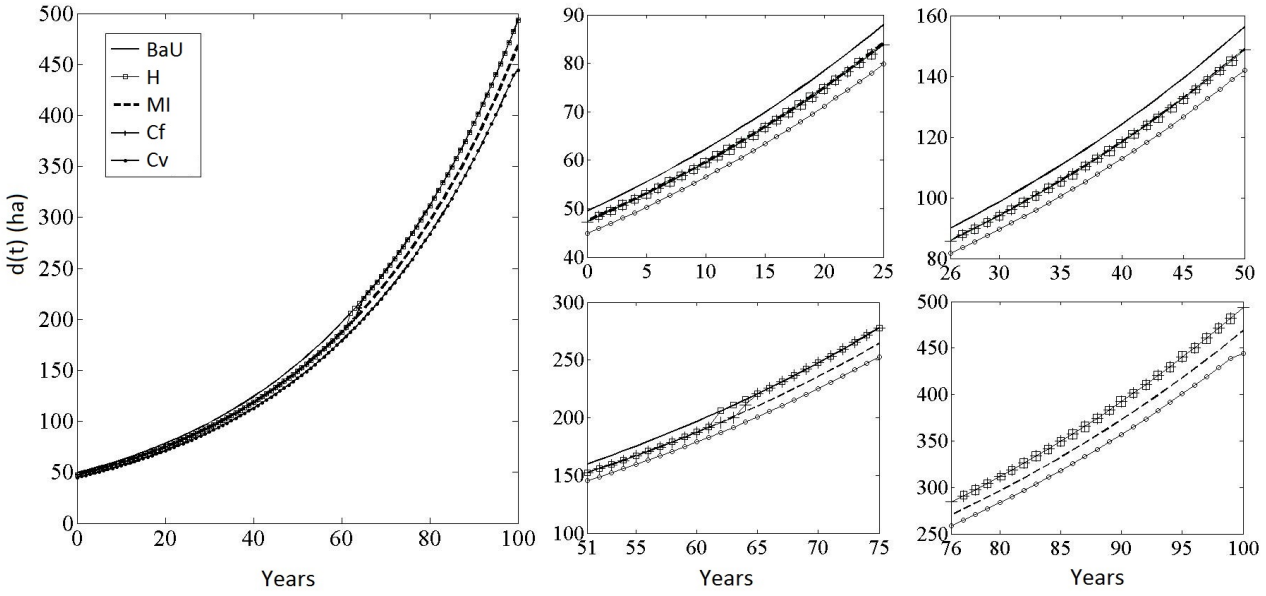

Fig. 3.B.3: Optimal deforestation paths under BaU and different REDD baselines, detailed for sub-periods of 25 years.

3.C Efficiency of the single-threshold and corridor approaches

Proposition: The single-threshold baseline approach is more efficient that the corresponding corridor approach, that is:

$$E_3^H \leq E_3^{Cf} \tag{3.C.1}$$
$$E_3^{MI} \leq E_3^{Cv} \tag{3.C.2}$$

where $E_3^i = \frac{SRR^i}{S_{Tot}^{BaU} - S_{Tot}^i}$, $SRR^i = \int_0^T RR^i(t)dt$, $S_{Tot}^i = \int_0^T d^i(t)dt$, $i \in \{H, MI, Cf, Cv\}$, and BaU stands for business-as-usual.

Proof:
Let ST refer to the single-threshold approach and C to the corresponding corridor approach. For the proof we will use three results from Section 3.3.1. First, we have seen in Section 3.3.1 that:

$$RR^{ST}(t) \leq RR^C(t) \tag{3.C.3}$$

Since Relation (3.C.3) holds $\forall t \in [0; T]$, we can write that:

$$\int_0^T RR^{ST}(t)dt \leq \int_0^T RR^C(t)dt \Leftrightarrow SRR^{ST} \leq SRR^C \tag{3.C.4}$$

Let us denote then:

$$SRR^{ST} = (1-a)SRR^C \tag{3.C.5}$$

with $a \in [0; 1]$ such that Relation (3.C.5) is satisfied.
We have seen in Section 3.3.1 that:

$$E_1^{ST} \leq E_1^C \tag{3.C.6}$$

From the definition of E_1^i, it follows that:

$$\frac{S_{Tot}^{BaU} - S_{Tot}^{ST}}{S_{Tot}^{BaU}} \leq \frac{S_{Tot}^{BaU} - S_{Tot}^C}{S_{Tot}^{BaU}} \Leftrightarrow S_{Tot}^{BaU} - S_{Tot}^{ST} \leq S_{Tot}^{BaU} - S_{Tot}^C \tag{3.C.7}$$

Let us denote then:

$$S_{Tot}^{BaU} - S_{Tot}^{ST} = (1-b)\left(S_{Tot}^{BaU} - S_{Tot}^C\right) \tag{3.C.8}$$

where $b \in [0; 1]$ such that Relation (3.C.7) is satisfied.
Third, we observe from Table 3.4 that $a > b$, i.e. that the percentage gain in welfare (a) achieved by the corridor relative to the single-threshold is larger than its gain in effectiveness (b). Therefore, accounting for Relations (3.C.5) and (3.C.8), we can compare the efficiency of the single-threshold and corridor approaches:

$$E_3^{ST} - E_3^C = \frac{SRR^{ST}}{S_{Tot}^{BaU} - S_{Tot}^{ST}} - \frac{SRR^C}{S_{Tot}^{BaU} - S_{Tot}^C} = \frac{(1-a)SRR^C}{(1-b)(S_{Tot}^{BaU} - S_{Tot}^C)} - \frac{SRR^C}{S_{Tot}^{BaU} - S_{Tot}^C} \tag{3.C.9}$$

$$E_3^{ST} - E_3^C = \frac{SRR^C}{S_{Tot}^{BaU} - S_{Tot}^C}\frac{b-a}{1-b} \tag{3.C.10}$$

With $a > b$, we get that:

$$E_3^{ST} \leq E_3^C \tag{3.C.11}$$

3.D Parameter calibration and sensitivity analysis

This section verifies the robustness of our results to several key calibration parameters, namely: the carbon content of the forest, the discount rate, and the growth rates of the composite commodity and REDD permit prices.

3.D.1 The forest carbon content (Ω)

REDD programs aim to achieve reductions in emissions from deforestation below business-as-usual levels. While deforestation can be measured in terms of hectares of land where forest has been removed, the GHG emissions coming from deforestation depend on the carbon content stored in the trees. The carbon content of one hectare of forest can vary across geographical regions, depending on tree type and forest density.

Across the REDD candidate countries, the average carbon content varies widely. Fig. 3.D.1 captures the distribution of average above and below ground carbon content of 85 REDD countries, grouped according to their deforestation patterns and the geographical region[27]. The variability of the carbon content is very large even within each geographical and FTT group.

The forest carbon content varies not only from country to country, but also within countries. Fig. 3.D.3 shows the above ground carbon content across the territory of Peru[28], which takes values from 0 to more than 150 tC/ha. The existence of large differences between the carbon content of different regions brings a strong argument for the need to design REDD projects that take into account regional characteristics.

The success of REDD is likely to depend on its ability to provide payments that correctly reflect the carbon content of each project area. We test the sensitivity of the baseline performance to different levels of carbon content per hectare of forest. This setting depicts a situation where REDD projects are implemented in several regions of a country, with the average carbon content varying from region to region. Holding everything else constant, we assume identical conditions regarding the composite commodity and REDD permit markets across the different regions.

Fig. 3.D.2 illustrates the performance of the four REDD baselines across different levels of average carbon content. It demonstrates the robustness of the baseline ranking presented in Section 3.3.1. The variable corridor (Cv) continues to be the most effective in reducing deforestation. The fixed corridor (Cf) offers the highest increase in welfare from BaU. The model-implied baseline (MI) is the most efficient, having the lowest costs per hectare of avoided deforestation.

Additionally, we observe an increase in the difference in performance of the static versus dynamic baselines at higher carbon contents. The results are particularly interesting in terms of effectiveness; it results that REDD projects employing the variable corridor (Cv) approach will have a high potential in reducing deforestation and the inherent GHG emissions, especially if they target high carbon content (HCC) areas. With the current international fora inclined to direct REDD programs towards high carbon content areas, it appears especially important to understand and underline the benefits of the variable corridor approach.

[27] Data source is the OSIRIS v.3-4 spreadsheet, available online at http://sp10.conservation.org/osiris/Pages/overview.aspx.

[28] Of course, not the entire territory of Peru is covered with forest and eligible for REDD projects. As mentioned in Section 3.2.3, Peru has about 68 million hectares of tropical forest, covering nearly 53% of its territory.

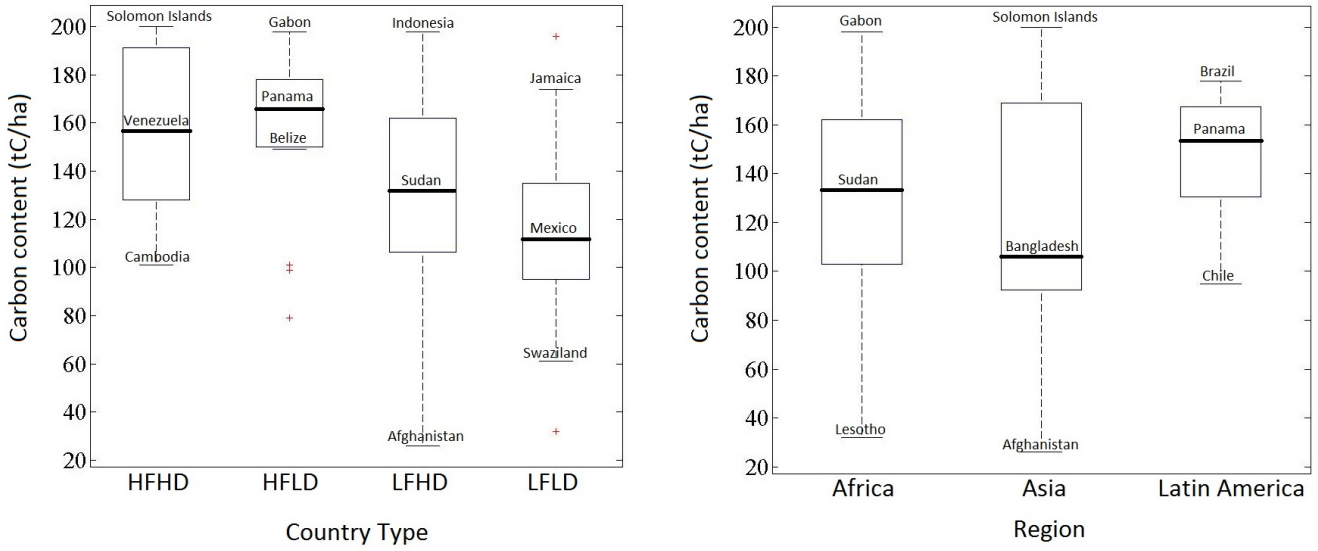

Fig. 3.D.1: Distributions of the average above and below ground carbon content across different stages of FTT and world regions.

Note: The right panel groups countries according to the geographical region. The left panel groups countries based on their deforestation patterns according to the Forest Transition Theory (FTT). HFHD is high forest, high deforestation; HFLD is high forest, low deforestation; LFHD is low forest, high deforestation; LFLD is low forest, low deforestation. Source: Authors' own calculations based on OSIRIS v.3-4.

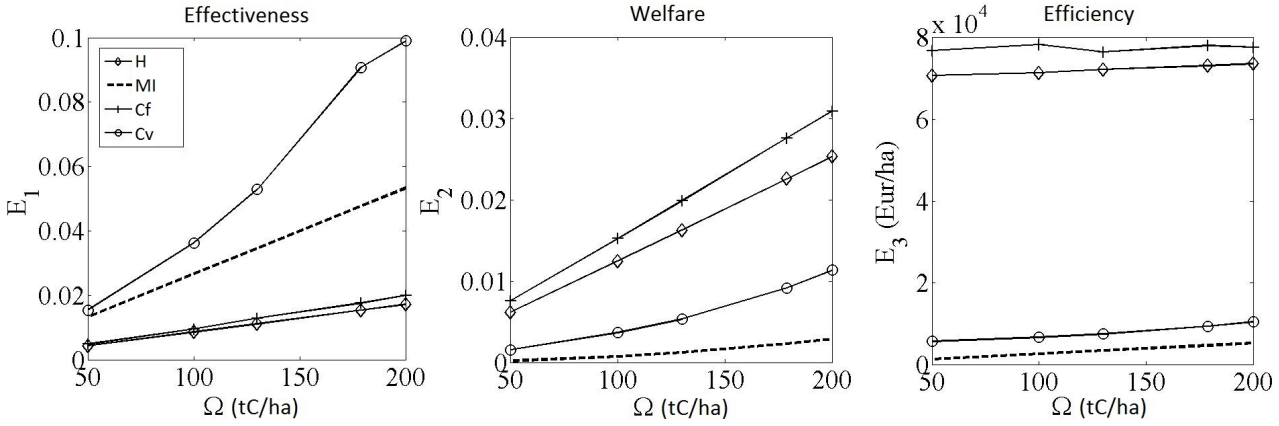

Fig. 3.D.2: Baseline performance across different average forest carbon contents (Ω).

Note: The figure captures the performance of the four baselines for different average carbon contents per hectare of forest. The historical deforestation rate (dB) is 200 ha/year. Corridor width is $x = 0.1$.

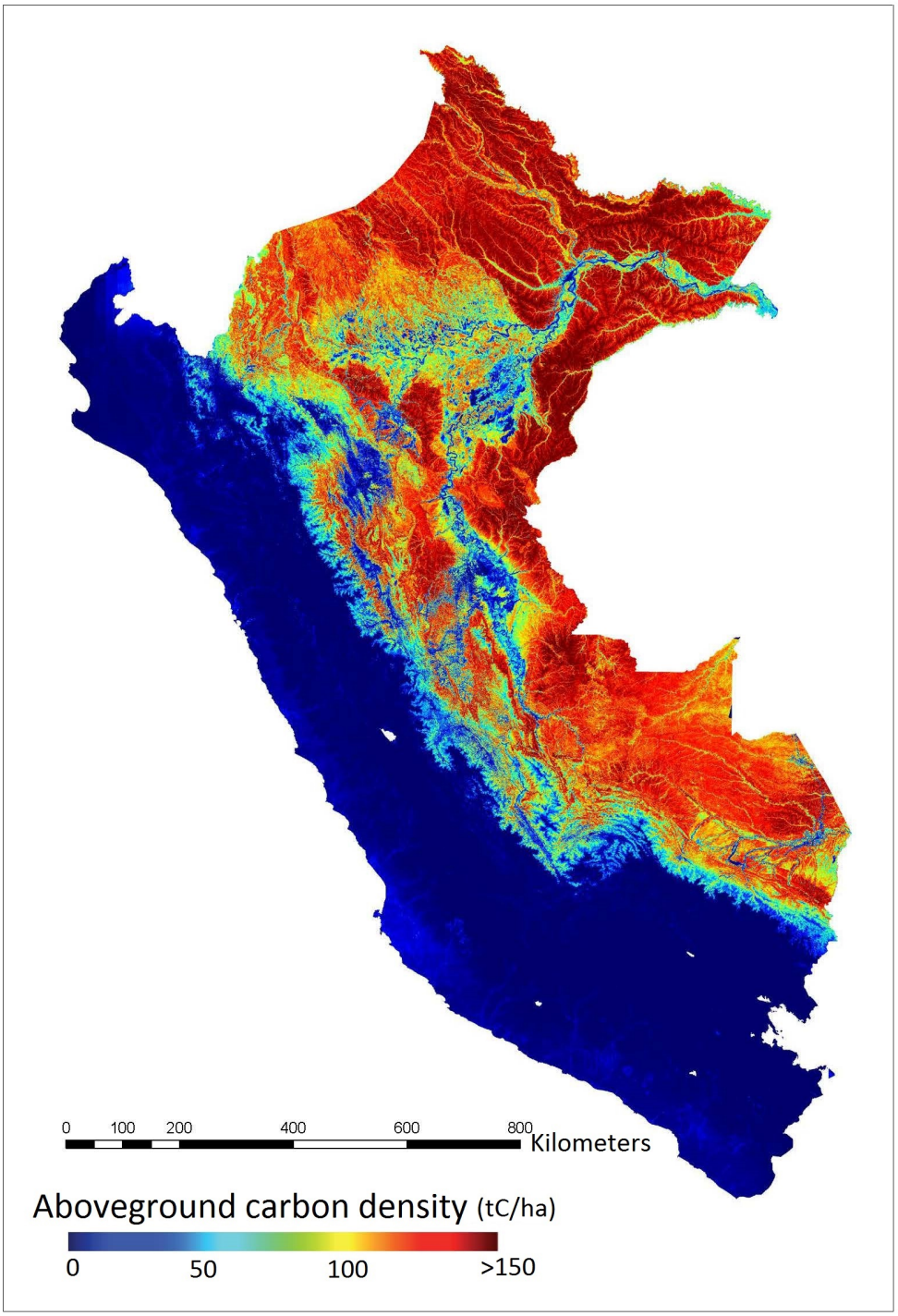

Fig. 3.D.3: Aboveground carbon content in Peru.

Source: *The High-resolution Carbon Geography of Peru*, Carnegie Institution for Science, 2014, available online at http://carnegiescience.edu/news/per%C3%BA%E2%80%99s_carbon_quantified_economic_and_conservation_boon.

3.D.2 The crediting threshold in the static baselines

In this section, we verify the change in the performance of the static baseline approaches to different crediting levels. The REDD rewards of the historical and fixed corridor approaches depend on the fixed threshold dB (Table 3.5). As mentioned in the baseline presentation (Section 3.2.2), the fixed threshold can be set equal to the average past deforestation in the area. Aside from data availability and estimation issues, linking rewards to a single value over a larger horizon can result in payments that reflect only partially actual efforts. There remains a certain level of risk involved in choosing a fixed threshold, and we check now the sensitivity of baseline performance to various levels (dB) against which rewards are accrued for the historical and fixed corridor schemes. The results are displayed in Fig. 3.D.4.

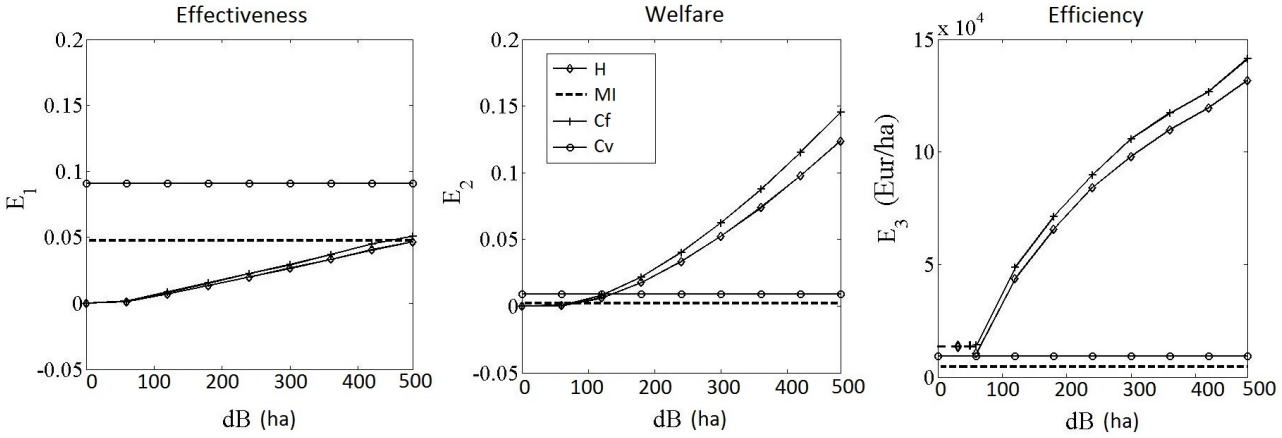

Fig. 3.D.4: Baseline performance across different fixed thresholds.

Note: The ranking of the four baselines changes across different historical deforestation rates. For the historical and fixed corridor baselines, efficiency is not defined for deforestation averages below 60 ha/year, where deforestation reduction and REDD costs are zero. Corridor width is $x = x_0 = 0.1$.

We find that the ranking of baselines is robust to variations in the fixed threshold level dB. The historical and the fixed corridor baselines gain ground at larger fixed thresholds, both in terms of effectiveness and welfare. However, these improvements come at the high cost of large losses in efficiency.

The increase in welfare at higher dBs follows from the fact that the REDD revenues of the historical and fixed corridor schemes are an increasing function of the fixed threshold. This is confirmed by the positive partial derivatives of the REDD revenue functions of the static baselines with respect to dB. Moreover, the higher REDD revenues foster increases in effectiveness, but also reductions in efficiency.

Our findings show that, if a static baseline is selected, the fixed threshold should be set above the average predicted deforestation rate in order to achieve stronger effectiveness and welfare results.

3.D.3 The discount rate (r)

In our initial calibration, the discount rate was chosen slightly below the growth rates of the composite commodity and REDD permit prices, depicting a setting in which forest exploitation and REDD bring higher financial benefits than saving at the discount rate. However, the discount rate in many developing countries varies widely from country to country and across time. Fig. 3.D.5 shows the discount rates for the years 2000 and 2012 in the Latin America region, with r taking values in the range [0.5%, 19.5%].

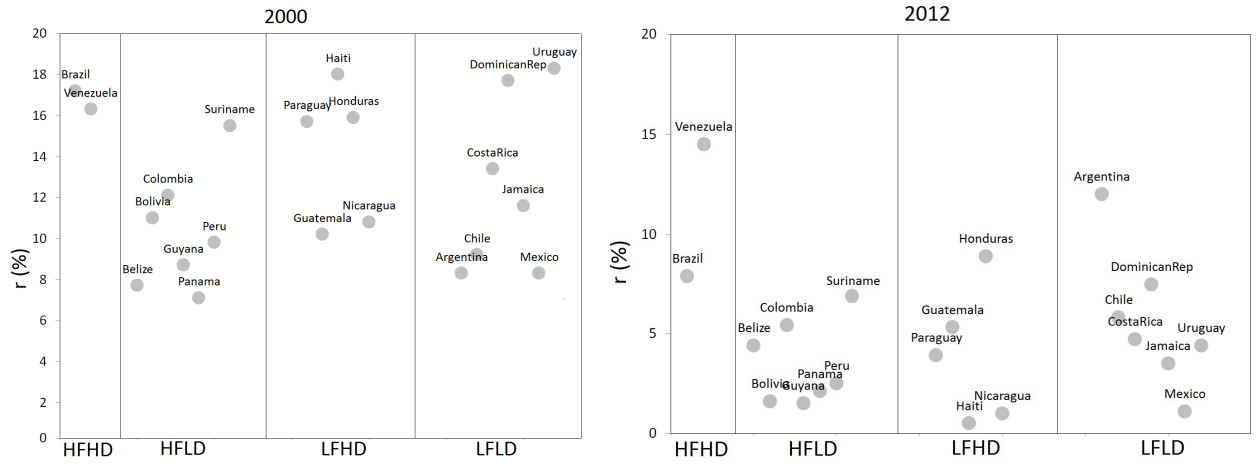

Fig. 3.D.5: Deposit rates (r) in the Latin America region in the years 2000 and 2012.

Source: Authors' own graphical representation based on the data provided by the World Bank, World Development Indicators, available online at http://wdi.worldbank.org/table/4.15.

We test the sensitivity of our results to changes in the discount rate. Fig. 3.D.6 shows the total deforested area under BaU and the four REDD baseline methodologies. The BaU optimal deforestation rate is a decreasing function in r (Eq. (3.A.11)), with higher impacts at later periods of time (as t approaches T). We detail the impact on the static and the dynamic baselines separately:

- Higher discount rates lower the total deforestation the static baselines. The landowner switches from REDD to BaU in the second part of the optimisation horizon; see Fig. 3.D.7. After the switch, the optimal deforestation follows the BaU path, achieving reductions in deforestation due to higher r.
- For the prospective baselines, whose reference levels depend on the BaU deforestation ($dB(t) = d_{BaU}(t)$), the impact of an increase in r on total deforestation is non-monotonous. The plots of total deforestation at different r present an inflection point (at $r = 8\%$ for MI and $r = 2\%$ for Cv). For r lower than the inflection point, an increase in r leads to a decrease in total deforestation; for r higher than the inflection point, an increase in r leads to higher deforestation. Below the inflection point, an increase in r results in lower $dB(t)$, requiring stronger reductions in deforestation for obtaining the same REDD profits. Reducing the deforestation rate pays off until some point (the inflection point), above which the time-varying threshold is so low that the opportunity costs of REDD exceed the benefits, and the landowner is better off following the BaU scenario (exiting REDD and increasing deforestation); see Fig. 3.D.7.

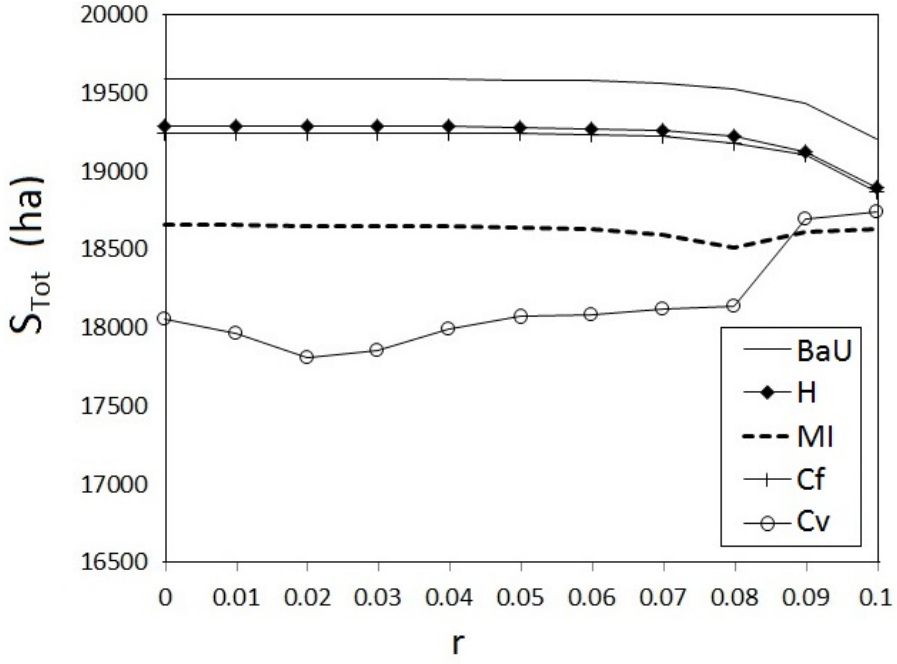

Fig. 3.D.6: Total deforestation across different baselines and discount rates (r).

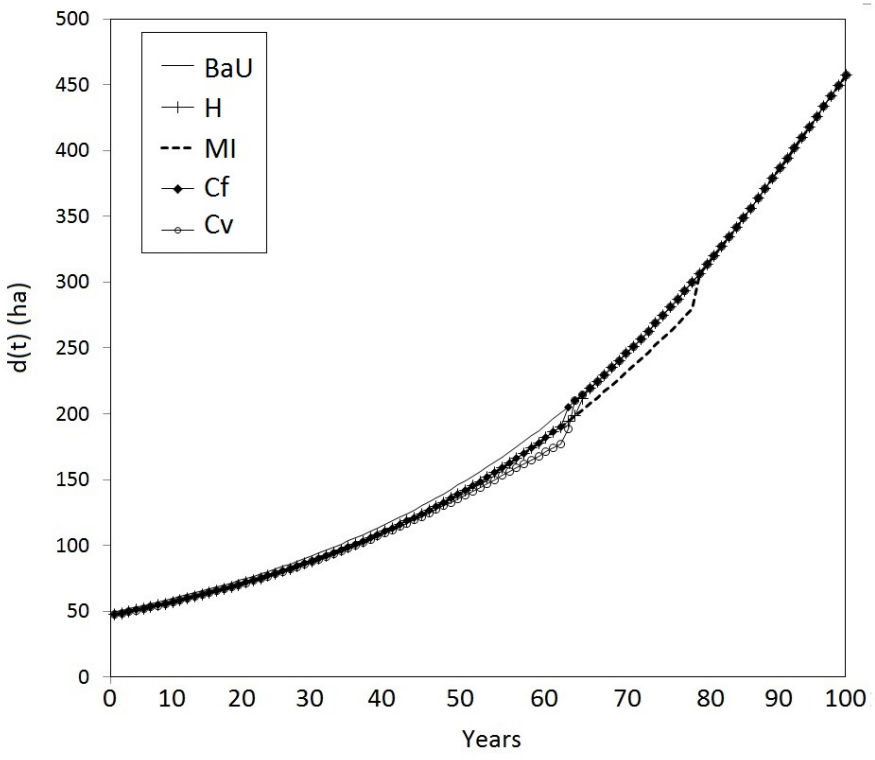

Fig. 3.D.7: Optimal deforestation across different baselines ($r = 0.1$).

Fig. 3.D.8 shows that the ranking of baselines across the three performance measures is robust across different discount rates. Additionally, for higher discount rates, the difference in performance between the static and dynamic baselines decreases in terms of effectiveness and efficiency, but widens considerably in terms of welfare. The results need to be interpreted carefully. First, at higher r, both BaU and static baselines result in lower total welfare. The impact of higher r on the change in welfare from BaU is measured by the E_2 indicator. With the income under the static baselines decreasing less than the BaU income, the percentage change in welfare appears to be increasing, despite the fact that

welfare itself is decreasing in r. Second, with efficiency measured as total discounted REDD revenues per hectares of avoided deforestation (the E_3 indicator), an increase in r reduces heavily the nominator (lower total discounted revenues), without increasing the forest area saved (we have seen that effectiveness is constant across different r). The improvement in efficiency at higher r is, therefore, just a discounting effect.

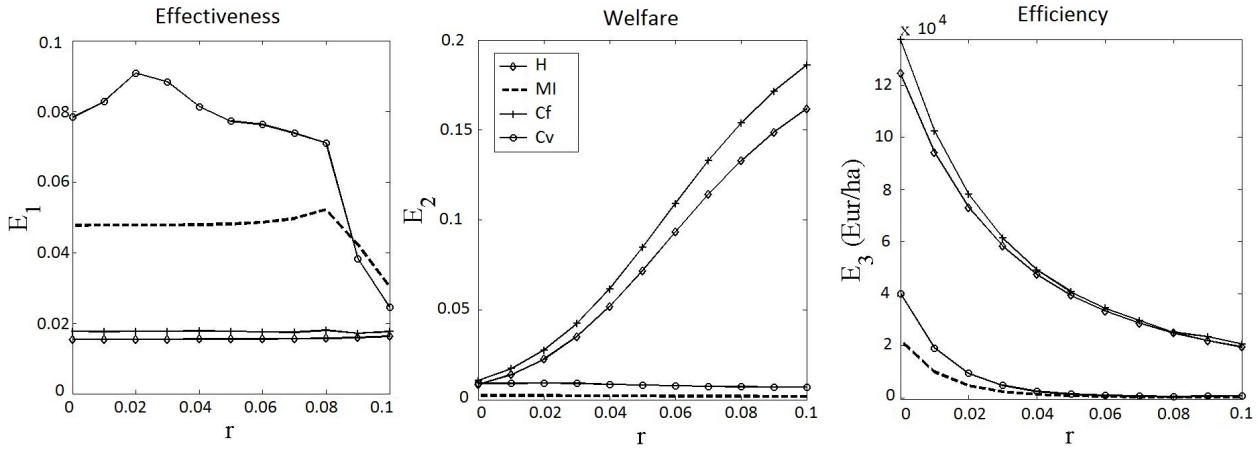

Fig. 3.D.8: Baseline performance across different discount rates (r).

Note: The figure captures the performance of the four baselines for different discount rates. The historical deforestation rate (dB) is at 200 ha/year. Corridor width is $x = 0.1$.

Summing up, we find that the ranking of baselines at different discount rates is consistent with the results presented under the initial calibration (Section 3.3.1). Higher discount rates lower the amount of total deforestation, especially for periods of time that are further away in the future. With lower deforestation also under the BaU, there is little room for additionality obtained by REDD, and the effectiveness of the different baselines decreases. We argue that policy makers interested in achieving high effectiveness, might prefer to direct REDD projects to countries of higher political stability, where discount rates are lower.

3.D.4 The growth rate of the composite commodity price (δ)

REDD programs are currently being designed in many developing countries, and the opportunity costs of avoiding deforestation are likely to vary widely across the different regions. The price dynamics of the alternative land use — in our model the growth rate of the composite commodity price (δ) — represents a key parameter influencing the opportunity costs of avoiding deforestation. Intuitively, the higher the growth rate of the composite commodity, the larger the price of the commodity in the future, strengthening the incentives to deforest more at later periods of time. With higher opportunity costs, REDD programs are expected to be less effective (Irawan et al., 2013).

We test the sensitivity of baseline ranking to different levels of opportunity costs, by varying the growth rate of the composite commodity. We observe that, with our calibration, for $\delta > 0.04$ REDD projects are no longer effective in reducing deforestation below BaU.

Fig. 3.D.9 shows that the ranking of baselines is consistent with the results presented in Section 3.3.1 across all values of δ. Higher values of δ increase deforestation under BaU and the four REDD scenarios, reducing the effectiveness of REDD, as expected. As δ gets higher, landowners opt out of REDD and follow the BaU, with their welfare converging to the BaU income. At lower effectiveness rates, payments for deforestation reductions under REDD are less cost-efficient.

The policy implication that arises from our analysis is that REDD programs need to be accompanied by payments that stand up to the specific opportunity costs of the region; otherwise, where opportunity costs are very high, REDD programs will be ineffective. This result is in line with the of findings of Irawan et al. (2013), who underline that REDD might not be able to compete with some alternative land uses that have prohibitive opportunity costs.

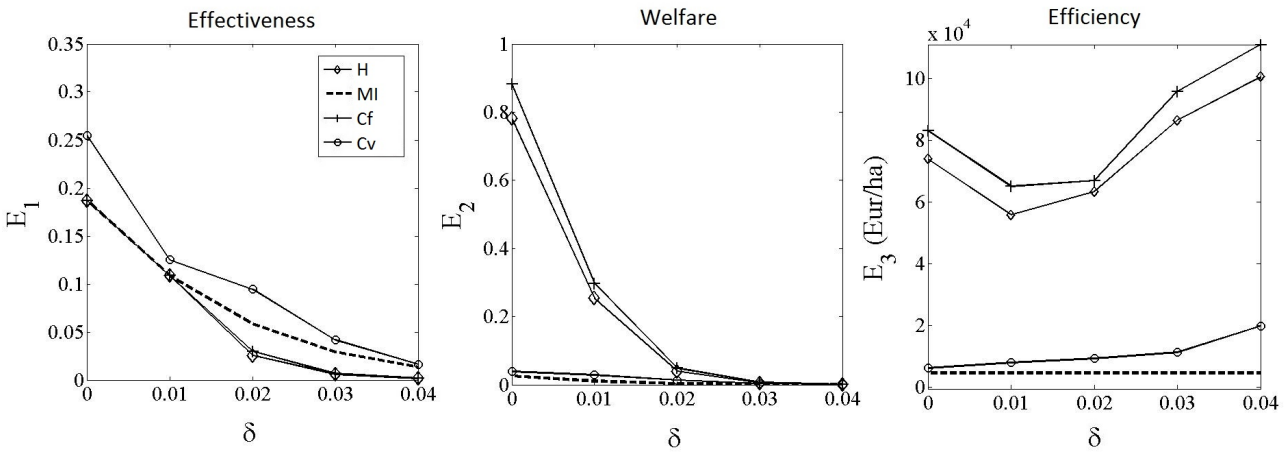

Fig. 3.D.9: Baseline performance across different growth rates of the composite commodity price (δ).

Note: The figure captures the performance of the four baselines for different growth rates of the composite commodity price. The historical deforestation rate (dB) is at 200 ha/year. Corridor width is $x = 0.1$.

3.D.5 The growth rate of the REDD permit price (γ)

The success of REDD is critically dependent on the incentive structure offered by the scheme. A key element is the amount of money rewarded per hectare of avoided deforestation, given by the REDD permit price (P^R) and its growth rate over time (γ).

Forest carbon projects have started their slow but steady increase at the end of the 1980s, and since then the largest part of demand for forest offsets has come from the voluntary carbon markets. Since 2005, forest carbon markets have experienced a significant boom, clearly marked by the development of REDD projects starting with 2010 (Diaz et al., 2011). REDD projects do not result in unique prices per ton of avoided emissions from deforestation; instead, prices vary according to demand levels, international regulation, and quality of the specific projects[29]. Fig. 3.D.10 captures the historical distribution of forest carbon prices and illustrates two key characteristics of the market: (i) forest carbon prices present large variability; and (ii) the trend in average prices after 2008 was increasing.

[29]Various international standards have emerged to distinguish between different forest projects, as for example the Panda Standard in China.

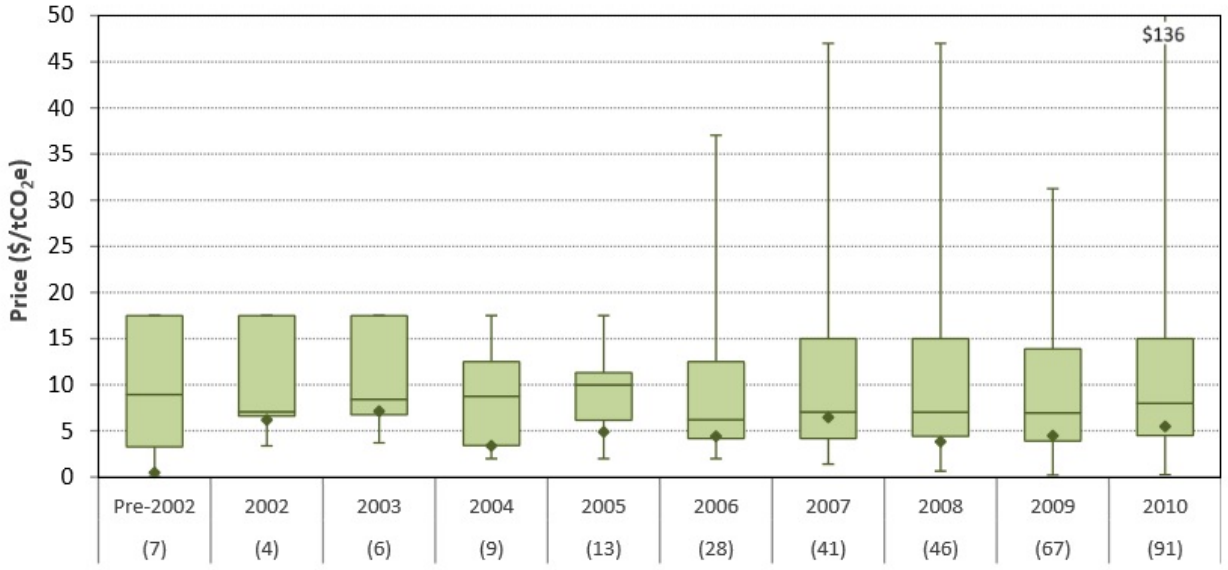

Fig. 3.D.10: Historical forest carbon price distributions (primary market).

Source: Diaz et al. (2011), Ecosystem Marketplace, available online at http://www.forest-trends.org/documents/files/doc_2963.pdf. Values in parentheses show the number of reported prices included in each year.

Motivated by the high price variability observed empirically, and by the fact that only increasing prices can motivate the sustained reduction of deforestation in the long run, we test the robustness of our results to different growth rates of the REDD credits price (γ).

Fig. 3.D.11 captures the performance of the four REDD baseline methodologies across different levels of γ. The baseline ranking presented in Section 3.3.1 is robust to changes in the growth rate of the REDD price. As expected, low future REDD prices diminish the incentives to avoid deforestation, and the modest reductions in deforestation are cost-inefficient. On the contrary, if the forest owner expects large future increases in REDD prices, he is motivated to keep the deforestation rates significantly lower than the BaU scenario; REDD projects are in this case likely to achieve high effectiveness. Moreover, the higher the growth rate, the larger becomes the difference in effectiveness between the static and the dynamic baselines.

The policy implication that results from our analysis is that it is not enough to ensure high future REDD payments in order to achieve large reductions in deforestation, but it is necessary to choose carefully the baseline methodology. While static baselines achieve limited effectiveness at high REDD rewards, a dynamic baseline approach, designed as a corridor around the estimated BaU deforestation rate, will strongly increase the effectiveness of REDD.

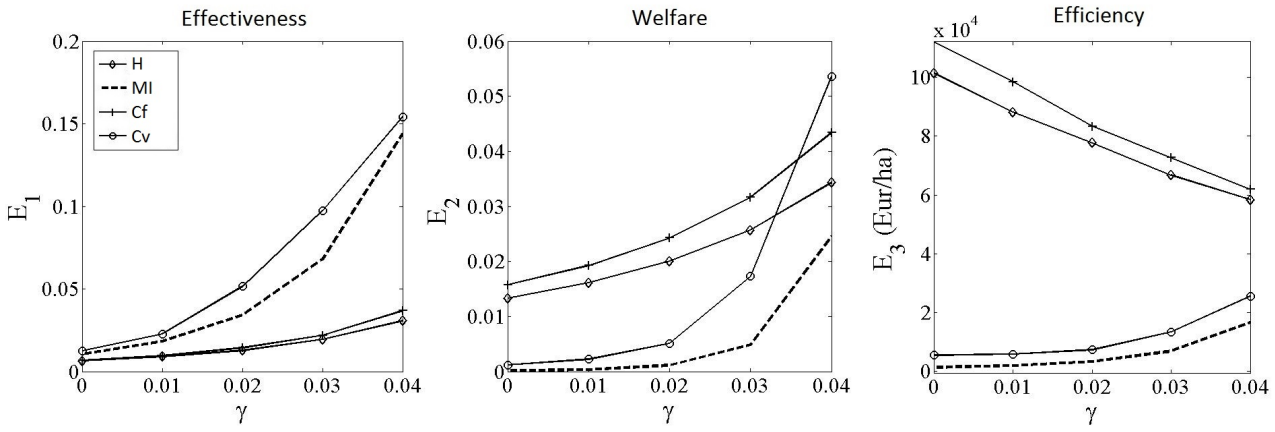

Fig. 3.D.11: Baseline performance across different growth rates of the REDD permit (γ).

Note: The figure captures the performance of the four baselines for different growth rates of the REDD permit price. The historical deforestation rate (dB) is at 200 ha/year. Corridor width is $x = 0.1$.

3.E Corridor bandwidth and symmetry

The fixed corridor

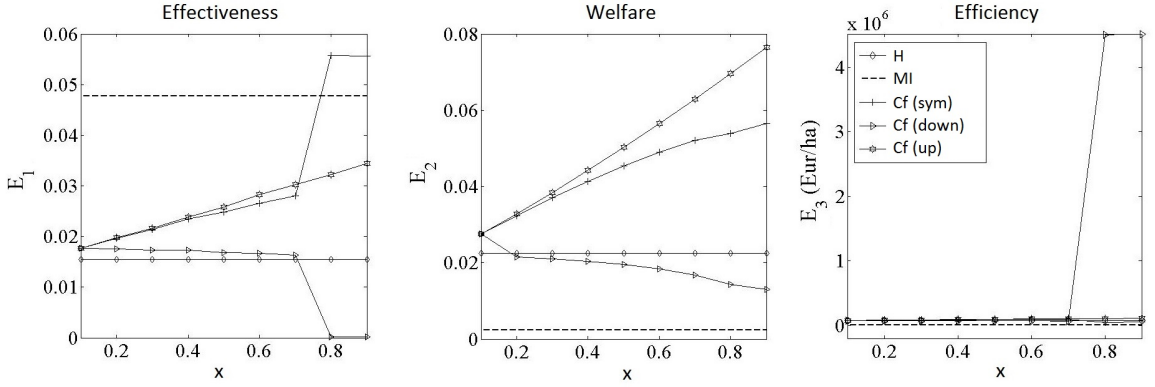

Fig. 3.E.1: Performance of the fixed corridor at different corridor bandwidths (x).

Note: The figure captures the performance of the fixed corridor for different corridor widths and symmetry assumptions. Considered corridors are symmetric (*sym*), upward (*up*), and downward-biased (*down*). Bounds in the downward-biased case are set as $dB^U = (1 + x_0)dB$, $dB^L = (1 - x)dB$; in the upward-biased case $dB^U = (1 + x)dB$, $dB^L = (1 - x_0)dB$, with $x \in [0.1, 0.9]$ and $x_0 = 0.1$

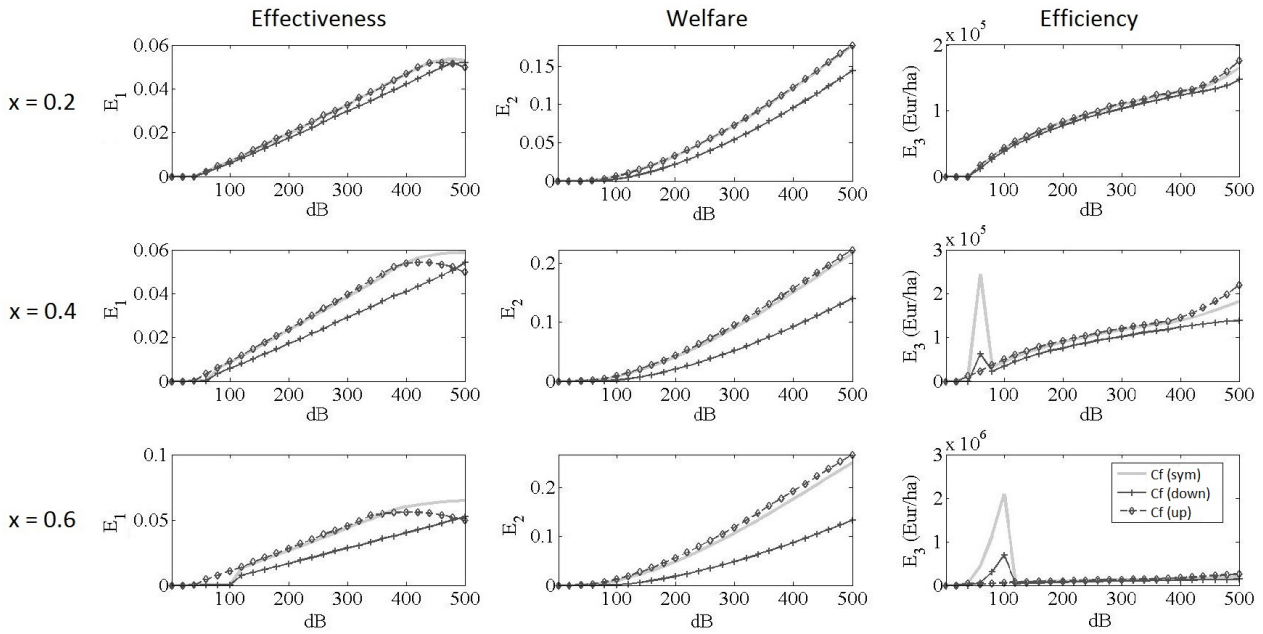

Fig. 3.E.2: Performance of the fixed corridor at different fixed thresholds (dB).

Note: The figure captures performance results of the fixed (symmetric, upward, and downward-biased) corridor. Three cases of corridor width are considered ($x \in \{0.2, 0.4, 0.6\}$) for different fixed thresholds ($dB \in [1, 500]$ ha/year).

Table 3.E.1: REDD revenues of fixed and variable corridors, detailed for different ranges of the deforestation rate.

Cf $RR(t) = P^R(t)\left(1 - \frac{(d(t)-dB^L)^+}{dB^U - dB^L}\right)(dB^U - d(t))^+$

Deforestation Range	Symmetric	Upward-biased	Downward-biased	Ranking
$d(t) \in [0,(1-x)dB]$	$P^R(t)((1+x)dB - d(t))$	$P^R(t)((1+x)dB - d(t))$	$P^R(t)((1+x_0)dB - d(t))$	$RR(t)^{up} = RR(t)^{sym} \geq RR(t)^{down}$
$d(t) \in ((1-x)dB,(1-x_0)dB]$	$P^R(t)\frac{((1+x)dB-d(t))^2}{2xdB}$	$P^R(t)((1+x)dB - d(t))$	$P^R(t)\frac{((1+x_0)dB-d(t))^2}{(x+x_0)dB}$	$RR(t)^{up} \geq RR(t)^{sym} \geq RR(t)^{down}$
$d(t) \in ((1-x_0)dB,(1+x_0)dB]$	$P^R(t)\frac{((1+x)dB-d(t))^2}{2xdB}$	$P^R(t)\frac{((1+x)dB-d(t))^2}{(x+x_0)dB}$	$P^R(t)\frac{((1+x_0)dB-d(t))^2}{(x+x_0)dB}$	$RR(t)^{up} \geq RR(t)^{sym} \geq RR(t)^{down}$
$d(t) \in ((1+x_0)dB,(1+x)dB]$	$P^R(t)\frac{((1+x)dB-d(t))^2}{2xdB}$	$P^R(t)\frac{((1+x)dB-d(t))^2}{(x+x_0)dB}$	0	$RR(t)^{up} \geq RR(t)^{sym} \geq RR(t)^{down}$
$d(t) \geq (1+x)dB$	0	0	0	$RR(t)^{up} = RR(t)^{sym} = RR(t)^{down}$

Cv $RR(t) = P^R(t)\left(1 - \frac{(d(t)-dB^L(t))^+}{dB^U(t) - dB^L(t)}\right)(dB^U(t) - d(t))^+$

Deforestation Range	Symmetric	Upward-biased	Downward-biased	Ranking
$d(t) \in [0,(1-x)dB(t)]$	$P^R(t)((1+x)dB(t) - d(t))$	$P^R(t)((1+x)dB(t) - d(t))$	$P^R(t)((1+x_0)dB(t) - d(t))$	$RR(t)^{up} = RR(t)^{sym} \geq RR(t)^{down}$
$d(t) \in ((1-x)dB(t),(1-x_0)dB(t)]$	$P^R(t)\frac{((1+x)dB(t)-d(t))^2}{2xdB(t)}$	$P^R(t)((1+x)dB(t) - d(t))$	$P^R(t)\frac{((1+x_0)dB(t)-d(t))^2}{(x+x_0)dB(t)}$	$RR(t)^{up} \geq RR(t)^{sym} \geq RR(t)^{down}$
$d(t) \in ((1-x_0)dB(t),(1+x_0)dB(t)]$	$P^R(t)\frac{((1+x)dB(t)-d(t))^2}{2xdB(t)}$	$P^R(t)\frac{((1+x)dB(t)-d(t))^2}{(x+x_0)dB(t)}$	$P^R(t)\frac{((1+x_0)dB(t)-d(t))^2}{(x+x_0)dB(t)}$	$RR(t)^{up} \geq RR(t)^{sym} \geq RR(t)^{down}$
$d(t) \in ((1+x_0)dB(t),(1+x)dB(t)]$	$P^R(t)\frac{((1+x)dB(t)-d(t))^2}{2xdB(t)}$	$P^R(t)\frac{((1+x)dB(t)-d(t))^2}{(x+x_0)dB(t)}$	0	$RR(t)^{up} \geq RR(t)^{sym} \geq RR(t)^{down}$
$d(t) \geq (1+x)dB(t)$	0	0	0	$RR(t)^{up} = RR(t)^{sym} = RR(t)^{down}$

Table 3.E.2: Change in REDD revenues when varying corridor bandwidth and deforestation rate.

Note: Columns 3 and 4 show results for first partial derivatives of REDD revenues with respect to corridor width across different symmetry scenarios for the fixed and the variable corridor. Columns 5 and 6 display results of the second partial derivative of REDD revenues, first with respect to corridor width, and then with respect to deforestation rate. A distinction is made between the case when the deforestation rate is below the lower boundary and the case when it is inside the corridor.

Symmetry	Boundaries	$\frac{\partial RR(t)}{\partial x}$	$\frac{\partial RR(t)}{\partial x}$	$\frac{\partial^2 RR(t)}{\partial x \partial d(t)}$	$\frac{\partial^2 RR(t)}{\partial x \partial d(t)}$
Cf		$d(t) \in [0, dB^L]$	$d(t) \in (dB^L, dB^U)$	$d(t) \in [0, dB^L]$	$d(t) \in (dB^L, dB^U)$
Symmetric	$dB^L = (1-x)dB$ $dB^U = (1+x)dB$	$P^R(t)dB > 0$	$P^R(t)\frac{((1+x)dB-d(t))((x-1)dB+d(t))}{2x^2 dB} > 0$	0	$P^R(t)\frac{dB-d(t)}{x^2 dB} > 0$ $(\forall d(t) \in (dB^L, dB])$
Upward-biased	$dB^L = (1-x_0)dB$ $dB^U = (1+x)dB$	$P^R(t)dB > 0$	$P^R(t)\frac{((1+x)dB-d(t))((x+2x_0-1)dB+d(t))}{(x_0+x)^2 dB} > 0$	0	$2P^R(t)\frac{(1-x_0)dB-d(t)}{(x_0+x)^2 dB} < 0$
Downward-biased	$dB^L = (1-x)dB$ $dB^U = (1+x_0)dB$	0	$-P^R(t)\frac{((1+x_0)dB-d(t))^2}{(x_0+x)^2 dB} < 0$	0	$2P^R(t)\frac{(1+x_0)dB-d(t)}{(x_0+x)^2 dB} > 0$
Cv		$d(t) \in [0, dB^L(t)]$	$d(t) \in (dB^L(t), dB^U(t))$	$d(t) \in [0, dB^L(t)]$	$d(t) \in (dB^L(t), dB^U(t))$
Symmetric	$dB^L(t) = (1-x)dB(t)$ $dB^U(t) = (1+x)dB(t)$	$P^R(t)dB(t) > 0$	$P^R(t)\frac{((1+x)dB(t)-d(t))((x-1)dB(t)+d(t))}{2x^2 dB(t)} > 0$	0	$P^R(t)\frac{dB(t)-d(t)}{x^2 dB(t)} > 0$ $(\forall d(t) \in (dB^L(t), dB(t)])$
Upward-biased	$dB^L(t) = (1-x_0)dB(t)$ $dB^U(t) = (1+x)dB(t)$	$P^R(t)dB(t) > 0$	$P^R(t)\frac{((1+x)dB(t)-d(t))((x+2x_0-1)dB(t)+d(t))}{(x_0+x)^2 dB(t)} > 0$	0	$2P^R(t)\frac{(1-x_0)dB(t)-d(t)}{(x_0+x)^2 dB(t)} < 0$
Downward-biased	$dB^L(t) = (1-x)dB(t)$ $dB^U(t) = (1+x_0)dB(t)$	0	$-P^R(t)\frac{((1+x_0)dB(t)-d(t))^2}{(x_0+x)^2 dB(t)} < 0$	0	$2P^R(t)\frac{(1+x_0)dB(t)-d(t)}{(x_0+x)^2 dB(t)} > 0$

Table 3.E.3: Double impact of varying the corridor width on REDD revenues.

Symmetry	Characteristics	Linear impact on REDD credits (n)	Non-linear impact on weight (ω)
Cf			
Symmetric	$dB^L = (1-x)dB$ $dB^U = (1+x)dB$ $n = (1+x)dB - d(t)$ $\omega = 1 - \frac{d(t)-(1-x)dB}{(1+x)dB-(1-x)dB}$	$\frac{\partial n}{\partial x} = dB > 0$	$\frac{\partial \omega}{\partial x} = \frac{d(t)-dB}{2x^2 dB}$ ($\frac{\partial \omega}{\partial x} < 0$ if $d(t) < dB$) ($\frac{\partial \omega}{\partial x} \geq 0$ if $d(t) \geq dB$)
Upward-biased	$dB^L = (1-x_0)dB$ $dB^U = (1+x)dB$ $n = (1+x)dB - d(t)$ $\omega = 1 - \frac{d(t)-(1-x_0)dB}{(1+x)dB-(1-x_0)dB}$	$\frac{\partial n}{\partial x} = dB > 0$	$\frac{\partial \omega}{\partial x} = \frac{d(t)-(1-x_0)dB}{(x+x_0)^2 dB} > 0$
Downward-biased	$dB^L = (1-x)dB$ $dB^U = (1+x_0)dB$ $n = (1+x_0)dB - d(t)$ $\omega = 1 - \frac{d(t)-(1-x)dB}{(1+x_0)dB-(1-x)dB}$	$\frac{\partial n}{\partial x} = 0$	$\frac{\partial \omega}{\partial x} = \frac{d(t)-(1+x_0)dB}{(x+x_0)^2 dB} < 0$
Cv			
Symmetric	$dB^L(t) = (1-x)dB(t)$ $dB^U(t) = (1+x)dB(t)$ $n = (1+x)dB(t) - d(t)$ $\omega(t) = 1 - \frac{d(t)-(1-x)dB(t)}{(1+x)dB(t)-(1-x)dB(t)}$	$\frac{\partial n}{\partial x} = dB(t) > 0$	$\frac{\partial \omega(t)}{\partial x} = \frac{d(t)-dB(t)}{2x^2 dB(t)} < 0$ (since optimal $d(t) < dB(t)$)
Upward-biased	$dB^L(t) = (1-x_0)dB(t)$ $dB^U(t) = (1+x)dB(t)$ $n = (1+x)dB(t) - d(t)$ $\omega(t) = 1 - \frac{d(t)-(1-x_0)dB(t)}{(1+x)dB(t)-(1-x_0)dB(t)}$	$\frac{\partial n}{\partial x} = dB(t) > 0$	$\frac{\partial \omega(t)}{\partial x} = \frac{d(t)-(1-x_0)dB(t)}{(x+x_0)^2 dB(t)} > 0$
Downward-biased	$dB^L(t) = (1-x)dB(t)$ $dB^U(t) = (1+x_0)dB(t)$ $n = (1+x_0)dB(t) - d(t)$ $\omega(t) = 1 - \frac{d(t)-(1-x)dB(t)}{(1+x_0)dB(t)-(1-x)dB(t)}$	$\frac{\partial n}{\partial x} = 0$	$\frac{\partial \omega(t)}{\partial x} = \frac{d(t)-(1+x_0)dB(t)}{(x+x_0)^2 dB(t)} < 0$

Chapter 4

Who is driving the volatility of the CO_2 permit price? Evidence from EU ETS Phase I

Abstract

This paper studies the relation between the trading activity and the volatility of the European Emission Allowance (EUA) price during Phase I of the European Union Emission Trading System (EU ETS). Our focus rests on the contrasting roles of different types of traders. We distinguish market players according to three criteria: emission regulation, initial endowment of permits relative to realized emissions, and exposure to other markets.
We find evidence of a positive and significant trading activity - volatility relation, which appears stronger when distinguishing between different types of traders. The positive relation can be mainly attributed to the energy providers. In contrast, industrial companies seem to have traded more frequently when volatility levels were lower. Finally, the non-liable players, mostly represented by financial intermediaries, appear to have taken the role of a flexible counterparty, adjusting to the needs of the liable sectors by trading more with the energy sector when volatility was higher, and more with the industrial firms when volatility was lower. We discuss possible explanations for these contrasted positions.
Understanding the link between the trading activity of different market players and price volatility is relevant for evaluating the efficiency of the EU ETS. Although the trading activity - volatility relation is generally positive, many players remained often inactive and traded mostly when volatility levels were lower. In this setting, new information is expected to be more slowly incorporated into prices and market efficiency is not maximized.

Keywords: EU ETS; Permit price; Volatility; Liable and non-liable participants; Market efficiency.

Acknowledgements: This paper has benefited greatly from the suggestions and insights of Regina Betz, Johanna Cludius, Jakub Rojcek, Kathrin De Greiff, Delia Coculescu, and Souvik Datta. The author is especially thankful to Regina Betz and Johanna Cludius for providing access to and continuous support with the EUTL dataset.

4.1 Introduction

Due to the pressing dangers of climate change and the low progress on mitigation agreements at the international level, countries and regions have started to develop domestic solutions to reduce emissions. The proposed regulations take different forms around the world, relying on cap-and-trade schemes, carbon taxes, subsidies for energy efficiency improvements, and setting of energy efficiency standards.

The theoretical fundaments of emission allowance markets have been consolidated in the last half decade (Dales, 1968; Montgomery, 1972; Rubin, 1996; Cronshaw and Kruse, 1996), putting forth the idea that tradable pollution rights would lead to a cost-efficient solution to handle externalities from production. The European Union Emission Trading System (EU ETS) and the regional carbon markets set in China[1] are examples of existing *quantity*[2] approaches to pollution regulation.

The EU ETS started its activity in 2005 and aims to regulate the greenhouse gas (GHG) emissions of its area.[3] The EU ETS has been divided into four compliance phases so far: Phase I 2005-2007, Phase II 2008 - 2012, Phase III 2013-2020, and Phase IV 2021 - 2028. The first period was intended to test and evaluate the performance of the emission market. The second phase (2008 - 2012) imposed an emission reduction target in line with the Kyoto Protocol's first commitment period. The third trading period (2013 - 2020) brought along considerable revisions to the system's operational design, concerning, in particular, the permit allocation procedure and the imposition of an EU-wide emissions cap. The rules of the expected fourth phase are still under development. In this paper, we focus on the (pilot) Phase I of the EU ETS.

The EU ETS works on a *cap-and-trade* principle. The heavy polluters of the European industry are periodically assigned an overall limit for their emissions. At the beginning of each compliance year, liable entities are allocated a number of European Union Allowance Units (EUAs). While the allocation was done almost entirely for free in the first years of the EU ETS, beginning with 2013, auctioning became the main method for allocating allowances. Within the cap, liable entities can trade EUAs according to their compliance needs. For emission levels below the cap, unused permits are eligible for sale; at the end of each compliance year, penalties and additional permits need to be provided in case of uncovered emissions. On the carbon markets, both regulated (liable) and non-regulated (non-liable) entities can trade permits.

During the several years since the opening of the EU ETS, the permit price has diverted significantly from its theoretical optimum, namely the marginal abatement cost. Instead, EUA prices have been fairly volatile, experiencing at times jumps, and converging to zero due to excess

[1] In China, several ETS schemes have opened since 2013 in six provinces: Beijing, Guangdong, Hubei, Shanghai, Shenzhen, and Tianjin, making China the second largest carbon market in the world after the EU ETS (World Bank, 2014).

[2] A pollution regulation based on a tax system is known as a *price* approach.

[3] The EU ETS currently covers more than 11,000 installations in 31 countries: the 28 European states as well as Iceland, Lichtenstein, and Norway. The GHGs covered are carbon dioxide (CO_2), nitrous oxide (N_2O), and perfluorocarbons (PFCs). About 45% of the total EU emissions are currently covered by the EU ETS (European Commission, 2015).

supply (Paolella and Taschini, 2008; Daskalakis et al., 2009; Uhrig-Homburg and Wagner, 2009; Hintermann, 2010, 2012).

An extended thread of literature has steadily evolved since the opening of the EU ETS, trying to pinpoint the drivers behind the atypical evolution of prices on this compliance market. The first branch of literature considers that, in an efficient market, prices are related to fundamentals. For Phase I, several studies identify energy prices and weather conditions as the main drivers of carbon prices (Christensen et al., 2005; Bunn and Fezzi, 2007; Mansanet-Bataller et al., 2007). Alberola et al. (2008a) confirm that carbon prices react to changes in energy prices, and underline the additional influence played by unanticipated temperature changes during colder periods. Finally, they show that institutional decisions regarding permit allocation exercise at times a stronger impact on EUA prices than fundamentals. Hintermann (2010) finds that carbon prices were more likely to reflect marginal abatement costs after April 2006, when fuel prices, temperature levels, and precipitation began to exercise influence over EUA prices.

Due to the low evidence of abatement and highly volatile prices, researchers started to look for price drivers that go beyond fundamentals related to abatement. The specificities of the carbon market, as an artificially created one, make it susceptible to various market design properties, such as the possibility of permits transferability from one compliance period to the next (banking) and the allocation process (grandfathering). More importantly, the penalty level and the (perceived) difference between allocated permits and realized emissions have shown a strong influence on price formation (Chesney and Taschini, 2012; Hintermann, 2012).

The properties of the EUA price have also been analyzed from a time series perspective. During Phase I, the carbon price has been documented to exhibit structural breaks, jumps, and heavy tails (Paolella and Taschini, 2008; Daskalakis et al., 2009; Uhrig-Homburg and Wagner, 2009). Recent studies draw attention to the indisputable presence of jumps; Chevallier and Sévi (2014) show that, for the period 2009 - 2010, carbon futures prices do not seem to contain a continuous (Brownian motion) component, and can be better characterized by a centered Lévy or Poisson process.

In this paper, we contribute to the discussion on the dynamics of the EUA price by taking a players-oriented approach. Namely, we examine the relation between the volatility of the allowance price and the trading activity of different types of participants in the carbon market. On mature financial markets, previous literature documents a strong and positive trading activity - volatility relation (Clark, 1973; Harris and Raviv, 1993; Shalen, 1993). Moreover, the association is better explained when distinguishing between different types of traders (Daigler and Wiley, 1999). Our focus is on the artificially created EU ETS market for emission compliance, whose special setting is likely to allow for traders with significantly different characteristics.

A study closely related to ours is the one of Kalaitzoglou and Ibrahim (2013). The authors use high frequency data in order to analyse the microstructure of the carbon futures market in Phases I and II. Based on the volumes traded and the duration between consecutive trades, they identify three categories of distinct traders, which they name as: informed, fundamental, and uninformed. The authors provide, however, no evidence that the trader types actually possess the characteristics of their category title, i.e. if they actually have access to different information or not. First, they find that the *informed* players trade high volumes at low duration. Second, the *fundamental* traders time their trades, and prolong the revelation of the information that the order flow of informed trades started. Third, the *uninformed* players have both lower volumes and longer duration. The authors show that, during the first two phases of the EU ETS, most players acted similarly to the *uninformed* type, trading for compliance

reasons; however, some periods of intense trading with fast information arrival can be identified, where the informed type had a dominating strategic behavior.

In this paper, we are also interested in identifying different categories of market participants. Unlike the work of Kalaitzoglou and Ibrahim (2013), we define trader types according to characteristics that go beyond the observed trading behavior; instead, we focus on the special design of the EU ETS as a compliance market. For trader type classification we rely on three criteria: (i) compliance regulation, (ii) initial endowment of permits relative to actual emissions, and (iii) players' exposure to other markets.

Our study uses the European Union Transactions Log (EUTL) to track daily permit transfers across the individual accounts of the liable and non-liable players in Phase I of the EU ETS (2005 - 2007). Relying on the procedure suggested by Bessembinder and Seguin (1993) and Daigler and Wiley (1999) for financial markets, we estimate the trading activity - volatility relation during the first phase of the EU ETS. Our procedure consists in simultaneously estimating returns and volatility, via a series of iterations between two equations describing conditional daily price changes and volatility.

Three main findings result from our analysis. First, we show that, common to most financial markets, volatility is persistent and clusters. Evidence of seasonality is also documented, with volatility being especially high in April when, under the EU ETS design, liable firms need to surrender allowances covering their cumulated emissions, and the amount of verified emissions for the preceding year is publicly disclosed. Second, the trading activities of stronger intensity (larger volumes and higher number of transfers) are generally positively and significantly associated with higher volatility levels for the analysed period. Third, the trading activity - volatility relation can be better captured when specifying the sector initiating the trade, the specific counterparty, and whether or not the player acted as a buyer or a seller. The positive association can be attributed in particular to the energy sector, which appears to have traded more during times of higher volatility levels. In contrast, the industrial sector tended to trade more often when volatility was lower. The non-liable players, mostly represented by financial intermediaries, seem to have acted as a flexible counterparty, answering to the differentiated needs of the liable sectors, by trading more with the energy sector when volatility levels were higher, and more with the industrial companies when volatility levels were lower.

Characterising the trading activity - volatility link is relevant for several reasons. First, estimating price differences and volatility on autoregressive terms reveals the degree of market predictability and maturity. Second, estimating permit price volatility brings insights into how the design of the EU ETS can help the European Union reach its target of reducing emissions.[4] The aim of the EU ETS is to generate a price signal that can encourage firms to reduce their emissions (Paolella and Taschini, 2008; Bredin et al., 2014) through investments in cleaner technologies. In an efficient market, permit prices should come close to the marginal abatement cost. From a theoretical point of view, price volatility and trading activity should be positively correlated, allowing new information to be incorporated into prices and market participants to adjust their permit holdings accordingly. However, we find that a large share of market participants remained often inactive during Phase I, and tended to trade, on average, more when price volatility was lower. This indicates lower liquidity contributions by some sectors at times of intense information revelation, and could suggest that price adjustment was slower than in well-established, more efficient markets.

[4]The commitment taken by the European Union was to reduce emissions by 8% by 2012, primarily through its cap-and-trade scheme. Starting in 2013, the cap is reduced by 1.74% every year, such that by 2020 the GHGs of the liable sectors are expected to be 21% lower than in 2005.

The policy implications of our analysis are direct; a cap-and-trade market is unlikely to achieve efficiency if many players are inactive and reluctant to trade during periods of intense information arrival. A directed engagement of less active players could possibly counteract this trend and lead to improved market efficiency.

The rest of the paper is organized as follows. In Section 4.2, we discuss the existing theories formalizing the trading activity - volatility relation. The methodology employed for estimation is described in Section 4.3. Section 4.4 describes the dataset used and the main characteristics of the EU ETS. Section 4.5 presents the results. Section 4.6 discusses possible explanations for our findings. Section 4.7 concludes and reviews interesting avenues for further research.

4.2 Trading activity - volatility relation

Our study is related to the branch of literature that associates changes in prices with trading activities, such as transacted volumes or number of daily transactions. Two complementary theories have been developed to explain this empirically observed link. On one hand, the 'mixture of distributions' theory considers volume and volatility to be contemporaneously determined by the arrival of new information and predict a positive volume - volatility association (Clark, 1973; Tauchen and Pitts, 1983; Harris, 1986). On the other hand, the 'dispersion of beliefs' theory, developed among others by Harris and Raviv (1993) and Shalen (1993), considers that traders differ in the way they interpret new information and trade according to their distinctive beliefs. The dispersion of expectations creates a positive correlation between traded volumes and price variability.

The positive volume - volatility relation on established financial markets has been empirically documented since a long time (an early review is given in Karpoff (1988)). Further studies have shown that partitioning volume into expected and unexpected components increases the fit of the models, with unexpected volumes playing a dominating role (Bessembinder and Seguin, 1992, 1993). A complementary branch of literature (Jones et al., 1994) points to the fact that the number of daily transactions is strongly related to price change variability. They conclude that the trading activity relevant for price movements is the number of daily trades, and not the volume levels *per se*.

Assuming heterogeneous agents, with different characteristics or diverging interests, one could expect that the sign and strength of the trading activity - volatility relation depend on the type of agent that participates in the trade. Indeed, this prediction is confirmed by empirical evidence. Daigler and Wiley (1999) analyse several commodity futures markets and find that, depending on the type of trader (classified in their work according to the distance to the trading floor), the association between volumes and volatility can be either positive or negative.

In this paper, we study the trading activity - volatility relation on the EU ETS market during Phase I. In this trial period, the carbon market exhibited many features of an emerging market, with low initial liquidity and large variations in prices. Fig. 4.1 shows the evolution of carbon spot prices and traded volumes. Permit prices experienced large jumps caused by the arrival of compliance information[5] (Alberola et al., 2008a). Fig. 4.1 gives a first impression on the relation between volumes and price changes. It appears that larger movements in prices can be matched with contemporaneous spikes in volumes.

[5]Such events include the April 2006 publication of realized emissions for 2005, and the October 2006 announcement of reduced allocation for the EU ETS second phase.

The special setting of this market allows for players that are different from multiple perspectives. We identify three points of possible divergence in agents' characteristics, namely: (i) compliance regulation, (ii) initial endowment of permits relative to actual emissions, and (iii) exposure to other markets.

First, while most traders are subject to pollution compliance rules and need to acquire sufficient permits to cover their cumulated emissions, the EU ETS is open also to non-liable entities, such as non-emitting companies or individual and institutional investors. Their participation is expected to increase liquidity on the carbon markets, while trading for speculation or hedging purposes (Daskalakis and Markellos, 2008). Our analysis might be relevant for indicating possible benefits or disadvantages of opening the permit market to non-liable players.

Second, in the first phase of the EU ETS, the liable players started off with freely allocated permits. The extent of the initial permit allocation depended on several factors, including emission forecasts, self-declared historical emissions, the sector of activity, and the bargaining power of the emitter (Betz et al., 2004; Alberola et al., 2008b). As such, some players ended up being generally over-allocated with permits relative to their actual emissions, while others under-allocated. In a cap and trade system without banking or borrowing, where the supply of permits is fixed by initial allocation of permits and excess permits are worthless at the end of the compliance period, it is likely that players adopt different trading strategies depending on their expected over- or under-allocation status. Estimating the trading activity - volatility relation according to this dimension can bring insights into the different permit trading strategies of players depending on their excess or deficit of allowances.

Third, both liable and non-liable players operate primarily in other markets than the EU ETS and are, thus, exposed to different external risks and opportunities. Alberola et al. (2008b) show that, during Phase I, the annual growth rate of output production greatly depended on the sector of activity. Moreover, the authors find carbon price changes to be significantly related to the size of output production in three sectors: combustion, paper, and iron. Liable agents are likely to build their permit trading strategies and their output production decisions simultaneously; resulting permit trades may reflect the conditions on both markets. For example, Daskalakis and Markellos (2009) conjecture a positive relation between emission allowance spot returns and electricity risk-premia, possibly due to the coordination of the decisions regarding when and how much power to produce and when to abate emissions. In contrast, non-liable players, such as banks and insurance companies, are likely to regard the trading of carbon permits in a financial framework, for hedging or speculation (Engels, 2009). By grouping accounts along the sectoral breakdown, we intend to shed light on the trading strategies of players exposed to different primary business activities.

We have, thus, several reasons to believe that, in this designed market for pollution compliance, the involved market players differ in key aspects and that their permit trades reflect these differences. As such, our work makes similar assumptions to those in Shalen (1993) and Daigler and Wiley (1999), where agents are heterogeneous and their trades are expected to associate differently with price volatility. We dedicate the remaining of the paper to the investigation of the sign and the strength of the trading activity - volatility association, and to the analysis of whether or not this relation varies according to the type of agent involved in the trade.

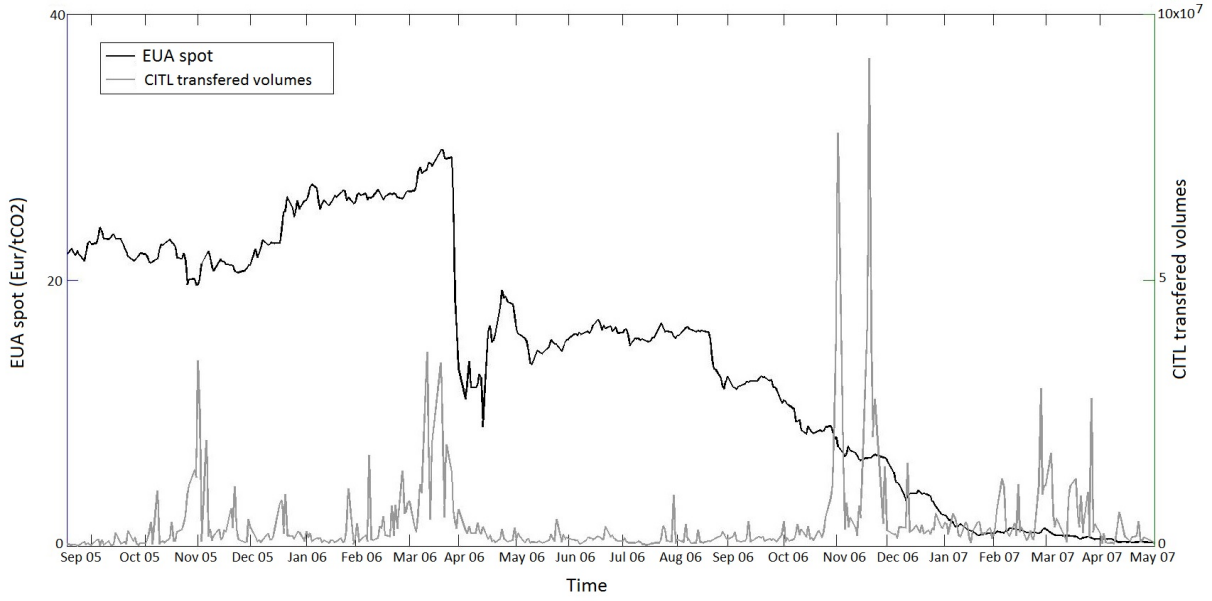

Fig. 4.1: EUA spot price and transferred volumes (Sept. 2005 - May 2007).

4.3 Methodology

In order to analyse the trading activity - volatility relation on the carbon market, we rely on the methodology proposed by Davidian and Carroll (1987), and applied to financial markets by Schwert (1990) and Bessembinder and Seguin (1992, 1993), among others. The procedure achieves the computation of unbiased estimates of the conditional daily return standard deviation, and simultaneously accounts for the persistence of volatility. Our paper is closely related to the study of Daigler and Wiley (1999), who estimate the association between the price volatility and the trading activity of different types of players on commodity futures markets.

Following the standard procedure in the literature, our methodology consists of iterating between a conditional mean and a conditional volatility equation of the type:

$$D_t = \alpha + \sum_{j=1}^{n} \nu_j D_{t-j} + \sum_{j=1}^{n} \mu_j \hat{\sigma}_{t-j} + U_t \tag{4.1}$$

$$\hat{\sigma}_t = \delta + \sum_{j=1}^{n} \gamma_j \hat{\sigma}_{t-j} + \sum_{j=1}^{n} \beta_j \hat{U}_{t-j} + \sum_{k=1}^{m} \eta_k TA_{k,t} + e_t. \tag{4.2}$$

Above, D_t stands for the observed change in price (P_t) from one day to the next, i.e. $D_t = P_t - P_{t-1}$, and the residuals U_t are the unexpected price changes, with $\hat{U}_t = D_t - \hat{D}_t$.[6] $\hat{\sigma}_t = |\hat{U}_t|\sqrt{\frac{\pi}{2}}$ is the estimated conditional standard deviation. The fitted values from Eq. (4.1) represent price changes conditional on autoregressive terms and lagged volatilities.

[6]In the original models, D_t stands for the observed percentage change in price on day t. We opted for the change in price in order to avoid the inflation of volatility to very large levels in the second part of 2007, when the permit price basically converged to zero, and daily movements of one tick would result in returns of 100%.

Eq. (4.2) estimates conditional standard deviations based on lagged volatilities (to account for persistence), lagged price changes (to allow for effects of recent realized returns on volatility), and the trading activity (TA_t). Based on the findings of Daigler and Wiley (1999) and Jones et al. (1994), we proxy trading activity with the help of two indicators: (i) daily transferred EUA volumes and (ii) number of daily permit transfers. Several studies have documented that traded volumes are highly serially correlated and, thus, easily forecastable (Bessembinder and Seguin, 1993). We fit the transferred volumes with the help of an ARIMA(p,d,q) procedure, in order to distinguish between expected and unexpected trading activities. Following Bessembinder and Seguin (1992, 1993), we define expected volumes as the fitted values obtained from the ARIMA(p,d,q) procedure, while the residuals represent unexpected volumes. Distinguishing between the expected and unexpected components allows us to determine whether surprises or trend activity are more strongly associated with volatility. The number of daily permit transfers and the unexpected volumes represent contemporaneous variables with price change volatility; thus, our analysis will identify how the trading activity and volatility variables tend to covary in response to external factors, such as new information arrivals.

The iterative procedure between Eq. (4.1) and (4.2) consists of several steps, as detailed in Appendix 4.A. After having selected the number of autoregressive lags in price changes with the help of the Akaike Information Criterion (AIC), we first estimate Eq. (4.1) without the lagged volatility terms. The residuals from this estimation are then used for the volatility transformation, and the model in Eq. (4.2) is fitted. We then re-estimate the price changes via Eq. (4.1), using the fitted volatilities from the previous step. We recompute the unexpected price change ($\hat{U}_t$) and the volatility transformation ($\hat{\sigma}_t$), and re-estimate the conditional volatility with the help of Eq. (4.2).

4.4 Data

Our analysis uses the European Union Transactions Log (EUTL)[7] to track all daily permit transfers in Phase I of the EU ETS. The EUTL data is published with a five-year delay, currently offering information up to the end of 2009.[8] Due to the lack of availability until recently, this dataset has been analyzed in only a limited number of studies (Zaklan, 2013; Jaraite and Kazukauskas, 2013; Betz and Schmidt, 2015) that attempt to identify different patterns in the trading strategies of liable companies. The dataset offers information regarding the daily transfers of allowances, and specifies the parties and volumes involved in each transaction. However, no information is available regarding the price at which the permit transfers have been concluded.

In Phase I, the allocation of permits to the liable companies was done almost entirely for free (in percentage of 99%). To exchange permits, all interested entities could open trading accounts. Three types of accounts could be opened for permit management: (i) mandatory Operator Holding Accounts (OHAs) opened by the liable companies; (ii) Person Holding Accounts (PHAs) that could be opened by any interested entity, liable or not; and (iii) mandatory country accounts opened by the member countries of the EU ETS for administrative purposes. As revealed by Betz and Schmidt (2015), the vast majority of accounts remained mostly inactive during the Phase I.

[7]The EUTL is a central transaction log, run by the European Commission, which checks and records all transactions taking place within the trading system.

[8]In contrast, US trading schemes have registry data available in real time (Betz and Schmidt, 2015).

4.4.1 Trading activity of heterogeneous agents

In our study, we use the transfer data provided by the EUTL to proxy the daily volume traded on the carbon markets. This dataset gives us the unique possibility to distinguish the volumes traded by each account holder,[9] and to group daily transfers according to different criteria.

As mentioned in Section 4.2, EU ETS market players are likely to differ in three dimensions: (i) compliance regulation, (ii) initial endowment of permits relative to actual emissions, and (iii) exposure to other markets. First, we distinguish between liable and non-liable players depending on whether or not the account was subject to compliance regulation. Second, not all players operating in the EU ETS have started Phase I under the same permit allocation conditions. Depending on the initial endowment of permits relative to actual emissions, we group traders into over-allocated, under-allocated, and non-liable.[10] The partition criterion consists of comparing the number of initially allocated allowances with the number of allowances surrendered at the end of the compliance period. Third, the EU ETS players operate primarily on other financial or output markets, and belong thus to different sectors of activity. Based on each account's corresponding sector code, we distinguish three categories of players, which for simplicity we denote as: the energy sector, the industrial firms, and the financial institutions.[11] The players entering the financial institutions category are non-liable entities, and during the analysis of results we will refer to them as non-liable, to maintain consistency with the other criteria for differentiating players.

Table 4.1 presents information regarding the trading activity of market players grouped according to the three criteria. While the liable group consists of a large number of players, only few accounts enter the non-liable category. Nonetheless, the number of transfers and the volumes have been fairly balanced between the two groups. This implies that the non-liable players, consisting mostly in financial intermediaries, have been much more active, on average, than a common liable player. Among the liable accounts, the energy providers appear to have been the most active market participants. According to the initial permit endowment information, most liable players have received more permits than finally surrendered, both among the energy and the industrial firms. Being over-allocated appears to have been associated, on average, with a more intense trading activity, both in terms of the number of transfers and volumes.

Table 4.2 lists the correlation coefficients characterising the trading activity of players grouped according to the three sectors of primary business activity. Two indicators of trading activity are considered: (i) transferred volume levels and (ii) number of transfers. The coefficients are positive and one can notice the higher connectedness between the trading activities of the energy and the industry sector, as well as the energy and the non-liable one. Higher coefficient values are observed for the number of transfers. It appears that the number of permits each

[9] The account holder name is relevant for all transactions registered under one name and it aggregates, if needed, several different account IDs belonging to the same holder. For more information regarding the aggregation, please refer to Cludius (2015).

[10] The under-/over-allocation analysis needs to be interpreted with care. When analysing the data, some inconsistencies have been found in the information regarding the initial allocation of permits. Namely, some liable accounts appear with zero initial permit allocation. This is inconsistent with reality, where all liable accounts benefited from grandfathering. We believe the problem arises due to the late opening of some registries, therefore missing some of the initial permit activity. However, the number of concerned accounts is limited and we expect this problem not to significantly influence the results.

[11] In our classification, the accounts of the *energy* sector belong to: electricity and heat, energy service providers, mining, and refineries. The accounts of the *industrials* sector include: airport and trade fairs; automotive and transport; bricks and ceramics; cement and chalk; chemicals and pharmaceuticals; food, beverages, and tobacco; glass, machinery, and electronics; non-ferrous metals; paper and wood; steel; textiles and printing; university, research, and health; waste, water and property management. The players entering the *financials* sector are only PHAs and refer to: banks, brokers, consultancy, exchanges, fund managers, governmental, NGOs, and own-account traders.

type of trader exchanged depends on their characteristic size and compliance needs; instead, how often each trader category traded seems to depend on commonly observed information and to be more strongly correlated.

The summary statistics presented in Tables 4.1 and 4.2 indeed support the hypothesis that the permit trading strategy of EU ETS market players differs significantly along the three classification criteria. Further details on the trading activity of different types of agents are presented in Appendix 4.C.

Table 4.1: Statistics on the trading activity of market participants grouped according to three criteria.

Note: The table lists summary statistics related to the trading activity of different participants in the EU ETS. The number of accounts represents the number of different account IDs that have traded at least once. The under- or over-allocation status of each account can vary from year to year. Volumes are presented in 100,000 units, where total number of transferred permits is 1,841,282,785. Numbers in brackets refer to percentages in total. The analyzed period is 15.09.2005 - 31.05.2007.

Compliance regulation		Exposure to other markets		Initial permit endowment	
A. Non-liable		**A.1. Financial institutions**		Zero allocation	
Nr. accounts	192 (5.1%)				
Nr. transfers	13,761 (42.8%)				
Volume	568 (30.9%)				
B. liable		**B.1. Energy**		**B.1.1. Over-allocated**	
Nr. accounts	3,596 (94.9%)	Nr. accounts	2,448 (64.6%)	Nr. accounts	1,844 (48.7%)
Nr. transfers	18,420 (57.2%)	Nr. transfers	14,996 (46.6%)	Nr. transfers	12,702 (39.5%)
Volume	1,273 (69.1%)	Volume	1,095 (59.5%)	Volume	809 (44.0%)
				B.1.2. Under-allocated	
				Nr. accounts	875 (23.1%)
				Nr. transfers	2,294 (7.1%)
				Volume	286 (15.5%)
		B.2. Industrials		**B.2.1. Over-allocated**	
		Nr. accounts	1,148 (30.3%)	Nr. accounts	845 (22.3%)
		Nr. transfers	3,426 (10.7%)	Nr. transfers	2,682 (8.3%)
		Volume	178 (9.7%)	Volume	144 (7.8%)
				B.2.2. Under-allocated	
				Nr. accounts	394 (10.4%)
				Nr. transfers	741 (2.3%)
				Volume	34 (1.8%)

Table 4.2: Correlation coefficients for the trading activities of different sectors.

Note: The table lists the correlation coefficients characterising the trading activity of EU ETS market participants grouped into three sectors. The analyzed period is 15.09.2005 - 31.05.2007.

Indicator	Position	Correlation coefficient		
		Energy - Industrials	Energy - Financials	Industrials - Financials
Volume	Buy+Sell	0.1965	0.2392	0.0834
	Buy	0.0946	0.1742	0.0169
	Sell	0.2507	0.2102	0.1409
Nr. transfers	Buy+Sell	0.5888	0.6384	0.5477
	Buy	0.3591	0.6191	0.3516
	Sell	0.6540	0.5839	0.5699

4.4.2 European carbon markets and EUA daily price changes

Several organized exchanges have operated during Phase I, covering about 30% of all permit transactions. This percentage was split between the ECX (London), the NordPool (Oslo), the EEX (Leipzig), the Eurex (Stuttgart), the BlueNext (Paris), the EXAA (Vienna), and the Climex (Utrecht). The remaining dominating share of about 70% of transactions took place over-the-counter (Rittler, 2012). The EUTL database gives information on all transfers of permit ownership, both exchange and OTC.[12]

The spot price on the different exchanges followed a very similar trend, with no significant discrepancies. Our analysis relies on spot prices, publicly available from the European Environmental Agency (EEA). To avoid periods of very low liquidity and less meaningful price levels,[13] we restrict the analysis horizon to September 2005 - May 2007, similar to Hintermann (2010).[14] With low market liquidity and permit over-allocateion, the EUA price varied widely during Phase I, from an initial level around 30 EUR/tCO_2e, down to 0.1 EUR/tCO_2e at the end of the compliance period in 2007.

Table 4.3 captures the main descriptive statistics regarding the EUA daily spot price, daily percent change (return), and daily differences in the EUA price; see Appendix 4.B for the graphical illustration. The normality assumption is rejected for all three series. The return distribution exhibited fat tails and was slightly positively skewed. When prices declined to almost zero at the end of the analyzed period, daily changes consisted in only few ticks,[15] but large absolute percentage changes. Similarly to Hintermann (2010), our analysis relies on daily price differences; these capture the level of price variation and can be related to actual driving factors, unlike returns which appear inflated at the end on Phase I. The daily price change series had a mean close to zero, exhibited low standard deviation, negative skewness, and fat tails. While the spot and log returns series are non-stationary, the daily price difference series is stationary, as revealed by the KPSS test.

Table 4.3: Descriptive statistics for the EUA spot price level, return, and difference series.

Note: The table presents descriptive statistics of the daily EUA spot prices (P_t), returns (R_t), and price differences (D_t) during 15.09.2005 - 31.05.2007. Returns are computed as the natural logarithm of the price ratio in consecutive days, i.e. $R_t = log\,(P_t/P_{t-1})$, and are unitless. Daily price differences are computed as $D_t = P_t - P_{t-1}$ (EUR/tCO_2e). Nr. observations = 433.

Statistic	Spot (P_t)	Log Returns (R_t)	Price Changes (D_t)
Mean	14.30	-0.01	-0.05
Median	15.60	-0.001	-0.02
Maximum	29.75	0.58	7.10
Minimum	0.26	-0.37	-7.50
St. Deviation	8.99	0.07	0.72
Skewness	-0.20	0.09	-0.99
Excess Kurtosis	-1.23	18.49	51.10
Lilliefors (p-value)	0.10 (0.00)	0.20 (0.00)	0.19 (0.00)
KPSS (p-value)	7.73 (<0.1)	0.95 (<0.1)	0.01 (>0.1)

[12] Our analysis excludes administrative transfers, i.e. allowance issuance, retirement, and cancellation.
[13] In the second half of 2007 prices converged and stayed close to zero; see Fig. 4.1.
[14] The EUA data provided by the European Environmental Agency starts on 15.09.2005.
[15] One tick is of Eur 0.01.

4.5 Results

This section presents the empirical results from the estimation of the trading activity - volatility association on the EU ETS market. We first present the results related to the fitting of the daily spot price differences. Then, we focus on the regressions of volatility on the trading activity of different market players.

4.5.1 Daily spot price differences

We start the analysis by first fitting an autoregressive model to the price difference series. The Akaike Information Criterion (AIC) indicates that the first twenty five lags (approximately one month) have explanatory power for price differences. Selecting a number of autoregressive terms below this threshold results in autocorrelated errors.

After performing a first iteration on the fitting of price differences and volatility, we re-estimate Eq. (4.1) using the fitted volatilities from the previous step, together with the autoregressive terms. The results are presented in Table 4.4. We first show the results of a model where in the previous step of the iteration process, volatility is regressed only on autoregressive terms and lagged unexpected price differences ($\mathcal{M}1$). Then, in models $\mathcal{M}2$ and $\mathcal{M}3$, total transferred volumes and total number of transfers by all market participants are included in the first estimation of volatility, respectively.

The coefficients of the lagged price differences are significant and negative, showing that larger past price differences tended to reduce current price changes. In contrast, lagged volatility terms appear to have positive coefficient signs and are jointly significant, consistent with previous empirical studies (Bessembinder and Seguin, 1993) and with the literature predicting a positive relation between required rates of return and expected levels of volatility (French et al., 1987).

The adjusted R^2 is around 23%, considerably higher than the 3% that is commonly documented for commodities futures markets (Bessembinder and Seguin, 1993). This result signals that the market efficiency of the EU ETS during Phase I was much weaker than that of established financial markets, where predictability is lower. The result concurs with the findings of Montagnoli and de Vries (2010) and Palao and Pardo (2012), who point to the inefficiency of the carbon market during Phase I.

4.5.2 Price volatility and permit trading

Implementing the methodology described in Section 4.3, we analyse the trading activity - volatility relation by estimating Eq. (4.2). The dependent variable is the volatility of daily spot price differences. The conditional daily volatility is estimated as a function of autoregressive terms, past unexpected price differences, and trading activity variables. We test the association between trading activity and permit price volatility by examining first the relation with daily volume levels and then with number of transfers.

Kalaitzoglou and Ibrahim (2013) analyse the carbon futures market during the first two phases of the EU ETS and find it to be buyer-dominated, where the duration (the time passed between consecutive trades of the same day) of buyer-initiated transactions was always longer than that of the seller-initiated transactions. To account for potential differences between acquisitions and sales of permits, we estimate the trading activity - volatility relation by looking at: (i) overall trading activity (buy and sell); (ii) only acquisitions (buy); and (iii) only sales (sell).

Table 4.4: Autoregressive models for daily EUA price differences.

Note: The table presents results from the second iteration of the estimation of Eq. (4.1) based on the results from the first estimation of Eq. (4.2). The dependent variable is the daily spot price difference series. 'No trading activity', 'Volumes', and 'Nr. transfers' refer to the trading activity included in the first estimation of Eq. (4.2). The analysed period is 15.09.2005 - 31.05.2007. For all estimated coefficients, standard errors are presented in brackets. F-test statistics are listed for $\sum_{j=1}^{n=25} \hat{\nu}_j$ and $\sum_{j=1}^{n=25} \hat{\mu}_j$. The Box-Pierce statistic is computed with $k = 2\sqrt{N}$, N = 359.

	No trading activity ($\mathcal{M}1$)	**Volumes** ($\mathcal{M}2$)	**Nr. transfers** ($\mathcal{M}3$)
Intercept	-0.09 (0.07)	-0.08 (0.07)	-0.07 (0.07)
$\sum_{j=1}^{n=25} \hat{\nu}_j$	0.00 (3.70)***	-0.02 (3.69)***	-0.03 (3.71)***
$\sum_{j=1}^{n=25} \hat{\mu}_j$	0.06 (2.61)***	0.04 (2.58)***	0.01 (2.63)***
R^2	0.34	0.34	0.34
Adj. R^2	0.23	0.23	0.23
AIC	778.90	779.71	778.39
Box-Pierce test (p-val)	11.43 (0.49)	10.96 (0.53)	11.95 (0.45)

$^{***}p < 0.001$, $^{**}p < 0.01$, $^{*}p < 0.05$, $^{\circ}p < 0.1$

4.5.2.1 Transferred volume levels

The first indicator of trading activity used is the level of daily transferred volumes. Depending on the selected definition of traded volume, several models are fitted; the results are displayed in Table 4.5.

We first regress daily volatility on autoregressive terms and past unexpected price differences, without considering the trading activity among the explanatory variables (Model $\mathcal{M}4$). Further, we estimate a model including the total daily volume traded by all market participants ($\mathcal{M}5$). In both cases, we find the autoregressive terms to be highly significant and positive, showing that past volatility levels have a large predictive power for realized volatility. This is consistent with the previously documented persistence of volatility (Schwert, 1990; Bessembinder and Seguin, 1993). The positive sign indicates the tendency of volatility to cluster. Moreover, the lagged unexpected returns have some explanatory power for the realized movements in volatility.

Including the total transferred volumes in the regressions slightly increases the explanatory power of the model; the coefficient of the total volume is positive, supporting the positive volume - volatility hypothesis, but not significant. We can infer that the association between total volumes and volatility was not particularly strong over the entire analysed horizon. This might be due to the different interests of the EU ETS market participants, which, if diverging, could have neutralized on the aggregate. Our prediction is that some types of players traded volumes that are correlated positively with volatility, while others negatively.

Motivated by this hypothesis, we continue the analysis of the volume-volatility relation by distinguishing between the type of traders involved in the permit transfer. Following our argumentation in Sections 4.2 and 4.4, we use three criteria of classification.

Liable and non-liable traders

In a first classification, we separate volumes according to the liable - non-liable partition. The estimation results are relegated to Appendix 4.D (Table 4.D.1). We find that only the volumes traded by the *liable* sectors have correlated significantly and positively with volatility. Distinguishing between expected and unexpected volumes reveals that the positive volume - volatility

association can be mainly attributed to the unexpected volumes traded by the liable sector. The explanatory power of the models is higher than that of the general models that do not distinguish among different types of players.

Under-allocated, over-allocated, and non-liable traders

The results of the volatility estimation when volumes are partitioned according to the permit allocation criterion are displayed in Appendix 4.D (Table 4.D.2). According to this partition, the relation between volume and volatility does not appear to have been significant, except for the models that distinguish between expected and unexpected volumes. Here, we find volatility to be positively associated with the unexpected volumes bought by the over-allocated accounts, but negatively with the expected volumes bought by the under-allocated ones. With this trader type classification, the explanatory power of the model increases to about 40%.

Energy providers, industrial firms, and financial institutions

Third, we classify traders according to their primary business activity and their implicit exposure to other output and financial markets. The results of the volatility estimation are displayed in Table 4.5 (Models $\mathcal{M}6$ - $\mathcal{M}8$). We find that the volumes traded by the energy sector have correlated significantly and positively with volatility. More precisely, the positive relation is driven by the unexpected trades of the energy sector.

Based on these findings, we are further interested in understanding whether we can capture a link between the two types of players whose trading activity has associated positively with volatility: the energy companies and the over-allocated players. Our intention is to test the connection between the exposure to the market of the primary business activity and the permit allocation status. For this, we regress daily volatility on traded volumes partitioned according to both business activity and allocation status; see Table 4.D.4 in Appendix 4.D. We find that the acquired unexpected volumes of the over-allocated accounts that have correlated positively with volatility belong to the industrial firms. The anticipated volumes bought by the under-allocated players that have correlated negatively with volatility belong to the energy companies.

Summing up, our analysis shows that the volume - volatility relation can indeed be better explained when distinguishing between different trader types. We find that higher unexpected volumes traded by either the liable, the over-allocated, or the energy participants, are correlated positively and significantly with price volatility.

Table 4.5: Regressions of volatility on expected and unexpected volumes from different sectors of primary business activity.

Note: The table presents results from the second iteration of the estimation of Eq. (4.2) based on the results from the first estimation of Eq. (4.1). The dependent variable is the volatility of daily spot EUA price differences. 'No trading activity', 'Total volume', and 'Expected and unexpected volume' refer to the trading activity included in the estimation of Eq. (4.2). The analysed period is 15.09.2005 - 31.05.2007. For all estimated coefficients, standard errors are presented in brackets. F-test statistics are listed for $\sum_{j=1}^{n=25} \hat{\beta}_j$ and $\sum_{j=1}^{n=25} \hat{\gamma}_j$. The Box-Pierce statistic is computed with $k = 2\sqrt{N}$, N = 334.

	No trading activity	**Total volume**	**Expected and unexpected volume**		
			Buy + Sell	**Buy**	**Sell**
	($\mathcal{M}4$)	($\mathcal{M}5$)	($\mathcal{M}6$)	($\mathcal{M}7$)	($\mathcal{M}8$)
Intercept	0.07 (0.06)	0.05 (0.06)	0.07 (0.07)	0.07 (0.07)	0.08 (0.07)
$\sum_{j=1}^{n=25} \hat{\gamma}_j$	0.84 (8.17)***	0.85 (8.51)***	0.81 (7.99)***	0.85 (7.97)***	0.81 (8.50)***
$\sum_{j=1}^{n=25} \hat{\beta}_j$	0.47 (1.39)	0.47 (1.42)°	0.35 (1.44)°	0.40 (1.66)*	0.35 (1.35)
Total volume		0.02 (0.01)			
Energy					
Expected			0.01 (0.04)	0.01 (0.03)	-0.02 (0.05)
Unexpected			0.05 (0.02)*	0.05 (0.02)*	0.04 (0.03)°
Industrials					
Expected			0.09 (0.12)	-0.09 (0.11)	0.14 (0.11)
Unexpected			0.05 (0.08)	0.01 (0.08)	0.09 (0.08)
Non-liable					
Expected			-0.01 (0.03)	-0.02 (0.03)	0.00 (0.02)
Unexpected			-0.02 (0.03)	-0.01 (0.02)	-0.01 (0.03)
R^2	0.46	0.47	0.47	0.47	0.48
Adj. R^2	0.36	0.37	0.36	0.37	0.37
AIC	532.71	525.4	538.29	532.4	530.42
Box-Pierce test (p-val)	14.93 (0.19)	15.53 (0.16)	16.99 (0.11)	15.06 (0.18)	18.59 (0.07)

$^{***}p < 0.001$, $^{**}p < 0.01$, $^{*}p < 0.05$, $^{\circ}p < 0.1$

4.5.2.2 The number of transfers

So far, the focus of our analysis has been on the volume - volatility relation in the EU ETS. A complementary stream of literature points to the strong association between the number of trades and price volatility on financial markets. Jones et al. (1994) show that the positive volume - volatility relation should be understood as the number of trades - volatility relation. They find that it is the number of transactions *per se* that is associated with volatility, and not necessarily their size. However, their findings are not confirmed for all markets by follow-up literature; Daigler and Wiley (1999) include the number of transactions in their regressions, but do not find evidence of significance when controlling also for volume size.

Motivated by this debate, we investigate the relation between the daily price volatility and the number of permit transfers. The results are in line with the findings of the volume - volatility relation from Section 4.5.2.1; see Table 4.6. On average over the analyzed period, the total number of transfers associated positively and significantly with volatility ($\mathcal{M}9$). We again partition trades according to the three criteria for trader classification. First, distinguishing between liable and non-liable accounts indicates that a higher number of transfers performed by the liable players correlated positively and significantly with volatility. Second, grouping players according to the over- and under-allocation status does not seem to result in a significant number of transfers - volatility relation for either player type. Third, the sectoral breakdown reveals that the positive trading activity - volatility relation can be attributed to the number of buying and selling transfers performed by the energy companies ($\mathcal{M}10$-$\mathcal{M}12$).

Table 4.6 shows that accounting for the number of daily permit transfers results in an increased explanatory power (compared to models $\mathcal{M}4$-$\mathcal{M}8$). Including both volume levels and number of transfers in the regressions does not improve the fitness of the models and reveals that only the number of transfers associated significantly with volatility, while the volume - volatility relation is rendered not significant; see Table 4.E.1 in Appendix 4.E. In line with the study of Jones et al. (1994) for futures markets, we find that traded volumes in the EU ETS have no marginal explanatory power when volatility is conditioned on the number of trades. It might seem surprising that the size of trades had on average no information content beyond that contained in the number of transfers. However, keeping in mind that the carbon market was generally over-allocated during Phase I, it seems reasonable that the frequency with which players trade is a better proxy for the trading activity than the volume size itself. As well, our results are in line with the findings of Chevallier and Sévi (2014), who show that the allowance price process can be represented by a centered jump process, with no continuous component. With a limited number of traders and infrequent orders, it seems reasonable that the frequency of trade be significantly associated with the unexpected changes in prices.

Regressing volatility on the number of transfers partitioned according to the primary business activity appears to provide the best fit. The analysis that follows uses the number of transfers to proxy the permit trading activity, and the business activity partition to distinguish between players.

Table 4.6: Regressions of volatility on the number of daily permit transfers by different trading sectors.

Note: The table presents results from the second iteration of the estimation of Eq. (4.2) based on the results from the first estimation of Eq. (4.1). The dependent variable is the volatility of daily spot EUA price differences. The analysed period is 15.09.2005 - 31.05.2007. For all estimated coefficients, standard errors are presented in brackets. F-test statistics are listed for $\sum_{j=1}^{n=25} \hat{\beta}_j$ and $\sum_{j=1}^{n=25} \hat{\gamma}_j$. The Box-Pierce statistic is computed with $k = 2\sqrt{N}$, N = 334.

	Nr. transfers			
	Total ($\mathcal{M}9$)	**Buy + Sell** ($\mathcal{M}10$)	**Buy** ($\mathcal{M}11$)	**Sell** ($\mathcal{M}12$)
Intercept	-0.05 (0.08)	-0.01 (0.08)	-0.00 (0.09)	-0.03 (0.08)
$\sum_{j=1}^{n=25} \hat{\gamma}_j$	0.81 (8.07)***	0.77 (8.67)***	0.76 (8.62)***	0.79 (8.52)***
$\sum_{j=1}^{n=25} \hat{\beta}_j$	0.61 (1.49)°	0.44 (1.59)*	0.43 (1.57)*	0.50 (1.56)*
Nr. transfers				
Total	0.13 (0.05)**			
Energy		0.30 (0.13)*	0.30 (0.12)*	0.25 (0.12)*
Industrials		-0.18 (0.44)	-0.17 (0.41)	-0.06 (0.37)
Non-liable		-0.02 (0.14)	-0.02 (0.12)	0.01 (0.14)
R^2	0.47	0.49	0.49	0.48
Adj. R^2	0.37	0.39	0.39	0.38
AIC	530.20	522.92	523.37	526.36
Box-Pierce test (p-val)	16.57 (0.12)	17.19 (0.10)	18.51 (0.07)	16.30 (0.13)

$^{***}p < 0.001$, $^{**}p < 0.01$, $^{*}p < 0.05$, $^{\circ}p < 0.1$

4.5.2.3 The April effect

Sections 4.5.2.1 and 4.5.2.2 showed that, on average, the positive trading activity - volatility relation has been related over the entire analyzed period with the traded volumes and the number of transfers of the energy sector. However, analysing the evolution of volatility and the trading activity over time, one can easily notice the large variations in the levels of both variables, with peaks in two particular months of each year, namely April and December; see again Fig. 4.1. These months correspond to important dates in the design of the EU ETS. Each phase of the EU ETS spans over several years, with December being the last month of each compliance year. December is, therefore, also the prevalent maturity date for most derivative contracts on allowances (futures, forwards, and options). However, liable companies are granted time until March 31st to submit to the European Commission the report regarding the verified emissions of the previous year. By the end of April, each liable entity needs to surrender the necessary allowances covering its total emissions for the precedent year. As well, in April until mid-May, the European Commission publicly reveals the cumulated emissions of the liable companies.[16] This brings information on the ratio between total realized emissions and overall market cap.

Motivated by the particular design of the EU ETS and the empirical observation of volatility levels and trading activity shooting high in some periods of the year, we run the regressions of volatility controlling also for month. Indeed, Table 4.7 confirms that price volatility has been significantly higher in April. In contrast, we find volatility levels to be lower in December, but the relation does not appear significant (Models $\mathcal{M}13$ - $\mathcal{M}15$). The permit trading activity of the energy sector remains significant even when controlling for seasonality. When including the month fixed effects, the explanatory power of the models increases significantly.

Lucia et al. (2014) suggest that the permit trading strategies of players could vary across the compliance year, being influenced by the specific timeline imposed by the EU ETS. Both the

[16]The specific timeline of the EU ETS is captured in Fig. 4.F.1 in Appendix 4.F.

number of transfers and the volumes have been significantly above the average in April for both energy and industrial companies; see Figs. 4.F.2 and 4.F.3 in Appendix 4.F. In order to understand if the trading behavior of the market players is associated differently with volatility in April, we introduce interaction terms between the number of transfers and the April dummy (Models $\mathcal{M}16$ - $\mathcal{M}18$). We find that the number of transfers led by the energy sector continues to be positively and significantly associated with volatility, and the association is indeed stronger in April. In contrast, the higher the number of permit transfers involving the industrial sector, the lower was the associated volatility. The negative relation appears to have been particularly strong for the number of acquisitions.

Let us analyse the results in light of the 'mixture of distributions' theory. When new relevant information is disclosed, the relation between price changes and trading activity will depend on how traders interpret the new information. If the news is uncertain, traders might interpret it in different ways and take opposing trading positions. In such a case, large price changes are expected to be accompanied by an intense trading activity (volumes and number of trades). However, if the new information is interpreted in the same way by all traders, a large price change would be associated with relatively low traded volumes (Clark, 1973; Tauchen and Pitts, 1983). In April, when the information on the cumulated emissions of liable players is publicly revealed, market participants can estimate the difference between the total amount of permits needed to be surrendered for compliance and the amount of permits allocated for free. In case this difference is negative, the market is in excess of permits, with prices being updated downwards. Since all players are exposed to the same information, they update their expectations in the same direction. This occurred in April 2006, when the permit price experienced a large negative jump. While the price process experienced a large change due to the arrival of information containing unequivocal implications, the associated trading activity has been much weaker after the announcement than before.[17, 18]

[17] Prior to April 26th, when the announcement of global market emissions has been made, transferred volumes have been very large, possibly due to the fact that the surrendering of permits for 2005 was due by the end of April. After April 26th, i.e. once the permit price experienced the large drop, volumes have been very low; see Fig. 4.F.8 in Appendix 4.F.

[18] Interestingly, Lucia et al. (2014) find that the speculative behavior became much smaller after April 2006, when the reports regarding the cumulated emissions were publicly released.

Table 4.7: Regressions of volatility on month dummies and nr. transfers led by agents sorted by business activity sector.

Note: The table presents results from the second iteration of the estimation of Eq. (4.2) based on the results from the first estimation of Eq. (4.1). The dependent variable is the volatility of daily spot EUA price differences. The analysed period is 15.09.2005 - 31.05.2007. For all estimated coefficients, standard errors are presented in brackets. F-test statistics are listed for $\sum_{j=1}^{n=25} \hat{\beta}_j$ and $\sum_{j=1}^{n=25} \hat{\gamma}_j$. The Box-Pierce statistic is computed with $k = 2\sqrt{N}$, N = 334.

	Model with month dummies			**Model with interaction terms**		
	Buy + Sell ($\mathcal{M}13$)	**Buy** ($\mathcal{M}14$)	**Sell** ($\mathcal{M}15$)	**Buy + Sell** ($\mathcal{M}16$)	**Buy** ($\mathcal{M}17$)	**Sell** ($\mathcal{M}18$)
Intercept	-0.03 (0.14)	-0.01 (0.14)	-0.08 (0.13)	0.06 (0.07)	0.08 (0.07)	0.02 (0.07)
$\sum_{j=1}^{n=25} \hat{\gamma}_j$	0.68 (10.28)***	0.66 (10.51)***	0.71 (9.59)***	0.67 (10.80)***	0.66 (11.32)***	0.71 (10.65)***
$\sum_{j=1}^{n=25} \hat{\beta}_j$	0.04 (2.37)***	0.01 (2.28)***	0.12 (2.31)***	-0.17 (2.24)***	-0.22 (2.28)***	-0.08 (1.96)**
Nr. transfers						
Energy	0.34 (0.13)**	0.32 (0.11)**	0.29 (0.12)*	0.24 (0.12)*	0.23 (0.11)*	0.19 (0.11)
Industrials	-0.43 (0.42)	-0.39 (0.40)	-0.24 (0.36)	-0.28 (0.45)	-0.10 (0.42)	-0.19 (0.37)
Non-liable	0.05 (0.15)	0.02 (0.13)	0.12 (0.15)	-0.09 (0.13)	-0.13 (0.11)	-0.01 (0.13)
Month dummies						
February	-0.08 (0.13)	-0.08 (0.13)	-0.06 (0.13)			
March	-0.07 (0.12)	-0.06 (0.12)	-0.07 (0.13)			
April	0.42 (0.16)**	0.42 (0.16)**	0.42 (0.16)**			
May	-0.06 (0.15)	-0.05 (0.15)	-0.06 (0.15)			
June	0.07 (0.18)	0.1 (0.18)	0.04 (0.19)			
July	0.09 (0.15)	0.09 (0.15)	0.11 (0.15)			
August	-0.00 (0.15)	0.00 (0.15)	0.01 (0.15)			
September	0.09 (0.15)	0.09 (0.15)	0.12 (0.15)			
October	0.13 (0.14)	0.11 (0.14)	0.14 (0.15)			
November	-0.03 (0.14)	-0.01 (0.14)	-0.03 (0.15)			
December	-0.24 (0.16)	-0.22 (0.15)	-0.27 (0.16)°			
Interaction terms						
Energy*April				0.80 (0.30)**	0.67 (0.27)*	0.74 (0.31)*
Industrials*April				-1.00 (0.83)	-1.38 (0.69)*	-0.31 (0.85)
Non-liable*April				0.04 (0.39)	0.30 (0.31)	-0.22 (0.45)
R^2	0.56	0.57	0.55	0.57	0.58	0.56
Adj. R^2	0.46	0.46	0.44	0.48	0.5	0.47
AIC	476.49	473.65	487.90	422.86	423.75	442.66
Box-Pierce test (p-val)	21.19 (0.03)	23.85 (0.01)	17.70 (0.09)	15.02 (0.18)	17.23 (0.10)	14.66 (0.20)

$^{***}p < 0.001$, $^{**}p < 0.01$, $^{*}p < 0.05$, $^{\circ}p < 0.1$.

4.5.2.4 Counterparties in permit transfers

Our analysis so far has focused mostly on the association between permit price volatility and the trading activity of different players. However, a trade is never the action of one player alone, and each transaction can be characterized by a buyer and a seller. It might be that the trading activity of one player is correlated positively with volatility when trading with one sector, but negatively when trading with other sectors.

Table 4.8 provides information regarding the frequency at which each sector traded permits with the other sectors during the analyzed period. Both in terms of acquisitions and sales, the energy sector preferred to trade with other companies from the same sector, and secondly with the non-liable institutions. The industry sector bought mainly within the sector, but preferred to sell to non-liable players. Finally, the non-liable sector diversified its acquisitions and sales among energy and other non-liable players.

Table 4.8: Transfer counterparties for players grouped according to primary business activity.

Note: The table presents the share of trades concluded by each sector with the other players, and distinguishes between acquisitions and sales.

		Counterparty		
Transfer position	Sector	Energy	Industry	Financials
Buyer	Energy	60.37%	5.96%	33.67%
	Industry	26.11%	46.22%	27.67%
	Non-liable	40.68%	14.31%	45.01%
Seller	Energy	56.06%	4.40%	39.55%
	Industry	20.33%	28.59%	51.09%
	Non-liable	39.24%	5.85%	54.91%

As shown in the previous sections, the trades of the energy sector have been positively associated with permit price volatility. By specifying the sector of the buyer and the seller, we intend now to understand whether it was the trades of the energy sector in general that coincided with increased levels of volatility, or only the trades between the energy sector and a specific counterparty.

We partition the number of trades executed between the different sectors, such that both the buyer and the seller are identified (Models $\mathcal{M}19$ - $\mathcal{M}20$ in Table 4.9). The estimation of volatility is performed both with and without the monthly fixed effects; results appear consistent across the two models. Our findings show that all three sectors tended to trade more frequently within their own sector when volatility levels were lower. In times of high volatility levels, the energy sector tended to trade more frequently outside their sector, and find counterparties among the industrial (as seller) and non-liable sectors. In contrast, it appears that the industrial companies traded more frequently when volatility levels were lower. Finally, the non-liable players behaved indeed like financial intermediaries and acted as counterparties to trades whenever the liable sectors needed it: they traded more with the energy sector whenever volatility was higher, and more often with the industrial sector when volatility was lower.

Table 4.9: Regressions of volatility on the number of daily permit transfers by different trading sectors after distinguishing between buyer and seller.

Note: The table presents results from the second iteration of the estimation of Eq. (4.2) based on the results from the first estimation of Eq. (4.1). The dependent variable is the volatility of daily spot EUA price differences. The analysed period is 15.09.2005 - 31.05.2007. For all estimated coefficients, standard errors are presented in brackets. F-test statistics are listed for $\sum_{j=1}^{n=25} \hat{\beta}_j$ and $\sum_{j=1}^{n=25} \hat{\gamma}_j$. The Box-Pierce statistic is computed with $k = 2\sqrt{N}$, N = 334.

	No Month Dummy ($\mathcal{M}19$)	**With Month Dummy** ($\mathcal{M}20$)
Intercept	0.00 (0.09)	-0.01 (0.14)
$\sum_{j=1}^{n=25} \hat{\gamma}_j$	0.68 (10.67)***	0.56 (12.04)***
$\sum_{j=1}^{n=25} \hat{\beta}_j$	0.35 (1.58)*	0.01 (2.66)***
Nr. transfers (Buyer - Seller)		
Energy - Industrials	3.46 (1.23)**	2.99 (1.12)**
Energy - Non-liable	0.77 (0.39)*	1.00 (0.37)**
Industrials - Non-liable	-0.04 (1.08)	-0.20 (1.12)
Energy - Energy	-0.09 (0.17)	-0.07 (0.16)
Industrials - Industrials	-0.02 (0.55)	-0.14 (0.53)
Non-liable - Non-liable	-0.41 (0.24)°	-0.43 (0.24)
Industrials - Energy	-0.17 (1.11)	-0.30 (1.05)
Non-liable - Energy	0.66 (0.38)°	0.71 (0.36)*
Non-liable - Industrials	-1.11 (0.61)°	-1.22 (0.59)*
Month Dummy		
February		-0.04 (0.13)
March		-0.10 (0.12)
April		0.43 (0.17)*
May		-0.04 (0.14)
June		0.13 (0.18)
July		0.10 (0.15)
August		-0.03 (0.15)
September		0.12 (0.15)
October		0.12 (0.15)
November		-0.01 (0.15)
December		-0.17 (0.16)
R^2	0.55	0.61
Adj. R^2	0.45	0.51
AIC	513.77	466.89
Box-Pierce test (p-val)	14.94 (0.19)	23.20 (0.02)

$^{***}p < 0.001$, $^{**}p < 0.01$, $^{*}p < 0.05$, $^{\circ}p < 0.1$

4.6 Discussion

Our analysis reaches the following conclusions:

1. In Phase I of the EU ETS, the carbon market lacked in efficiency, with an observed larger predictability of price differences than on common financial markets.

2. The volatility of the allowance price is explained to a large extent by autoregressive terms, suggesting that the volatility process was persistent and that it clustered, common to established financial markets.

3. Including the trading activity of market players into the volatility estimation increases the explanatory power of the models. Two indicators of trading activity have been considered: volume and number of transfers. Between the two, the number of transfers seems to better explain movements in volatility. As a robustness check, we use the number of active traders each day as a proxy for daily trading activity; see Appendix 4.I. The results are similar to the

number of transfers - volatility analysis and reveal a strong and positive relation. It results that, in a market with excess allowances, the number of permits traded contains arguably less information that the number of transfers or the number of active traders. These last two variables seem to indeed constitute better indicators of changes in market information and of daily liquidity.

4. The volatility of the allowance price is found to contain seasonal patterns, seemingly strongly related to the specific EU ETS design. In particular, price changes have higher magnitudes each year in April, when liable players need to surrender enough allowances to cover their realized emissions for the previous calendar year and when the information regarding the aggregated market emissions are made public. Moreover, the trading activity of market players is more strongly related to volatility in April.

5. The trading activity - volatility relation can be better explained when accounting for the type of trader. The special setting of the EU ETS market is likely to include traders with significantly different characteristics. We distinguished between trader types based on three criteria: (i) compliance regulation, (ii) initial endowment of permits relative to actual emissions, and (iii) players' exposure to other markets. First, we find a positive and significant relation between the trading activity of the liable participants and volatility. Second, the sign of the relation depends on the over- or under-allocation status. Third, the relation is best explained when accounting for traders with different exposures to other markets. Namely, the energy sector appears to be the one whose trading activity was positively and most strongly correlated with volatility. In contrast, the industrial sector appears to have traded more when volatility levels were lower. The trading activity of the non-liable sector appears to be associated positively, although not significantly, with volatility.

6. We find that the trading activity - volatility relation depends also on the specific counterparties concluding the trade and on who held the buyer or the seller position. As a buyer, the activity of the energy sector was correlated positively with volatility, regardless of the counterparty. The non-liable sector, mainly represented by financial intermediaries, tended to trade more with the energy sector when volatility levels were higher, and more with the industrials sector when volatility levels were lower.

Our results are confirmed by several robustness tests, as presented in Appendix 4.H. Several dimensions have been tested for: (i) subsample analysis, as delimited by the April 2006 crash; (ii) lagged trading activity terms; (iii) including one type of trader at a time; and (iv) daily changes in trading activity.

The main finding of our analysis is that the relation between the trading activity and the volatility of the permit price depended indeed on the specific counterparty in the trade and whether or not the player acted as a buyer or a seller. The question arises as to why did the energy sector tend to trade more frequently when volatility was higher, while the industrials when volatility was lower, and the non-liable sector had a trading intensity that related with volatility positively or negatively depending on the counterparty. In this section, we discuss how these results could be justified.

Trading experience

One likely hypothesis is that each sector had a different previous experience with trading activities. With the creation of the EU ETS and its regulation, companies were suddenly exposed to a new market and needed to develop strategies for reaching compliance. This included the designation of an organizational department to deal with permit trading activities and to incorporate this trading activity into the accounting system of the company (Engels, 2009).

The energy sector consists of generally larger players with a stronger experience in trading, and therefore more likely to seek profit opportunities from trading permits when price volatility is higher. In contrast, the industrial sector consists of smaller-sized companies, less exposed to trading in their primary business activity, and therefore more relentless to trade in times of higher market turbulences. Finally, the non-liable sector, mostly represented by financial intermediaries, can be expected to have had enough trading experience to be able to match their permit trading strategies with the specific trading patterns of the counterparties.

Coordinated output and permit trading decisions
A second proposition is that each sector took both primary business and permit trading decisions in a coordinated manner. For instance, Daskalakis and Markellos (2009) document a positive relation between EUA spot returns and electricity risk premia.[19] The authors propose that electricity producers have more information regarding the demand and supply of electricity than other electricity market participants, such as speculators, hedgers, and arbitrageurs; as well, they own a stock of freely allocated allowances. They are, thus, likely to design power production and permit trading strategies that account for this extra information. Moreover, energy producers face a stochastic demand that needs to be fully satisfied (Hintermann, 2012). Daskalakis and Markellos (2009) argument that the demand can be satisfied by either producing electricity or by purchasing it on futures/forward markets. The decision on how to satisfy demand will be influenced by EUA price movements. For example, in case of increasing EUA prices, instead of producing it, power could be bought on the futures/forward market and fewer EUAs would be needed for compliance. This would put pressure on the demand for electricity and increase prices for future delivery of electricity, increasing the electricity risk premium. In contrast, in case of decreasing EUA prices, electricity producers would prefer to produce electricity and sell it on the futures/forward market, putting pressure on the supply for electricity and decreasing electricity prices in the forward markets. This would result in lower electricity risk premia, and larger acquisitions of EUAs. The positive link between the allowance returns and electricity risk premia finds further support in the analysis of Keppler and Mansanet-Bataller (2010), who show that the allowance price Granger caused electricity prices during Phase I.

On one hand, we find that higher unexpected changes in EUA price differences are positively associated with the trading activity of the energy sector. We think these findings are in line with the argumentation of Daskalakis and Markellos (2009) and with the 'mixture of distribution' theory. Namely, the higher the volatility of permit prices, the more often will the energy sector need to adjust their permit positions, resulting in a larger number of transfers and larger traded volumes.

On the other hand, the industrial sector faces generally a stochastic demand on output markets that does not necessarily have to be fully satisfied. Moreover, their output has usually a longer storability period, such that producers can adjust permit and output positions when market conditions are more favorable for them, i.e. when EUA volatility is lower. This argument is in line with our findings that the industrial sector tended to trade less when permit volatility levels were higher.

Market concentration and exposure to international competition
Tightly connected to the argument above, a third hypothesis states that, depending on the degree of competition on output markets, the liable companies adopted different permit trading strategies. Some authors argue that, during the first phase of the EU ETS, the energy sector,

[19]The electricity risk premium is defined as the difference between expected (futures/forwards) and current (spot) electricity prices.

not exposed to non-EU competition, could have passed on a significant share of the permit compliance costs to their customers, cashing in windfall profits. In the light of this argument, it might be that when the permit price volatility was higher and the permit price was steadily decreasing, some energy companies attempted to trade more (especially acquire more) in order to bring the permit price back to higher levels and be able to continue collecting windfall profits. This hypothesis is in line with our findings that the energy sector realized on average large losses from the trading of permits due to their acquisitions when permit prices were high; see Appendix 4.J. Moreover, Hintermann (2014) shows that a number of electricity firms accumulated a large allowance surplus by the end of Phase I, which could indicate their intention to keep permit prices high. Provided that a player receives enough free permit allocation and has a dominant position on both output and permit markets, it might find it profitable to increase the price even in a position of net buyer, as argued by Hintermann (2011). Since the passing on of compliance costs did not function for the other sectors, which were exposed to non-EU competition, they did not seem to share the same permit trading strategy.

The permit price manipulation hypothesis is not endorsed by our anaylsis. We study the degree of market concentration in the EU ETS and find that during Phase I the carbon market was generally highly competitive, with a sufficient number of active market players; see Appendix 4.I. This finding is in line with Hintermann (2014). Moreover, we find no statistical significance in the relation between permit price volatility and the trading activity of the biggest players, and we cannot, thus, validate the market manipulation theory. Two caveats are in order. First, our market concentration analysis is done at the aggregate level, over all permit transfers; in reality, several carbon markets were in place, and it might indeed be that on some of them a few players held a significant market share. Second, the concentration analysis includes the entire analysed horizon; in reality, on a market with limited liquidity, such as the EU ETS, it is likely that some players have held large market shares in some particular periods, although not over the aggregate.

4.7 Conclusion

Our analysis focused on the relation between the permit price volatility and the trading activity of market participants during the first phase of the EU ETS. We find evidence of a generally positive relation between trading activity and volatility. Our analysis indicates that this association is contemporaneous, where both variables vary in relation to common external factors, in line with the 'mixture of distributions' theory.

Our study was directed at estimating not only the sign of the association between the trading activity and the movements in prices, but also the specific relation with the trades of different trader types. The sign and strength of the trading activity - volatility relation are found to depend on the sector initiating the trade, the specific counterparty, and whether or not the player acted as a buyer or a seller. Several hypotheses are formulated to explain the contrasting associations between trader types and volatility. Among these, we give strongest support to the conjecture that, depending on their specific situation, players have designed coordinated output and permit trading decisions that resulted in a specific association with price volatility. It is important that further research focuses on the theoretical validation or disapproval of this hypothesis. Perhaps even more important is the need to fully grasp the link between the trading activity - volatility relation and the incentives to abate emissions.

Although the trading activity - volatility relation was found to be generally positive, this only held due to the dominance of the energy sector and against the contribution of the industrial

one. A cap-and-trade market is unlikely to be efficient if many players remain mostly inactive and are reluctant to trade during periods of intense information arrival. The policy implications that follow from our analysis point to the desirability of a directed engagement of less active players. Possibly, an intensified participation on carbon markets of financial intermediaries acting as market makers and information gatherers, provided their speculative behavior does not distort the market, is expected to favor the entry of small liable players, who have been predominantly absent from the trading platforms during the first phases of the EU ETS. This could possibly help with the dissemination of information regarding the cumulated emissions - permit allocation balance, and avoid large market destabilizations in the future due to infrequent arrivals of important news.

The European carbon market has been shown to achieve higher efficiency levels in the years following the first compliance period (Montagnoli and de Vries, 2010; Palao and Pardo, 2012), with allowance prices coming closer to fundamentals (Creti et al., 2012; Koch, 2014). Kalaitzoglou and Ibrahim (2013) link the increase in market stability and maturity with the increased availability of data on emissions at the installation level and the higher stability of order flow. Future research could extend our study by analysing the trading activity - volatility relation in the subsequent phases of the EU ETS, once EUTL data is made available. This could help generalize our findings that the sector whose trading activity was mostly associated with higher volatility were the energy companies and provide further insights into the reasons behind. As well, accounting for the different rules introduced in the EU ETS in Phases II and III could better reveal the link between market design, price volatility, and abatement.

Appendix Chapter 4

4.A Estimation steps for the trading activity - volatility relation

For the estimation of the trading activity - volatility association, we rely on the methodology proposed by Davidian and Carroll (1987), as detailed in Section 4.3. The estimation steps are summarized below:

1. We select the optimal number of autoregressive lags (p) in EUA price differences.
2. We run the autoregressive model for EUA price differences.

$$D_t = \alpha + \sum_{i=1}^{p} \nu_i D_{t-i} + U_t \tag{4.A.1}$$

3. We apply the volatility transformation:

$$\hat{\sigma}_t = |\hat{U}_t| \sqrt{\frac{\pi}{2}} \tag{4.A.2}$$

where:

$$\hat{U}_t = D_t - \hat{D}_t \tag{4.A.3}$$

$$\hat{D}_t = \hat{\alpha} + \sum_{i=1}^{p} \hat{\nu}_i D_{t-i} \tag{4.A.4}$$

4. We estimate volatility as an autoregressive model of lagged volatility, lagged unexpected returns, and the trading activity variables. We use different proxies for the trading activity ($TA_{k,t}$): transferred volumes, expected and unexpected transferred volumes, number of daily permit transfers, and daily number of unique trading agents.

$$\hat{\sigma}_t = \alpha + \sum_{i=1}^{p} \gamma_i \hat{\sigma}_{t-i} + \sum_{i=1}^{p} \beta_i \hat{U}_{t-i} + \sum_{k=1}^{m} \eta_k TA_{k,t} + \epsilon_t \tag{4.A.5}$$

5. We re-estimate price differences using the fitted volatility:

$$D_t = \alpha + \sum_{j=1}^{p} \gamma_j \hat{\sigma}_{t-j} + \sum_{j=1}^{p} \beta_j D_{t-j} + U_t \tag{4.A.6}$$

where the fitted volatility is given by:

$$\hat{\sigma}_t = \hat{\alpha} + \sum_{j=1}^{p} \hat{\gamma}_j \hat{\sigma}_{t-j} + \sum_{j=1}^{p} \hat{\beta}_j \hat{U}_{t-j} + \sum_{k=1}^{m} \hat{\eta_k} TA_{k,t} \tag{4.A.7}$$

6. We compute the unexpected EUA price differences as:

$$\hat{U}_t = D_t - \hat{D}_t \tag{4.A.8}$$

and redo the volatility transformation:

$$\hat{\sigma}_t = |\hat{U}_t| \sqrt{\frac{\pi}{2}} \tag{4.A.9}$$

7. We re-estimate EUA volatility using $\hat{\sigma}_t$ and $\hat{U}_{t-i}$ estimated in Step 6:

$$\hat{\sigma}_t = \alpha + \sum_{i=1}^{p} \gamma_i \hat{\sigma}_{t-i} + \sum_{i=1}^{p} \beta_i \hat{U}_{t-i} + \sum_{k=1}^{m} \eta_k TA_{k,t} + \epsilon_t \tag{4.A.10}$$

4.B The emission allowance price in the EU ETS Phase I

We define the EUA returns (R_t) and daily price differences (D_t) as:

$$R_t = \frac{S_t - S_{t-1}}{S_{t-1}} \tag{4.B.1}$$

$$D_t = S_t - S_{t-1} \tag{4.B.2}$$

where S_t represents the EUA spot price at time t. Fig. 4.B.1 captures the evolution of the EUA spot, returns, and daily price differences over the analysed horizon 19.09.2005 - 31.05.2007.

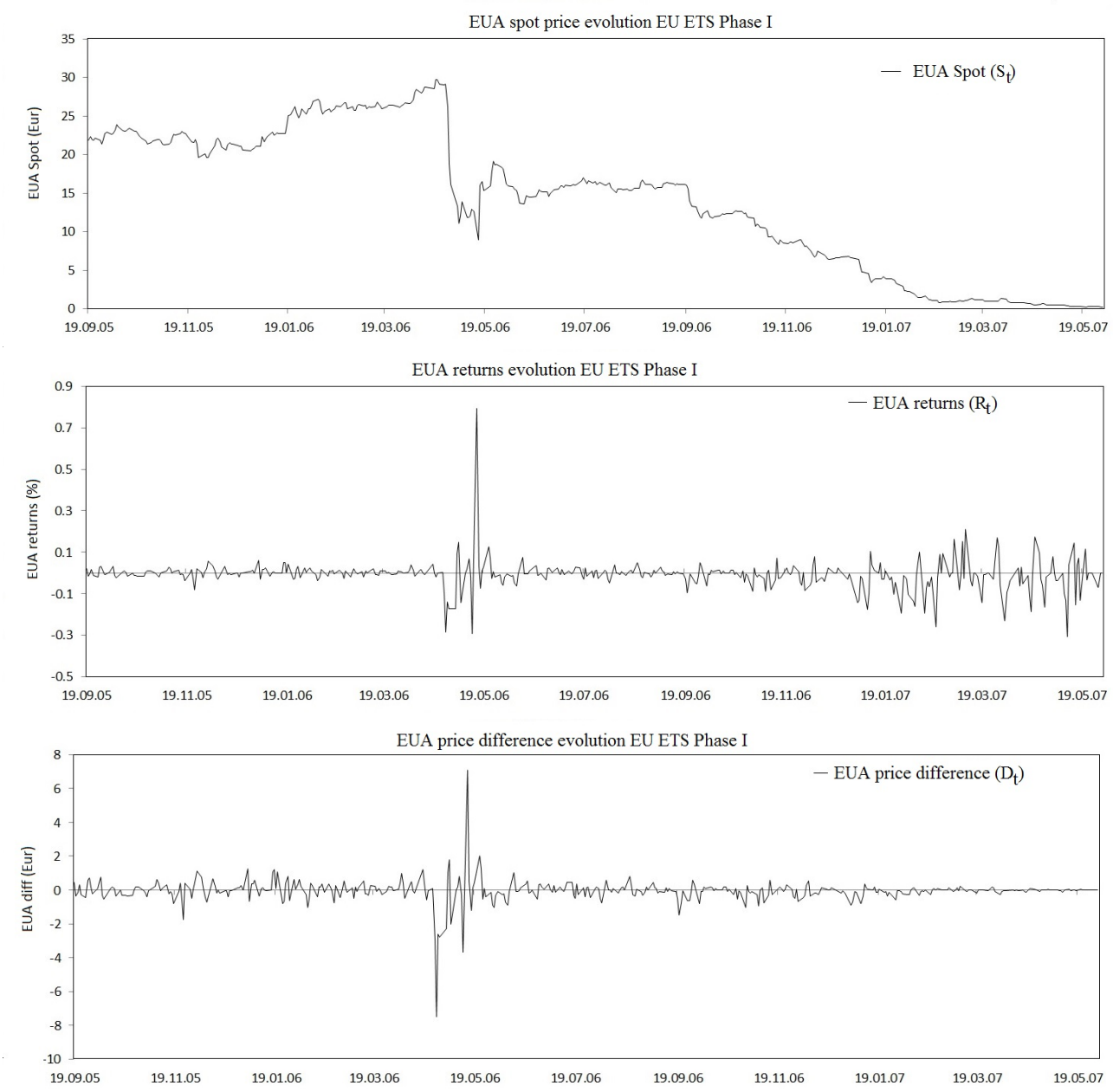

Fig. 4.B.1: EUA spot, daily returns, and daily price differences during Phase I of the EU ETS.

In Fig. 4.B.2, the histograms of the three price series are presented. While the EUA spot appears comparably uniformly distributed over the 0 - 30 Eur/tCO_2 space, both the returns and the price difference series are centered around zero.

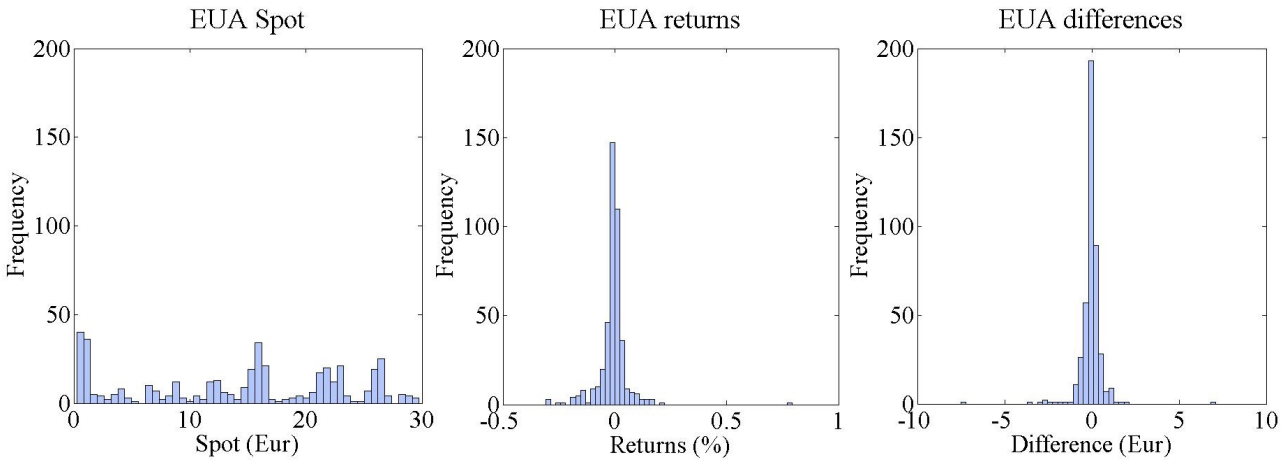

Fig. 4.B.2: Historical distributions for spot prices, daily returns, and daily price differences during Phase I of the EU ETS (19.09.2005 - 31.05.2007).

In order to determine the number of autoregressive lags in price differences, we examine in Fig. 4.B.3 the autocorrelation and partial autocorrelation plots for the entire price difference series. As indicated by the plots, even lags of order higher than 20 are significant. For the regression analysis, we choose to rely on 25 autoregressive terms. This choice results in non-autocorrelated errors.

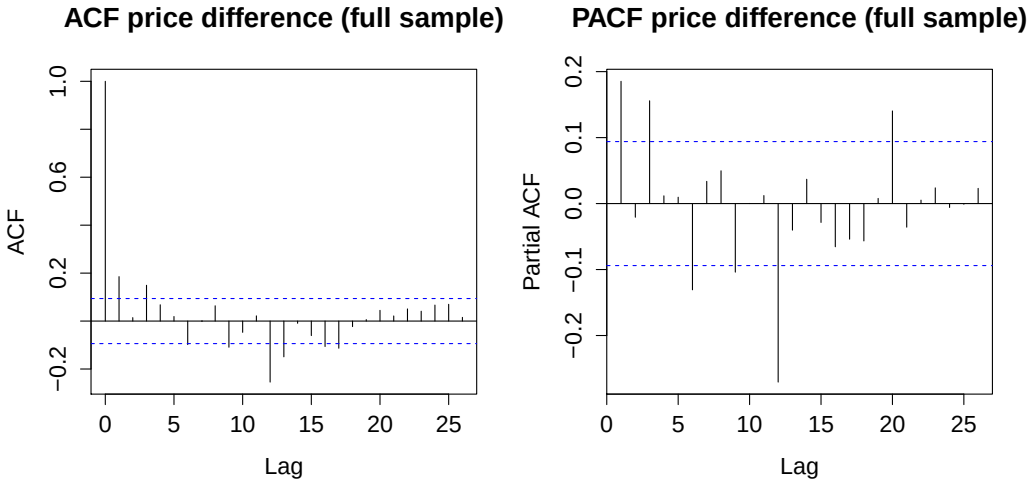

Fig. 4.B.3: Autocorrelation and partial autocorrelation in daily price differences.

4.C The permit trading activity in the EU ETS Phase I

In this section, we present key summary statistics describing the trading activity on the market for emission allowances. Fig. 4.C.1 captures the evolution over time of total traded volumes and number of daily transfers during 15.09.2005 - 31.05.2007. The two variables appear to be positively correlated and have spikes in particular periods of the year, e.g. in December and April of each year. These seasonality can be explained by the specific design of the EU ETS, as explained in Section 4.5.2.3.

In our analysis, we are interested in understanding the trading behavior of different types of players. One criteria for player differentiation is the sector of primary business activity. Table 4.C.1 presents the main statistics linked to the trading activity of different activity sectors. As motivated in the main text, we group players into three main groups: energy, industrials, and non-liable. Table 4.C.1 reveals significant differences among the three players, with the energy sector taking the largest share in terms of volumes, number of accounts, and number of transfers. The non-liable sector,

composed mainly of financial intermediaries, is perhaps on average the most active in terms of trading days and average volumes per trader.

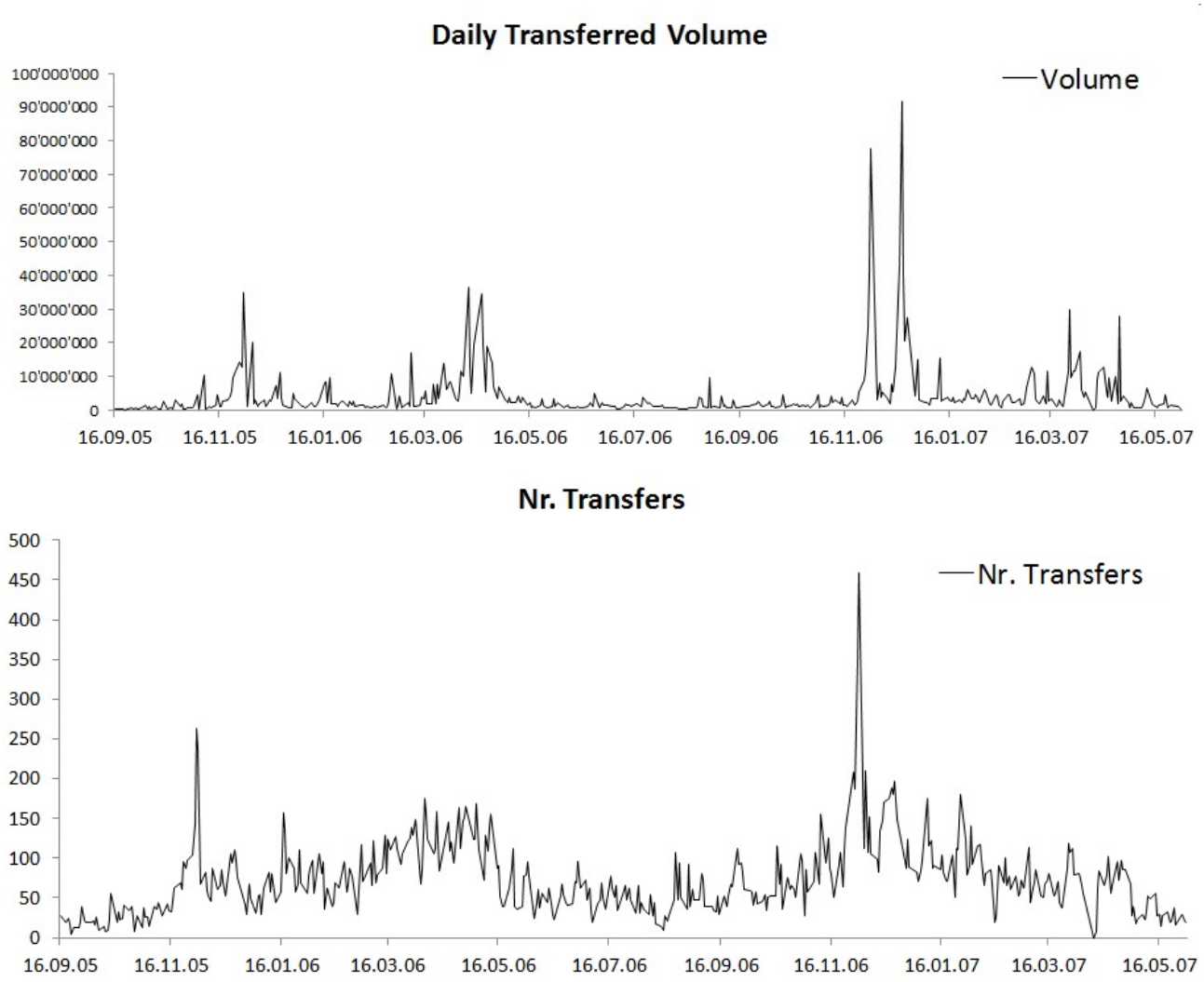

Fig. 4.C.1: Daily transferred volumes and number of transfers in the EU ETS Phase I.

Table 4.C.1: Daily transferred volumes detailed for each sector of activity.

Note: The table captures descriptive statistics for the trading activity of active accounts in the EU ETS during 19.09.2005 - 31.05.2007. Active accounts are defined as those that performed at least one selling or buying operation during the analysed period.

Sector	**Nr. accounts**		**Nr. transfers**		**Volumes**		**Nr. days active**	
Activity	Buy	Sell	Buy	Sell	Buy	Sell	Buy	Sell
Energy								
Combustion Installations	1'192	1'872	12'594	13'862	1'036'724'213	986'140'726	451	459
Mineral oil refineries	67	79	1'913	1'763	87'881'015	96'549'893	388	377
Total energy	**1'259**	**1'951**	**14'507**	**15'625**	**1'124'605'228**	**1'082'690'619**	**455**	**461**
Industrials								
Coke ovens	2	2	3	182	238'000	7'161'000	3	120
Metal ore roasting/sintering	4	5	25	40	316'002	3'072'806	21	29
Pig iron or steel	48	65	189	395	43'469'642	82'284'484	136	198
Cement clinker or lime	65	114	390	577	4'4886'624	58'480'005	169	243
Glass including glass fibre	68	112	196	358	7'369'199	13'118'245	95	174
Ceramic products by firing	120	228	258	548	2'315'181	5'482'803	122	231
Pulp, paper, and board	155	245	739	1'290	9'936'118	18'890'200	275	334
Aircraft operator activities	1	1	1	1	13'996	13'996	1	1
Other activities opted-in	63	62	5'547	3'092	310'161'138	277'397'718	435	410
Total industrials	**526**	**834**	**7'348**	**6'483**	**418'705'900**	**465'901'257**	**407**	**439**
Non-liable								
Bank	86	81	3'337	3'508	107'455'384	106'836'423	424	421
Broker	13	10	85	49	1'369'637	1'306'020	58	37
Consultancy	16	16	6'115	5'702	167'337'887	162'603'299	429	423
Exchange	3	3	13	15	515'002	515'002	11	8
Fund manager	2	1	6	5	40'309	2'432	4	3
Trader	1	1	3	1	2'100	328	3	1
Trust	6	6	36	42	918'816	668'751	22	24
Governmental	1	0	3	0	404	0	3	0
NGO	90	83	828	851	29'123'682	29'550'218	291	294
Total non-liable	**218**	**201**	**10'426**	**10'173**	**306'763'221**	**301'482'473**	**453**	**443**

Another important criterion of trader classification is the number of permits initially allocated for free. Table 4.C.2 presents summary statistics on the number of permits over-allocated to each sector (energy, industrials, and non-liable). The number of permits over-allocated is computed as the number of permits initially received for free minus the number of permits surrendered at the end of each compliance year (the number of permits covering total realized emissions). The information is presented for each compliance year in Phase I. We observe that the energy sector has been generally under-allocated over Phase I, although it had a large number of excess permits in 2005. The industrials sector has been generally over-allocated, explaining the higher propensity of the sector to participate in the permit market on the sell side, rather than on the buy side. The non-liable players have entered the market voluntarily and were by definition non subject to emission regulation under the EU ETS. As such, their initial permit allocation (and over-allocation) was zero.

Table 4.C.2: Descriptive statistics regarding the over-allocation of permits per sector of activity.

Note: The table presents key descriptive statistics regarding the initial permit allocation status of three sectors of activity (energy, industrials, and non-liable institutions) for 19.09.2005 - 31.05.2007. The number of permits over-allocated is computed as the difference between initially allocated allowances (for free) and the final number of surrendered allowances.

	Sector of activity		
Indicator	Energy	Industrials	Non-liable
Nr. permits over-allocated			
2005	261'422'527	159'129'599	0
2006	-261'635'140	-47'905'466	0
2007	-51'059'179	40'760'772	0
2005-2007	-51'271'792	151'984'905	0
Nr. accounts over-allocated			
(% in total)			
2005	63.82%	68.87%	0
2006	50.32%	46.76%	0
2007	62.67%	55.42%	0

4.D Volatility and transferred volumes: supporting results

This section presents supporting results for the anaylsis undertaken in Section 4.5.2.1. Tables 4.D.1 - 4.D.4 present the estimation results of the regressions of daily price difference volatility on different proxies of the trading volumes. According to trader type, four categorizations of volumes are made: (i) regulated and non-regulated volumes; (ii) volumes traded by under- and over-allocated agents; (iii) volumes separated according to the sector of primary business activity of the trader (energy, industrials, non-liable), and (iv) volumes separated according to both the under- and over-allocated status and the sector of activity of the trader. The results of the different models are discussed in Section 4.5.2.1.

Table 4.D.1: Regressions of volatility on liable and non-liable volumes.

Note: The table presents results from the second iteration of the estimation of Eq. (4.2) based on the results from the first estimation of Eq. (4.1). The dependent variable is the volatility of daily spot EUA price differences. The analysed period is 15.09.2005 - 31.05.2007. For all estimated coefficients, standard errors are presented in brackets. F-test statistics are listed for $\sum_{j=1}^{n=25} \hat{\beta}_j$ and $\sum_{j=1}^{n=25} \hat{\gamma}_j$. The Box-Pierce statistic is computed with $k = 2\sqrt{N}$, N = 334.

	Total Volume			**Expected and Unexpected Volume**		
	Buy + Sell ($\mathcal{M}$ A1)	**Buy** ($\mathcal{M}$ A2)	**Sell** ($\mathcal{M}$ A3)	**Buy + Sell** ($\mathcal{M}$ A4)	**Buy** ($\mathcal{M}$ A5)	**Sell** ($\mathcal{M}$ A6)
Intercept	0.05 (0.06)	0.05 (0.06)	0.05 (0.06)	0.07 (0.06)	0.07 (0.06)	0.07 (0.06)
$\sum_{j=1}^{n=25} \hat{\gamma}_j$	0.82 (8.71)***	0.83 (8.60)***	0.83 (8.72)***	0.83 (8.82)***	0.83 (8.67)***	0.84 (8.78)***
$\sum_{j=1}^{n=25} \hat{\beta}_j$	0.39 (1.36)	0.40 (1.36)	0.40 (1.38)	0.43 (1.37)	0.44 (1.36)	0.45 (1.37)
Liable						
Total	0.04 (0.02)°	0.04 (0.02)*	0.04 (0.02)			
Expected				0.00 (0.03)	0.01 (0.03)	-0.00 (0.03)
Unexpected				0.05 (0.02)*	0.05 (0.02)*	0.05 (0.02)*
Non-liable						
Total	-0.01 (0.02)	-0.01 (0.02)	-0.00 (0.02)			
Expected				-0.00 (0.03)	-0.01 (0.03)	0.01 (0.02)
Unexpected				-0.01 (0.02)	-0.01 (0.02)	-0.00 (0.03)
R^2	0.48	0.47	0.48	0.48	0.48	0.48
Adj. R^2	0.38	0.38	0.38	0.38	0.38	0.38
AIC	525.85	526.26	526.52	525.37	526.60	527.37
Box-Pierce test (p-val)	16.79 (0.11)	16.48 (0.12)	16.74 (0.12)	18.52 (0.07)	18.21 (0.08)	17.69 (0.09)

$^{***}p < 0.001$, $^{**}p < 0.01$, $^{*}p < 0.05$, $^{\circ}p < 0.1$

Table 4.D.2: Regressions of volatility on volumes traded by over-allocated, under-allocated, and non-liable agents.

Note: The table presents results from the second iteration of the estimation of Eq. (4.2) based on the results from the first estimation of Eq. (4.1). The dependent variable is the volatility of daily spot EUA price differences. The analysed period is 15.09.2005 - 31.05.2007. For all estimated coefficients, standard errors are presented in brackets. F-test statistics are listed for $\sum_{j=1}^{n=25} \hat{\beta}_j$ and $\sum_{j=1}^{n=25} \hat{\gamma}_j$. The Box-Pierce statistic is computed with $k = 2\sqrt{N}$, N = 334.

	Total Volume			**Expected and Unexpected Volume**		
	Buy + Sell ($\mathcal{M}$ A7)	**Buy** ($\mathcal{M}$ A8)	**Sell** ($\mathcal{M}$ A9)	**Buy + Sell** ($\mathcal{M}$ A10)	**Buy** ($\mathcal{M}$ A11)	**Sell** ($\mathcal{M}$ A12)
Intercept	0.06 (0.06)	0.06 (0.06)	0.05 (0.06)	0.06 (0.06)	0.13 (0.07)	0.06 (0.06)
$\sum_{j=1}^{n=25} \hat{\gamma}_j$	0.81 (8.60)***	0.79 (7.97)***	0.83 (8.42)***	0.81 (8.56)***	0.78 (7.88)***	0.81 (8.92)***
$\sum_{j=1}^{n=25} \hat{\beta}_j$	0.32 (1.42)°	0.30 (1.71)*	0.42 (1.45)°	0.32 (1.45)°	0.19 (2.18)**	0.41 (1.58)*
Over-allocated						
Total	0.04 (0.04)	0.04 (0.03)	0.04 (0.03)			
Expected				0.00 (0.05)	0.04 (0.04)	0.04 (0.04)
Unexpected				0.05 (0.04)	0.05 (0.03)°	0.04 (0.03)
Under-allocated						
Total	0.04 (0.08)	0.04 (0.04)	0.03 (0.05)			
Expected				0.12 (0.11)	-0.17 (0.05)**	0.02 (0.10)
Unexpected				0.04 (0.08)	0.06 (0.04)	0.03 (0.05)
Non-liable						
Total	-0.01 (0.02)	-0.01 (0.02)	-0.00 (0.02)			
Expected				-0.00 (0.03)	-0.03 (0.02)	-0.00 (0.02)
Unexpected				-0.01 (0.03)	-0.02 (0.02)	-0.00 (0.02)
R^2	0.48	0.47	0.47	0.48	0.50	0.47
Adj. R^2	0.38	0.37	0.37	0.37	0.40	0.36
AIC	525.39	518.37	527.23	529.09	456.52	516.21
Box-Pierce test (p-val)	16.59 (0.12)	15.95 (0.14)	16.52 (0.12)	17.28 (0.10)	17.07 (0.11)	13.59 (0.26)

$^{***}p < 0.001$, $^{**}p < 0.01$, $^{*}p < 0.05$, $^{\circ}p < 0.1$.

Table 4.D.3: Regressions of volatility on volumes traded by agents sorted by business activity sector.

Note: The table presents results from the second iteration of the estimation of Eq. (4.2) based on the results from the first estimation of Eq. (4.1). The dependent variable is the volatility of daily spot EUA price differences. The analysed period is 15.09.2005 - 31.05.2007. For all estimated coefficients, standard errors are presented in brackets. F-test statistics are listed for $\sum_{j=1}^{n=25} \hat{\beta}_j$ and $\sum_{j=1}^{n=25} \hat{\gamma}_j$. The Box-Pierce statistic is computed with $k = 2\sqrt{N}$, N = 334.

	Total Volume			**Expected and Unexpected Volume**		
	Buy + Sell ($\mathcal{M}$ A13)	**Buy** ($\mathcal{M}$ A14)	**Sell** ($\mathcal{M}$ A15)	**Buy + Sell** ($\mathcal{M}$ A16)	**Buy** ($\mathcal{M}$ A17)	**Sell** ($\mathcal{M}$ A18)
Intercept	0.05 (0.06)	0.05 (0.07)	0.05 (0.06)	0.07 (0.07)	0.07 (0.07)	0.08 (0.07)
$\sum_{j=1}^{n=25} \hat{\gamma}_j$	0.81 (8.07)***	0.82 (7.34)***	0.82 (8.49)***	0.81 (7.99)***	0.85 7.97***	0.81 (8.50)***
$\sum_{j=1}^{n=25} \hat{\beta}_j$	0.34 (1.41)°	0.37 (1.45)°	0.36 (1.38)	0.35 (1.44)°	0.40 1.66*	0.35 (1.35)
Energy						
Total	0.04 (0.02)°	0.05 (0.02)*	0.03 (0.03)			
Expected				0.01 (0.04)	0.01 (0.03)	-0.02 (0.05)
Unexpected				0.05 (0.02)*	0.05 (0.02)*	0.04 (0.03)°
Industrials						
Total	0.04 (0.08)	0.00 (0.08)	0.07 (0.07)			
Expected				0.09 (0.12)	-0.09 (0.11)	0.14 (0.11)
Unexpected				0.05 (0.08)	0.01 (0.08)	0.09 (0.08)
Non-liable						
Total	-0.02 (0.02)	-0.02 (0.02)	-0.01 (0.02)			
Expected				-0.01 (0.03)	-0.02 (0.03)	0.00 (0.02)
Unexpected				-0.02 (0.03)	-0.01 (0.02)	-0.01 (0.03)
R^2	0.46	0.46	0.47	0.47	0.47	0.48
Adj. R^2	0.36	0.35	0.37	0.36	0.37	0.37
AIC	532.75	533.16	530.52	538.29	532.40	530.42
Box-Pierce test (p-val)	16.92 (0.11)	16.67 (0.12)	16.62 (0.12)	16.99 (0.11)	15.06 (0.18)	18.59 (0.07)

$^{***}p < 0.001$, $^{**}p < 0.01$, $^{*}p < 0.05$, $^{\circ}p < 0.1$.

Table 4.D.4: Regressions of volatility on volumes traded by agents sorted by business activity sector and permit allocation status.

Note: The table presents results from the second iteration of the estimation of Eq. (4.2) based on the results from the first estimation of Eq. (4.1). The dependent variable is the volatility of daily spot EUA price differences. The analysed period is 15.09.2005 - 31.05.2007. For all estimated coefficients, standard errors are presented in brackets. F-test statistics are listed for $\sum_{j=1}^{n=25} \hat{\beta}_j$ and $\sum_{j=1}^{n=25} \hat{\gamma}_j$. The Box-Pierce statistic is computed with $k = 2\sqrt{N}$, N = 334.

	Total Volume			**Expected and Unexpected Volume**		
	Buy + Sell ($\mathcal{M}$ A19)	**Buy** ($\mathcal{M}$ A20)	**Sell** ($\mathcal{M}$ A21)	**Buy + Sell** ($\mathcal{M}$ A22)	**Buy** ($\mathcal{M}$ A23)	**Sell** ($\mathcal{M}$ A24)
Intercept	0.06 (0.06)	0.07 (0.06)	0.05 (0.06)	0.05 (0.07)	0.17 (0.06)**	0.04 (0.07)
$\sum_{j=1}^{n=25} \hat{\gamma}_j$	0.81 (8.26)***	0.78 (8.94)***	0.83 (8.18)***	0.86 (9.01)***	0.70 (8.77)***	0.96 (8.10)***
$\sum_{j=1}^{n=25} \hat{\beta}_j$	0.37 (1.42)°	0.21 (1.64)*	0.45 (1.57)*	0.56 (1.25)	0.04 (2.00)**	0.60 (1.09)
Energy						
Over-allocated						
Total	0.05 (0.04)	0.05 (0.03)°	0.04 (0.03)			
Expected				0.07 (0.06)	-0.01 (0.04)	0.03 (0.05)
Unexpected				0.05 (0.05)	0.05 (0.03)	0.08 (0.03)*
Under-allocated						
Total	0.00 (0.08)	0.01 (0.05)	0.01 (0.06)			
Expected				-0.18 (0.13)	-0.20 (0.07)**	-0.20 (0.12)°
Unexpected				0.03 (0.09)	0.04 (0.05)	-0.01 (0.05)
Industrials						
Over-allocated						
Total	-0.00 (0.09)	0.02 (0.07)	0.02 (0.09)			
Expected				-0.15 (0.14)	0.19 (0.13)	-0.12 (0.13)
Unexpected				-0.01 (0.09)	0.17 (0.08)*	-0.02 (0.08)
Under-allocated						
Total	0.45 (0.32)	0.59 (0.4)	0.21 (0.17)			
Expected				1.45 (0.5)**	0.67 (0.41)	0.25 (0.22)
Unexpected				0.57 (0.33)°	0.5 (0.4)	0.22 (0.16)
Non-liable						
Total	-0.02 (0.02)	-0.01 (0.02)	-0.01 (0.02)			
Expected				-0.01 (0.03)	-0.02 (0.02)	-0.00 (0.02)
Unexpected				-0.00 (0.02)	-0.02 (0.02)	-0.02 (0.02)
R^2	0.47	0.49	0.47	0.5	0.52	0.47
Adj. R^2	0.37	0.39	0.37	0.4	0.42	0.35
AIC	527.68	487.62	532.30	530.60	452.98	507.55
Box-Pierce test (p-val)	14.87 (0.19)	19.28 (0.06)	14.33 (0.21)	23.17 (0.02)	17.83 (0.09)	16.36 (0.13)

$^{***}p < 0.001$, $^{**}p < 0.01$, $^{*}p < 0.05$, $^{\circ}p < 0.1$.

4.E Volatility and number of permit transfers: supporting results

The number of daily permit transfers is another proxy for the trading activity. This section presents regression results in support for the anaylsis undertaken in Section 4.5.2.2. Table 4.E.1 presents the results of the estimation of volatility on the number of daily permit transfers when agents are grouped according to their emission regulation liability and the over-/under-allocation status. The interpretation of results can be found in Section 4.5.2.2. Substituting traded volumes with the number of daily permit transfers confirms the previous findings and results in models with a higher explanatory power. Table 4.E.2 includes both volumes and number of transfers in the regressions of volatility. We find that volumes have no additional explanatory power beyond that contained in the number of daily permit transfers. We believe that, in this generally over-allocated market, the number of trades has been more sensitive to relevant arriving information than the size of the trades.

Table 4.E.1: Regressions of volatility on the number of transfers led by agents sorted according to the compliance regulation and the permit allocation status.

Note: The table presents results from the second iteration of the estimation of Eq. (4.2) based on the results from the first estimation of Eq. (4.1). The dependent variable is the volatility of daily spot EUA price differences. The analysed period is 15.09.2005 - 31.05.2007. For all estimated coefficients, standard errors are presented in brackets. F-test statistics are listed for $\sum_{j=1}^{n=25} \hat{\beta}_j$ and $\sum_{j=1}^{n=25} \hat{\gamma}_j$. The Box-Pierce statistic is computed with $k = 2\sqrt{N}$, N = 334.

	Liable and non-liable			**Over-allocated, under-allocated, and non-liable**		
	Buy + Sell ($\mathcal{M}$ A25)	**Buy** ($\mathcal{M}$ A26)	**Sell** ($\mathcal{M}$ A27)	**Buy + Sell** ($\mathcal{M}$ A28)	**Buy** ($\mathcal{M}$ A29)	**Sell** ($\mathcal{M}$ A30)
Intercept	-0.04 (0.08)	-0.05 (0.08)	-0.04 (0.08)	-0.03 (0.08)	-0.03 (0.07)	-0.04 (0.08)
$\sum_{j=1}^{n=25} \hat{\gamma}_j$	0.79 (8.32)***	0.80 (8.24)***	0.79 (8.34)***	0.78 (8.44)***	0.78 (8.46)***	0.80 (8.33)***
$\sum_{j=1}^{n=25} \hat{\beta}_j$	0.51 (1.51)°	0.53 (1.51)°	0.52 (1.50)°	0.47 (1.55)*	0.45 (1.56)*	0.54 (1.51)°
Nr. transfers						
Liable	0.23 (0.1)*	0.24 (0.1)*	0.20 (0.09)*			
Non-liable	-0.01 (0.14)	0.01 (0.12)	0.01 (0.14)	-0.01 (0.14)	0.01 (0.12)	0.02 (0.14)
Over-allocated				0.21 (0.13)	0.19 (0.14)	0.21 (0.10) *
Under-allocated				0.30 (0.4)	0.39 (0.31)	0.09 (0.35)
R^2	0.48	0.47	0.48	0.48	0.48	0.48
Adj. R^2	0.38	0.38	0.38	0.38	0.38	0.38
AIC	528.04	528.65	528.38	523.04	518.71	529.36
Box-Pierce test (p-val)	18.18 (0.08)	17.99 (0.08)	18.02 (0.08)	17.69 (0.09)	16.59 (0.12)	18.09 (0.08)

$^{***}p < 0.001$, $^{**}p < 0.01$, $^{*}p < 0.05$, $^{\circ}p < 0.1$.

Table 4.E.2: Regressions of volatility on volumes and number of transfers led by agents sorted by business activity sector.

Note: The table presents results from the second iteration of the estimation of Eq. (4.2) based on the results from the first estimation of Eq. (4.1). The dependent variable is the volatility of daily spot EUA price differences. The analysed period is 15.09.2005 - 31.05.2007. For all estimated coefficients, standard errors are presented in brackets. F-test statistics are listed for $\sum_{j=1}^{n=25} \hat{\beta}_j$ and $\sum_{j=1}^{n=25} \hat{\gamma}_j$. The Box-Pierce statistic is computed with $k = 2\sqrt{N}$, N = 334.

	Total Volume			**Expected and Unexpected Volume**		
	Buy + Sell ($\mathcal{M}$ A31)	**Buy** ($\mathcal{M}$ A32)	**Sell** ($\mathcal{M}$ A33)	**Buy + Sell** ($\mathcal{M}$ A34)	**Buy** ($\mathcal{M}$ A35)	**Sell** ($\mathcal{M}$ A36)
Intercept	-0.06 (0.09)	-0.05 (0.09)	-0.06 (0.09)	-0.04 (0.09)	-0.07 (0.09)	-0.05 (0.09)
$\sum_{j=1}^{n=25} \hat{\gamma}_j$	0.78 (7.71)***	0.77 (7.78)***	0.78 (7.54)***	0.77 (7.95)***	0.84 (8.37)***	0.78 (7.91)***
$\sum_{j=1}^{n=25} \hat{\beta}_j$	0.62 (1.77)*	0.60 (1.80)*	0.63 (1.68)*	0.64 (1.72)*	0.72 (2.05)**	0.66 (1.54)°
Energy						
Volume						
Total	-0.02 (0.03)	-0.01 (0.03)	-0.03 (0.03)			
Expected				-0.07 (0.05)	-0.06 (0.04)	-0.10 (0.06)°
Unexpected				-0.01 (0.03)	-0.01 (0.03)	-0.02 (0.03)
Nr. transfers	0.28 (0.17)°	0.29 (0.15) °	0.27 (0.16)°	0.32 (0.17)°	0.30 (0.15)°	0.31 (0.16)*
Industrials						
Volume						
Total	-0.03 (0.08)	-0.02 (0.08)	-0.02 (0.08)			
Expected				0.00 (0.13)	-0.17 (0.12)	0.00 (0.13)
Unexpected				-0.01 (0.08)	-0.04 (0.08)	-0.00 (0.08)
Nr. transfers	-0.04 (0.47)	-0.06 (0.43)	0.03 (0.40)	-0.05 (0.48)	0.29 (0.44)	0.05 (0.40)
Non-liable						
Volume						
Total	-0.03 (0.03)	-0.04 (0.03)	-0.02 (0.03)			
Expected				-0.03 (0.03)	-0.03 (0.03)	-0.02 (0.03)
Unexpected				-0.03 (0.03)	-0.03 (0.03)	-0.02 (0.03)
Nr. transfers	0.11 (0.16)	0.1 (0.14)	0.12 (0.17)	0.12 (0.17)	0.09 (0.14)	0.13 (0.17)
R^2	0.47	0.48	0.46	0.48	0.5	0.48
Adj. R^2	0.37	0.37	0.36	0.37	0.4	0.36
AIC	540.25	534.68	545.73	540.25	527.10	541.23
Box-Pierce test (p-val)	13.17 (0.28)	13.76 (0.25)	12.83 (0.30)	15.79 (0.15)	15.98 (0.14)	16.38 (0.13)

$^{***}p < 0.001$, $^{**}p < 0.01$, $^{*}p < 0.05$, $^{\circ}p < 0.1$.

4.F The April effect: supporting results

This section provides additional supporting results for the analysis undertaken in Section 4.5.2.3. As mentioned before, the EU ETS is an artificially created market whose rules and their changes have an impact on market variables. In particular, we observe that both the permit price process and the trading activity of market participants is characterized by seasonality. More precisely, an intensification in the trading activity as well as an increase in the magnitude of daily price changes can be observed in specific periods of the year. Two months stand out for their intensified activity, namely December and April of each year. Fig. 4.F.1 captures the most important annual events taking place in the European compliance market. This information motivates our decision to check for seasonality patterns in volatility by including month dummies.

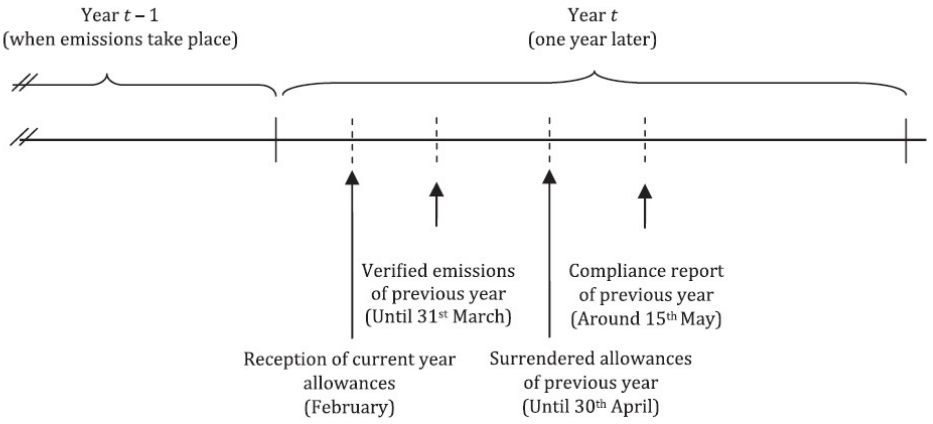

Fig. 4.F.1: The EU ETS compliance timeline. Source: Lucia et al. (2014).

Table 4.F.1 presents the results of the regressions of volatility on month dummies and volumes traded by agents sorted according to their sector of activity. The results confirm our findings when proxying the trading activity by the number of daily transfer. In particular, volatility is generally higher in April. Table 4.F.2 presents the results of the analysis when including an interaction term between traded volumes and the April dummy. We find that the volumes traded by the non-liable sector in April are significantly and positively correlated with the price change volatility. The results are further discussed in Section 4.5.2.3.

Table 4.F.1: Regressions of volatility on month dummies and volumes traded by agents sorted by business activity sector.

	Total Volume			**Expected and Unexpected Volume**		
	Buy + Sell ($\mathcal{M}$ A37)	**Buy** ($\mathcal{M}$ A38)	**Sell** ($\mathcal{M}$ A39)	**Buy + Sell** ($\mathcal{M}$ A40)	**Buy** ($\mathcal{M}$ A41)	**Sell** ($\mathcal{M}$ A42)
Intercept	0.07 (0.11)	0.07 (0.11)	0.06 (0.11)	0.05 (0.11)	0.09 (0.11)	0.06 (0.12)
$\sum_{j=1}^{n=25} \hat{\gamma}_j$	0.84 (8.90)***	0.84 (8.61)***	0.83 (9.31)***	0.90 (9.78)***	0.88 (8.97)***	0.91 (9.77)***
$\sum_{j=1}^{n=25} \hat{\beta}_j$	0.04 (2.07)**	0.02 (2.23)***	0.06 (1.97)**	0.15 (1.87)**	0.08 (2.34)***	0.17 (1.75)*
Month Dummy						
February	-0.13 (0.13)	-0.14 (0.13)	-0.12 (0.13)	-0.13 (0.13)	-0.17 (0.13)	-0.12 (0.13)
March	-0.10 (0.13)	-0.10 (0.12)	-0.10 (0.12)	-0.08 (0.12)	-0.08 (0.12)	-0.07 (0.12)
April	0.41 (0.16)*	0.43 (0.16)*	0.39 (0.16)*	0.40 (0.16)*	0.47 (0.16)**	0.38 (0.16)*
May	-0.23 (0.14)	-0.24 (0.14) °	-0.21 (0.14)	-0.24 (0.14) °	-0.27 (0.14) °	-0.22 (0.14)
June	-0.07 (0.17)	-0.08 (0.17)	-0.05 (0.17)	-0.03 (0.17)	-0.05 (0.17)	-0.06 (0.17)
July	-0.00 (0.15)	-0.00 (0.15)	0.01 (0.15)	-0.03 (0.15)	-0.04 (0.15)	-0.00 (0.14)
August	-0.08 (0.15)	-0.08 (0.15)	-0.08 (0.15)	-0.07 (0.14)	-0.10 (0.15)	-0.09 (0.14)
September	0.03 (0.15)	0.03 (0.15)	0.04 (0.15)	0.03 (0.15)	0.01 (0.15)	0.03 (0.14)
October	0.04 (0.15)	0.04 (0.15)	0.05 (0.15)	0.02 (0.14)	0.03 (0.14)	0.01 (0.14)
November	-0.01 (0.15)	-0.01 (0.15)	-0.00 (0.15)	0.00 (0.15)	-0.01 (0.15)	-0.00 (0.14)
December	-0.23 (0.17)	-0.23 (0.17)	-0.21 (0.17)	-0.23 (0.17)	-0.20 (0.17)	-0.18 (0.17)
Volumes						
Energy						
Total	0.05 (0.02)°	0.04 (0.02)*	0.04 (0.03)			
Expected				0.04 (0.04)	0.01 (0.04)	0.03 (0.05)
Unexpected				0.05 (0.02)*	0.04 (0.02) °	0.05 (0.03)*
Industrials						
Total	-0.07 (0.08)	-0.10 (0.08)	-0.03 (0.07)			
Expected				-0.22 (0.11)*	-0.26 (0.10)*	-0.21 (0.11) °
Unexpected				-0.09 (0.08)	-0.11 (0.08)	-0.04 (0.07)
Non-liable						
Total	-0.00 (0.02)	-0.01 (0.02)	0.00 (0.02)			
Expected				0.01 (0.03)	-0.01 (0.03)	0.01 (0.02)
Unexpected				-0.00 (0.02)	-0.00 (0.02)	-0.00 (0.02)
R^2	0.53	0.53	0.53	0.55	0.55	0.55
Adj. R^2	0.42	0.42	0.42	0.43	0.43	0.43
AIC	497.03	493.18	496.04	486.39	489.70	479.92
Box-Pierce test (p-val)	23.80 (0.01)	24.44 (0.01)	21.22 (0.03)	18.39 (0.07)	20.00 (0.05)	21.24 (0.03)

$^{***}p < 0.001$, $^{**}p < 0.01$, $^{*}p < 0.05$, $^{\circ}p < 0.1$.

Table 4.F.2: Regressions of volatility on the daily volumes of permits and interaction with April month dummy by different trading sectors.

Note: The table presents results from the second iteration of the estimation of Eq. (4.2) based on the results from the first estimation of Eq. (4.1). The dependent variable is the volatility of daily spot EUA price differences. The analysed period is 15.09.2005 - 31.05.2007. For all estimated coefficients, standard errors are presented in brackets. F-test statistics are listed for $\sum_{j=1}^{n=25} \hat{\beta}_j$ and $\sum_{j=1}^{n=25} \hat{\gamma}_j$. The Box-Pierce statistic is computed with $k = 2\sqrt{N}$, N = 334.

	Volume		
	Buy + Sell ($\mathcal{M}$ A43)	**Buy** ($\mathcal{M}$ A44)	**Sell** ($\mathcal{M}$ A45)
Intercept	0.1 (0.06)	0.1 (0.06)	0.11 (0.06)
$\sum_{j=1}^{n=25} \hat{\gamma}_j$	0.65 (7.97)***	0.67 (7.90)***	0.63 (7.76)***
$\sum_{j=1}^{n=25} \hat{\beta}_j$	-0.15 (2.30)***	-0.19 (2.17)**	-0.14 (2.41)***
Volumes			
Energy	0.02 (0.03)	0.03 (0.02)	0.01 (0.04)
Industrials	0.05 (0.29)	-0.14 (0.32)	0.10 (0.20)
Non-liable	-0.02 (0.02)	-0.03 (0.02)	-0.02 (0.02)
Interaction Volume-April Dummy			
Energy*April	-0.06 (0.05)	-0.05 (0.05)	-0.07 (0.05)
Industrials*April	-0.11 (0.3)	0.11 (0.33)	-0.18 (0.21)
Non-liable*April	2.96 (0.56)***	2.28 (0.52)***	3.61 (0.58)***
R^2	0.51	0.50	0.52
Adj. R^2	0.41	0.40	0.42
AIC	481.84	493.94	469.01
Box-Pierce test (p-val)	19.77 (0.05)	17.77 (0.09)	22.35 (0.02)

$^{***}p < 0.001$, $^{**}p < 0.01$, $^{*}p < 0.05$, $^{\circ}p < 0.1$

To have a better grasp of the April effect, we plot the volumes and number of permit transfers conducted by each sector during the analysed horizon; see Figs. 4.F.2 - 4.F.7. In each plot, the trading activity is aggregated at the monthly horizon. We observe that at the monthly level, the trading activity of the three sectors followed different patterns, most likely due to the initial permit allocation status (over-, under-allocated, or no allocation). Specifically, the energy sector tended to align its monthly bought and sold volumes, with net traded volumes close to zero. The trading activity of the industrial sector has been more intense on the sell than the buy side, as could be expected from the fact that the sector was generally over-allocated. The non-liable sector, with no initial allocation tended to acquire more permits than sell over the year, with the exception of the month of December, when most probably the permits underlying various futures/forward contracts reached maturity and permits have been transferred to liable counterparties.

Trying to link the monthly trading activity with the April effect, we observe that it spiked in April of each year for all sectors, both in terms of volumes and number of trades. This might be the result of excessive trading before the final surrendering of permits for the previous compliance year. It might also be that volumes have reflected the drop in permit prices due to the general acknowledgment of market over-allocation after the publication of total realized emissions in April.

Looking specifically at the daily permit trading activity characterising the days around the April 2006 crash, we observe that spikes in traded volumes took place immediately before the crash; see Fig. 4.F.8. The main trading players were the energy and industrial representatives, with the non-liable sector having a fairly uniformly distributed amount of volumes before and after the crash. Taking a look at the number of transfers reveals that these presented similar magnitudes before and after the April 2006 crash, revealing that the average volumes transferred per transaction have been higher than usually before the crash for the energy and industrials sectors.

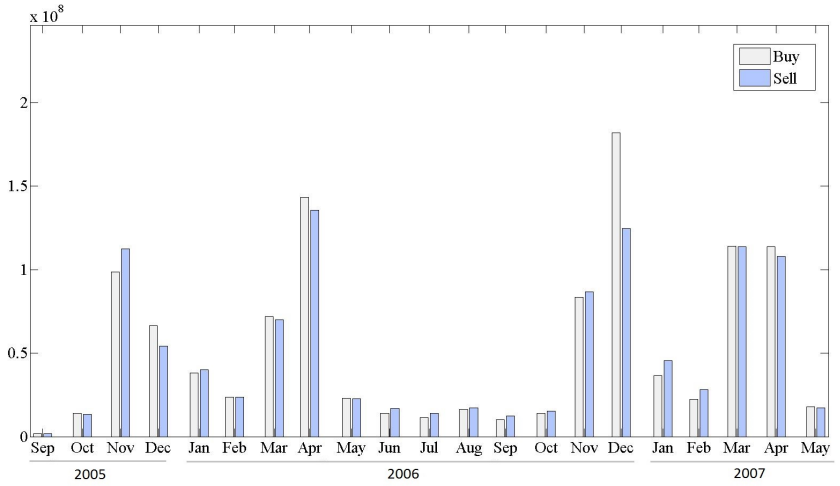

Fig. 4.F.2: Volumes bought and sold by the energy sector during Phase I.

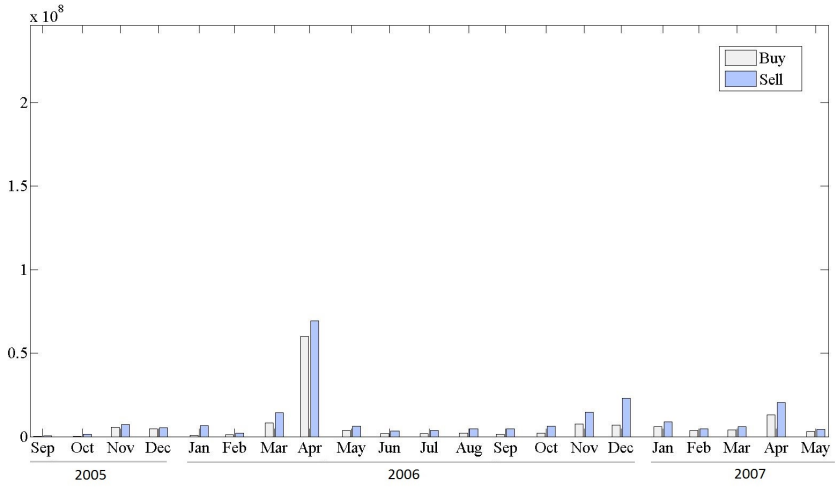

Fig. 4.F.3: Volumes bought and sold by the industrial sector during Phase I.

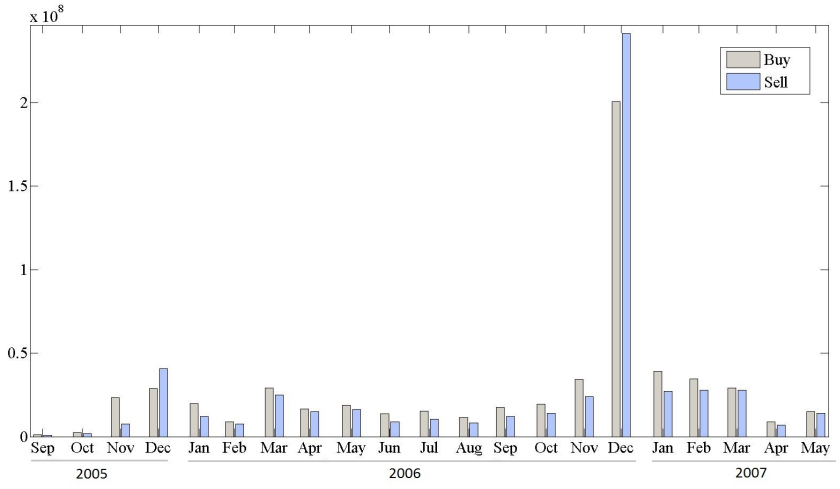

Fig. 4.F.4: Volumes bought and sold by the non-liable sector during Phase I.

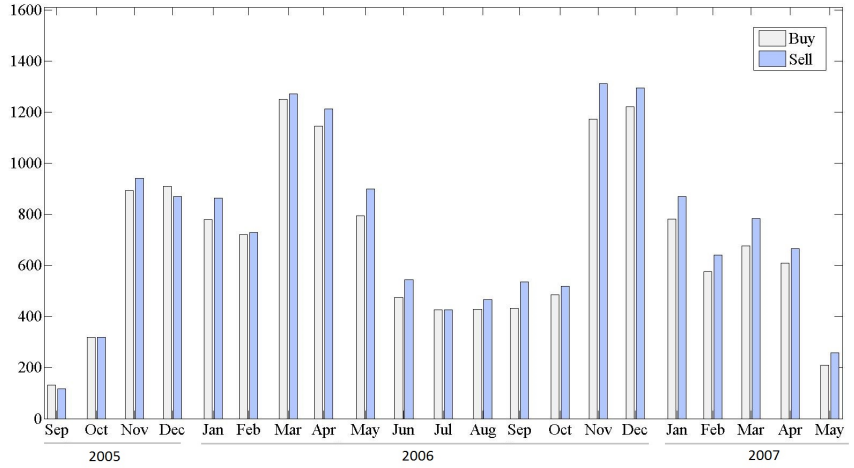

Fig. 4.F.5: Number of monthly transfers performed by the energy sector during Phase I.

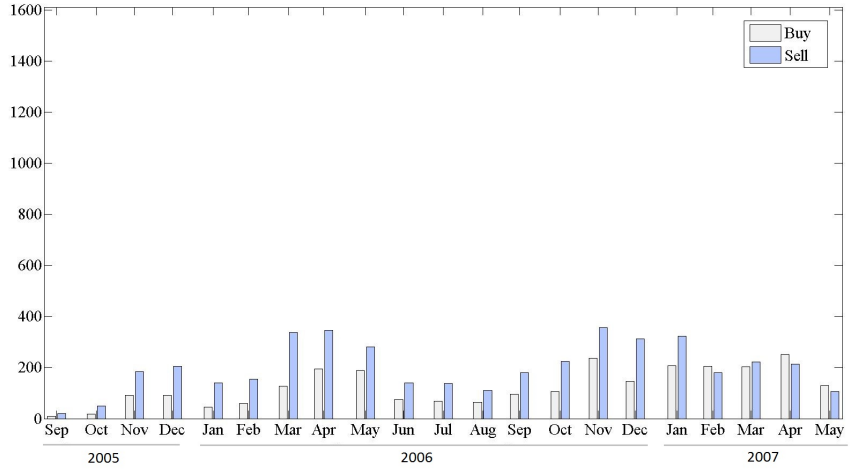

Fig. 4.F.6: Number of monthly transfers performed by the industrial sector during Phase I.

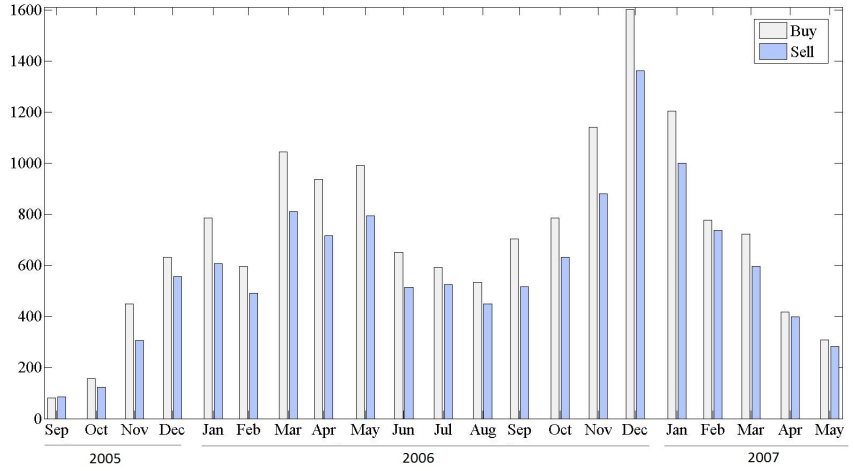

Fig. 4.F.7: Number of monthly transfers performed by the financial sector during Phase I.

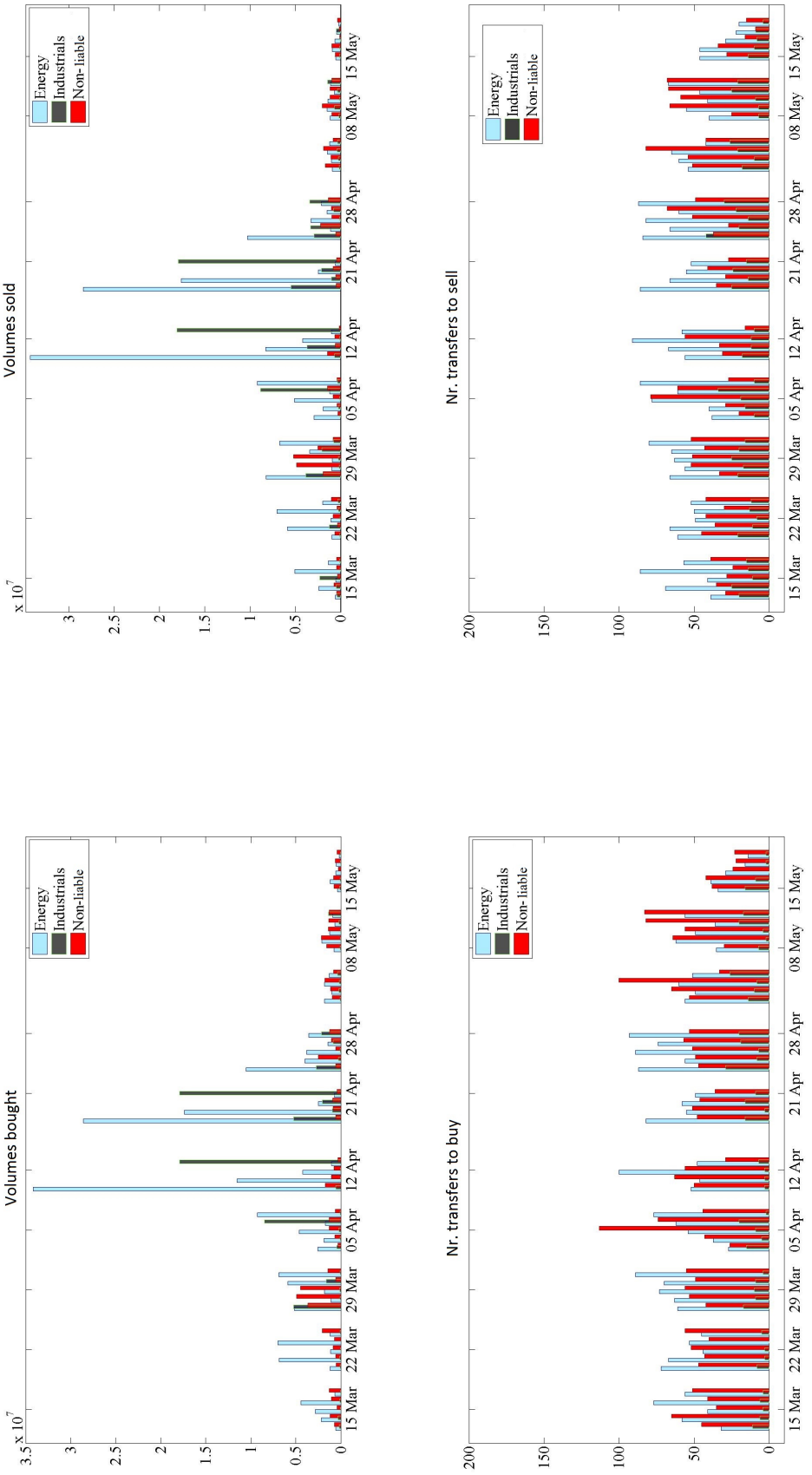

Fig. 4.F.8: Traded volumes and number of daily transfers on the EU ETS during March-May 2006.

4.G Counterparties in permit transfers: supporting results

This section presents additional information in support of the analysis led in Section 4.5.2.4. Our view is that when analysing the trading activity of different types of players, one should consider not only the total trades undertaken by each agent, but also the specific counterparty of the trade. So far, our analysis has shown that the trading activity of the energy sector was the one that, on average, correlated the most with price difference volatility. Accounting for the counterparty of each permit transfer, we are interested in understanding whether it was the energy sector in general that associated positively and significantly with volatility, or only their trades with a specific counterparty.

Figs. 4.G.1 and 4.G.2 display the evolution of the number of daily trades within and across sectors. Figs. 4.G.3 - 4.G.8 provide further information regarding the division of trades according to buys and sales. Two key observations come out. First, as expected, financial intermediaries constituting the non-liable sector used to trade the least within their own sector. Second, most across sector transfers took place between the non-liable and the energy sector. It is no surprise then that the trading activity of the energy sector with the non-liable sector as counterparty was the one to correlate the strongest with volatility.

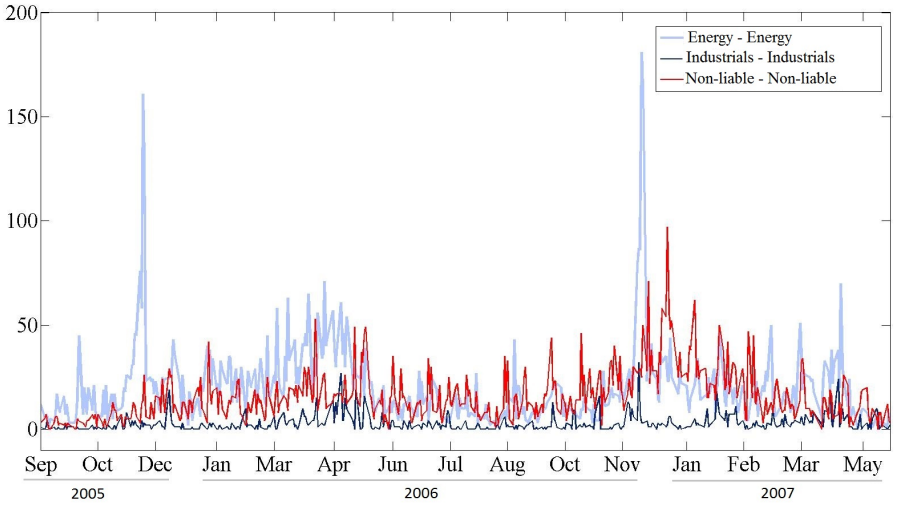

Fig. 4.G.1: Number of daily transfers to the same sector during EU ETS Phase I.

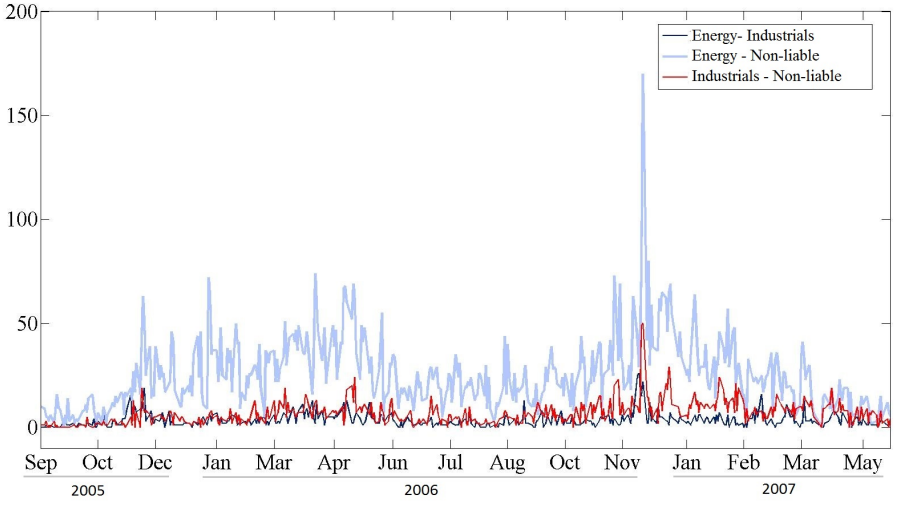

Fig. 4.G.2: Number of daily transfers across different sectors during EU ETS Phase I.

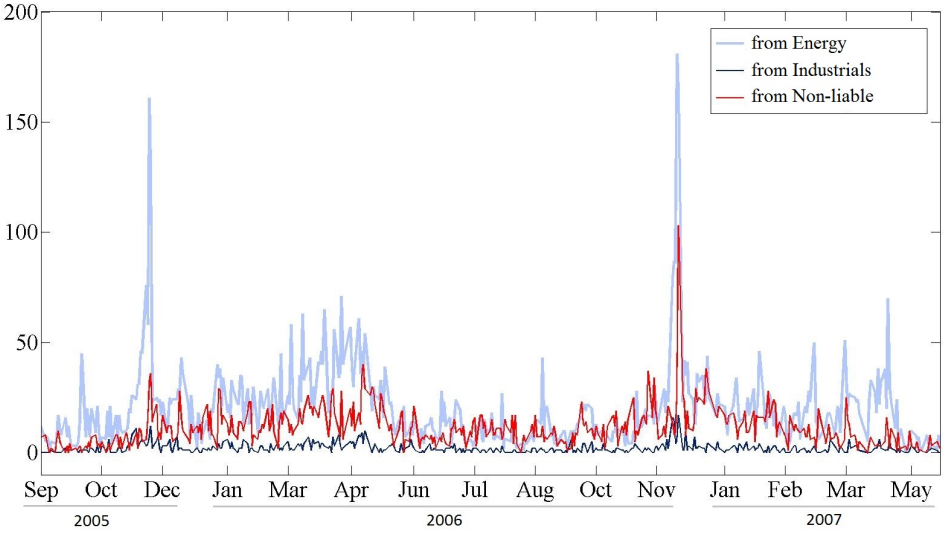

Fig. 4.G.3: Number of daily transfers with the energy sector as a buyer during EU ETS Phase I.

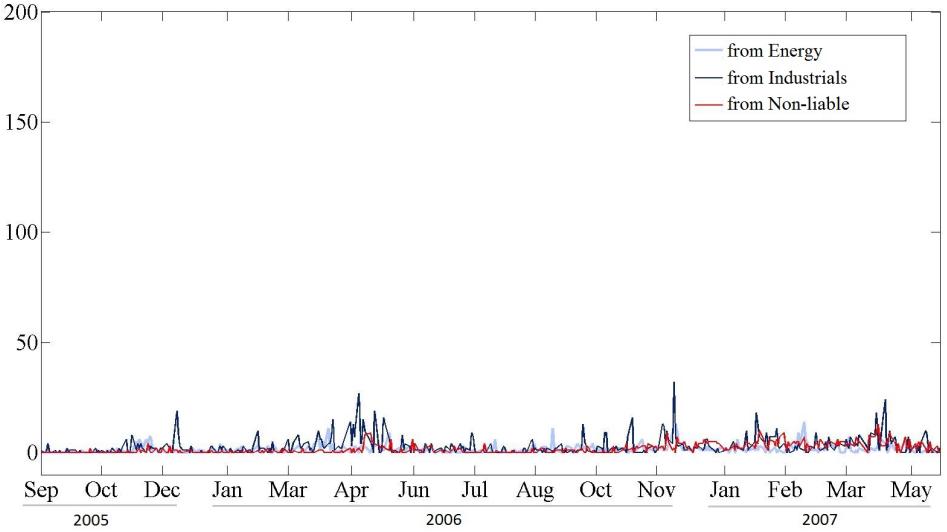

Fig. 4.G.4: Number of daily transfers with the industrials sector as a buyer during EU ETS Phase I.

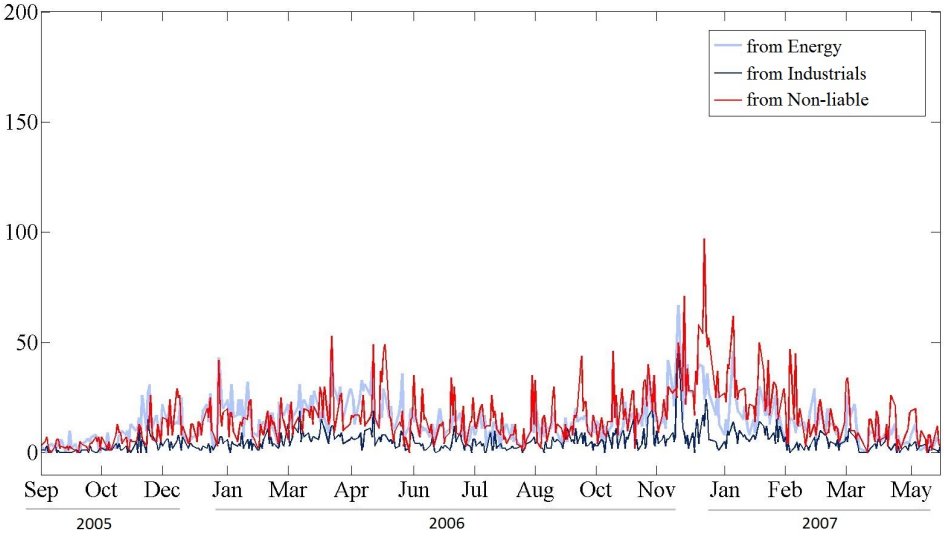

Fig. 4.G.5: Number of daily transfers with the non-liable sector as a buyer during EU ETS Phase I.

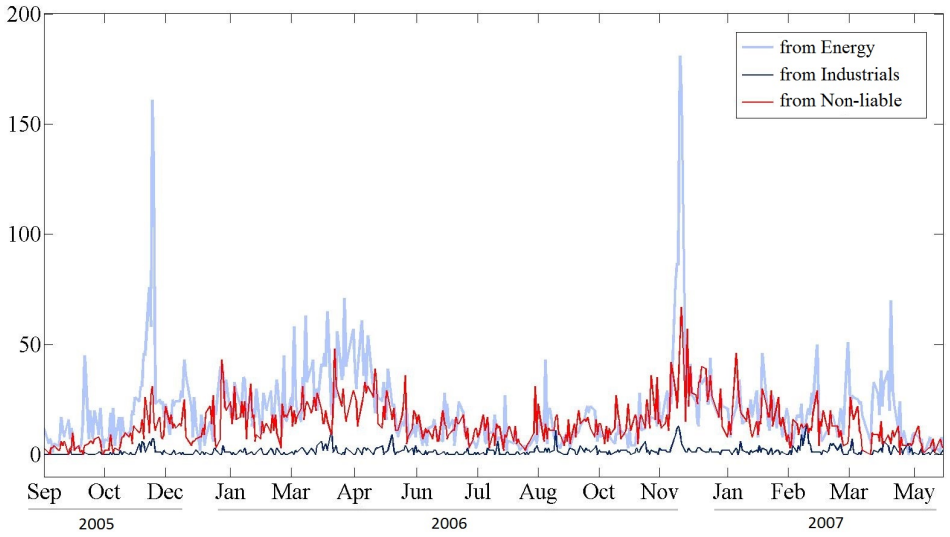

Fig. 4.G.6: Number of daily transfers with the energy sector as a seller during EU ETS Phase I.

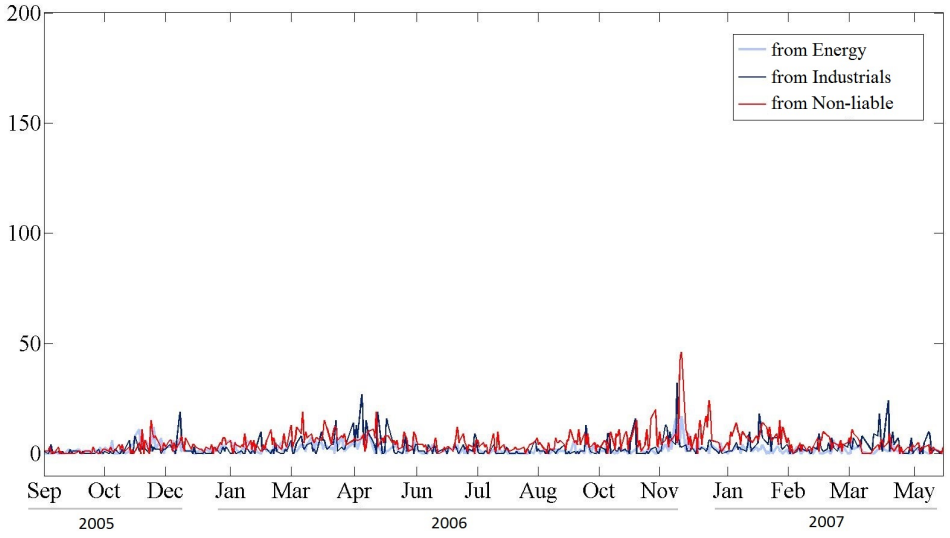

Fig. 4.G.7: Number of daily transfers with the industrials sector as a seller during EU ETS Phase I.

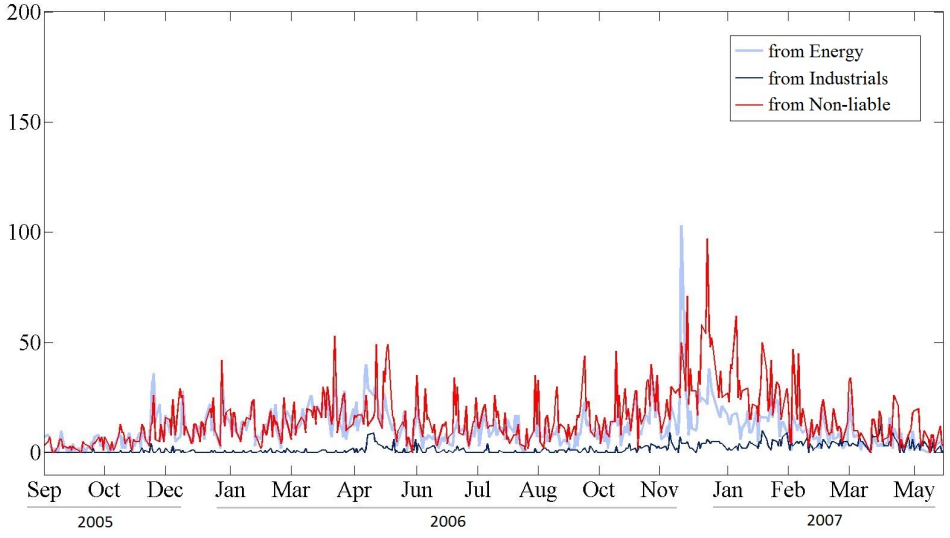

Fig. 4.G.8: Number of daily transfers with the non-liable sector as a seller during EU ETS Phase I.

4.H Robustness tests

4.H.1 Subsample analysis

In this section, we test the robustness of our results by rerunning the analysis over subsamples of the entire analyzed period. The main point of change in the spot price series is represented by the crash of April 2006, when the EUA price has been suddenly adjusted downwards, following the release of public information that too many allowances were available on the market compared to the total realized emissions. As seen in Table 4.3 in the main text, the April 2006 crash marks a regime shift in the EUA price series, making the price sample non-stationary. On the contrary, the daily price change series, i.e. the variable of interest for our analysis, is stationary with similar sample characteristics before and after the crash. The subsample analysis is expected to confirm the robustness of our results regarding the entire sample.

In order to understand the properties of the price difference series before and after the event of April 2006, we present in Fig. 4.H.1 the autocorrelation and partial autocorrelation plots for the *pre-crash* and *post-crash* periods.

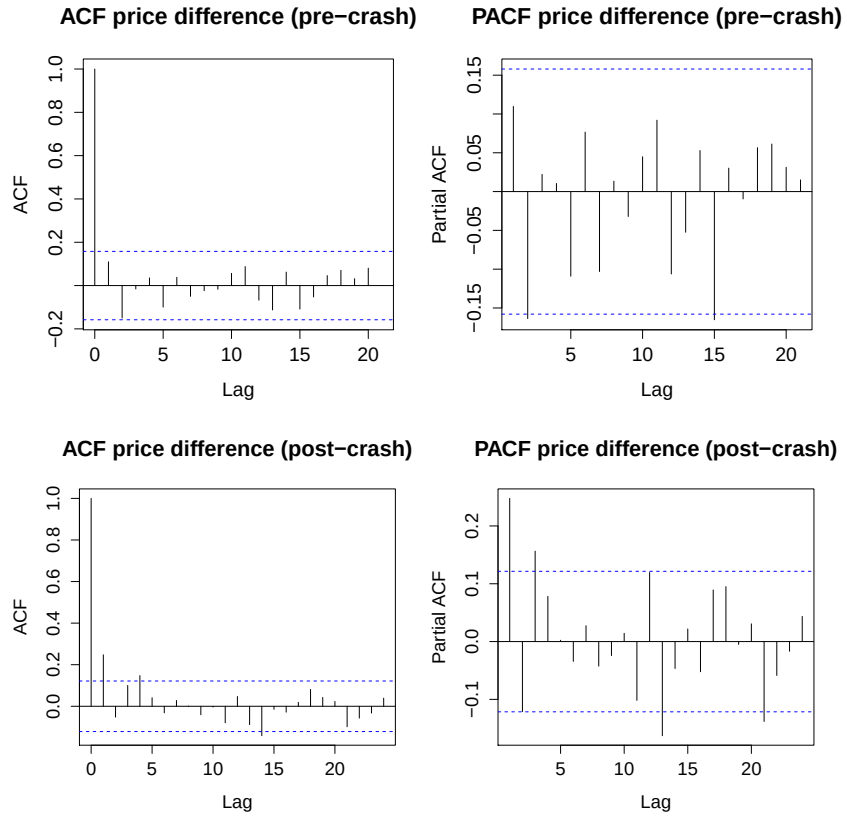

Fig. 4.H.1: Autocorrelation and partial autocorrelation in daily price differences (pre- and post- the April 2006 crash).

Table 4.H.1 presents summary statistics on EUA daily price differences. Excluding the data points during the April 2006 crash eliminates the extreme values encountered in the full sample, leaving the pre- and post-crash series with closer minimum and maximum values, as well as reduced standard deviation.

Table 4.H.1: Summary statistics on EUA daily price differences (full sample, pre-crash, and post-crash).

Sample	**N**	**Min**	**Median**	**Mean**	**Max**	**St. dev.**	**ADF** (p-value)	**KPSS** (p-value)
Full sample (15.09.05-31.05.07)	433	-7.50	-0.02	-0.05	7.10	0.72	-6.66 (< 0.01)	0.01 (> 0.1)
Pre-crash (15.09.05-25.04.06)	155	-2.95	0.05	0.02	1.25	0.45	-4.31 (< 0.01)	0.08 (> 0.1)
Post-crash (16.05.06-31.05.07)	266	-1.50	-0.02	-0.06	2.03	0.35	-6.64 (< 0.01)	0.14 (> 0.1)

Tables 4.H.2 and 4.H.3 present the results of the estimations of volatility on autoregressive lags, past unexpected price differences, and different trading activity indicators.

For the period preceding the April 2006 crash, we find that past volatility terms are significantly and negatively correlated with current levels of volatility. This observation is in line with the fact that the price difference series before the crash exhibited significant negative partial autocorrelation terms; see again Fig. 4.H.1. It appears that periods of high volatility have been followed by periods of low volatility, similar to a mean-reverting process. Moreover, the trading activity seems not to have had a significant association with price volatility. Although the coefficients are predominantly positive, only the association between the total daily number of transfers and price volatility is significant. The breakdown of volumes and of number of transfers according to the sector initiating the permit transfer does not seem to provide further insights into the trading activity - volatility relation. The explanatory power of the models is much lower than for the entire analysed sample.

For the period after the April 2006 crash, results are more in line with what is observed for the entire sample, also due to the larger number of observations in the post-crash period than pre-crash. First, lagged volatility terms are positively and significantly associated with current volatility levels, suggesting that volatility is persistent and clusters. Second, the total number of daily permit transfers correlates positively and significantly with volatility. Third, for the period after the April 2006 crash, it appears that the volumes traded by the non-liable sector (the financial intermediaries) had a negative impact on volatility levels. In other words, the non-liable sector preferred to trade more when volatility levels were lower. The explanatory power of the models is higher than in the pre-crash period, but still below that what is observed for the entire sample.

Table 4.H.2: Regressions of volatility on volumes and nr. transfers in the period before the April 2006 crash.

Note: The table presents results from the second iteration of the estimation of Eq. (4.2) based on the results from the first estimation of Eq. (4.1). The dependent variable is the volatility of daily spot EUA price differences. The analysed period is 16.05.2006 - 31.05.2007. For all estimated coefficients, standard errors are presented in brackets. F-test statistics are listed for $\sum_{j=1}^{n=15} \hat{\beta}_j$ and $\sum_{j=1}^{n=15} \hat{\gamma}_j$. The Box-Pierce statistic is computed with $k = 2\sqrt{N}$, N = 95.

	No trading activity ($\mathcal{M}$ A43)	**Total volume** ($\mathcal{M}$ A44)	**Total nr. transfers** ($\mathcal{M}$ A45)	**Sectoral nr. transfers** ($\mathcal{M}$ A46)	**Sectoral volumes** ($\mathcal{M}$ A47)	**Exp. and unexp. volumes** ($\mathcal{M}$ A48)
Intercept	0.72** (0.22)	0.69** (0.22)	0.61** (0.22)	0.52* (0.23)	0.60** (0.21)	0.48* (0.21)
$\sum_{j=1}^{n=15} \hat{\gamma}_j$	-0.86 (2.00)*	-0.88 (1.92)*	-1.35 (2.12)*	-1.21 (1.44)	-0.67 (1.88)*	-0.28 (1.48)
$\sum_{j=1}^{n=15} \hat{\beta}_j$	0.91 (1.25)	0.95 (1.25)	1.14 (1.47)	1.08 (1.15)	0.87 (1.14)	0.21 (1.40)
Total volume		0.02 (0.03)				
Total nr. transfers			0.22* (0.09)			
Energy						
Nr. transfers				0.14 (0.25)		
Total volume					0.03 (0.04)	
Expected volume						0.05 (0.07)
Unexpected volume						0.02 (0.04)
Industrials						
Nr. transfers				0.24 (0.62)		
Total volume					0.02 (0.07)	
Expected volume						0.10 (0.11)
Unexpected volume						-0.09 (0.08)
Non-liable						
Nr. transfers				0.41 (0.29)		
Total volume					0.02 (0.17)	
Expected volume						-0.16 (0.22)
Unexpected volume						0.02 (0.19)
R^2	0.43	0.43	0.48	0.43	0.43	0.47
Adj. R^2	0.17	0.15	0.23	0.12	0.12	0.13
AIC	101.45	103.48	97.92	108.57	102.19	103.29
Box-Pierce test (p-val)	4.09 (0.39)	4.09 (0.30)	11.28 (0.02)	10.66 (0.03)	5.44 (0.25)	8.62 (0.07)

$^{***}p < 0.001$, $^{**}p < 0.01$, $^{*}p < 0.05$, $^{\circ}p < 0.1$

Table 4.H.3: Regressions of volatility on volumes and nr. transfers in the period after the April 2006 crash.

Note: The table presents results from the second iteration of the estimation of Eq. (4.2) based on the results from the first estimation of Eq. (4.1). The dependent variable is volatility of daily spot EUA price differences. The analysed period is 15.09.2005 - 25.04.2006. For all estimated coefficients, standard errors are presented in brackets. F-test statistics are listed for $\sum_{j=1}^{n=25} \hat{\beta}_j$ and $\sum_{j=1}^{n=25} \hat{\gamma}_j$. The Box-Pierce statistic is computed with $k = 2\sqrt{N}$, N = 166.

	No trading activity ($\mathcal{M}$ A49)	**Total volume** ($\mathcal{M}$ A50)	**Total nr. transfers** ($\mathcal{M}$ A51)	**Sectoral nr. transfers** ($\mathcal{M}$ A52)	**Sectoral volumes** ($\mathcal{M}$ A53)	**Exp. and unexp. volumes** ($\mathcal{M}$ A54)
Intercept	0.05 (0.04)	0.05 (0.04)	0.06 (0.04)	0.04 (0.04)	0.07 (0.04)	0.07 (0.04)
$\sum_{j=1}^{n=25} \hat{\gamma}_j$	1.14 (2.82)***	1.19 (2.72)***	1.02 (2.72)***	0.98 (2.48)***	1.26 (2.87)***	1.31 (2.54)***
$\sum_{j=1}^{n=25} \hat{\beta}_j$	0.97 (1.56)°	1.15 (1.50)°	1.03 (1.49)°	0.88 (1.70)*	1.11 (1.64)*	1.10 (1.59)°
Total volume		0.00 (0.01)				
Total nr. transfers			0.04 (0.02)°			
Energy						
Nr. transfers				0.08 (0.06)		
Total volume					0.01 (0.01)	
Expected volume						0.00 (0.01)
Unexpected volume						0.02 (0.01)
Industrials						
Nr. transfers				-0.15 (0.21)		
Total volume					0.03 (0.07)	
Expected volume						0.07 (0.10)
Unexpected volume						0.03 (0.08)
Non-liable						
Nr. transfers				0.02 (0.06)		
Total volume					-0.02 (0.01)°	
Expected volume						-0.03 (0.01)*
Unexpected volume						-0.02 (0.01)°
R^2	0.49	0.48	0.49	0.49	0.51	0.51
Adj. R^2	0.27	0.25	0.26	0.25	0.28	0.26
AIC	-104.90	-99.79	-99.91	-108.48	-100.70	-97.68
Box-Pierce test (p-val)	13.00 (0.00)	10.44 (0.00)	11.40 (0.00)	14.81 (0.00)	14.09 (0.00)	14.14 (0.00)

$^{***}p < 0.001$, $^{**}p < 0.01$, $^{*}p < 0.05$, $^{\circ}p < 0.1$

4.H.2 Lagged trading activity terms

During our analysis, we have noted that the association between trading activity and volatility is significant and positive, where both trading activity and volatility are observed at the same time. However, the analysis is not actually fit for saying anything about the direction of the relation, e.g. if trading activity had an influence on price volatility. To get a hint on whether the trading activity had any influence on price volatility, we rerun the models with lagged trading activity terms, i.e. volatility observed at time t is regressed on trading activity at time $t-1$. Table 4.H.4 presents the results of the regressions on volatility of lagged trading activity variables, over the entire analysed horizon.

The explanatory power of the models stays similar to that of the models of contemporaneous trading activity and volatility. We find that total volume and total number of transfers are no longer significantly associated with price volatility. It appears that only the past trading activity of the industrial sector is positively and significantly associated with volatility, giving some basis to the interpretation that volatility tended on average to be higher after the industrial sector traded more (higher volumes or more frequently).

The results of the regressions on lagged trading activity bring some clarity over the interpretation of results for the contemporaneous trading activity - volatility relation. We have previously seen that, when studying the contemporaneous trading activity - volatility relation, the energy sector seems to have the strongest association with volatility. In light of the new results, it seems that we cannot talk about an increase in volatility due to the trading behavior of the energy sector, but rather that both have reacted on average in similar ways to the arrival of information on the market. In this sense, these new results tend to support the hypothesis that an exogenous variable (the arrival of information) has a simultaneous impact on both price volatility and traded volumes.

Table 4.H.4: Regressions of volatility on lagged volumes and nr. transfers.

Note: The table presents results from the second iteration of the estimation of Eq. (4.2) based on the results from the first estimation of Eq. (4.1). The dependent variable is the volatility of daily spot EUA price differences. The analysed period is 15.09.2005 - 31.05.2007. The trading activity variables (volume and nr. transfers) are lagged by one observation. For all estimated coefficients, standard errors are presented in brackets. F-test statistics are listed for $\sum_{j=1}^{n=25} \hat{\beta}_j$ and $\sum_{j=1}^{n=25} \hat{\gamma}_j$. The Box-Pierce statistic is computed with $k = 2\sqrt{N}$, N = 333.

	No trading activity ($\mathcal{M}$ A55)	**Total volume** ($\mathcal{M}$ A56)	**Total nr. transfers** ($\mathcal{M}$ A57)	**Sectoral nr. transfers** ($\mathcal{M}$ A58)	**Sectoral volumes** ($\mathcal{M}$ A59)
Intercept	0.06 (0.06)	0.05 (0.06)	0 (0.08)	-0.05 (0.08)	0.07 (0.06)
$\sum_{j=1}^{n=25} \hat{\gamma}_j$	0.86 (8.23)***	0.86 (8.23)***	0.85 (8.66)***	0.89 (8.86)***	0.79 (8.79)***
$\sum_{j=1}^{n=25} \hat{\beta}_j$	0.56 (1.44)°	0.57 (1.53)°	0.62 (1.52)°	0.72 (1.82)*	0.40 (2.04)**
Total volume		0.01 (0.01)			
Total nr. transfers			0.07 (0.05)		
Energy					
Nr. transfers				-0.07 (0.13)	
Volume					-0.01 (0.02)
Industrials					
Nr. transfers				0.81 (0.44)°	
Volume					0.14 (0.08)°
Non-liable					
Nr. transfers				0.07 (0.14)	
Volume					0.01 (0.02)
R^2	0.46	0.47	0.48	0.49	0.50
Adj. R^2	0.37	0.37	0.38	0.40	0.40
AIC	527.59	525.46	520.27	519.63	504.56
Box-Pierce test (p-val)	15.03 (0.18)	14.03 (0.23)	14.51 (0.21)	10.98 (0.45)	17.55 (0.09)

$^{***}p < 0.001$, $^{**}p < 0.01$, $^{*}p < 0.05$, $^{\circ}p < 0.1$

4.H.3 Including one sector at a time

The analysis in the main text of the paper has shown that the strongest association between the trading activity and volatility can be encountered in the case of the energy sector (both for volumes and number of transfers). To investigate whether possible correlations between sectoral activities do not hide the significant association with the industrials or non-liable sectors, we rerun the models by including only the trading activity of a sector at a time.

As Table 4.H.5 reveals, our previous results are robust. In terms of volumes, it is indeed only the trading activity of the energy sector that correlates positively and significantly with volatility. In terms of the number of daily transfers, we observe that by including only one sector at a time, the positive association between the number of transfers of the energy sector and volatility is maintained and appears even stronger (model $\mathcal{M}$ A61 compared to model $\mathcal{M}$ A60). The number of transfers of the industrial and non-liable sectors appear also significant and positive when included separately into the regressions, signaling the potential existence of some correlation effects in the model with all three sectors. Moreover, the explanatory power of the two models excluding the energy sector is lower than of the models that include with energy, hinting to the fact that it is indeed the energy sector who bears the strongest association with volatility.

In Table 4.H.6, we continue the robustness analysis by running the regressions of volatility on the number of transfers, while testing for possible seasonality evidence. The left panel presents the results when the model includes month dummies, while the right panel allows for interactions between the number of transfers from each sector and the April dummy. First, the models with month dummies confirm our previous results, i.e. the number of transfers carried out by the energy sector correlated positively and significantly with volatility and volatility is higher in April. Including only one sector at a time decreases the explanatory power of the model. Second, according to the models with interaction terms, including only one sector at a time reveals that the number of transfers from each sector has correlated positively and significantly with volatility in April, especially for the energy and non-liable sectors. Again, the explanatory power of the models is considerably lower when the sectors are included separately (in models $\mathcal{M}$ A73-75 compared to $\mathcal{M}$ A72), showing that accounting for the activity of all three sectors simultaneously manages to extract most information.

Table 4.H.5: Regressions of volatility on volumes and nr. transfers (separate inclusion of sectors).

Note: The table presents results from the second iteration of the estimation of Eq. (4.2) based on the results from the first estimation of Eq. (4.1). The dependent variable is the volatility of daily spot EUA price differences. The analysed period is 15.09.2005 - 31.05.2007. For all estimated coefficients, standard errors are presented in brackets. F-test statistics are listed for $\sum_{j=1}^{n=25} \hat{\beta}_j$ and $\sum_{j=1}^{n=25} \hat{\gamma}_j$. The Box-Pierce statistic is computed with $k = 2\sqrt{N}$, N = 334.

	Nr. transfers				**Volume**			
	All sectors ($\mathcal{M}$ A60)	**Energy** ($\mathcal{M}$ A61)	**Industrials** ($\mathcal{M}$ A62)	**Non-liable** ($\mathcal{M}$ A63)	**All sectors** ($\mathcal{M}$ A64)	**Energy** ($\mathcal{M}$ A65)	**Industrials** ($\mathcal{M}$ A66)	**Non-liable** ($\mathcal{M}$ A67)
Intercept	-0.01 (0.08)	-0.04 (0.07)	-0.01 (0.08)	-0.01 (0.08)	0.05 (0.06)	0.05 (0.06)	0.07 (0.06)	0.07 (0.06)
$\sum_{j=1}^{n=25} \hat{\gamma}_j$	0.77 (8.67)***	0.79 (8.81)***	0.85 (8.02)***	0.83 (8.45)***	0.81 (8.07)***	0.84 (8.57)***	0.83 (7.94)***	0.84 (8.11)***
$\sum_{j=1}^{n=25} \hat{\beta}_j$	0.44 (1.59)*	0.48 (1.57)*	0.56 (1.38)	0.64 (1.39)	0.34 (1.41)°	0.43 (1.42)°	0.43 (1.41)°	0.47 (1.38)
Nr. transfers								
Energy	0.30 (0.13)*	0.28 (0.08)**						
Industrials	-0.18 (0.44)		0.60 (0.35)°					
Non-liable	-0.02 (0.14)			0.19 (0.10)°				
Volume								
Energy					0.04 (0.02)°	0.04 (0.02)°		
Industrials					0.04 (0.08)		0.05 (0.08)	
Non-liable					-0.02 (0.02)			-0.00 (0.02)
R^2	0.49	0.49	0.46	0.44	0.46	0.47	0.45	0.46
Adj. R^2	0.39	0.40	0.36	0.34	0.36	0.38	0.35	0.36
AIC	522.92	519.13	535.77	539.85	532.75	523.30	536.64	535.94
Box-Pierce test (p-val)	17.19 (0.10)	17.61 (0.09)	17.69 (0.09)	14.23 (0.22)	16.92 (0.11)	17.68 (0.09)	14.44 (0.21)	14.97 (0.18)

$^{***}p < 0.001$, $^{**}p < 0.01$, $^{*}p < 0.05$, $^{\circ}p < 0.1$

Table 4.H.6: Regressions of volatility on nr. transfers including month dummies (separate inclusion of sectors).

Note: The table presents results from the second iteration of the estimation of Eq. (4.2) based on the results from the first estimation of Eq. (4.1). The dependent variable is the volatility of daily spot EUA price differences. The analysed period is 15.09.2005 - 31.05.2007. For all estimated coefficients, standard errors are presented in brackets. F-test statistics are listed for $\sum_{j=1}^{n=25} \hat{\beta}_j$ and $\sum_{j=1}^{n=25} \hat{\gamma}_j$. The Box-Pierce statistic is computed with $k = 2\sqrt{N}$, N = 334.

	Models with month dummies				**Models with interaction terms**			
	All sectors ($\mathcal{M}$ A68)	**Energy** ($\mathcal{M}$ A69)	**Industrials** ($\mathcal{M}$ A70)	**Non-liable** ($\mathcal{M}$ A71)	**All sectors** ($\mathcal{M}$ A72)	**Energy** ($\mathcal{M}$ A73)	**Industrials** ($\mathcal{M}$ A74)	**Non-liable** ($\mathcal{M}$ A75)
Intercept	-0.03 (0.14)	-0.05 (0.12)	0.06 (0.13)	-0.05 (0.14)	0.06 (0.07)	-0.01 (0.06)	0.05 (0.08)	0.07 (0.07)
$\sum_{j=1}^{n=25} \hat{\gamma}_j$	0.68 (10.28)***	0.69 (9.71)***	0.81 (9.10)***	0.77 (8.52)***	0.67 (10.80)***	0.70 (10.31)***	0.78 (7.78)***	0.71 (7.35)***
$\sum_{j=1}^{n=25} \hat{\beta}_j$	0.04 (2.37)***	0.10 (2.19)***	0.12 (1.86)**	0.19 (1.93)**	-0.17 (2.24)***	-0.07 (1.49)°	0.24 (1.14)	-0.07 (1.14)
Nr. transfers								
Energy	0.34 (0.13)**	0.32 (0.10)**			0.24 (0.12)*	0.17 (0.08)*		
Industrials	-0.43 (0.42)		0.30 (0.37)		-0.28 (0.45)		0.17 (0.39)	
Non-liable	0.05 (0.15)			0.23 (0.13)°	-0.09 (0.13)			0.02 (0.10)
Month dummies								
February	-0.08 (0.13)	-0.07 (0.13)	-0.12 (0.14)	-0.04 (0.14)				
March	-0.07 (0.12)	-0.08 (0.12)	-0.09 (0.13)	-0.03 (0.13)				
April	0.42 (0.16)**	0.38 (0.16)*	0.37 (0.16)*	0.45 (0.16)**				
May	-0.06 (0.15)	-0.05 (0.14)	-0.19 (0.15)	-0.07 (0.15)				
June	0.07 (0.18)	0.06 (0.18)	-0.02 (0.18)	0.01 (0.19)				
July	0.09 (0.15)	0.11 (0.15)	0.01 (0.16)	0.1 (0.16)				
August	0 (0.15)	0.01 (0.15)	-0.08 (0.15)	-0.01 (0.15)				
September	0.09 (0.15)	0.12 (0.15)	0.04 (0.15)	0.10 (0.15)				
October	0.13 (0.14)	0.13 (0.15)	0.04 (0.15)	0.11 (0.15)				
November	-0.03 (0.14)	-0.03 (0.15)	-0.01 (0.15)	0.03 (0.15)				
December	-0.24 (0.16)	-0.23 (0.15)	-0.18 (0.16)	-0.24 (0.16)				
Interaction terms								
Energy*April					0.80 (0.30)**	0.60 (0.13)***		
Industrials*April					-1.00 (0.83)		1.02 (0.53)°	
Non-liable*April					0.04 (0.39)			0.82 (0.19)***
R^2	0.56	0.55	0.52	0.51	0.57	0.54	0.45	0.45
Adj. R^2	0.46	0.44	0.41	0.40	0.48	0.45	0.35	0.35
AIC	476.49	487.38	497.84	497.86	422.86	467.64	539.71	507.82
Box-Pierce test (p-val)	21.19 (0.03)	19.61 (0.05)	17.45 (0.09)	17.64 (0.09)	15.02 (0.18)	13.47 (0.26)	17.20 (0.10)	11.26 (0.42)

$^{***}p < 0.001$, $^{**}p < 0.01$, $^{*}p < 0.05$, $^{\circ}p < 0.1$

4.H.4 Daily changes in trading activity

This section discusses the relation between the change in number of transfers and volatility. The results of the estimation are presented in Table 4.H.7. The significant association seems to hold also for volatility and changes in trading activity. We find that volatility is positively associated not only with trading activity levels, but also with changes in trading activity levels.

Table 4.H.7: Regressions of volatility on the change in the number of daily permit transfers by different trading sectors.

Note: The table presents results from the second iteration of the estimation of Eq. (4.2) based on the results from the first estimation of Eq. (4.1). The dependent variable is the volatility of daily spot EUA price differences. The analysed period is 15.09.2005 - 31.05.2007. For all estimated coefficients, standard errors are presented in brackets. F-test statistics are listed for $\sum_{j=1}^{n=25} \hat{\beta}_j$ and $\sum_{j=1}^{n=25} \hat{\gamma}_j$. The Box-Pierce statistic is computed with $k = 2\sqrt{N}$, N = 333.

	Nr. transfers			
	Total ($\mathcal{M}$ A76)	**Buy + Sell** ($\mathcal{M}$ A77)	**Buy** ($\mathcal{M}$ A78)	**Sell** ($\mathcal{M}$ A79)
Intercept	0.06 (0.07)	0.06 (0.06)	0.06 (0.06)	0.06 (0.07)
$\sum_{i=1}^{n=25} \hat{\gamma}_i$	0.86 (7.80)***	0.87 (8.75)***	0.86 (8.56)***	0.87 (8.32)***
$\sum_{i=1}^{n=25} \hat{\beta}_i$	0.55 (1.46)°	0.54 (1.85)**	0.51 (1.65)*	0.59 (1.86)**
Nr. transfers				
Total	0.11 (0.06)°			
Energy		0.43 (0.13)**	0.37 (0.12)**	0.32 (0.12)**
Industrials		-0.65 (0.35)°	-0.35 (0.35)	-0.53 (0.29)°
Non-liable		-0.11 (0.13)	-0.10 (0.12)	0.01 (0.13)
R^2	0.46	0.50	0.49	0.49
Adj. R^2	0.36	0.40	0.39	0.39
AIC	537.31	521.41	526.64	527.55
Box-Pierce test (p-val)	16.93 (0.11)	15.35 (0.17)	16.83 (0.11)	13.43 (0.27)

$^{***}p < 0.001$, $^{**}p < 0.01$, $^{*}p < 0.05$, $^{\circ}p < 0.1$

4.I Market concentration

This section focuses on the extent of market concentration in the EU ETS Phase I. When analysing the trading activity - volatility relation, it is interesting to understand whether the trading activity on the emission allowance market can be mainly attributed to a few players, that is the market is highly concentrated, or is well spread among many different players.

To evaluate the extent of market concentration and its link with price volatility, we proceed with a three-step analysis. First, we check how many agents operated on the market and what were the volumes they traded. We group agents according to their sector of activity. We observe that many agents have entered the market just once or twice, while others have traded very frequently. Second, we compute two indexes relevant for the extent of market concentration and equality of distribution in the market of trading activities in the market. Third, we regress daily EUA price difference volatility on the number of unique agents that have traded each day in the market in order to understand whether price changes have been sensitive to higher or lower market concentration.

Fig. 4.I.1: The trading activity and extent of market presence of agents.

Note: The figure captures the number of active agents and their traded volumes in the EU ETS Phase I. We group agents according to their sector of activity. Active agents are defined as those trading in at least a threshold number of days (displayed on the X-axis). The threshold takes values between 0 and 400 out of a maximum of 434 days. Only one agent (belonging to the non-liable sector) has traded on more than 400 out of 434 days.

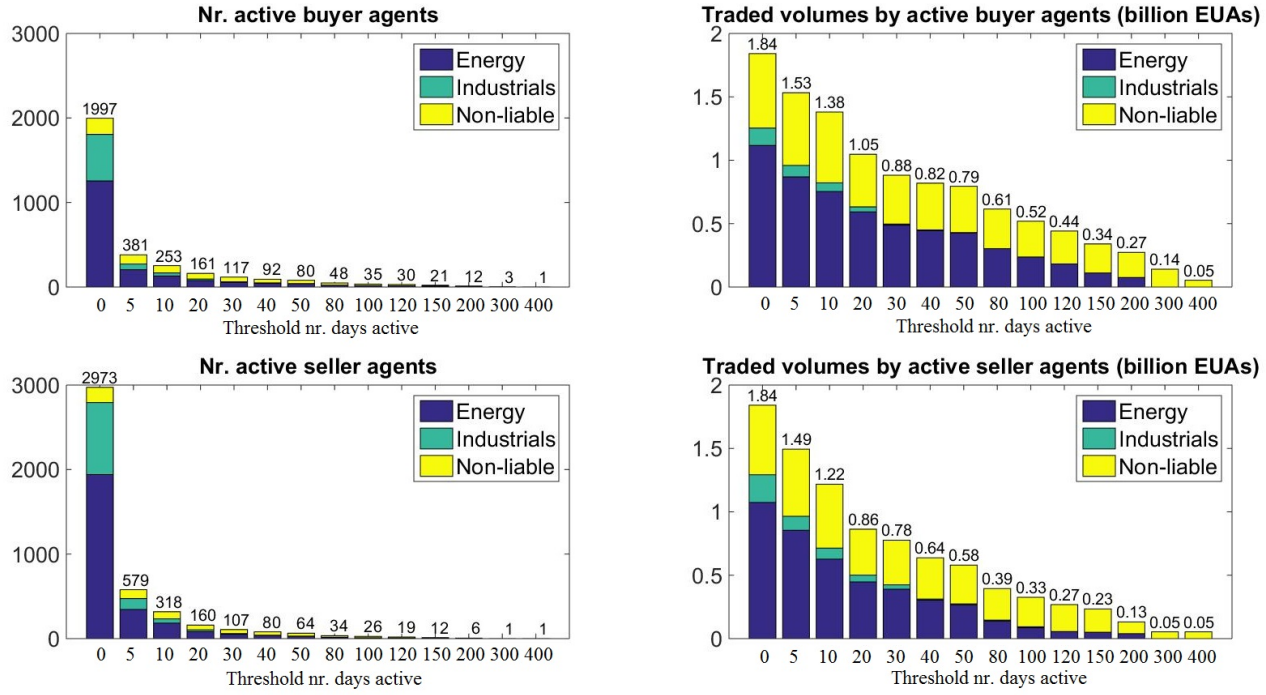

In the Phase I of the EU ETS, it appears that although many agents have participated with at least one trade in the market, only very few have actually traded regularly. Fig. 4.I.1 shows that the most active players belong the energy and the non-liable sectors. Both among the buyers and the sellers, less than 15 agents traded in more than half of the days in the analysed horizon. The effect is more pronounced for sellers. However, the number of active players is large enough to describe a competitive market, with possibly no major players dominating the trades, as indicated by the Herfindahl Index for market concentration displayed in Table 4.I.1. When analysing the Herfindahl Index at the sector level, it appears that the non-liable sector presents higher market concentration than the energy or industrial ones. This observation holds only for the number of transfers, not for volumes.

Table 4.I.1: Indicators of market concentration.

Note: The table presents the Herfindahl Index relevant for the extent of market concentration. The index is computed based on two trading activity variables (volume and nr. transfers) during 15.09.2005 - 31.05.2007. The statistics are presented separately for buy and sell transactions. The index is computed first for the entire market and then at the sector level (energy, industrials, and non-liable). The Herfindahl Index (HI) is computed as the sum of squared market shares, i.e. $HI = \sum_{i=1}^{N} s_i^2$ where N is the number of buyers or sellers, $s_i = TA_i/TA$, TA_i the trading activity of agent i and TA the total trading activity.

Market position	Sector	**Herfindahl Index**	
		Nr. transfers	**Volumes**
Buy	All	0.0261	0.0108
	Energy	0.0149	0.0164
	Industrials	0.0113	0.0590
	Non-liable	0.1044	0.0442
Sell	All	0.0230	0.0095
	Energy	0.0068	0.0141
	Industrials	0.0064	0.0297
	Non-liable	0.1436	0.0482

Furthermore, we check whether we can detect any significant association between volatility and the number of unique players trading each day. Table 4.I.2 shows that this trading activity proxy leads to similar results as the number of daily

trades. We find evidence of a significant and positive association between the number of agents operating each day in the market and volatility. In particular, the more agents traded on behalf of the energy sector, the higher the volatility level. The explanatory power of these models is higher than for the models with the number of transfers. We find, thus far, no evidence of a significant link between high market concentration and volatility.

Table 4.I.2: Regressions of volatility on the number of trading agents grouped by sector of activity.

Note: The table presents results from the second iteration of the estimation of Eq. (4.2) based on the results from the first estimation of Eq. (4.1). The dependent variable is the volatility of daily spot EUA price differences. The analysed period is 15.09.2005 - 31.05.2007. For all estimated coefficients, standard errors are presented in brackets. F-test statistics are listed for $\sum_{j=1}^{n=25}\hat{\beta}_j$ and $\sum_{j=1}^{n=25}\hat{\gamma}_j$. The Box-Pierce statistic is computed with $k = 2\sqrt{N}$, N = 334.

	Nr. agents			
	Total ($\mathcal{M}$ A80)	**Buy + Sell** ($\mathcal{M}$ A81)	**Buy** ($\mathcal{M}$ A82)	**Sell** ($\mathcal{M}$ A83)
Intercept	-0.11 (0.09)	-0.04 (0.10)	0.04 (0.10)	-0.10 (0.09)
$\sum_{j=1}^{n=25}\hat{\gamma}_j$	0.81 (8.47)***	0.74 (9.10)***	0.65 (9.14)***	0.59 (8.83)***
$\sum_{j=1}^{n=25}\hat{\beta}_j$	0.60 (1.49)°	0.43 (1.64)*	0.21 (1.67)*	0.15 (1.56)*
Nr. agents				
Total	0.18 (0.06)**			
Energy		0.40 (0.18)*	0.44 (0.16)**	0.25 (0.15)°
Industrials		-0.58 (0.51)	-0.88 (0.47)°	-0.10 (0.36)
Non-liable		0.10 (0.28)	0.02 (0.23)	0.16 (0.23)
R^2	0.48	0.5	0.5	0.49
Adj. R^2	0.38	0.41	0.41	0.40
AIC	525.15	517.84	515.68	523.46
Box-Pierce test (p-val)	15.58 (0.16)	15.11 (0.18)	15.61 (0.16)	14.49 (0.21)

$^{***}p < 0.001$, $^{**}p < 0.01$, $^{*}p < 0.05$, $^{\circ}p < 0.1$

Table 4.I.3 presents the results of the regressions of volatility on the number of daily transfers or volume levels traded by the most active agents. The most active agents are defined here as those that have traded for more than 300 days out of the 434 of the analysed horizon. We find no significant associations between the trading activity of the most active agents and volatility. Taking into account the fact that these 4 most active agents belong exclusively to the non-liable sector, i.e. they are financial intermediaries, we can infer that their trading strategy was following a pattern, which was only weakly related to allowance price volatility. Finding no significant association between the trading activity of the most active players (both in terms of frequency and volumes) leads us to conclude once again that the EU ETS market has been quite competitive during the analysed period, and find no evidence of market concentration.

Table 4.I.3: Regressions of volatility on the number of transfers and volumes traded by the most active agents (nr. trading days larger than 300 out of 434).

Note: The table presents results from the second iteration of the estimation of Eq. (4.2) based on the results from the first estimation of Eq. (4.1). The dependent variable is the volatility of daily spot EUA price differences. The analysed period is 15.09.2005 - 31.05.2007. For all estimated coefficients, standard errors are presented in brackets. F-test statistics are listed for $\sum_{j=1}^{n=25}\hat{\beta}_j$ and $\sum_{j=1}^{n=25}\hat{\gamma}_j$. The Box-Pierce statistic is computed with $k = 2\sqrt{N}$, N = 334.

	Nr. transfers		**Volumes**	
	Buy ($\mathcal{M}$ A84)	**Sell** ($\mathcal{M}$ A85)	**Buy** ($\mathcal{M}$ A86)	**Sell** ($\mathcal{M}$ A87)
Intercept	0.00 (0.08)	-0.00 (0.08)	0.05 (0.07)	0.06 (0.06)
$\sum_{j=1}^{n=25}\hat{\gamma}_j$	0.83 (7.16)***	0.83 (7.08)***	0.85 (8.14)***	0.86 (8.39)***
$\sum_{j=1}^{n=25}\hat{\beta}_j$	0.61 (1.34)	0.63 (1.39)	0.53 (1.38)	0.53 (1.46)°
Trading activity	0.36 (0.24)	0.45 (0.26)°	0.00 (0.00)	0.00 (0.00)
R^2	0.43	0.43	0.46	0.47
Adj. R^2	0.33	0.33	0.36	0.37
AIC	543.89	547.48	534.06	526.72
Box-Pierce test (p-val)	13.01 (0.29)	14.37 (0.21)	14.95 (0.18)	15.37 (0.17)

$^{***}p < 0.001$, $^{**}p < 0.01$, $^{*}p < 0.05$, $^{\circ}p < 0.1$

4.J Gains and losses in the EU ETS Phase I

This section analyses the monetary results generated by the trading strategies of market players. We look at three sectors of activity (energy, industrials, and non-liable) and compute the associated profit and loss to their transactions. For the computation, we use daily EUA market prices; as such, the results presented below constitute just an approximation. In reality, permit transfers have been possibly conducted at personalised price levels (many transactions have been over-the-counter) and we lack this information.

Fig. 4.J.1 presents the daily profit and loss (PnL) levels as well as the cumulated profit and loss ($cPnL$) of the three sectors of activity. We observe that, most of the days, the daily profit and loss is very close to zero, suggesting that in general each sector tried to balance the incoming and outgoing level of permits. This might be generated by the preference to trade within the sector, with buying and selling transactions netting each other out. Several spikes are striking, mostly in December of each year, as well as around the April 2006 crash.

Observing the cumulated profit and loss, significant discrepancies appear in the trading revenues obtained by the different sectors. On average, the industrial sector appears as the most successful one, starting slowly but achieving rapidly positive cumulated profits. This trend is increasing through time, in line with the cumulated number of permits each sector decided to hold. As shown in Fig. 4.J.2, the cumulated number of net permits held by each sector followed different trajectories. First, the industrial sector, which was over-allocated initially, chose to be a net seller of permits, supporting the observation that their cumulated revenues from permit trading have been positive at the cumulated level. Second, the energy sector had cumulated profits close to zero for a significant amount of time, but these turned negative in 2007 as the sector became a net buyer of profits, albeit at a low permit price. Third, the strategy chosen by the non-liable players is perhaps the most intriguing one. The non-liable sector appears on the aggregate to have had the most significant losses during Phase I, buying heavily at the beginning of the compliance period when permit prices were high, and trying to exit the market towards the end of the compliance period by selling the permits at much lower prices. Our results are in line with Cludius (2015), who analyses the winners and losers on the EU ETS market during Phase I and shows that the gains and losses obtained by market participants through permit trading depended mostly on the number of initially allocated permits. As such, the author finds that big industrial companies that have been over-allocated, managed to obtain the largest gains, while the under-allocated energy companies suffered losses. The author also draws the readers' attention to the fact that the losses made by energy companies on the EU ETS have been significantly smaller than the gains they made on the energy markets as a results of compliance price pass-through.

Our analysis is to be interpreted with care since three caveats are in order. First, we abstract from discounting of revenue over time. This might have an influence over the estimated cumulated revenues, since sectors had access on average to differentiated financing conditions, e.g. the non-liable sector, mostly represented by financial intermediaries, is expected to have been able to borrow funds at lower interest rates than the other sectors. Second, the transfer of permits reflects not only spot transactions, but also transfers of permits from derivative products, such as forwards and futures. These derivative contracts are usually concluded at different points in time and price conditions, but such details are not accounted for in our analysis. Third, many of the permit transactions have been concluded over-the-counter, sometimes at personalized price and quantity conditions. Lacking information on the actual transaction price, our analysis uses the EUA average daily price and achieves only a proxy of the actual profits and losses.

Notwithstanding the shortcomings of our profit and loss analysis, it appears that indeed the energy and the non-liable sectors tended to make less money over all from permit trading than the industrial sector. This observation might represent a hint as to why did the trading activity of these two sectors tend to correlate significantly and positively with price volatility. Being on a path of cumulated losses, the two sectors might have been tempted to trade more when volatility levels were higher since they were more exposed to the permit market.

Fig. 4.J.1: Daily and cumulated gains and losses from permit trading by sector of activity.

Note: The figure captures the estimated gains and losses during 15.09.2005 - 31.05.2007. Agents are grouped according to their sector of activity. The upper panel presents the daily profit and loss (PnL); the lower panel captures the evolution of the cumulated profit and loss ($cPnL$). $PnL(t) = [V_s(t) - V_b(t)] \cdot P(t)$ and $cPnL(t) = \sum_{i=0}^{t} PnL(i)$, where V_s and V_b are the nr. of permits bought and sold at time t, and $P(t)$ is the EUA price.

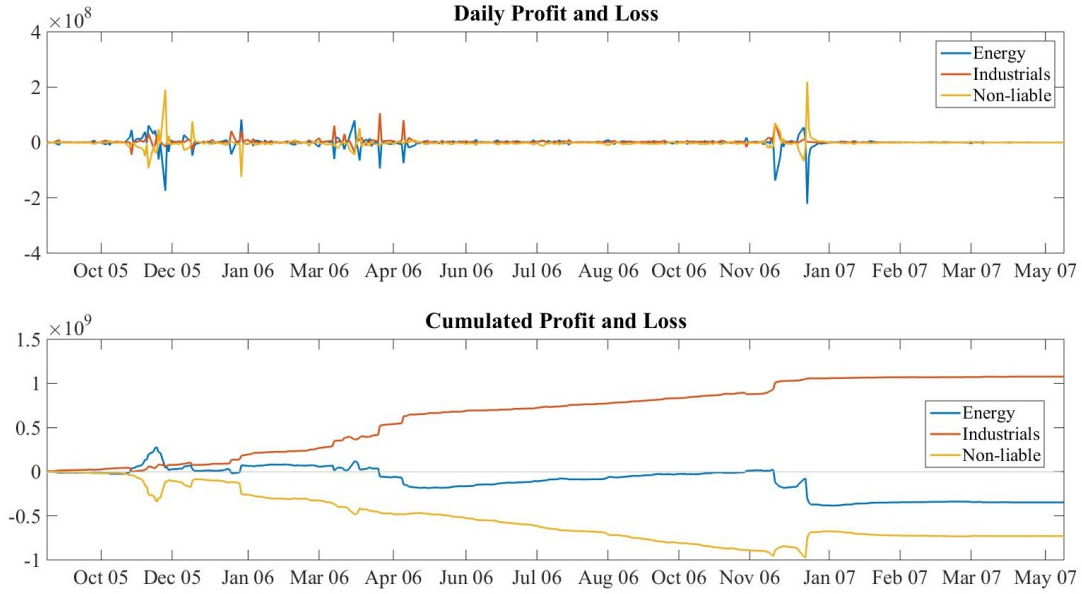

Fig. 4.J.2: Daily and cumulated net permit volumes by sector of activity.

Note: The figure captures daily traded volumes during 15.09.2005 - 31.05.2007. Agents are grouped according to their activity sector. The upper panel presents daily net transferred volumes (nV); the lower panel captures cumulated net volumes (cnV). $nV(t) = V_s(t) - V_b(t)$ and $cnV(t) = \sum_{i=0}^{t} nV(i)$, where V_s and V_b are the number of permits bought and sold at time t.

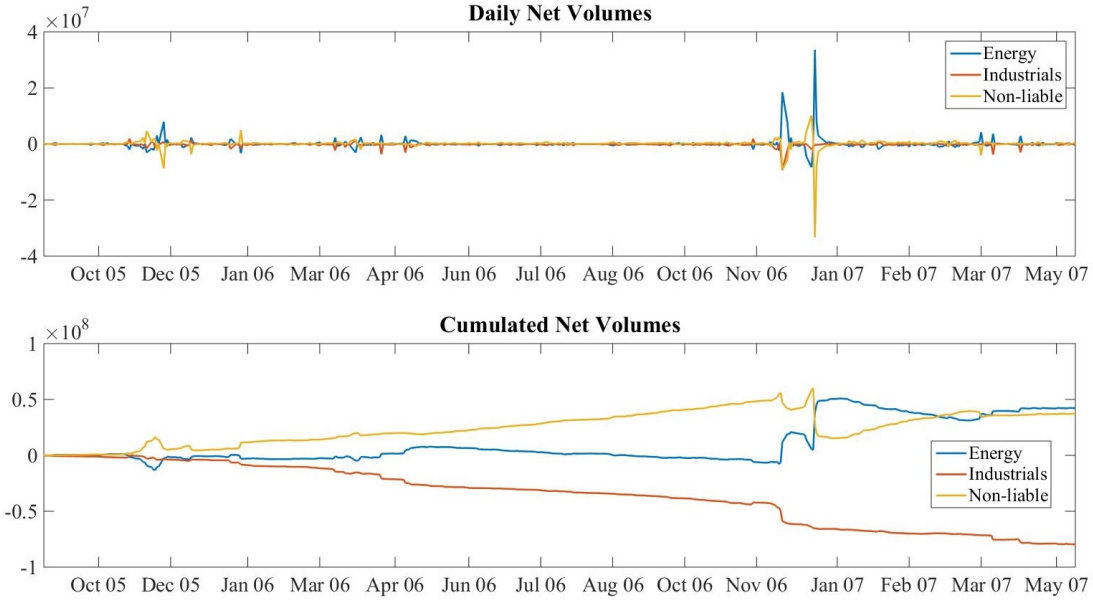

Bibliography

Adams, J., Mann, M., Ammann, C., 2003. Proxy evidence for an El Niño-like response to volcanic forcing. Nature 426, 274 – 278.

Adger, W., Agrawala, S., et al, 2007. Assessment of adaptation practices, options, constraints and capacity, in: Parry, M., Canziani, O., Palutikof, J., van der Linden, P., Hanson, C. (Eds.), Climate Change 2007: Impacts, Adaptation and Vulnerability. Cambridge University Press, Cambridge, UK. Contribution of Working Group II to the Fourth Assessment Report of the Intergovernmental Panel on Climate Change, pp. 717–743.

Agrawala, S., Bosello, F., Carraro, C., De Bruin, K., De Cian, E., Dellink, R., Lanzi, E., 2011. Plan or react? Analysis of adaptation costs and benefits using integrated assessment models. Climate Change Economics 2, 175–208.

Alberola, E., Chevallier, J., Cheze, B., 2008a. Price drivers and structural brakes in European carbon prices 2005-2007. Energy Policy 36, 787–797.

Alberola, E., Chevallier, J., Cheze, B., 2008b. The EU emissions trading scheme: the effects of industrial production and CO_2 emissions on carbon prices. Economie Internationale 116, 93–126.

Andreae, M.O., Jones, C.D., Cox, P.M., 2005. Strong present-day aerosol cooling implies a hot future. Nature 435, 1187–1190.

Angelsen, A., 1996. Deforestation: Population or market driven? Different approaches in modelling agricultural expansion. Chr. Michelsen Institute Working Paper 9 (http://hdl.handle.net/10202/324).

Angelsen, A., 1999. Agricultural expansion and deforestation: Modelling the impact of population, market forces and property rights. Journal of Development Economics 58 (1), 185–218.

Angelsen, A., 2007. Forest cover change in space and time: Combining the von Thünen and Forest Transition Theories. The World Bank Policy Research Working Paper, CIFOR and UBM.

Angelsen, A., 2008a. Moving ahead with REDD: Issues, Options and Implications. Center for International Forestry Research (CIFOR), Bogor, Indonesia. http://www.cifor.org/online-library/browse/view-publication/publication/2601.html.

Angelsen, A., 2008b. REDD models and baselines. International Forestry Review 10(3), 465–475.

Angelsen, A., 2010. The 3 REDD I's. Journal of Forest Economics 16, 253–256.

Angelsen, A., Brown, S., Loisel, C., Peskett, L., Streck, C., Zarin, D., 2009. Reducing emissions from deforestation and forest degradation (REDD): An options assessment report. Meridian Insititute, Document prepared for the Government of Norway www.climatefocus.com/documents/reducing_emissions_from_deforestation_and_forest_degradation.

Assante, P., 2011. Carbon sequestration and the optimal economic harvest decision. Ph.D. thesis. The Faculty of Graduate Studies and Research, Edmonton, Alaberta.

Bahn, O., Chesney, M., Gheyssens, J., 2012. The effect of proactive adaptation on green investment. Environmental Science & Policy 18, 9–24.

Bala, G., Duffy, P.B., Taylor, K.E., 2008. Impact of geoengineering schemes on the global hydrological cycle. Proceedings of the National Academy of Sciences 105 (22), 7664–7669.

Ban-Weiss, G.A., Caldeira, K., 2010. Geoengineering as an optimization problem. Environmental Research Letters 5.

Barrett, S., 2008. The incredible economics of geoengineering. Environmental and Resource Economics 39, 45–54.

Barrett, S., Lenton, T.M., et al, 2014. Climate engineering reconsidered. Nature Climate Change 4, 527 – 529.

Bellamy, R., Chilvers, J., Vaughan, N., Lenton, T., 2013. 'opening up' geoengineering appraisal: Multi-criteria mapping of options for tackling climate change. Global Environmental Change .

Bessembinder, H., Seguin, P.J., 1992. Futures-trading activity and stock price volatility. The Journal of Finance 47(5), 2015–2034.

Bessembinder, H., Seguin, P.J., 1993. Price volatility, trading volume, and market depth: Evidence from futures markets. Journal of Financial and Quantitative Analysis 28(1), 21–39.

Betz, R., Eichhammer, W., Schleich, J., 2004. Designing national allocation plans for EU-Emissions Trading - a first analysis of the outcomes. Energy & Environment 15 (3), 375–425.

Betz, R.A., Schmidt, T.S., 2015. Transfer patterns in Phase I of the EU Emissions Trading System: a first reality check based on cluster analysis. Climate Policy DOI: 10.1080/14693062.2015.1028319.

Bickel, J., 2013. Climate engineering and climate tipping-point scenarios. Environmental Systems & Decisions 33, 152–167, doi:10.1007/s10669–013–9435–8.

Bickel, J., Agrawal, S., 2012. Reexamining the economics of aerosol geoengineering. Climatic Change 119, 993–1006.

Blackstock, J., Battisti, D., Caldeira, K., Eardley, D., Katz, J., Keith, D., Patrinos, A., Schrag, D., Socolow, R., Soonin, S., 2009. Climate engineering responses to climate emergencies. Novim, Santa Barbara .

Blom, B., Sunderland, T., Murdiyarso, D., 2010. Getting REDD to work locally: Lessons learned from integrated conservation and development projects. Environmental Science and Policy 13(2), 164–172.

Borras Jr, S.M., Franco, J.C., Gomez, S., Kay, C., Spoor, M., 2012. Land grabbing in Latin America and the Caribbean. Journal of Peasant Studies 39, 845–872.

Bosello, F., Carraro, C., De Cian, E., 2010. Climate policy and the optimal balance between mitigation, adaptation and unavoided damage. Climate Change Economics 1, 71–92.

Brasseur, G.P., Roeckner, E., 2005. Impact of improved air quality on the future evolution of climate. Geophysical Research Letters 32, L23704, doi:10.1029/2005GL023902.

Bredin, D., Hyde, S., Muckley, C., 2014. A microstructure analysis of the carbon finance market. International Review of Financial Analysis 34, 222–234.

Brockett, C.D., 1990. Land, power, and poverty: Agrarian transformation and political conflict in Central America. Unwin Hyman Publishing House, London, UK.

Brovkin, V., Petoukhov, V., Claussen, M., Bauer, E., Archer, D., Jaeger, C., 2009. Geoengineering climate by stratospheric sulfur injections: Earth system vulnerability to technological failure. Climatic Change 92, 243–259.

de Bruin, K., 2011. Distinguishing between proactive (stock) and reactive (flow) adaptation. Working Paper 8 CERE Umea Sweden.

de Bruin, K., Dellink, R., 2011. How harmful are restrictions on adapting to climate change? Global Environmental Change 21, 34–45.

de Bruin, K., Dellink, R., Tol, R., 2009. AD-DICE: An implementation of adaptation in the DICE model. Climatic Change 95, 63–81.

Bunn, D., Fezzi, C., 2007. Interaction of European carbon trading and energy prices. Fondazione Eni Enrico Mattei Working Paper 123.

Busch, J., Godoy, F., Turner, W.R., Harvey, C.A., 2011. Biodiversity co-benefits of reducing emissions from deforestation under alternative reference levels and levels of finance. Conservation Letters 4(2), 101–115.

Busch, J., Lubowski, R., Godoy, F., Steininger, M., Yusuf, A., Austin, K., Hewson, J., Juhn, D., Farid, M., Boltz, F., 2012. Structuring economic incentives to reduce emissions from deforestation within Indonesia. Proceedings of the National Academy of Sciences 109(4), 1062–1067.

Busch, J., Strassburg, B., Cattaneo, A., Lubowski, R., Bruner, A., Rice, R., Creed, A., Ashton, R., Boltz, F., 2009. Comparing climate and cost impacts of reference levels for reducing emissions from deforestation. Environmental Research Letters 4, DOI:10.1088/1748–9326/4/4/044006.

Caldeira, K., Bala, G., Cao, L., 2013. The science of geoengineering. Annual Review of Earth and Planetary Sciences 41(1), 231–256.

Cao, L., Caldeira, K., 2008. Atmospheric co_2 stabilization and ocean acidification. Geophysical Research Letters 35.

Carlin, A., 2007. Global climate change control: is there a better strategy than reducing greenhouse gas emissions? Univ PA Law Review 155, 128–156.

Carlson, J.M., Doyle, J., 2002. Complexity and robustness. Proceedings of the National Academy of Sciences of the United States of America 99, 2538–2545.

Cattaneo, A., Lubowski, R., Busch, J., Creed, A., Strassburg, B., Boltz, F., Ashton, R., 2010. On international equity in reducing emissions from deforestation. Environmental Science & Policy 13, 742–753.

Chesney, M., Taschini, L., 2012. The endogenous price dynamics of emission allowances and an application to CO_2 option pricing. Applied Mathematical Finance 19, 447–475.

Chevallier, J., Sévi, B., 2014. On the stochastic properties of carbon futures prices. Environmental and Resource Economics 58, 127–153.

Chiang, A., 1992. Elements of Dynamic Optimization. McGraw-Hill International Editions, Economic Series.

Christensen, A., Arvanitakis, A., Tangen, K., Hasselknippe, H., 2005. Price determinants in the EU Emissions Trading S. Climate Policy 5, 15–30.

Clark, P.K., 1973. A subordinated stochastic process model with finite variances for speculative prices. Econometrica 41, 135–155.

Cludius, J., 2015. Distributional Effects of Energy and Climate Policy. PhD thesis in Economics. Ph.D. thesis. UNSW Business School, UNSW Australia, forthcoming.

Corbera, E., Schroeder, H., 2011. Governing and implementing REDD+. Environmental Science and Policy 14, 89–99.

Creti, A., Jouvet, P., Mignon, V., 2012. Carbon price drivers: Phase I versus phase II equilibrium? Energy Economics 34, 327–334.

Cronshaw, M.B., Kruse, J.B., 1996. Regulated firms in pollution permit markets with banking. Journal of Regulatory Economics 9, 179–189.

Crutzen, P., 2006. Albedo enhancement by stratospheric sulfur injections: a contribution to resolve a policy dilemma? Climatic Change 77, 211–219.

Daigler, R.T., Wiley, M.K., 1999. The impact of trader type on the futures volatility-volume relation. The Journal of Finance 54(6), 2297–2316.

Dales, J., 1968. Pollution property and prices. University of Toronto Press .

Daskalakis, G., Markellos, R., 2008. Are the European carbon markets efficient? Review of Futures Markets 17 (2), 103–128.

Daskalakis, G., Markellos, R.N., 2009. Are electricity risk premia affected by emission allowance prices? Evidence from EEX, Nord Pool and Powernext. Energy Policy 37, 2594–2604.

Daskalakis, G., Phychoyios, D., Markellos, R.N., 2009. Modeling CO_2 emission allowance prices and derivatives: Evidence from the European trading scheme. Journal of Banking and Finance 33, 1230–1241.

Davidian, M., Carroll, R.J., 1987. Variance function estimation. Journal of the American Statistical Association 82, 1079–1091.

Diaz, D., Hamilton, K., Johnson, E., 2011. State of the Forest Carbon Markets 2011: From canopy to currency. Ecosystem Marketplace http://www.forest-trends.org/publication_details.php?publicationID=2963.

Doney, S.C., Fabry, V.J., Feely, R.A., Kleypas, J.A., 2009. Ocean acidification: The other co2 problem. Annual Review of Marine Science 1, 169–192.

Doupé, P., 2014. The costs of error in setting reference rates for reduced deforestation. Working paper version 10 July 2014. Available online at http://www.patrickdoupe.net/wp-content/uploads/2014/01/timeSeries.pdf.

Edenhofer, O., Pichs-Madruga, R., et al (Eds.), 2014. IPCC, 2014: Climate Change 2014: Mitigation of Climate Change. Cambridge University Press, Cambridge, United Kingdom and New York, NY, USA.

Engels, A., 2009. The European Emissions Trading Scheme: an exploratory study of how companies learn to account for carbon. Accounting, Organization and Society 34, 488 – 498.

English, J., Toon, O., Mills, M., 2012. Microphysical simulations of sulfur burdens from stratospheric sulfur geoengineering. Atmospheric Chemistry and Physics 12, 4775–4793.

Entenmann, S., Schmitt, C., 2013. Actors' perceptions of forest biodiversity values and policy issues related to REDD+ implementation in Peru. Biodiversity and Conservation 22, 1229–1254.

European Commission, 2015. The EU Emissions Trading System (EU ETS) Factsheet. Technical Report. European Commission. Available online at $http://ec.europa.eu/clima/publications/docs/factsheet_ets_en.pdf$.

FAO, 2005. Peru country profile, Forest Area Statistics, FAO Global Forest Resources Assessment 2005.

FAO, 2010. Global Forest Resources Assessment Main report. Technical Report. Food and Agriculture Organization of the United Nations, http://www.fao.org/docrep/013/i1757e/i1757e.pdf.

FCPF Carbon Fund, 2013. FCPF Carbon Fund Methodological Framework. Technical Report. Forest Carbon Partnership Facility. Available online at https://www.forestcarbonpartnership.org/sites/fcp/files/2014/MArch/March/FCPF

French, K.R., Schwert, G.W., Stambaugh, R.F., 1987. Expected stock returns and volatility. Journal of Financial Economics 19, 3–30.

Goes, M., Tuana, N., Keller, K., 2011. The economics (or lack thereof) of aerosol geoengineering. Climatic Change 109, 719–744.

Gramstad, K., Tjotta, S., 2010. Climate engineering: Cost benefit and beyond. Working papers in economics, University of Bergen, Norway.

Griscom, B., Shoch, D., Stanley, B., Cortez, R., Virgilio, N., 2009. Sensitivity of amounts and distribution of tropical forest carbon credits depending on baseline rules. Environmental Science and Policy 12, 897–911.

Guariguata, M.R., Cornelius, J.P., Locatelli, B., Forner, C., Sánchez-Azofeifa, G.A., 2008. Mitigation needs adaptation: Tropical forestry and climate change. Mitigation and Adaptation Strategies for Global Change 13(8), 793–808.

Gunderson, L.H., 2003. Adaptive dancing: Interactions between social resilience and ecological crises. Navigating socialecological systems: Building resilience for complexity and change. Cambridge University Press, Cambridge, UK 2003, 33–52.

Hajek, F., Ventresca, M., Scriven, J., Castro, A., 2011. Regime-building for REDD+: Evidence from a cluster of local initiatives in South-Eastern Peru. Environmental Science and Policy 14, 201–215.

Harris, L., 1986. Cross-security tests of the mixture of distributions hypothesis. Journal of Financial and Quantitative Analysis 21, 39–46.

Harris, M., Raviv, A., 1993. Differences of opinion make a horse race. Review of Financial Studies 6, 473–506.

Hintermann, B., 2010. Allowance price drivers in the first phase of the EU ETS. Journal of Environmental Economics and Management 59, 43–56.

Hintermann, B., 2011. Market power, permit allocation and efficiency in emission permit markets. Journal of Environment and Resource Economics 49, 327–349.

Hintermann, B., 2012. Pricing emission permits in the absence of abatement. Energy Economics 34, 1329–1340.

Hintermann, B., 2014. Market power in emission permit markets: theory and evidence. Working paper Switzerland, University of Basel.

Holling, C.S., 1973. Resilience and stability of ecological systems. Annual review of ecology and systematics 4, 1–23.

Huettner, M., Leemans, R., Kok, K., Ebeling, J., 2009. A comparison of baseline methodologies for 'Reducing Emissions from Deforestation and Degradation'. Carbon Balance and Management 4(4), DOI: 10.1186/1750–0680–4–4.

Huneeus, N., Boucher, O., et al, 2014. Forcings and feedbacks in the GeoMIP ensemble for a reduction in solar irradiance and increase in CO_2. Journal of Geophysical Research: Atmospheres 119(9), 5226–5239.

IPCC, 2014. Climate Change 2014 Synthesis Report Summary for Policymakers. Technical Report. IPCC.

Irawan, S., Tacconi, L., Ring, I., 2013. Shareholders' incentives for land-use change and REDD+: The case of Indonesia. Ecological Economics 87, 75–83.

ITTO, 2010. Annual Review and Assessment of the World Timber Situation 2010. Prepared by the Division of Economic Information and Market Intelligence, ITTO, Yokohama, Japan. http://www.itto.int/annual_review/.

Janssen, M.A., Anderies, J.M., Ostrom, E., 2007. Robustness of social-ecological systems to spatial and temporal variability. Society and Natural Resources 20, 307–322.

Jaraite, J., Kazukauskas, A., 2013. Firm trading behavior and transaction costs in the European Union's Emission Trading Scheme: An empirical assessment. Working paper presented at the EAERE conference in Toulouse, France, 2013. Available online at: $http://papers.ssrn.com/sol3/papers.cfm?abstract_id = 2013891$.

Joanneum Research Institute, E.R., 2006. Reducing Emissions from Deforestation in Developing Countries: Potential Policy Approaches and Positive Incentives, Submission to the UNFCCC/SBSTA. Technical Report. Joanneum Research Institute of Energy Research, Union of Concerned Scientists, Woods Hole Research Center, Instituto de Pesquisa Ambiental da Amazonia.

Jones, A., Haywood, J., et al, 2013. The impact of abrupt suspension of solar radiation management (termination effect) in experiment G2 of the Geoengineering Model Intercomparison Project (GeoMIP). Journal of Geophysical Research 118, 97439752.

Jones, C.M., Kaul, G., Lipson, M.L., 1994. Transactions, volume, and volatility. The Review of Financial Studies 7(4), 631–351.

Kalaitzoglou, I., Ibrahim, B.M., 2013. Does order flow in the European carbon futures market reveal information? Journal of Financial Markets 16, 604–635.

Karpoff, J.M., 1988. The relation between price changes and trading volume: a survey. Journal of Financial Research 11, 173–188.

Keith, D., 2000. Geoengineering the climate: history and prospect. Annual Review of Energy and the Environment 25, 245–284.

Keller, K., Robinson, A., Oppenheimer, D.B.M., 2007. The regrets of procrastination in climate policy. Environmental Research Letters 2.

Keppler, J.H., Mansanet-Bataller, M., 2010. Causalities between CO_2, electricity, and other energy variables during phase I and phase II of the EU ETS. Energy Policy 38, 3329–3341.

Kindermann, G., Obersteiner, M., Sohngen, B., Sathaye, J., Andrasko, K., Rametsteiner, E., Schlamadinger, B., Wunder, S., Beach, R., 2008. Global cost estimates of reducing carbon emissions through avoided deforestation. Proceedings of the National Academy of Sciences 105, 10302–10307.

Klein, R., Eriksen, S., Næss, L., Hammill, A., Tanner, T., Robledo, C., O'Brien, K., 2007. Portfolio screening to support the mainstreaming of adaptation to climate change into development assistance. Climatic Change 84, 23–44.

Koch, N., 2014. Dynamic linkages among carbon, energy and financial markets: a smooth transition approach. Applied Economics 46 (7), 715–729.

Kravitz, B., Rasch, P., et al, 2013. An energetic perspective on hydrological cycle changes in the Geoengineering Model Intercomparison Project. Journal of Geophysical Research 118 (23), 13087–13102.

Kravitz, B., Robock, A., Oman, L., Stenchikov, G., Marquardt, A., 2009. Sulfuric acid deposition from stratospheric geoengineering with sulfate aerosols. Journal of Geophysical Research 114 (D14).

Lu, H., Liu, G., 2013. Distributed land use modeling and sensitivity analysis for REDD+. Land Use Policy 33, 54–60.

Lucia, J.J., Mansanet-Bataller, M., Pardo, A., 2014. Speculative and hedging activities in the European carbon market. Energy Policy 82, 342 – 351.

MacMynowski, D., Keith, D., Caldeira, K., Shin, H., 2011a. Can we test geoengineering? Royal Society Journal of Energy and Environmental Science 4 (12), 5044–5052.

MacMynowski, D., Shin, H., Caldeira, K., 2011b. The frequency response of temperature and precipitation in a climate model. Geophysical Research Letters 38(L16711).

Macnaghten, P., Szerszynski, B., 2013. Living the global social experiment: An analysis of public discourse on solar radiation management and its implications for governance. Global Environmental Change 23(2), 465–474.

Manne, A., Richels, R., 2005. MERGE: An integrated assessment model for global climate change, in: Loulou, R., Waaub, J.P., Zaccour, G. (Eds.), Energy and Environment. Springer. volume 3 of *GERAD 25th Anniversary Series*, pp. 175–189.

Mansanet-Bataller, M., Pardo, A., Valor, E., 2007. CO_2 prices, energy and weather. The Energy Journal 3, 67–86.

Margulis, S., Narain, U., 2009. The Costs to Developing Countries of Adapting to Climate Change: New Methods and Estimates. Global Report of the Economics of Adaptation to Climate Change Study. The World Bank. Washington, DC.

Markusson, N., Ginn, F., Singh Ghaleigh, N., Scott, V., 2013. 'In case of emergency press here': framing geoengineering as a response to dangerous climate change. Wiley Interdisciplinary Reviews: Climate Change http://doi.wiley.com/10.1002/wcc.263, ISSN: 17577780.

Millard-Ball, A., 2012. The tuvalu syndrome. can geoengineering solve the climate's collective action problem? Climatic Change 110, 1047–1066.

Montagnoli, A., de Vries, F.P., 2010. Carbon trading thickness and market efficiency. Energy Economics 32, 1331–1336.

Montgomery, W., 1972. Markets in licences and efficient pollution control programs. Journal of Economic Theory 5.

Moreno-Cruz, J.B., Keith, D.W., 2013. Climate policy under under uncertainty: a case for solar geoengineering. Climatic Change 121, 431–444.

Mosnier, A., Havlik, P., Obersteiner, M., Aoki, K., Schmid, E., Fritz, S., McCallum, I., Leduc, S., 2014. Modeling impact of development trajectories and a global agreement on Reducing Emissions from Deforestation on Congo Basin forests by 2030. Environmental and Resource Economics 57, 505–525.

Niemeier, U., Schmidt, H., Alterskjr, K., Kristjnsson, J., 2013. Solar irradiance reduction via climate engineering: Impact of different techniques on the energy balance and the hydrological cycle. Journal of Geophysical Research 118 (21), 11905–11917.

NIFCI, 2011. Real-time evaluation of Norway's International and Climate Initiative. Contributions to National REDD+ Processes 2007-2010. Technical Report. Norway's International and Climate Initiative. Available online at http://www.climatefundsupdate.org/listing/norway-s-international-climate-and-forest-initiative.

Nordhaus, W., 2001. Global warming economics. Science 294, 1283–1284.

Nordhaus, W., 2007. Alternative measures of output in global economic-environmental models: purchasing power parity or market exchange rates? Energy Economics 29(3), 349–372.

Nordhaus, W., 2008. A question of balance. Yale University Press .

Nordhaus, W.D., Boyer, J., 2000. Warning the World: Economic Models of Global Warming. MIT Press (MA).

Ollivier, H., 2012. Growth, deforestation and the efficiency of the REDD mechanism. Journal of Environmental Economics and Management 64, 312 – 327.

Orr, J.C., Fabry, V.J., et al., 2005. Anthropogenic ocean acidification over the twenty-first century and its impact on calcifying organisms. Nature 437, 681–686.

Palao, F., Pardo, A., 2012. Assessing price clustering in european carbon markets. Applied Energy 92, 51–56.

Palmer, C., 2010. Property right and liability for deforestation under REDD+: Implications for 'permanence' in policy design. Ecological Economics 70, 571–576.

Paolella, M.S., Taschini, L., 2008. An econometric analysis of emission allowance prices. Journal of Banking and Finance 32, 2022–2032.

Parker, C., Mitchell, A., Trivedi, M., Mardas, N., 2008. The little REDD book: A guide to governmental and non-governmental proposals for reducing emissions from deforestation and degradation. Global Canopy Programme, Oxford, UK.

Penman, J., Gytarsky, M., Hiraishi, T., Krug, T., Kruger, D., Pipatti, R., Buendia, L., Miwa, K., Ngara, T., Tanabe, K., Wagner, F., 2003. Good practice guidance for land use, land use change and forestry. Intergovernmental Panel on Climate Change, Institute for Global Environmental Strategies (IGES) .

Pfaff, A., Amacher, G., Sills, E., 2013. Realistic REDD: Improving the forest impacts of domestic policies in different settings. Review of Environmental Economics and Policy 7 (1), 114–135.

Pindyck, R.S., 2013. Climate change policy: What do the models tell us? Working paper 19244 NBER.

Pinker, R.T., Zhang, B., Dutton, E.G., 2005. Do satellites detect trends in surface solar radiation? Science 308, 850–854.

Ramanathan, V., Crutzen, P., Kiehl, J., Rosenfeld, D., 2001. Aerosols, climate, and the hydrological cycle. science 294, 2119–2124.

Rasch, P., Tilmes, S., et al, 2008. An overview of geoengineering of climate using stratospheric sulphate aerosols. Philosophical Transactions of The Royal Society 366, 4007–4037.

Rittler, D., 2012. Price discovery and volatility splillovers in the European Union emissions trading scheme: A high-frequency analysis. Journal of Banking and Finance 36, 774–785.

Robock, A., MacMartin, D., Duren, R., Christensen, M., 2013. Studying geoengineering with natural and anthropogenic analogs. Climatic Change 121, 445–458.

Robock, A., Marquardt, A., Kravitz, B., Stenchikov, G., 2009. Benefits, risks, and costs of stratospheric geoengineering. Geophysical Research Letters 36.

Robock, A., Oman, L., Stenchikov, G., 2008. Regional climate responses to geoengineering with tropical and Arctic SO_2 injections. Journal of Geophysical Research 113.

Rubin, J.D., 1996. A model of intertemporal emission trading, banking and borrowing. Journal of Environmental Economics and Management 31, 269–286.

Sathaye, J., Andrasko, K., Chan, P., 2011. Emissions scenarios, costs, and implementation considerations of REDD-plus programs. Environment and Development Economics 16, 361–380.

Schaller, N., Cermak, J., Wild, M., Knutti, R., 2013. The sensitivity of the modeled energy budget and hydrological cycle to CO_2 and solar forcing. Earth System Dynamics 4, doi:10.5194/esd–4–253–2013.

Schlamadinger, B., Ciccarese, L., Dutschlke, M., Fearnside, P., Brown, S., Mudiyarso, D., 2005. Should we include avoidance of deforestation in the international response to climate change?, in: Carbon Forestry: Who Will Benefit? Proceedings of Workshop on Carbon Sequestration and Sustainable Livelihoods, held in Bogor on 16-17 February 2005. Center for International Forestry Research (CIFOR), Bogor, Indonesia.

Schwert, G.W., 1990. Stock volatility and the crash of '87. The Review of Financial Studies 3(1), 77–102.

Shalen, C.T., 1993. Volume, volatility, and the dispersion of beliefs. Review of Financial Studies 6, 405–434.

Shepherd, J., 2009. Geoengineering the climate; science, governance and uncertainty. The Royal Society .

Solomon, S., Plattnera, G.K., Knutti, R., Friedlingstein, P., 2009. Irreversible climate change due to carbon dioxide emissions. Proceedings of the National Academy of Sciences 106, 1704–1709.

Stainforth, D.A., Aina, T., Christensen, C., Collins, M., Faull, N., Frame, D.J., Kettleborough, J.A., Knight, S., Martin, A., Murphy, J.M., Piani, C., Sexton, D., Smith, L.A., Spicer, R.A., Thorpe, A.J., Allen, M.R., 2005. Uncertainty in predictions of the climate response to rising levels of green house gases. Nature 433, 403–406.

Stanhill, G., Cohen, S., 2001. Global dimming: A review of the evidence for a widespread and significant reduction in global radiation with discussion of its probable causes and possible agricultural consequences. Agricultural and Forest Meteorology 107.

Stenchikov, G., Kirchner, I., et al, 1998. Radiative forcing from the 1991 Mount Pinatubo volcanic eruption. Journal of Geophysics Research 103, 13837–13857.

Stern, N., 2006. The Economics of Climate Change: The Stern Review. Cambridge University Press, Cambridge, UK.

Stern, N., 2008. Key elements of a global deal on climate change. London School of Economics and Political Science, London, UK.

Stern, N., 2013. The structure of economic modeling of the potential impacts of climate change: Grafting gross underestimation of risk onto already narrow science models. Journal of Economic Literature 51(3), 838–859.

Tauchen, G.E., Pitts, M., 1983. The price variability - volume relationship on speculative markets. Econometrica 51, 485–505.

The German REDD Early Movers Program, 2014. Available online at http://theredddesk.org/markets-standards/germanys-redd-early-movers-programme.

von Thünen, J., 1826. Der isolierte Staat. Beziehung auf Landwirtschaft und Nationalökonomie. Akademie Verlag Berlin.

Tilmes, S., Mueller, R., Salawitch, R., 2008. The sensitivity of polar ozone depletion to proposed geoengineering schemes. Science 320, 1201–1204.

Tol, R., 2005. Adaptation and mitigation: Trade-offs in substance and methods. Environmental Science and Policy 8, 572–578.

Trenberth, K., Dai, A., 2007. Effects of Mount Pinatubo volcanic eruption on the hydrological cycle as an analog of geoengineering. Geophysical Research Letters 34.

Uhrig-Homburg, M., Wagner, M., 2009. Futures price dynamics of CO_2 emission allowances: An empirical analysis of the trial period. The Journal of Derivatives 17(2), 73–88.

UNFCCC, 2009. Decision 4/CP.15 Methodological guidance for activities relating to reducing emissions from deforestation and forest degradation and the role of conservation, sustainable management of forests and enhacement of forest carbon stocks in developing countries. Technical Report. United Nations Framework Convention on Climate Change.

UNFCCC, 2011. Decision 12/CP.17 Guidance on systems for providing information on how safeguards and addressed and respected and modalities relating to forest reference emission levels and forest reference levels as referred to in decision 1/CP.16. Technical Report. United Nations Framework Convention on Climate Change.

Vaughan, N., Lenton, T., 2011. A review of climate geoengineering proposals. Climatic Change 109, 745–790.

Verburg, P.H., Schot, P.P., Dijst, M.J., Veldkamp, A., 2004. Land use change modelling: Current practice and research priorities. GeoJournal 61, 309–324.

Verissimo, A., Barreto, P., Mattos, M., Tarifa, R., Uhl, C., 1992. Logging impacts and prospects for sustainable forest management in an old Amazonian frontier: The case of Paragominas. Forest Ecology and Management 55, 169–199.

Victor, D.G., 2008. On the regulation of geoengineering. Oxford Review of Economic Policy 24, 322–336.

Vitel, C.S.M.N., Carrero, G.C., Cenamo, M.C., Leroy, M., Graça, P.M.L.A., Fearnside, P.M., 2013. Land-use change modeling in a Brazilian indigenous reserve: Construction of a reference scenario for the Suruí REDD project. Human Ecology 41 (6), 807–826.

Wassenaar, T., Gerbera, P., Verburg, P., Rosales, M., Ibrahim, M., Steinfeld, H., 2007. Projecting land use changes in the Neotropics: The geography of pasture expansion into forest. Global Environmental Change Volume 17, 86 – 104.

van der Werf, G.R., Morton, D., DeFries, R., Olivier, J.G.J., Kasibhatla, P.S., Jackson, R.B., Collatz, G., Randerson, J.T., 2009. CO_2 emissions from forest loss. Nature Geoscience 2, 737–738.

Wigley, T., 2006. A combined mitigation/geoengineering approach to climate stabilization. Science 314, 452–454.

World Bank, 2014. States and Trends of Carbon Pricing 2014. World Bank, Washington DC.

Wright, M.J., Teagle, D.H., Feetham, P.M., 2014. A quantitative evaluation of the public response to climate engineering. Nature Climate Change 4(2), 106–110.

Zaklan, A., 2013. Why do emitters trade carbon permits? Firm-level evidence from the European Emissions Trading Scheme. Working paper presented at the EAERE conference in Toulouse, France, 2013. Available online at: $http://papers.ssrn.com/sol3/papers.cfm?abstract_id = 2239656$.

Appendix

A Published manuscript, Journal of Environmental Science and Policy 48, 2015, p67-76: *Is there room for geoengineering in the optimal climate policy mix?*

ENVIRONMENTAL SCIENCE & POLICY 48 (2015) 67–76

Available online at www.sciencedirect.com

ScienceDirect

journal homepage: www.elsevier.com/locate/envsci

Is there room for geoengineering in the optimal climate policy mix?

O. Bahn [a], M. Chesney [b,*], J. Gheyssens [d], R. Knutti [c], A.C. Pana [b]

[a] GERAD and Department of Decision Sciences, HEC Montréal, Canada
[b] Institute of Banking and Finance, University of Zurich, Switzerland
[c] Institute for Atmospheric and Climate Science, ETH Zurich, Switzerland
[d] UNEP Financial Initiative, Geneva, Switzerland

ARTICLE INFO

Article history:
Available online 14 January 2015

Keywords:
Climate change
Integrated assessment
Adaptation
Mitigation
Geoengineering

JEL classification:
Q43
Q48
Q54
Q58

ABSTRACT

We investigate geoengineering as a possible substitute for mitigation and adaptation measures to address climate change. Relying on an integrated assessment model, we distinguish between the effects of solar radiation management (SRM) on atmospheric temperature levels and its side-effects on the environment. The optimal climate portfolio is a mix of mitigation, adaptation, and SRM. When accounting for uncertainty in the magnitude of SRM side-effects and their persistency over time, we show that the SRM option lacks robustness. We then analyse the welfare consequences of basing the SRM decision on wrong assumptions about its side-effects, and show that total output losses are considerable and increase with the error horizon. This reinforces the need to balance the policy portfolio in favour of mitigation.

1. Introduction

Climate change due to anthropogenic greenhouse gas (GHG) emissions is viewed as one of the most serious challenges faced by humankind (Stern, 2006). Strategies for dealing with climate change enter three main categories: mitigation, adaptation, and climate geoengineering. International agreements call for reductions in GHG emissions – the mitigation approach. Despite its direct impact on temperature levels, its technical feasibility, and its ethical appeal, several factors limit the implementation of mitigation: (i) the strong inertia in the carbon cycle creates a gap between present abatement costs and future climate benefits (Keller et al., 2007); (ii) the decades-to-millennia-long lifespan of GHG render mitigation ineffective in case of abrupt climate changes; (iii) the atmosphere is a common good and unilateral actions are discouraged by the possibility of free riding (Millard-Ball, 2012).

An alternative for dealing with climate change is adaptation, the development of strategies that effectively reduce climate change impacts (Tol, 2005). Adaptation covers a large array of sectors, and can be 'proactive' or 'reactive' (de Bruin, 2011). While proactive adaptation is directed towards infrastructure and medium-to-long-term economic transformations (Agrawala et al., 2011), reactive adaptation can be deployed almost instantaneously to mitigate unforeseen or underestimated damages. Several features distinguish adaptation from mitigation: (i) adaptation can be implemented

* *Corresponding author*. Tel.: +41 44 634 45 80.
E-mail address: marc.chesney@bf.uzh.ch (M. Chesney).
http://dx.doi.org/10.1016/j.envsci.2014.12.014
1462-9011/

unilaterally, giving full control of the benefits to the countries implementing it; (ii) adaptation is expected to exhibit a fast implementation – fast benefits feature, avoiding deadlocks from discounting preferences. However, investments in adaptation have been limited so far due, in particular, to difficulties in forecasting its effectiveness.

Given the increasing risk of an unmanageable temperature path, geoengineering has been proposed as an alternative strategy. It corresponds to a deliberate modification of the climate system in order to alleviate climate change impacts (Keith, 2000; Caldeira et al., 2013). One may distinguish between two main techniques: Carbon Dioxide Removal (CDR) and Solar Radiation Management (SRM). In this paper, we focus on an SRM approach that targets the reduction of incoming solar radiation by injection of sulfur in the stratosphere, believed to be one of the most efficient geoengineering strategies to reduce global temperature (Wigley, 2006; Shepherd et al., 2009). Its premise is the ability to keep temperature levels artificially low, instead of reducing GHG emissions. SRM presents several advantages: (i) it involves low implementation costs (Robock et al., 2009); (ii) in case of rapid climate changes (when tipping points are reached), with rare but catastrophic impacts, SRM could act as a quick and effective temperature 'backstop' (Crutzen, 2006); (iii) it can be implemented either unilaterally or cooperatively (Barrett, 2008).

SRM brings along also important risks, as it may produce unintended consequences and harmful side-effects (Victor, 2008). A comprehensive summary is given in Barrett et al. (2014). Injecting sulfur particles into the upper atmosphere is expected to cause polar ozone depletion (Crutzen, 2006; Tilmes et al., 2008; Solomon et al., 2009), acid deposition at the poles (Kravitz et al., 2009), alter ecosystems (Stanhill and Cohen, 2001; Adams et al., 2003; Rasch et al., 2008), and trigger regional imbalances (e.g., in the patterns of surface temperature, radiation, and the hydrological cycle; Trenberth and Dai, 2007; Bala et al., 2008; Brovkin et al., 2009; Kravitz et al., 2013; Niemeier et al., 2013; Schaller et al., 2013; Huneeus and Boucher, 2014). Simulations of sulphate injection predict disruptions in the Asian and African summer monsoons (Robock et al., 2008). Stratospheric aerosol loading impacts the ratio of direct to diffuse light, with consequences for terrestrial and marine photosynthesis and for technologies relying on direct light (Rasch et al., 2008; Vaughan and Lenton, 2011).

Furthermore, SRM achieves only an artificial reduction in temperature levels. With a continued increase in GHG concentrations, the injection of aerosols would need to raise proportionally, and a disruption would lead to a significant jump in temperatures at the corresponding concentration level (Brasseur and Roeckner, 2005; Brovkin et al., 2009; Jones et al., 2013) with probable dire consequences. Additionally, SRM will not be able to counteract other negative consequences coming from high GHG concentrations, such as ocean acidification (Orr et al., 2005; Doney et al., 2009), CO_2 fertilisation of land plants, and other biogeochemical modifications (Ban-Weiss and Caldeira, 2010). Finally, with a lack of assessment of SRM impacts on human societies and on ecosystems, there remains the possibility for unexpected consequences – unknown unknowns (Kravitz et al., 2009). The uncertainty is reinforced by the fact that expected consequences of SRM (both positive and negative) are estimated by comparison with natural volcanic eruptions, which are an imperfect analog to continuous anthropogenic stratospheric forcing (Robock et al., 2013). Finally, there are important societal and political dimensions to geoengineering (Macnaghten and Szerszynski, 2013; Wright et al., 2014).

Given these important caveats, support for geoengineering measures has been inconclusive so far. Crutzen (2006), Wigley (2006), Carlin (2007), and Bickel (2013) advocate additional research on geoengineering before a robust recommendation could be formulated. More recent studies focus on modelling decision-making in the context of multiple sources of risk. Goes et al. (2011) use an integrated assessment model (IAM) where the total damage from climate change is a function of a rate-dependent temperature component, and account for the failure to sustain aerosol forcing and for the subsequent unraveling of drastic climate changes. In such a case, SRM is found to be uneconomical. Bickel and Agrawal (2012) rely on the model of Goes et al. (2011) and show that under modified assumptions some totally different conclusions regarding the use of SRM can be found.

In this paper, we assess the optimal mix of policies to deal effectively with climate change. Our methodology relies on the Ada-BaHaMa model (Bahn et al., 2012), which allows for mitigation and proactive adaptation, and enriches it by explicitly considering reactive adaptation and SRM. We account for different effects of SRM. While the *desired* effects of SRM on radiative forcing can be estimated with a considerable degree of confidence (Crutzen, 2006), the magnitude of *undesired* side-effects of sulfur injection on natural and socio-economic systems remains a significant unknown. We focus on this second uncertainty source, and unlike previous IAMs that consider SRM side-effects to be constant over time (Goes et al., 2011; Bickel and Agrawal, 2012), we model side-effects as a time-varying and persistent process with a stochastic component.

Our original contribution consists in assessing within an integrated assessment framework the optimal policy mix when mitigation, adaptation, and SRM are available. We show that the optimal strategy for dealing with climate change involves the joint use of all three strategies. While mitigation and adaptation are optimally employed in the vast majority of analysed scenarios, SRM passes a cost–benefit test only when its side-effects are low. Moreover, small deviations from expected side-effects can potentially cause large welfare losses, further weakening the case for SRM.

This paper is structured as follows. Section 2 details our dynamic IAM and its calibration. Sections 3 and 4 provide numerical results and analyse specific uncertainties related to SRM. Section 5 concludes.

2. Modelling approach

This section briefly reviews the original Ada-BaHaMa model and details the new modelling features: (i) the introduction of SRM as an instrument to control temperature increase and (ii) a separate accounting of proactive and reactive adaptation.

The model distinguishes between two types of economy: a 'carbon' economy (our present economy), where production generates a high level of GHG emissions, and a 'low-carbon' economy. More precisely, production (Y) occurs in the two

economies according to an extended Cobb–Douglas function in three inputs: capital (K), labor (L), and energy (measured through GHG emissions E). Capital stock in each economy evolves according to the choice of investment (I) and a standard depreciation relation.

2.1. Climate dynamics in the presence of SRM

GHG stocks evolve according to the dynamic equations of the DICE model (Nordhaus, 2008) that distinguishes between three reservoirs: (i) an atmospheric one (M_{AT}), (ii) a quickly mixing one in the upper oceans and the biosphere (M_{UP}), and (iii) a slowly mixing deep-ocean reservoir (M_{LO}) which acts as a long-term sink.

We extend the original Ada-BaHaMa to account for a solar radiation management (SRM) strategy that increases the albedo effect through sulfur injection in the lower stratosphere. The sulphate aerosols formed increase the stratospheric reflection of shortwave radiation back to space (Stenchikov et al., 1998), reducing the radiative forcing (F) from an increase in CO_2 concentrations:

$$F(t) = \eta \log_2\left(\frac{M_{AT}(t)}{M_{AT}(1750)}\right) + F_{EX}(t) - F_{GE}(t) \quad (1)$$

where t is the time period ($t \in [2005, 2155]$), $\eta = 3.7$ W m^{-2} is the radiative forcing for a doubling of atmospheric CO_2 concentrations, F_{EX} the exogenous radiative forcing term, and F_{GE} is the radiative forcing created by the sulphates. The radiative forcing from SRM depends on the amount of sulfur injected, the size of the particles, and the location of injection (Vaughan and Lenton, 2011). Sulfur injection simulations show that at high injection rates (above 40 Tg S) the efficacy on radiative forcing levels off (English et al., 2012). However, for smaller injection rates, a linear relation approximates well the impact of sulfur injected on radiative forcing.[1] We follow Crutzen (2006) and allow for a linear relation:

$$F_{GE}(t) = \omega G(t) \quad (2)$$

where ω is the effectiveness factor of SRM ($\omega = 0.75$ W m^{-2} per Tg S), and G the yearly amount of sulfur injected in the stratosphere measured in tetragrams of sulfur (Tg S).

The other elements of the climatic model remain unchanged from Ada-BaHaMa and follow the DICE model to compute the earth's mean surface temperature (T_{AT}) and the average temperature of the deep oceans (T_{LO}).

2.2. Climate change damages and SRM side-effects

Ada-BaHaMa follows the approach used in MERGE (Manne and Richels, 2005) to link climate change damages and their economic impacts. Here, we additionally account for negative externalities from sulfur injection. Yearly damages (D) on production (Y) come from atmospheric temperature increase ($D_{T_{AT}}$) and side-effects from sulfur injection (D_{GE}):

$$D(t) = D_{T_{AT}}(t) + D_{GE}(t) \quad (3)$$

[1] In our simulations, the optimal amount of sulfur injected never exceeds 15 Tg S per annum.

2.2.1. Climate change damages and adaptation

The increase in temperature (T_{AT}) from pre-industrial levels entails damages that can be alleviated through adaptation (AD):

$$D_{T_{AT}}(t) = \mathrm{AD}(t)\left(\frac{T_{AT}(t) - T_d}{cat_T - T_d}\right)^2 \quad (4)$$

where T_d is the temperature deviation (from pre-industrial levels) at which damages start to occur, while cat_T represents the 'catastrophic' temperature level at which the entire production would be wiped out. To have a comparable basis with the current literature on IAM with adaptation, T_d and cat_T are calibrated to replicate the damage intensity in DICE; see Bahn et al. (2012).

We distinguish between reactive (flow) and proactive (stock) adaptation, similar to Bosello et al. (2010) and Agrawala et al. (2011). We model the effectiveness of the two adaptation strategies in reducing climate change damages as follows:

$$\mathrm{AD}(t) = 1 - \alpha_{\mathrm{AD}_p}(t)\frac{K_3(t)}{K_{3\max}(t)} - \alpha_{\mathrm{AD}_r}(t)\frac{S_3(t)}{S_{3\max}(t)} \quad (5)$$

where α_{AD_p} (respectively, α_{AD_r}) is the maximum proactive (resp. reactive) adaptation effectiveness, K_3 (resp. S_3) the amount of proactive adaptation capital (resp. reactive adaptation spending), $K_{3\max}$ (resp. $S_{3\max}$)[2] the maximum amount of adaptation capital (resp. spending) that would ensure the optimal effectiveness of the proactive (resp. reactive) adaptation measures. Like $K_{3\max}$ in our original model, $S_{3\max}$ is modelled as an increasing function of the temperature level:

$$S_{3\max}(t) = \beta_{\mathrm{AD}_r}\left(\frac{T_{AT}(t)}{T_d}\right)^{\gamma_{\mathrm{AD}_r}} \quad (6)$$

where β_{AD_r} and γ_{AD_r} are calibration parameters. The two options are assumed to be complementary, in that the implementation of one enhances the effectiveness of the other. On the one hand, reactive adaptation requires the existence of some infrastructure; for instance, the deployment of new crops (better suited to new climatic condition) possibly requires that tests have been conducted beforehand (pro-actively) in R&D facilities. On the other hand, since investments in (proactive) adaptation are initiated much earlier than their first use, they are based on expectations and can result in inadequate solutions when damages start to occur. Reactive adaptation can marginally modify the solution to ensure maximum effectiveness. Adaptation effectiveness is modelled as follows:

$$\alpha_{\mathrm{AD}_p}(t) = (\overline{\alpha_{\mathrm{AD}_p}} - \underline{\alpha_{\mathrm{AD}_p}})\left(\gamma_1\frac{K_3(t)}{K_{3\max}(t)} + \gamma_2\frac{S_3(t)}{S_{3\max}(t)}\right) + \underline{\alpha_{\mathrm{AD}_p}} \quad (7)$$

$$\alpha_{\mathrm{AD}_r}(t) = (\overline{\alpha_{\mathrm{AD}_r}} - \underline{\alpha_{\mathrm{AD}_r}})\left(\gamma_1\frac{S_3(t)}{S_{3\max}(t)} + \gamma_2\frac{K_3(t)}{K_{3\max}(t)}\right) + \underline{\alpha_{\mathrm{AD}_r}} \quad (8)$$

where $\underline{\alpha_{\mathrm{AD}_p}}$ and $\overline{\alpha_{\mathrm{AD}_p}}$ (resp., $\underline{\alpha_{\mathrm{AD}_r}}$ and $\overline{\alpha_{\mathrm{AD}_r}}$) are the minimum and maximum effectiveness values for proactive (resp., reactive) adaptation, and γ_1, γ_2 calibration parameters

[2] We impose $K_3(t) \le K_{3\max}(t)$ and $S_3(t) \le S_{3\max}(t)$ at all time periods.

($\gamma_1 > \gamma_2$, $\gamma_1 + \gamma_2 = 1$). We model adaptation effectiveness such that: (i) the absence of one adaptation strategy does not make the other ineffective, but reduces its potential; and (ii) only maximum capital level ($K_3(t) = K_{3max}(t)$) and spending ($S_3(t) = S_{3max}(t)$) ensure maximum effectiveness. The online Supplemental material provides information on the calibration of all parameters concerning adaptation.

2.2.2. SRM measures and side-effects

SRM implementation is expected to be inexpensive and fast (Barrett, 2008). Following Moreno-Cruz and Keith (2013), we allow for linear SRM implementation costs (S_4) in the yearly amount of sulfur injected in the atmosphere (G):

$$S_4(t) = p_{GE}(t)G(t) \tag{9}$$

where p_{GE} is the cost of sulfur injection. Following Crutzen (2006), p_{GE} equals \$25 billion per Tg S annually.

Despite low implementation costs, SRM is believed to bring along important risks. We have presented in the introduction a comprehensive, but not exhaustive, list of expected side-effects, whose true magnitude and economic effects remain to be quantified (Robock et al., 2013). We model the magnitude of SRM side-effects (D_{GE}) following the approach of Goes et al. (2011), where sulfur injection damages depend on an intensity factor ($\alpha_{GE} \in [0, 1]$) and the radiative forcing created by SRM (F_{GE}), normalised by the radiative forcing for a doubling of atmospheric CO_2 concentrations (η). However, unlike previous IAMs that consider SRM side-effects (parameter α_{GE}) to be constant over time (Goes et al., 2011; Bickel and Agrawal, 2012), we model side-effects as a time-varying and persistent process. Modifying the radiative forcing through sulphate injection is expected to impact different Earth system processes, whose consequences will be felt for periods beyond the lifetime of sulphates in the stratosphere (Brovkin et al., 2009; Vaughan and Lenton, 2011). Therefore, we account for persistency in damages and allow the intensity factor (α_{GE}) to vary over time:

$$D_{GE}(t + \Delta t) = \lambda D_{GE}(t) + \alpha_{GE}(t + \Delta t)\frac{F_{GE}(t + \Delta t)}{\eta} AD_{GE}(t) \tag{10}$$

where λ (<1) is a constant depreciation rate,[3] α_{GE} a random process, F_{GE} the radiative forcing created through SRM, η the radiative forcing for a doubling of atmospheric CO_2 concentrations, and $AD_{GE} \in [0, 1]$ a parameter describing the effectiveness of adaptation to damages from sulfur injection. It could also be possible to reduce SRM side-effects through adaptation measures, in a similar manner to damages from temperature increase (see Eq. (4)). However, we are not aware of any literature investigating this issue, and the costs of reducing the highly uncertain SRM damages are still to be estimated. Given this, we do not allow for adaption to side-effects and set $AD_{GE}(t) = 1$, $\forall$ t. Thus, we disregard both benefits and costs of such adaptation. Instead, we focus on many possible values in the magnitude of SRM side-effects (α_{GE}); see below.

SRM is likely to impact a multitude of systems and generate complex feedback loops. Hence, we assume its short- and long-term disturbances to be unpredictable and to evolve in a possibly non-monotonic manner.[4] While some of the responses to stratospheric sulfur injection are believed to be fast (e.g., precipitation), others would come with longer time scales (e.g., oceanic responses) (MacMynowski et al., 2011a,b; Robock et al., 2013). We rely on a binomial tree representation in order to model the evolution of (monetary) side-effects over time ($\alpha_{GE}(t)$) and capture the uncertainty and variability in their size. The binomial representation assumes that at each moment of time, side-effects can either increase or decrease compared to the previous state, such that:

$$\alpha_{GE}(t) \begin{cases} \alpha_{GE}(t + \Delta t) = (1 + u)\,\alpha_{GE}(t) \\ \alpha_{GE}(t + \Delta t) = (1 - d)\,\alpha_{GE}(t) \end{cases}$$

with u and d respectively the percentage increase and decrease.

The parameter α_{GE} refers to percentage losses in total production (Y) due to side-effects from SRM, when the radiative forcing created through sulfur injections equals the radiative forcing for a doubling of atmospheric CO_2 concentrations ($F_{GE} = \eta$). To capture all possible (from highly optimistic to very pessimistic) side-effect scenarios, we allow parameter α_{GE} to take values between 0 and 100% of total production. We define three levels of side-effects: an initial level $\alpha_{GE}(2005)$, and two boundary values for the final time period (year 2155) defining a minimum ($\alpha_{GE} = 0$) and a maximum level ($\alpha_{\bar{GE}} = 1$). Similarly to Goes et al. (2011), we run different scenarios in which the initial size of side-effects ($\alpha_{GE}(2005)$) takes values in the range [0, 0.1].[5]

Parameter u is calibrated to link $\alpha_{GE}(2005)$ to $\alpha_{\bar{GE}}$ in a monotonically increasing path over 15 decades (until 2155): $\alpha_{\bar{GE}} = (1 + u)^{15}\,\alpha_{GE}(2005)$. Similarly, a monotonically decreasing path is obtained for $\alpha_{GE} = (1 - d)^{15}\,\alpha_{GE}(2005)$. Based on the binomial representation, for each initial $\alpha_{GE}(2005)$ we obtain 32,768 (= 2^{15}) different scenarios. Perfect foresight is assumed regarding each of the distinctive α_{GE} scenarios.

3. Optimal policy mix

3.1. Selected scenarios for SRM side-effects

This section analyses the optimal decisions regarding investments and spendings for production and climate measures, and the impact on temperature levels and atmospheric GHG stocks, when three different climate policy portfolios are available: (i) mitigation only; (ii) mitigation and adaptation; (iii) mitigation, adaptation, and SRM.

[3] Given the lack of evidence on the strength of the persistency of SRM side-effects, we run a sensitivity analysis for λ, with $\lambda \in \{0, 0.25, 0.5, 0.75, 1\}$.

[4] This time-varying representation of SRM side-effects is motivated by the view that ecosystems present dynamic and non-linear resilience to shocks and perturbations (Holling, 1973; Gunderson, 2003). Complex socio-ecological systems can have a highly optimised tolerance to a certain set of disturbances (Carlson and Doyle, 2002; Janssen et al., 2007), but they would suffer if the disturbances evolve or change outside of their optimised tolerance zone, causing them to move to new equilibria.

[5] Goes et al. (2011) consider constant $\alpha_{GE} \in \{0, 0.01, 0.02, 0.03, 0.05\}$.

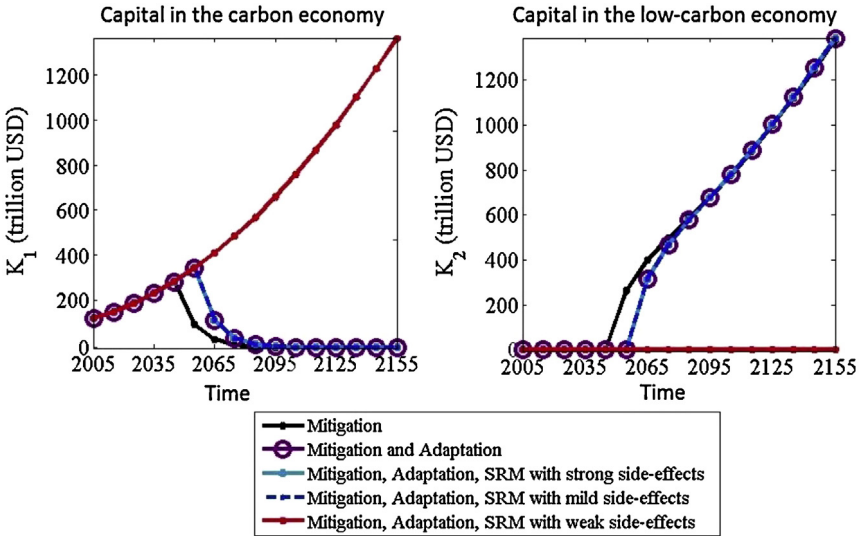

Fig. 1 – Capital accumulation in the two economies.

We consider three illustrative scenarios for SRM side-effects. Following Goes et al. (2011), we first choose a constant path for SRM side-effects ($\alpha_{GE}(t) = 0.015$, $\forall t$), entitled the *mild* scenario.[6] Additionally, we consider two cases where the side-effect paths are time-varying. In a *strong* damage scenario, α_{GE} increases monotonically from $\alpha_{GE}(2005) = 0.015$ to $\alpha_{GE}(2155) = \bar{\alpha_{GE}}$. It corresponds to the upper edge of the distribution (of all possible paths for side-effects starting at 0.015) when all forecasted impacts would be triggered and the total magnitude would be amplified by cross-interactions. In a *weak* damages scenario, α_{GE} decreases monotonically from $\alpha_{GE}(2005) = 0.015$ to $\alpha_{GE}(2155) = \underline{\alpha_{GE}}$. It corresponds to the lower edge of the distribution when SRM has only modest side-effects.

Addressing climate change requires mitigation, which corresponds in our model to a transition from the carbon economy to the low-carbon one. Fig. 1 illustrates the optimal capital accumulation in the two economies. In the 'mitigation only' portfolio, there is a clear transition between the two economies: the carbon-intensive capital is rapidly phased out after 2055 and completely replaced by the low-carbon capital before the end of the century. When adaptation is also available as a policy tool ('mitigation and adaptation' portfolio), this transition does take place, but starts one decade later. The SRM option has contrasted implications: under mild and strong side-effects, the transition takes place similarly to the 'mitigation and adaptation' portfolio, whereas the transition never occurs under weak side-effects. In line with Barrett (2008), our results indicate that there is no incentive to curb GHG emissions if SRM is available and its side-effects are benign.

Fig. 2 captures adaptation and SRM decisions. When its side-effects are weak, SRM is the main instrument to address climate change. It is used after 2045 (substituting for mitigation efforts), together with low proactive adaptation efforts (after 2095). When its side-effects are mild, SRM is only used (for two decades 2065–2085) as a complement to adaptation and mitigation strategies. SRM is not used when its side-effects are strong. Concerning adaptation, we note that: (i) the accumulation of proactive adaptation capital starts before spending on reactive adaptation; and (ii) the decreasing trend in adaptation towards the end of the horizon reflects the stabilisation of temperature (see Fig. 3) reached through SRM and/or mitigation. An interesting aspect is the relative dynamics of reactive adaptation and SRM, as they share the advantages of rapid implementation and immediate reduction of damages. The weight given to each strategy depends on the magnitude of SRM side-effects: (i) for strong side-effects, only adaptation is used; (ii) for mild and weak side-effects, both strategies enter the policy portfolio, with more weight given to SRM when its side-effects are lower. This results from the limited effectiveness of reactive adaptation.

Fig. 3 reveals that temperature is kept below the 2 °C threshold proposed by the Copenhagen Accord only when SRM side-effects are weak. This is achieved at the expense of: (i) a large deployment of SRM; and (ii) high GHG concentrations, due to the absence of mitigation. In the other scenarios, concentrations and then temperature decrease slowly with the transition to the low-carbon economy. When SRM side-effects are mild, the use of SRM for two decades (2065–2085) reduces the temperature deviation for this period below the 'mitigation only' portfolio; as SRM is stopped in 2085, the temperature level begins to increase and converges to the weak side-effects path, reflecting the accumulation of GHGs in the atmosphere. The use of adaptation (in the 'mitigation and adaptation', and 'mitigation, adaptation, and SRM with strong side-effects' portfolios) reduces the damages from climate change, postponing the transition to the clean economy and resulting in higher temperature increases than the 'mitigation only' portfolio.

Imposing the 2 °C limit yields an earlier implementation of mitigation and/or SRM. With strong side-effects, investments in mitigation are advanced by two decades (2035); with weak side-effects, SRM remains predominant and is implemented from 2035 on. To reduce climate change damages, adaptation is still used with a similar timing (compared to the unconstrained temperature cases) but requires less funding.

[6] This level has been chosen such that SRM is optimally employed in at least one decade over the horizon 2005–2155.

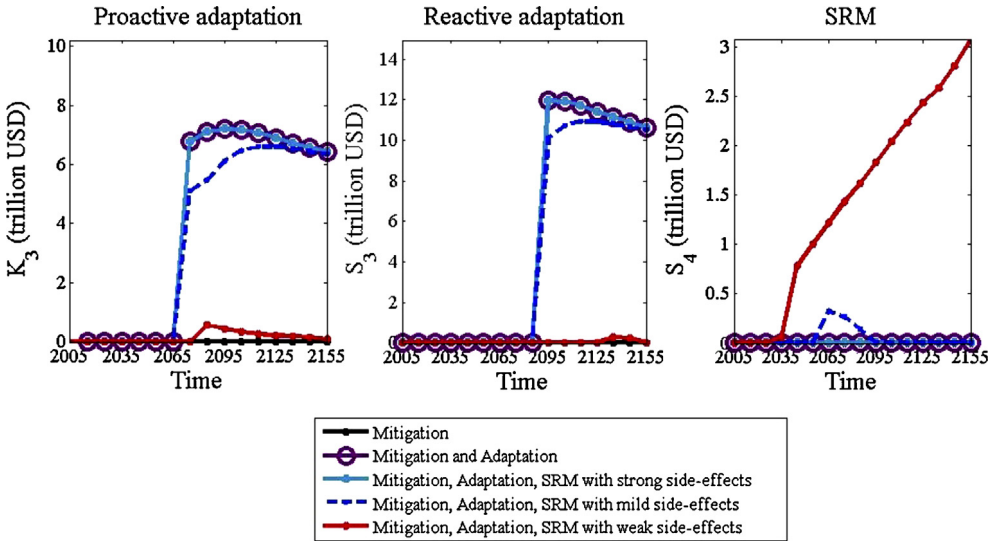

Fig. 2 – Capital accumulation in proactive adaptation, and decade spending with reactive adaptation and SRM.

3.2. *Distributional analysis for SRM side-effects*

In this section, we consider the 'mitigation, adaptation, and SRM' portfolio and extend the previous analysis in two directions. One the one hand, we consider different initial SRM side-effect levels ($\alpha_{GE}(2005)$). On the other hand, for each of these initial levels, we analyse 32,768 paths describing the evolution of side-effects over time based on the binomial representation; see Section 2.2.2.

We analyse first the frequency with which the different climate policies are used. The frequency indicator is computed as the number of scenarios in which the policy is employed in at least one decade over the 2005–2155 horizon, divided by the total number of scenarios corresponding to each $\alpha_{GE}(2005)$. However, this indicator is not evaluating the probability associated with the different α_{GE} paths.

Fig. 4 illustrates first that the optimal policy mix depends on the initial value of SRM damages. The use of SRM is strongly dependent on its initial side-effects, such that this strategy is implemented in at least one decade in almost 100% of the scenarios when $\alpha_{GE}(2005)$ is 0.1%, declining abruptly for larger values, to the point that SRM is employed in about 11% of the scenarios when $\alpha_{GE}(2005)$ is 10%. Despite the availability of the inexpensive SRM option, mitigation and adaptation strategies are an important part of the optimal climate policy portfolio. Proactive and reactive adaptation strategies are employed in all scenarios, independent of the SRM side-effects. The use of mitigation increases from about 80% when initial side-effects are low, to 93% of the scenarios when $\alpha_{GE}(2005) = 0.1$.

Another parameter that strongly influences the use of SRM is the persistency of its side-effects over time (parameter λ). Fig. 4 illustrates also that for moderate initial SRM damages ($\alpha_{GE}(2005) = 0.03$), this strategy is used mostly as a complement to mitigation and adaptation even when its side-effects are active only during the implementation period ($\lambda = 0$). The frequency of SRM use decreases sharply for higher persistency

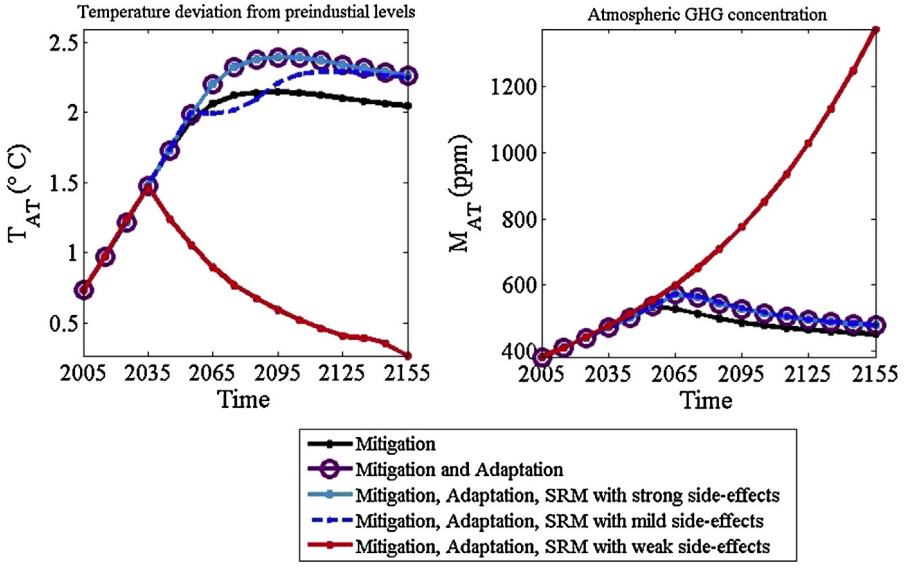

Fig. 3 – Atmospheric temperature and GHG concentrations.

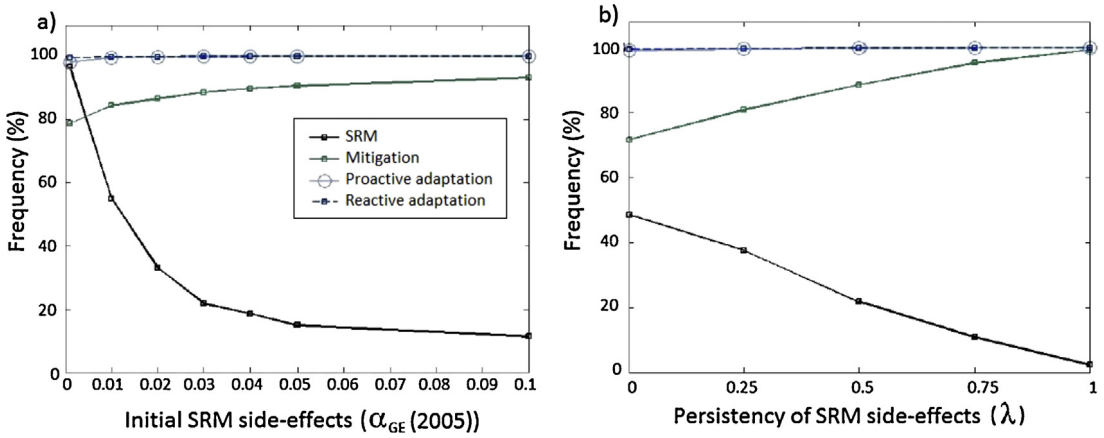

Fig. 4 – Policy frequency for different α_{GE}(2005) (at λ = 0.5) and λ (at α_{GE}(2005) = 0.03).

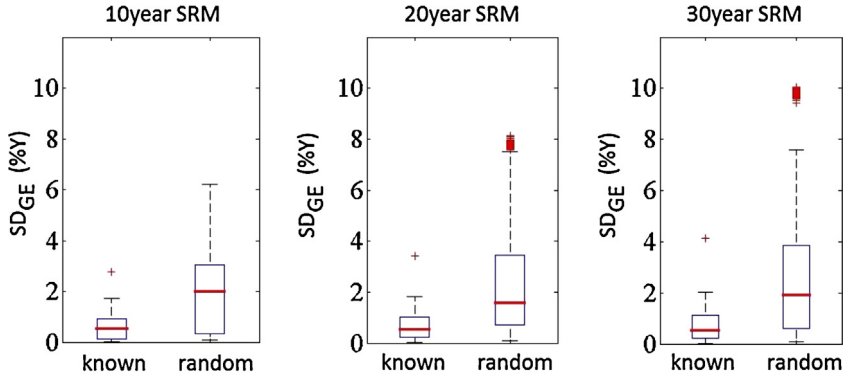

Fig. 5 – Distribution of output losses under known and random SRM damages for different error horizons ($SD_{GE} = \sum_{t_{GE}}^{t_{GE}+h\Delta t} D_{GE}(t)$, α_{GE}(2005) = 0.03, λ = 0.5).

levels. Moreover, in these cases, SRM is only implemented at the end of the decision horizon; see the online Supplemental material.

Due to the uncertainty in the size of initial side-effects and in their persistency over time, the variability in SRM use is very large. Thus, SRM does not seem to be a robust climate policy. Even with low initial side-effects, SRM mostly plays the role of a complement to adaptation and mitigation, and rarely a substitute.

4. Unexpected SRM side-effects

The previous section indicates that SRM should be used when its side-effects are low and their persistency is limited. Here, we discuss possible economic impacts of making wrong assumptions about SRM side-effects and analyse the resulting adjustments in the optimal policy mix. Other important concerns raised in previous literature (Orr et al., 2005; Robock et al., 2009; Goes et al., 2011), such as (i) the failure to continue with SRM and (ii) high GHG concentrations, are discussed in the online Supplemental material.

Up to now, the optimal policy mix was evaluated under perfect foresight, assuming that the side-effects were known along each scenario. Here, we study the consequences of incurring a different (random) side-effect path than the one presumed. First, we compute following Eq. (10) the *presumed* SRM damages ($D_{GE}(t, s)$) that translate into output losses, where s is given by each SRM side-effects path from the binomial representation. Next, we compute *unexpected* output losses ($D_{GE}(t, s')$) that would arise if a different side-effect path s' occurs. More precisely, we replace in Eq. (10) $\alpha_{GE}(t)$ by a factor chosen randomly from the possible side-effect paths, while keeping the same levels for sulfur injection. Holding wrong assumptions regarding the side-effects should only last for short periods. Indeed, although the earth system presents some inertia, the magnitude of side-effects is ex-post observable via decreases in production. However, it might take several decades until true realisations are identified.

As an illustration, we consider an error horizon of one to three decades and compare output losses[7] under known (presumed) and random (unexpected) side-effect paths. Fig. 5 reveals that output losses double on average when the side-effect path is different than the one expected, even for a

[7] For each scenario $s \in [1, 32, 768]$, we compute the sum of presumed damages as: $SD_{GE} = \sum_{t=t_{GE}}^{t_{GE}+h\Delta t} D_{GE}(t, s)$, where t_{GE} is the first period of SRM implementation in scenario s, and $h \in \{1, b, 3\}$ are decades of SRM implementation. Unexpected damages are computed as: $\frac{1}{5000}\sum_{i=1}^{5000}\sum_{t=t_{GE}}^{t_{GE}+h\Delta t} D_{GE}(t, s'_i)$, where $\alpha_{SE}(t, s'_i)$ is randomly selected from the initial side-effect distribution over 5000 simulations.

ten-year horizon. With a twenty to thirty-year horizon, the variance and right skewness of output losses increases further on average, indicating that extreme losses have a high chance of occurrence. The output loss is higher in the case of larger initial SRM side-effects, showing that when SRM implementation is optimal in only few of the possible α_{GE} paths, misestimating the damages can be very punitive; see also the online Supplemental material.

Next, we study the adjustments to the optimal policy mix after observing the true damages. As an example, we examine the (extreme) case where side-effects were assumed to be weak, but turn out to be strong. With (presumed) weak side-effects, SRM is first implemented in 2065 at the expense of any mitigation efforts. But suppose that after three decades the policy maker realises that side-effects are actually strong. We simulate this situation by running the model from 2065 on with the true α_{GE} values, keeping all investment and spending decisions blocked for the error horizon (2065–2085). The policy maker reacts by stopping all SRM activities from 2095 on. A quick transition to the low-carbon economy takes place, but cannot prevent a temperature increase to almost 3 °C. To alleviate some of the climate damages, adaptation (especially reactive) is extensively used; see also the online Supplemental material. Overall, deviating during the error horizon from the optimal policy in case of strong side-effects results in lower consumption levels for the remaining horizon.

5. Conclusions

This paper extends the Ada-BaHaMa model with an explicit representation of reactive adaptation and geoengineering (SRM). Reactive adaptation is modelled as a flow, and allows for its benefits to be internalized once with its costs, representing a climate policy that may avoid problems with discounting preferences. SRM is a potential alternative to traditional climate strategies, and we distinguish between its (desired) effects on temperature levels and its (undesired and uncertain) side-effects on the environment. To the best of our knowledge, this is the first paper to assess, within an integrated assessment framework, the optimal policy mix when mitigation, proactive and reactive adaptation, and SRM strategies are available. We focus on the possible interactions and substitutions between these different policies, while accounting for the possible variability and persistency in the side-effects of SRM.

Our analysis reveals that the climate portfolio should give primary weight to mitigation and adaptation. With large predominance, SRM is a complement to mitigation and adaptation, and rarely a substitute, revealing that SRM will not provide an easy way out of the climate problem. The use of SRM is strongly dependent on the magnitude of its side-effects and their persistency through time. Due to uncertainty in these two features, the variability in SRM use is very large, leading us to conclude that the SRM option lacks robustness.

An extensive use of SRM brings additional concerns. We investigate possible welfare losses due to incorrect assumptions about SRM side-effects. Our analysis shows that output losses rise considerably when side-effects are different than presumed, even for short error horizons. Besides, longer horizons are more costly, with extreme losses having a higher chance of occurrence. Accounting for such concerns reduces the use of SRM.

In our cost–benefit approach, despite the predominant role of mitigation, we note that investments in the low-carbon economy start after 2055 at the earliest. However, when following a cost-effectiveness approach to limit temperature increase to 2 °C, climate policies are implemented 20 years earlier. Meeting the agreed 2 °C temperature target would thus require earlier actions.

Our analysis could be improved along the following lines. First, being derived in a cost-benefit framework, our results (and in particular the timing of mitigation) critically depend on the magnitude of the estimated climate change damages, calibrated in our model on DICE and AD-DICE. Recent papers (Stern, 2013; Pindyck, 2013) signal possible underestimations of such damages in the DICE-like integrated assessment models; further research could help address these issues. Besides, one could perform additional sensitivity analysis on climate parameters, especially the climate sensitivity. Second, the deployment of SRM depends on various unknowns, such as the type and magnitude of side-effects, and the process governing their variability through time. The calibration of all involved parameters in our model will benefit from revisions reflecting scientific advances. Third, our model assumes exogenous technological progress. With an endogenous formulation, one might expect that (R&D) investments in low-carbon technologies start earlier to get on-time the needed technologies for mitigation. Finally, our model assumes the existence of a well-functioning international cooperation for undertaking mitigation and SRM at a global level. Future research could improve our understanding of the two policies by accounting for differentiated geographical impacts and investigating strategic country behaviour.

Appendix A. Supplementary data

Supplementary data associated with this article can be found, in the online version, at http://dx.doi.org/10.1016/j.envsci.2014.12.014.

REFERENCES

Adams, J., Mann, M., Ammann, C., 2003. Proxy evidence for an El Niño-like response to volcanic forcing. Nature 426, 274–278.

Agrawala, S., Bosello, F., et al., 2011. Plan or react? Analysis of adaptation costs and benefits using integrated assessment models. Clim. Change Econ. 2, 175–208.

Bahn, O., Chesney, M., Gheyssens, J., 2012. The effect of proactive adaptation on green investment. Environ. Sci. Policy 18, 9–24.

Bala, G., Duffy, P.B., Taylor, K.E., 2008. Impact of geoengineering schemes on the global hydrological cycle. Proc. Natl. Acad. Sci. U. S. A. 105 (22), 7664–7669.

Ban-Weiss, G.A., Caldeira, K., 2010. Geoengineering as an optimization problem. Environ. Res. Lett. 5 .

Barrett, S., 2008. The incredible economics of geoengineering. Environ. Resour. Econ. 39, 45–54.

Barrett, S., Lenton, T.M., et al., 2014. Climate engineering reconsidered. Nat. Clim. Change 4, 527–529.
Bickel, J., 2013. Climate engineering and climate tipping-point scenarios. Environ. Syst. Decis. 33, 152–167, http://dx.doi.org/10.1007/s10669-013-9435-8.
Bickel, J., Agrawal, S., 2012. Reexamining the economics of aerosol geoengineering. Clim. Change 119, 993–1006.
Bosello, F., Carraro, C., De Cian, E., 2010. Climate policy and the optimal balance between mitigation, adaptation and unavoided damage. Clim. Change Econ. 1, 71–92.
Brasseur, G.P., Roeckner, E., 2005. Impact of improved air quality on the future evolution of climate. Geophys. Res. Lett. 32, L23704, http://dx.doi.org/10.1029/2005GL023902.
Brovkin, V., Petoukhov, V., et al., 2009. Geoengineering climate by stratospheric sulfur injections: Earth system vulnerability to technological failure. Clim. Change 92, 243–259.
de Bruin, K., 2011. Distinguishing between proactive (stock) and reactive (flow) adaptation. Working Paper 8 CERE. Umea, Sweden. .
Caldeira, K., Bala, G., Cao, L., 2013. The science of geoengineering. Annu. Rev. Earth Planet. Sci. 41 (1), 231–256.
Carlin, A., 2007. Global climate change control: is there a better strategy than reducing green house gas emissions? Univ. PA Law Rev. 155, 128–156.
Carlson, J.M., Doyle, J., 2002. Complexity and robustness. Proc. Natl. Acad. Sci. U. S. A. 99, 2538–2545.
Crutzen, P., 2006. Albedo enhancement by stratospheric sulfur injections: a contribution to resolve a policy dilemma? Clim. Change 77, 211–219.
Doney, S.C., Fabry, V.J., Feely, R.A., Kleypas, J.A., 2009. Ocean acidification: the other CO_2 problem. Annu. Rev. Mar. Sci. 1, 169–192.
English, J., Toon, O., Mills, M., 2012. Microphysical simulations of sulfur burdens from stratospheric sulfur geoengineering. Atmos. Chem. Phys. 12, 4775–4793.
Goes, M., Tuana, N., Keller, K., 2011. The economics (or lack thereof) of aerosol geoengineering. Clim. Change 109, 719–744.
Gunderson, L.H., 2003. Adaptive Dancing: Interactions Between Social Resilience and Ecological Crises. Navigating Socialecological Systems: Building Resilience for Complexity and Change. Cambridge University Press, Cambridge, UK33–52.
Holling, C.S., 1973. Resilience and stability of ecological systems. Annu. Rev. Ecol. Syst. 4, 1–23.
Huneeus, N., Boucher, O., et al., 2014. Forcings and feedbacks in the GeoMIP ensemble for a reduction in solar irradiance and increase in CO_2. J. Geophys. Res. Atmos. 119 (9), 5226–5239.
Janssen, M.A., Anderies, J.M., Ostrom, E., 2007. Robustness of social–ecological systems to spatial and temporal variability. Soc. Nat. Resour. 20, 307–322.
Jones, A., Haywood, J., et al., 2013. The impact of abrupt suspension of solar radiation management (termination effect) in experiment G2 of the Geoengineering Model Intercomparison Project (GeoMIP). J. Geophys. Res. 118, 9743–9752.
Keith, D., 2000. Geoengineering the climate: history and prospect. Annu. Rev. Energy Environ. 25, 245–284.
Keller, K., Robinson, A., Oppenheimer, D.B.M., 2007. The regrets of procrastination in climate policy. Environ. Res. Lett. 2.
Kravitz, B., Rasch, P., et al., 2013. An energetic perspective on hydrological cycle changes in the Geoengineering Model Intercomparison Project. J. Geophys. Res. 118 (23), 13087–13102.
Kravitz, B., Robock, A., Oman, L., Stenchikov, G., Marquardt, A., 2009. Sulfuric acid deposition from stratospheric geoengineering with sulfate aerosols. J. Geophys. Res. 114 (D14) .
MacMynowski, D., Keith, D., Caldeira, K., Shin, H., 2011a. Can we test geoengineering? R. Soc. J. Energy Environ. Sci. 4 (12), 5044–5052.
MacMynowski, D., Shin, H., Caldeira, K., 2011b. The frequency response of temperature and precipitation in a climate model. Geophys. Res. Lett. 38 (L16711) .
Macnaghten, P., Szerszynski, B., 2013. Living the global social experiment: an analysis of public discourse on solar radiation management and its implications for governance. Global Environ. Change 23 (2), 465–474.
Manne, A., Richels, R., 2005. MERGE: an integrated assessment model for global climate change. In: Loulou, R., Waaub, J.P., Zaccour, G. (Eds.), Energy and Environment. GERAD 25th Anniversary Series, vol. 3. Springer, pp. 175–189.
Millard-Ball, A., 2012. The Tuvalu syndrome. Can geoengineering solve the climate's collective action problem? Clim. Change 110, 1047–1066.
Moreno-Cruz, J.B., Keith, D.W., 2013. Climate policy under uncertainty: a case for solar geoengineering. Clim. Change 121, 431–444.
Niemeier, U., Schmidt, H., Alterskjr, K., Kristjnsson, J., 2013. Solar irradiance reduction via climate engineering: impact of different techniques on the energy balance and the hydrological cycle. J. Geophys. Res. 118 (21), 11905–11917.
Nordhaus, W., 2008. A Question of Balance. Yale University Press.
Orr, J.C., Fabry, V.J., et al., 2005. Anthropogenic ocean acidification over the twenty-first century and its impact on calcifying organisms. Nature 437, 681–686.
Pindyck, R.S., 2013. Climate change policy: what do the models tell us? Working Paper 19244 NBER. .
Rasch, P., Tilmes, S., et al., 2008. An overview of geoengineering of climate using stratospheric sulphate aerosols. Philos. Trans. R. Soc. 366, 4007–4037.
Robock, A., MacMartin, D., Duren, R., Christensen, M., 2013. Studying geoengineering with natural and anthropogenic analogs. Clim. Change 121, 445–458.
Robock, A., Marquardt, A., Kravitz, B., Stenchikov, G., 2009. Benefits, risks, and costs of stratospheric geoengineering. Geophys. Res. Lett. 36, L19703, http://dx.doi.org/10.1029/2009GL039209.
Robock, A., Oman, L., Stenchikov, G., 2008. Regional climate responses to geoengineering with tropical and Arctic SO_2 injections. J. Geophys. Res. 113.
Schaller, N., Cermak, J., Wild, M., Knutti, R., 2013. The sensitivity of the modeled energy budget and hydrological cycle to CO_2 and solar forcing. Earth Syst. Dyn. 4, http://dx.doi.org/10.5194/esd-4-253-2013.
Shepherd, J., Caldeira, K., et al., 2009. Geoengineering the Climate. Science, Governance and Uncertainty. Technical Report. The Royal Society.
Solomon, S., Plattnera, G.K., Knutti, R., Friedlingstein, P., 2009. Irreversible climate change due to carbon dioxide emissions. Proc. Natl. Acad. Sci. U. S. A. 106, 1704–1709.
Stanhill, G., Cohen, S., 2001. Global dimming: a review of the evidence for a widespread and significant reduction in global radiation with discussion of its probable causes and possible agricultural consequences. Agric. For. Meteorol. 107, 255–278.
Stenchikov, G., Kirchner, I., et al., 1998. Radiative forcing from the 1991 Mount Pinatubo volcanic eruption. J. Geophys. Res. 103, 13837–13857.
Stern, N., 2006. The Economics of Climate Change: The Stern Review. Cambridge University Press, Cambridge, UK.
Stern, N., 2013. The structure of economic modeling of the potential impacts of climate change: grafting gross

underestimation of risk onto already narrow science models. J. Econ. Lit. 51 (3), 838–859.
Tilmes, S., Mueller, R., Salawitch, R., 2008. The sensitivity of polar ozone depletion to proposed geoengineering schemes. Science 320, 1201–1204.
Tol, R., 2005. Adaptation and mitigation: trade-offs in substance and methods. Environ. Sci. Policy 8, 572–578.
Trenberth, K., Dai, A., 2007. Effects of Mount Pinatubo volcanic eruption on the hydrological cycle as an analog of geoengineering. Geophys. Res. Lett. 34 .
Vaughan, N., Lenton, T., 2011. A review of climate geoengineering proposals. Clim. Change 109, 745–790.
Victor, D.G., 2008. On the regulation of geoengineering. Oxf. Rev. Econ. Policy 24, 322–336.
Wigley, T., 2006. A combined mitigation/geoengineering approach to climate stabilization. Science 314, 452–454.
Wright, M.J., Teagle, D.H., Feetham, P.M., 2014. A quantitative evaluation of the public response to climate engineering. Nat. Clim. Change 4 (2), 106–110.

B Published manuscript, Journal of Environmental Economics and Policy, 2015: Baseline choice and performance implications for REDD

Journal of Environmental Economics and Policy, 2015
http://dx.doi.org/10.1080/21606544.2015.1028465

Baseline choice and performance implications for REDD

Anca Claudia Pana[a]* and Jonathan Gheyssens[b]

[a]*Institute for Banking and Finance, University of Zurich, Plattenstrasse 32, 8032 Zurich, Switzerland;* [b]*REDD+ Finance and Sustainable Land Use, UNEP Finance Initiative, International Environment House, 11-15 Chemin des Anmones, CH-1219 Chtelaine, Geneva, Switzerland*

(*Received 8 May 2014; accepted 9 March 2015*)

Reducing Emissions from Deforestation and forest Degradation (REDD) projects are being designed and implemented across tropical countries, intending to curb the contribution of deforestation to greenhouse gas emissions. An important aspect of REDD implementation is the *baseline* against which reductions are measured. The baseline estimates the business-as-usual emissions from deforestation and forest degradation. We solve a dynamic model of land conversion from forest to agriculture in the presence of REDD, and assess the performance of four baselines. We show that none of the analysed baselines dominates in all performance aspects, and that the final baseline choice needs to maximise the trade-off between the effectiveness to reduce deforestation, cost-efficiency, and changes in income. The frequently used historical average baseline could be improved by using a forward-looking one, which is shown to better account for the opportunity costs faced by landowners. This result hinges on the ability of the baseline to predict deforestation rates without significant underestimations. We advocate the switch from a single-threshold baseline to a corridor methodology, which would provide continued incentives to reduce deforestation, even during periods of high opportunity costs. We finally show how the selection of certain baseline attributes, such as corridor bandwidth and symmetry, can enhance performance.

Keywords: deforestation; REDD; baselines; effectiveness and efficiency

1. Introduction

Emissions from deforestation and forest degradation rank as the second largest source of carbon dioxide in the atmosphere after fossil fuel combustion, contributing about 12% of global anthropogenic emissions (van der Werf et al. 2009). Programmes targeting the Reduction of Emissions from Deforestation and forest Degradation (REDD and REDD+)[1] have emerged as potential instruments for stabilising atmospheric CO_2 concentrations and mitigating climate change.

REDD programmes target forest preservation in tropical areas, where deforestation is the largest contributor to total greenhouse gas (GHG) emissions (van der Werf et al. 2009). Here, the major drivers of deforestation have often been identified as timbering, land conversion to agriculture, cattle ranching, and the establishment of new settlements (Pfaff et al. 2013). Restricting deforestation would limit the development of such land-use activities and alter the revenue flow of landowners. To compensate for the foregone income from deforestation, REDD schemes offer financial rewards for forest conservation.

*Corresponding author. Email: anca.pana@bf.uzh.ch

REDD programmes aim to achieve *additionality*, i.e. payments are intended to reward reductions in emissions from deforestation below business-as-usual (BaU) levels. However, the counterfactual deforestation rates and the corresponding emissions, which would occur in the absence of the policy, are not observable and, therefore, highly challenging to assess. Thus, REDD payments are linked to reductions below estimations of the BaU levels, called *baselines* or *reference levels*.

The reward system of REDD can be financed through the creation of special funds or be designed as a market mechanism (Palmer 2010; Corbera and Schroeder 2011). In the second case, reducing emissions from deforestation below a reference level generates credits eligible for sale on various carbon markets. International emitters[2] that are above their compliance level and short of CO_2 permits might find reducing emissions internally to be expensive (Diaz et al. 2011) and could benefit from the comparative affordability of REDD permits (Kindermann et al. 2008; Stern 2008). Despite this economic advantage, REDD projects remain complex to implement and prone to failure. Various aspects appear problematic: the measurement of reductions in emissions below BaU levels; raising sufficient funds for implementation or establishing a link with (immature) carbon markets; the risk that forest loss will be postponed in time (lack of permanence) or transferred to unregulated areas (leakage); and the existence of clear property rights that would rule out false permit claims from encroachers (Angelsen 2008a).

The success of REDD is critically sensitive to the incentive structure promoted by the schemes (Griscom et al. 2009; Cattaneo et al. 2010; Busch et al. 2012). A central aspect is the establishment of the baseline against which reductions in emissions from deforestation are measured and financial rewards are granted. However, setting the baseline is not a straightforward task. First of all, to encourage participation and ensure significant reductions in GHG emissions, the baseline design would need to ensure that REDD rewards cover the various opportunity costs of deforestation (Irawan et al. 2013). At the same time, the selected baseline should achieve emission reductions in a cost-efficient manner, avoiding that payments greatly exceed opportunity costs and result in windfall profits for landowners (Busch et al. 2012), instead of being used for reducing deforestation elsewhere. As well, flooding the carbon markets with REDD credits in large supply would drive the CO_2 permit price down and possibly reduce the effectiveness of the carbon markets (Doupé 2014).

Several organisations have emerged with the goal of assisting countries in participating successfully in REDD programmes, by offering technical, legal, and financial support. Among them, notable actors are the Forest Carbon Partnership Facility, the Amazon Fund, the UN-REDD programme, Norway's International Climate and Forest Initiative (NICFI), and the German REDD Early Movers Program. So far, the existing REDD initiatives supported by these organisations have endorsed the decision of the UNFCCC to compute reference levels based on past deforestation rates, adjusted to account for country circumstances[3] (UNFCCC 2009, Decision 4/CP.15). The decision to opt for historical reference levels is motivated by the desire to ensure transparency and credibility (The German REDD Early Movers Program 2014). In order to account for national circumstances, historical averages can be adjusted upwards for countries with historically low deforestation rates and high remaining forest areas; downward adjustments are allowed for countries with clear decreasing trends in deforestation (FCPF Carbon Fund 2013).

Despite its recognised advantages, the historical baseline lacks the ability to reflect future drivers of deforestation. Moreover, provided as an average, it neglects the variability observed in deforestation rates, coming from fluctuating economic conditions. The historical baseline might, therefore, fail to account properly for the true opportunity costs

that landowners face. Trying to address these issues, several baseline methodologies have been proposed; for an overview, see Huettner et al. (2009) and Griscom et al. (2009). Our paper attempts to provide further insights into how to choose the most robust and effective baseline methodology.

This paper joins the literature dedicated to the optimal contract design of REDD schemes (Huettner et al. 2009; Busch et al. 2009, 2011; Sathaye et al. 2011). We compare the impacts of four different baselines on REDD success. We focus on two of the most popular baseline categories: a retrospective baseline reflecting the historical average deforestation and a model-implied prospective baseline that proxies the BaU deforestation path in the absence of the REDD programme. We also analyse the so-called *fixed-corridor* approach, which replaces the historical threshold with a lower and an upper bound below and above the historical deforestation average (Schlamadinger et al. 2005). Additionally, we propose a new baseline type, the variable-corridor approach, which aims to gather the strong points of the model-implied and the corridor baselines.

Our analysis proceeds as follows. First, we show how to model land-use decisions in the presence of REDD in a dynamic setting. Second, we rank baselines according to different performance indicators: (1) a measure of forest preservation (effectiveness), (2) an indicator of the cost of this preservation per hectare (efficiency), and (3) a measure of changes in the total income of the landowner (change in welfare). In particular, we check what are the losses in effectiveness when the BaU deforestation path is estimated with error, impacting the REDD payments. The economic analysis is further put into perspective through a qualitative evaluation, accounting for environmental, technical, and social concerns with REDD. Finally, the paper explores different possibilities to improve the performance of the corridor baselines, by varying corridor width and symmetry.

Previous research on REDD design overlooked the inter-temporality dimension in forest decisions (Huettner et al. 2009; Busch et al. 2009, 2011). Huettner et al. (2009) ran a survey to qualitatively compare three types of retrospective baselines, based on the historical deforestation rate, with a forward-looking baseline. We extend the types of baselines analysed beyond those considered in Huettner et al. (2009) and focus on the economic incentives generated by each baseline. Busch et al. (2009) approach the ranking of different baselines via a one-period partial equilibrium model at the country level. They show that an effective national baseline simultaneously provides incentives to reduce deforestation in areas of high rates and ensures the continuation with low deforestation practices in areas of low previous forest loss. Busch et al. (2011) extend this approach by introducing different levels of annual REDD financing, either through funds or through access to a dedicated market. They highlight the importance of designing baselines that minimise leakage to unregulated areas and are generous enough to guarantee the participation of both countries with high or low deforestation rates. Cattaneo et al. (2010) use a static partial equilibrium model to compare five different baseline designs from an equity perspective. They show that the crediting schemes considered obtain similar reductions in deforestation, but differ greatly in terms of cost-efficiency and two measures of equity.

The highly dynamic nature of land-use practices has been studied in numerous papers and benefits from a large variety of models; for a review, see Verburg et al. (2004). However, only a few papers deal explicitly with dynamic land-use change in the presence of REDD (Ollivier 2012; Lu and Liu 2013; Vitel et al. 2013; Mosnier et al. 2014), and none of them tests for different baseline methodologies. We attempt to fill this gap by analysing our selected baselines with a dynamic land-use model. The dynamic model helps us illustrate the optimal deforestation decisions at several points in time, and show how landowners choose to take part in REDD depending on the time-varying opportunity costs for

deforestation. Anticipating our results, with the help of the dynamic approach we are able to demonstrate that some baseline methodologies offer continued incentives to keep deforestation below BaU levels, while others achieve only temporary effectiveness. This finding is key to understanding how we could potentially solve non-permanence issues with REDD and can only be grasped in a dynamic setting.

Another important decision concerning REDD implementation is the choice of the administrative level at which emission reductions are calculated and payments are made. While the accounting of emission reductions and the management of REDD payments is most likely to take place at the national level, land-use decisions are usually taken at the subnational (regional or household) level. This reinforces the need to understand the incentives received by the local landowners (Angelsen 2010; Busch et al. 2012). Our model describes the decisions of a single landowner who optimises over the rate of deforestation as he or she expands agriculture activities. The single-agent approach is in line with the literature on optimal forest extraction (Angelsen 2007) and with a new literature trend arguing that REDD will face the same issues as traditional integrated conservation and development projects, since it will have to account for incentives at the community and individual levels (Blom et al. 2010). It is not intended to suggest that the complexity of implementing REDD projects can be summarised into a single-player model; nonetheless, we believe that our approach is relevant for highlighting the behavioural changes at the micro level, which can then be used to inform national or jurisdictional policy decisions.

The choice of the administrative level for REDD is expected to impact the effectiveness in reducing deforestation. Implementing REDD at the site level, and then aggregating results at a larger (national) scale, may give way to leakage of deforestation to other areas (Busch et al. 2012), and raises questions regarding the organisation of carbon payments at the local level.[4] However, the estimation of reference levels is more likely to reflect the BaU deforestation path if set at the household level, since jurisdictions at lower scales may have better information regarding the specific drivers of deforestation in the area (Busch et al. 2012). Potential policies for avoiding leakage include (1) the monitoring of deforestation rates at the national level and (2) the setting of penalties for deforestation rates that exceed the estimated BaU level, coming from beneficiaries of REDD payments elsewhere. In this paper, we adopt the view that REDD should focus on providing incentives for reduced deforestation at the local level, while ensuring national monitoring.

Our analysis reaches several conclusions that we hold relevant for the design of forest carbon policies. First, solving for the optimal deforestation rate under a REDD regime, we show that the baseline choice impacts REDD performance at multiple economic, social, and environmental levels. None of the considered baselines can fulfil all REDD criteria simultaneously, and the baseline choice needs to maximise the trade-off between the different goals. We argue that the widespread current practice of rewarding emissions below the historical deforestation average could be improved by implementing a forward-looking baseline that would better account for the opportunity costs faced by landowners and would result in higher emission reductions. This result depends, however, on the ability of the forward-looking baseline to predict future deforestation rates without substantial underestimations. Finally, we advocate the switch from a single-threshold baseline approach to a corridor methodology; this reduces losses from estimation errors and provides continued incentives for reduced deforestation, even during periods of high opportunity costs.

The rest of the paper is organised as follows. Section 2 introduces our methodology and the main assumptions of the dynamic model. In Section 3, a numerical application is performed and the robustness of our results is tested. Section 4 concludes on the policy implications of our results and the link with broader issues of REDD implementation.

2. Methodology

2.1. Model setting

In our model, the owner of a large area of forested land decides if, when, and to what extent to exploit the forest for agricultural activities. To limit his or her deforestation, the owner is offered the possibility to take part in a REDD programme that grants carbon permits each time the deforestation rate is below a pre-specified threshold. We model the voluntary participation in REDD along the approach of Busch et al. (2009, 2011), where the owner can 'opt in' as long as he or she considers this to his or her advantage.[5] In our model, reforestation options are not accounted for; this assumes that costs for switching back from cropland to forest (together with the forgone discounted cash flows from agriculture) are large enough to render the reforestation option unattractive.

The landowner's revenues are a trade-off between the net income from land exploitation and REDD rewards. The more the owner deforests, the higher the incomes from selling timber and subsequently using land for agricultural activities, and the lower the number of received REDD permits. Alternatively, lower deforestation (below the defined baseline level) results in smaller incomes from agriculture and timbering, but higher REDD revenues. We choose an approach similar to Busch et al. (2009), where the owner's revenues from land exploitation are modelled as a unique composite commodity, representing both the harvesting value of timber and a perpetual discounted flow of agricultural activities on the land.[6]

The owner maximises the sum of total discounted profits, taking into account the parameters that define the decision environment: the state of the forest, the dynamics of composite commodity and REDD permit prices, and the specified deforestation baseline. In our model, the prices of the composite commodity ($P^{cc}(t)$) and of the REDD permit ($P^{R}(t)$) are exogenous and follow deterministic dynamics[7]:

$$dP^{cc}(t) = \delta P^{cc}(t)dt \tag{1}$$

$$dP^{R}(t) = \gamma P^{R}(t)dt \tag{2}$$

where δ and γ represent the respective growth rates of the two price processes. Being a composite price, $P^{cc}(t)$ is a simplification of the actual commodity flow generated from harvesting one hectare of forest and using the area for perpetual agricultural activities, which could be modelled as follows:

$$P^{cc}(t) = P_h(t) + \int_t^{\infty} A(t)e^{-\psi t}dt \tag{3}$$

where $P_h(t)$ represents the one-time timber harvest selling price, while $A(t)$ are the annual monetary flows from agricultural activities after land conversion. Land exploitation involves various operational costs that we model with the help of a quadratic function:

$$C(t) = a_1 d(t) + a_2 d(t)^2 \tag{4}$$

where $d(t)$ is the amount of forest converted to agriculture at time t. We assume the parameters of the cost function (a_1, a_2) to be constant. This stylised representation is in line with the classical approach of von Thünen (1826): when land is abundant and homogeneous, the agriculture expansion frontier depends on the cost of accessing new forest patches, which are farther away from the initial location and thus costlier to exploit (Angelsen 1999).

The offsetting scheme proposed by REDD imposes no liability: the owner is rewarded if the deforestation is below a certain reference level, but does not have to pay penalties in case this limit is exceeded (Griscom et al. 2009; Huettner et al. 2009; Joanneum Research Institute 2006). The owner's revenues from REDD ($RR(t)$) can be described by a step function:

$$RR(t) = P^R(t)(dB - d(t))^+ \tag{5}$$

where $P^R(t)$ is the REDD permit price at time t, dB the baseline level, and $d(t)$ the actual deforestation at t. REDD cash flows are zero for deforestation rates above the baseline, i.e. $(dB - d(t))^+ = 0$ if $d(t) \geq dB$. REDD programmes define reference levels (dB) in terms of tonnes of CO_2 equivalent per year. To simplify the presentation of results, we convert reference levels into hectares of avoided deforestation, as described in Section 2.3. Unlike in the traditional dynamic setting, we introduce a loose constraint on the total owned patch of forest at $t(0)$ $\left(\overline{F}(0)\right)$. However, we impose a time window [0, T] during which the optimisation occurs. While $\overline{F}(0)$ is not infinite, we consider its value so large that forest depletion is not likely[8]; we allow for a positive terminal stock at period T. However, future REDD schemes may have an explicit time frame[9] (Parker et al. 2008), which compels us to consider the time constraint as the most binding for the landowner.

We first solve the model for the BaU case (the benchmark when no REDD project is in place), and then for four REDD crediting baselines: historical, model implied, and two types of corridor. We proceed now with the presentation of each scenario, and then assess the incentives for avoiding deforestation observed in each case.

2.2. Baseline alternatives

2.2.1. Business-as-usual scenario (without REDD)

The BaU scenario illustrates the deforestation trend in the absence of REDD or other forest conservation projects. Here, the land brings only timbering and agriculture benefits, as reflected in the net cash flow ($\pi(\cdot)$) at time t:

$$\pi(d(t)) = P^{cc}(t)d(t) - (a_1 d(t) + a_2 d(t)^2) \tag{6}$$

where $P^{cc}(t)$ is the composite commodity price, $d(t)$ the deforestation rate, and a_1 and a_2 are the parameters of the cost function. The optimal control problem can be described as a maximisation over the deforestation rate of the total discounted net revenues resulting from land exploitation:

$$\max_{(d(t))_{t\in[0,T]}} \left\{ \int_0^T e^{-rt}\pi(d(t))dt \right\} \tag{7}$$

where r is the discount rate and T marks the end of the decision horizon. The variation in the stock of forested land is given by the following dynamics:

$$\dot{F} = -d(t) \tag{8}$$

where F is the stock of forest and $\dot{F}$ represents its variation between consecutive periods. We follow the solution approach of Chiang (1992) for determining the optimal deforestation path (see the Appendix). The rate of deforestation at each moment of time is recursively linked to the initial deforestation level:

$$d(t) = d(0)e^{rt} + \frac{P^{cc}(0)(e^{\delta t} - e^{rt}) - a_1(1 - e^{rt})}{2a_2} \tag{9}$$

Reflecting the optimal deforestation path in the BaU scenario, we denote $d(t) = d_{\mathrm{BaU}}(t)$; it will be used below for computing the REDD rewards in the model-implied and the variable-corridor scenarios.

2.2.2. *Historical baseline*

Most proposals include the historical average deforestation rate in the computation of the crediting baseline[10]; this comes as a recognition of the fact that the average past deforestation, although an imperfect measure, is one of the best predictors at hand for short- to medium-term deforestation (Angelsen et al. 2009). We thus start the analysis of the deforestation behaviour under REDD with a simple historical baseline, where the REDD threshold is flat and equal to the average past deforestation rate. This baseline type is a simplification of what has been proposed by Brazil (Parker et al. 2008).

The merit of the historical baseline consists of its fair simplicity of computation and implementation, as well as its appeal to countries and landowners who need to get used to new operation rules. The baseline has received support also for its ability to reflect local deforestation trends.

The historical reference level faces, however, a number of limitations. Most importantly, an imperfect predictor of future deforestation has high chances of undermining the additionality principle and of distorting country participation, especially if one considers the specific forest transition stage[11] of each country (Angelsen 2007). Forest-rich states with low past deforestation, but which expect increasing trends, might decide to stay out of REDD if the programmes are based on historical baselines. On the other hand, nations with large past deforestation rates and scarce remaining forests would gladly join, since rewards based on historical averages would be generous relative to the required additional efforts (Angelsen 2008a).

In the presence of REDD with a historical baseline, cash flows are generated by two counter-balancing activities, i.e. forest exploitation and REDD:

$$\pi(d(t)) = P^{cc}(t)d(t) - (a_1 d(t) + a_2 d(t)^2) + P^R(t)(dB - d(t))^+ \tag{10}$$

As captured in Equation (10), the landowner's profits are determined by the sales of the composite commodity, less the operational costs; additionally, REDD revenues are eligible for deforestation rates below the historical threshold (dB).

2.2.3. *Model-implied baseline*

An alternative to the retrospective historical baseline is the prospective method[12] that incorporates projections of future deforestation trends. The *model-implied* baseline relies on a time-varying level reflecting predicted deforestation paths under the BaU scenario. Here, the landowner is rewarded for deforesting less than in the absence of the REDD programme. If the forecasting is accurate, it enforces additionality, since only actual efforts would be rewarded. However, the model-implied baseline is not exempt from criticism that stems primarily from the baseline's vulnerability to forecasting errors and the reliance on model assumptions.

We incorporate the specificity of the model-implied baseline into the revenue function, accounting for the fact that the reference level ($dB(t)$) can fluctuate across time according to the projections of the model used:

$$\pi(d(t)) = P^{cc}(t)d(t) - (a_1 d(t) + a_2 d(t)^2) + P^R(t)(dB(t) - d(t))^+ \tag{11}$$

Compared to the methodology of the historical baseline (Equation (10)), the key difference in the model-implied approach is the modification of the baseline level from a static threshold (dB) to a dynamic one ($dB(t)$). In our model, $dB(t)$ is chosen to match the estimated deforestation pattern of the BaU scenario, such that

$$dB(t) = d_{\text{BaU}}(t) \quad \forall\, t \in [0, T] \tag{12}$$

where $d_{\text{BaU}}(t)$ is the optimal deforestation in the BaU scenario.

2.2.4. *Fixed corridor*

The corridor approach has been first proposed by Schlamadinger et al. (2005), and then reformulated jointly in 2006 by the Joanneum Research Institute, the Union of Concerned Scientists, the Woods Hole Research Center, and the Instituto de Pesquisa Ambiental da Amazonia (Griscom et al. 2009). This methodology modifies the historical baseline approach, by replacing the fixed threshold with a corridor whose bounds are computed as levels below and above the average past deforestation rate.

In this paper, we analyse the so-called *corridor 2* methodology,[13] whereby the possible deforestation range is divided into three regions: (1) deforestation levels above the upper boundary do not receive any REDD payments; (2) rates below the lower boundary are entirely eligible for REDD permits, as they would under a fixed-baseline scheme; and (3) deforestation levels within the corridor are discounted proportionally to the distance from the upper boundary, such that rewards are larger when deforestation approaches the lower bound, up to full payments if this lower bound is reached, and conversely, rewards are smaller for deforestation rates close to the upper bound, down to no payment if the upper bound is reached.

The corridor approach attempts to address an important feature of deforestation, namely its frequent fluctuations over time. Movements are usually caused by shifts in key market parameters, such as commodity prices, interest rates, or climate impacts (Joanneum Research Institute 2006). The corridor reward system admits that avoiding deforestation in boom years implies higher opportunity costs, and is, therefore, more difficult to sustain than conservation efforts in years of medium to low timber and agriculture prices. With the corridor system, the landowner is encouraged to keep deforestation rates close

to the average historical level, and is rewarded (although modestly) even if slightly above it. The corridor could also be useful when measurement errors hinder the estimation of the historical baseline. The corridor creates an 'error' band around the threshold, advantageous in the absence of incomplete information about past deforestation rates. In the words of Joanneum Research Institute (2006), the 'corridor approach reduces the risk of missing a single-level target'.

With the corridor approach for REDD, the shape of the profit function reflects the design of the reward programme:

$$\pi(d(t)) = P^{cc}(t)d(t) - (a_1 d(t) + a_2 d(t)^2) + P^R(t)w\big(dB^U - d(t)\big)^+ \tag{13}$$

where $dB^L = (1 - x)dB$ and $dB^U = (1 + x)dB$ represent the lower and upper bounds of the corridor, respectively, dB is the historical deforestation rate, and x the corridor width. $w \in [0, 1]$ is the weight (discount factor) imposed by the corridor. In Equation (13), the third term represents the income generated by the REDD project. The weighting system works as follows:

$$w = 1 - \frac{(d(t) - dB^L)^+}{dB^U - dB^L} = \begin{cases} 1 - \dfrac{d(t) - dB^L}{dB^U - dB^L}, & \text{if } \mathrm{d(t)} > dB^L \\ 1, & \text{if } \mathrm{d(t)} \le dB^L \end{cases}$$

If the deforestation rate lies within the corridor ($d(t) \in (dB^L, dB^U)$), a linear weighting procedure is activated: on one hand, fewer permits will be received than the difference between the deforestation rate and the upper boundary ($w < 1$). On the other hand, deforestation rates below the lower boundary are rewarded full permits ($w = 1$). The last term in the REDD income, $(dB^U - d(t))^+$, ensures that rewards are received only for deforestation rates below the upper bound of the corridor.

2.2.5. *Variable corridor*

Similar to the difference between the static historical baseline and its dynamic model-implied counterpart, we suggest to modify the fixed-corridor baseline by giving it a dynamic feature. The *variable* corridor replaces the constant lower and upper corridor bounds with time-varying levels, established below and above the deforestation rate of the dynamic BaU scenario. To the best of our knowledge, this is the first time this baseline approach is proposed.

The variable corridor aims at bringing together the strong points of both the model-implied and the fixed-corridor baselines. First, linking corridor bounds to the BaU deforestation trend is expected to offer not only a dynamic but also a forward-looking perspective on deforestation paths, more likely to ensure additionality. Second, the corridor reward system should be able to better deal with estimation errors of the BaU deforestation, and account for periodic fluctuations in deforestation levels, similarly to the fixed corridor. The revenue function follows the methodology of the fixed corridor, but introduces dynamic corridor bounds:

$$\pi(d(t)) = P^{cc}(t)d(t) - (a_1 d(t) + a_2 d(t)^2) + P^R(t)w(t)\big(dB^U(t) - d(t)\big)^+ \tag{14}$$

Table 1. REDD revenues under different baseline methodologies.

	Single threshold	Corridor
Static	$RR^{\mathrm{H}}(t) = P^{R}(t)(dB - d(t))^{+}$	$RR^{\mathrm{Cf}}(t) = P^{R}(t)\omega(dB^{U} - d(t))^{+}$
Dynamic	$RR^{\mathrm{MI}}(t) = P^{R}(t)(dB(t) - d(t))^{+}$	$RR^{\mathrm{Cv}}(t) = P^{R}(t)\omega(t)(dB^{U}(t) - d(t))^{+}$

Note: H stands for historical baseline, MI for model implied, Cf for fixed corridor, and Cv for variable corridor.

where the weighting factor is time varying due to the dynamic corridor bounds, with $w(t) = 1 - \frac{(d(t) - dB^{L}(t))^{+}}{dB^{U}(t) - dB^{L}(t)}$, $dB^{L}(t) = (1 - x)dB(t)$, $dB^{U}(t) = (1 + x)dB(t)$, $dB(t) = d_{\mathrm{BaU}}(t)$, and x the corridor width.

Summing up, in this paper we analyse four different REDD scenarios, namely two static and two dynamic, allowing for either a single-threshold or a corridor approach. While the static baselines are based on historical estimations of the deforestation rate, and are therefore retrospective, the dynamic baseline types are based on estimations of future deforestation trends, and are prospective. We denote the single-threshold approaches as H − the historical − and MI − the model implied. The fixed and variable corridors are labelled Cf and Cv, respectively, hereafter. To summarise, the REDD revenues ($RR(t)$) of each baseline methodology are presented in Table 1.

We solve for the optimal deforestation path under the BaU scenario and the four different baselines.[14] We tackle the non-linearity in the profit function with the help of a numerical approach (see the Appendix).

2.3. Model calibration

Our model is general enough to accommodate the characteristics of many regions where REDD could be implemented. For the numerical application, we take here the view of a forest owner from Peru. As the sensitivity analysis shows, the results are robust and generalisable to different regions of the world (see the Appendix).

Peru is an important REDD candidate in terms of forest resources[15] and market volume.[16] The annual deforestation rate for 1990−2005 is estimated at 0.14%, remaining at low levels relative to its neighbouring countries (FAO 2005). However, more recent estimates show that during 2000−2010 deforestation rates experienced an increasing trend,[17] which is predicted to persist in the near future mainly due to cropland expansion in the Andes (Wassenaar et al. 2007). Several local projects developing REDD credits are currently in the implementation phase in Peru[18] (Hajek et al. 2011; Entenmann and Schmitt 2013).

The list of parameters used for model fitting and their sources are presented in Table 2. In our model, the average deforestation rate obtained in the BaU scenario is about 200 ha/year. We allow the historical baseline level (dB) to vary in a large interval (between 1 ha and 500 ha per annum), in order to cover a broad spectrum of scenarios. While REDD credits are granted in terms of tons of CO_2 reduced per year, we present our results in terms of hectares of avoided deforestation. We convert the deforested area into tons of carbon emitted with the help of a parameter (Ω) whose value for Peru can be found in the OSIRIS model for the above and below ground biomass carbon and for soil carbon (Busch et al. 2009). Another converter (ψ) transforms the quantity of tons of carbon emitted into tons of CO_2 emitted (Assante 2011).

Table 2. Calibration parameters for the numerical solution.

Parameter	Explanation	Value	Source
$P^{cc}(0)$	Composite commodity price	500 Eur/m^3	ITTO (2010)
δ	Growth rate of $P^{cc}(t)$	2.3% per annum	ITTO (2010)
		S.A. [0, 0.4]% per annum	
λ	Eur/m^3 to Eur/ha	158 m^3/ha	Penman et al. (2003)
$P^R(0)$	REDD permit price	5 Eur/tCO_2	Diaz et al. (2011)
γ	Growth rate of $P^R(t)$	2.5% p.a.	Diaz et al. (2011)
		S.A. [0, 0.4]% per annum	
Ω	ha to tC emitted	179 tC/ha	Busch et al. (2009)
		S.A. [50, 200] tC/ha	
ψ	tC to tCO_2	3.67 tCO_2/tC	Assante (2011)
a_1	Cost parameter 1	3.3198 Eur/ha	Angelsen (1996), Verissimo et al. (1992)
a_2	Cost parameter 2	798.0811 Eur/ha^2	Angelsen (1996), Verissimo et al. (1992)
r	Discount rate	2% per annum	–
		S.A. [0, 0.1]% per annum	
dB	Historical baseline	200 ha per annum	–
		S.A. [1, 500] ha per annum	
dB^U	Corridor upper boundary	$(1 + x)$dB ha	–
dB^L	Corridor lower boundary	$(1 - x)$dB ha	–
x_0	Initial corridor width	0.1	–
x	Corridor width	[0.1, 0.9]	–
T	Time horizon	100 years	–

Note: The table captures values used for the calibration of the model parameters. S.A. stands for values used in the sensitivity analysis.

With the help of the parameter λ, we express the price of the composite commodity from Eur/m^3 into Eur/ha, relying on the IPCC Good Practice Guide LULUCF (Penman et al. 2003). The initial price of the commodity ($P^{cc}(0)$) and its growth rate (δ) are computed for the Peruvian market from the Annual Review and Assessment of the World Timber Situation (ITTO 2010). We use the State of the Forest Carbon Markets 2011 (Diaz et al. 2011) to set the initial REDD permit price ($P^R(0)$) and its growth rate. In our calibration, the growth rate of the REDD permit price is above the growth rate of the composite commodity price ($\delta > \gamma$). As a robustness check, we ran the analysis allowing for the opposite relationship ($\delta \leq \gamma$). This change impacts the amount of avoided deforestation, but does not modify the ranking of the baselines.

The chosen level for the discount rate (r) is 2%, placing it slightly lower than the growth rates of the composite commodity and the permit prices; we make here the assumption that forest exploitation and REDD bring higher financial benefits than saving at the discount rate.[19] In reality, discount rates in developing countries take usually larger values and vary widely over time (see the Appendix). Nonetheless, the sensitivity analysis shows that the ranking of baselines is consistent across different values of the discount rate ($r \in [0, 0.1]$).

Finally, for the calibration of the production cost, we adapt the cost function of Angelsen (1996), calibrating it to data from Verissimo et al. (1992) for the Amazonian forest.

Table 3. Performance indicators of baseline scenarios.

Indicator	Definition	Formula
(1) Effectiveness (E_1)	Avoided deforestation from BaU (%)	$E_1^i = \frac{S_{\text{Tot}}^{\text{BaU}} - S_{\text{Tot}}^i}{S_{\text{Tot}}^{\text{BaU}}}$ $S^i{}_{\text{Tot}} = \int_0^T d^i(t)dt$
(2) Landowner's welfare (E_2)	Change in income from BaU (%)	$E_2^i = \frac{\Pi_{\text{Tot}}^i - \Pi_{\text{Tot}}^{\text{BaU}}}{\Pi_{\text{Tot}}^{\text{BaU}}}$ $\Pi_{\text{Tot}} = \int_0^T e^{-rt}\pi(d^i(t))dt$
(3) Efficiency (E_3)	Average cost of avoiding 1 ha of deforestation from BaU (Eur/ha)	$E_3^i = \frac{SRR^i}{S_{\text{Tot}}^{\text{BaU}} - S_{\text{Tot}}^i}$ $SRR^i = \int_0^T e^{-rt} RR^i(t)dt$

Note: Three measures of REDD performance under different baselines are computed. $d(t)$ is the deforested area, $\pi(t)$ the total income from land, $RR(t)$ the REDD revenue at time t, and $i \in \{\text{H, MI, Cf, Cv}\}$; BaU: business-as-usual, H: historical, MI: model implied, Cf: fixed corridor, Cv: variable corridor.

2.4. *Performance indicators*

We evaluate the performance of REDD programmes under different baseline methodologies with the help of three indicators, in line with the *3E Criteria* proposed by Stern (2008).[20] The performance measures we consider are: effectiveness, landowner's welfare, and efficiency, as detailed in Table 3. First, the effectiveness indicator E_1 measures the avoided deforestation, and the inherent saved emissions. It quantifies the difference between the deforested area of BaU (no REDD) and the different baseline scenarios for REDD, being therefore a measure of additionality. Second, we measure the financial co-benefits of REDD with the help of the E_2 indicator, which quantifies the percentage change in landowner's income due to joining REDD. Finally, the efficiency indicator E_3 provides an estimate of the average cost of forest preservation per hectare of avoided deforestation. It divides the total received REDD revenues by the number of hectares of forest saved under each baseline type compared to the BaU scenario. Here, the cost of each baseline scheme reflects realised (additional) savings in emissions.

3. Results

This section presents the optimal deforestation paths for the BaU and the four REDD baseline approaches, and discusses the implications for baseline choice. Section 3.1 first ranks the baselines according to their performance, and then explains the observed differences by analysing the financial incentives offered by each baseline methodology. At the end of the section, we check the robustness of the baseline ranking to changes in key parameters. Section 3.2 relaxes the initial assumptions regarding corridor bandwidth and symmetry, and underlines possible design adjustments to increase baseline performance. Section 3.3 extends the analysis of baseline performance to technical, social, and environmental aspects of REDD.

3.1. *A first comparison*

We solve for the optimal deforestation paths under the BaU and the four REDD baselines (see Figure 1). With our initial calibration, under each baseline scheme the optimal deforestation path is increasing in time, as agricultural activities become more attractive due to rising composite commodity prices.[21] We compare the performance of the baseline methodologies

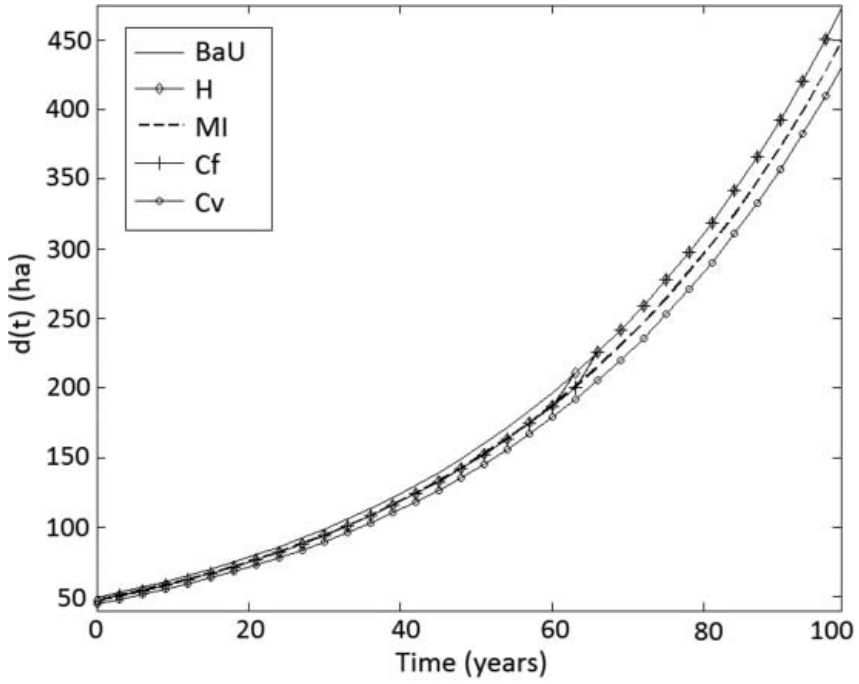

Figure 1. Optimal deforestation paths under BaU and different REDD baselines.
Note: H stands for historical baseline, MI for model implied, H for historical, Cf for fixed corridor, and Cv for variable corridor. The historical deforestation rate (dB) is 200 ha/year. Corridor width is $x = 0.1$.

based on the indicators introduced in Section 2.4. Table 4 shows that the baselines differ in their performance, with each indicator revealing a new ranking of baselines.

First, we compare the baselines in terms of the ability to reduce deforestation. Figure 1 is illustrative of the effectiveness of REDD. In all baseline scenarios, the area of deforested land remains lower or equal to the BaU case; over the aggregated time horizon, REDD programmes are effective in reducing deforestation.[22] However, the reduction in deforestation does not hold at all moments of time for the static baselines: our dynamic model shows that keeping reference levels constant while the opportunity costs of deforestation increase will determine the forest owner to opt out of the REDD project and follow the BaU path. This sheds light on the limited effectiveness of the static baselines, as opposed to the prospective ones that offer continued incentives for reducing deforestation. We argue that, with their temporary effectiveness, static baselines face higher non-permanence risks than dynamic baselines. Analysing the E_1 indicator, we indeed observe that the variable corridor achieves the best results, and it is followed at quite some distance by the model-implied baseline. The fixed-corridor and the historical baselines lag far behind in terms of effectiveness.

Table 4. Indicators of REDD performance under different baselines.

Baseline	Effectiveness E_1 (%)	Welfare E_2 (%)	Efficiency E_3 (Eur/ha)
H	1.54	2.26	73,096.66
MI	4.77	0.23	4,680.18
Cf	1.76	2.76	78,043.75
Cv	9.08	0.92	9,318.13

Second, imposing no liabilities for deforestation rates above the baseline, all scenarios have a positive impact on landowner's welfare compared to the BaU case (E_2). The increase in welfare across all baselines points to the ability of REDD to foster the voluntary opting-in of candidate countries, and alleviates some of the concerns with the need of additional enforcement measures. In particular, the static baselines prove to be more generous: the fixed corridor is the most attractive for the landowner, followed closely by the historical baseline. The remaining two baselines achieve only modest changes in welfare, with the model-implied baseline being the last ranked.

Third, in terms of cost-efficiency (E_3), the prospective baselines strongly outperform the static ones: the model-implied baseline is the top performer, with the variable corridor in the second position. The historical and fixed-corridor baselines require almost 20 times higher costs than MI.

3.1.1. The incentive structure of the baselines

In order to understand what drives the difference in baseline performance, we compare the incentive structure of the four baseline methodologies. To ease the comparison, we explicit the REDD revenues at different ranges of the deforestation rate (see Table 5). In particular, within the corridor we define the deforestation rate in terms of the reference level (dB, $dB(t)$), the corridor width (x), and a variable y, with $y \in (0, x)$, such that

(1) when $d(t) \in (dB^L, dB]$, we define $d(t) = (1 - x + y)dB$ for the Cf case, and $d(t) = (1 - x + y)dB(t)$ for Cv;
(2) when $d(t) \in (dB, dB^U)$, $d(t) = (1 + y)dB$ for the Cf case, and $d(t) = (1 + y)dB(t)$ for Cv, with $dB(t) = d_{\mathrm{BaU}}(t)$.

To account for possible misestimations in the BaU deforestation path and to increase participation rates, the corridor approaches reward landowners for choosing deforestation rates below an upper corridor bound, which is set above the corresponding single threshold ($dB^U = (1 + x)dB$, $dB^U(t) = (1 + x)dB(t)$, with $x > 0$). We observe from Table 5 that by design, for the same deforestation rate, a corridor approach always gives larger or equal financial incentives to participate in REDD to the corresponding single-threshold approach. For all $t \in [0, T]$

$$RR^{\mathrm{H}}(t) \leq RR^{\mathrm{Cf}}(t) \tag{15}$$

$$RR^{\mathrm{MI}}(t) \leq RR^{\mathrm{Cv}}(t) \tag{16}$$

The ranking of REDD payments influences the effectiveness of the baselines. Larger REDD revenues decrease the opportunity costs of deforestation, bringing stronger incentives to take part in REDD and keep deforestation below the baseline. Any decrease in deforestation will inevitably take place below $d_{\mathrm{BaU}}(t)$.[23] It follows that relations (15) and (16) hold also for effectiveness with unchanged signs:

$$E_1^{\mathrm{H}} \leq E_1^{\mathrm{Cf}} \tag{17}$$

$$E_1^{\mathrm{MI}} \leq E_1^{\mathrm{Cv}} \tag{18}$$

Table 5. REDD revenues ($RR(t)$) according to the range of the deforestation rate.

Static baselines				
	$d(t) \in [0, dB^L]$	$d(t) \in (dB^L, dB]$	$d(t) \in (dB, dB^U)$	$d(t) \geq dB^U$
H	$P^R(t)(dB - d(t))$	$P^R(t)(x - y)dB$	0	0
Cf	$P^R(t)((1 + x)dB - d(t))$	$P^R(t)\left(2(x - y) + \frac{y^2}{2x}\right)dB$	$P^R(t)\frac{(x-y)^2}{2x}dB$	0
Dynamic baselines				
	$d(t) \in [0, dB(t)^L]$	$d(t) \in (dB(t)^L, dB(t)]$	$d(t) \in (dB(t), dB(t)^U)$	$d(t) \geq dB(t)^U$
MI	$P^R(t)(dB(t) - d(t))$	$P^R(t)(x - y)dB(t)$	0	0
Cv	$P^R(t)((1 + x)dB(t) - d(t))$	$P^R(t)\left(2(x - y) + \frac{y^2}{2x}\right)dB(t)$	$P^R(t)\frac{(x-y)^2}{2x}dB(t)$	0

Finally, we analyse the impact of higher REDD revenues on efficiency. Our efficiency indicator (E_3) is defined as a measure of total REDD revenues divided by the hectares of reduced deforestation below BaU. Therefore, an increase in REDD revenues will have a double (yet opposed) impact on efficiency. First, higher $RR(t)$ lead to lower efficiency (higher E_3). Second, higher $RR(t)$ raise effectiveness (avoided deforestation), increasing efficiency (lower E_3). As can be observed from Table 4, the effect on welfare dominates the effect on effectiveness.[24] It follows that the single-threshold approaches, with lower welfare increases, are more efficient than the corresponding corridor approaches, with higher welfare increases. That is,

$$E_3^{\mathrm{H}} \leq E_3^{\mathrm{Cf}} \tag{19}$$

$$E_3^{\mathrm{MI}} \leq E_3^{\mathrm{Cv}} \tag{20}$$

Summing up, we have shown that the corridor approaches dominate the corresponding single-threshold approaches in terms of effectiveness and welfare increase, but lag behind in terms of efficiency. If sufficient funding is available, which remains to be seen, we argue that REDD promoters should opt for the corridor approach instead of the single-threshold one, in order to achieve the needed reductions in emissions.

3.1.2. *Sensitivity analysis*

REDD initiatives are currently being designed in a plethora of tropical countries, with several projects being already in the implementation phase (Angelsen 2010). In particular, Norway – through its International Climate and Forest Initiative (NICFI) – contributes to different multi- and bi-lateral REDD initiatives in several countries, including Brazil, Democratic Republic of Congo, Guyana, Indonesia, and Tanzania. These countries are distinct in terms of forest types, stages in the forest transition, and national forestry policies, apart from a large diversity in the economic, social, and political contexts. To reach the REDD goals, NICFI recognises the need to design projects that account for national and sub-national differences (NIFCI 2011). For instance, the Guyana–Norway cooperation agreed on a baseline that reflects both the historical average deforestation in Guyana and the mean deforestation rate in developing countries. Since Guyana had historically very low deforestation rates compared with other developing countries, the computed reference level is much higher than the country's past average deforestation rate. To allow for positive but limited increases in deforestation, payments are reduced linearly for deforestation rates that exceed a certain threshold, similarly to the fixed-corridor approach.

To be able to generalise our findings outside the region of Peru, we test the robustness of our results across different settings. We focus on several key calibration parameters, describing the forest type (the carbon content Ω), the crediting threshold of the static baselines (dB), the time preference of the forest owner (the discount rate r), and the variables describing the opportunity costs of deforestation and the received REDD financial incentives (the growth rates of the composite commodity (δ) and REDD permit prices (γ)). The detailed analysis can be found in the Appendix.

We find that the ranking of baselines is robust to different settings. The variable corridor continues to be the most effective in reducing deforestation. The fixed corridor offers the highest increase in welfare from BaU. The model-implied baseline is the most efficient, having the lowest costs per hectare of avoided deforestation. The sensitivity analysis underlines the importance of understanding the benefits of the variable-corridor

approach, whose performance can outpace significantly the other baselines, depending on the characteristics of the region where REDD is being implemented.

3.2. *Corridor bandwidth and symmetry*

When large uncertainties surround the BaU deforestation rate, or high variability in opportunity costs is to be expected, one might be tempted to advocate a corridor approach with a larger bandwidth, such that a broader range of deforestation rates would be accounted for in the REDD payments. The corridor bandwidth should in this case be carefully chosen, to provide effective incentives for forest protection and, at the same time, achieve cost-efficiency.

With this motivation, we test the sensitivity of baseline performance to two key adjustments to the corridor methodology, namely corridor wideness and symmetry. We allow for increasing bandwidths ($x \in [0.1, 0.9]$) that reflect different reward magnitudes granted for reducing deforestation. Additionally, we check the variation in performance when allowing for asymmetric corridors. Namely, we consider both an upward- and a downward-biased corridor. For the variable corridor, bounds are set such that

(1) in the upward-biased case, $dB^L(t) = (1 - x_0)dB(t)$ and $dB^U(t) = (1 + x)dB(t)$;
(2) in the downward-biased case, $dB^L(t) = (1 - x)dB(t)$ and $dB^U(t) = (1 + x_0)dB(t)$;

where $dB(t) = d_{\mathrm{BaU}}(t)$, $x \in [0.1, 0.9]$, and x_0 is fixed, with $x_0 = 0.1$. The same applies for the fixed corridor, but $dB(t)$ is replaced as usually by the constant dB. On one side, the upward-biased corridor approach raises the upper bound of the corridor, leading to an extension of the range of deforestation rates eligible for REDD revenues. This type of asymmetric corridor is in line with the proposal of Schlamadinger et al. (2005) who suggest setting the upper bound of the corridor so high that it minimises the probability that the deforestation rate will exceed this limit. In contrast, the downward-biased approach takes down the lower bound of the corridor, imposing therefore heavier discounts on REDD rewards for deforestation rates in the range (dB^L, dB] (($dB^L(t)$, $dB(t)$]) for the fixed (variable) corridor.

Figure 2 displays the performance results of the variable corridor. The change in the performance of the fixed corridor follows a similar pattern (see Figure E.1 in the Appendix). First, some effectiveness is always achieved ($E_1 > 0$), for all corridor bandwidths

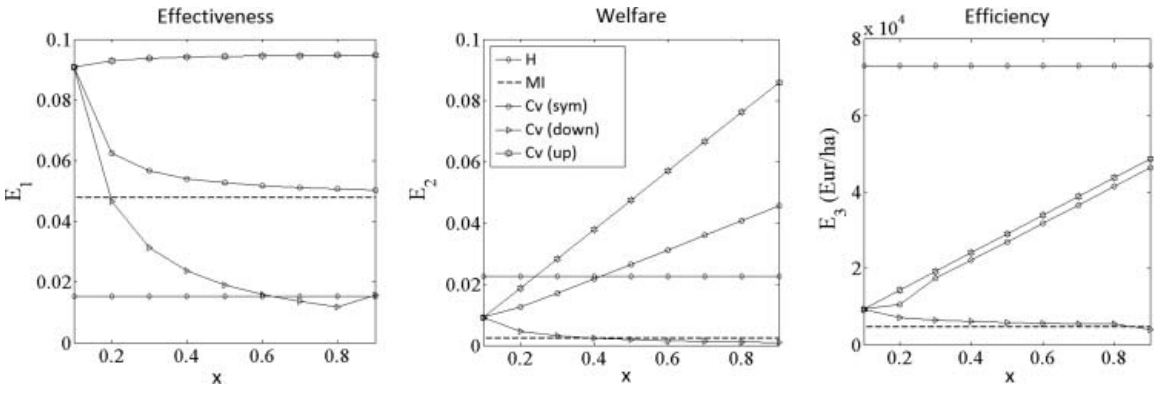

Figure 2. Performance of the variable corridor at different corridor widths.
Notes: The figure captures the performance of the variable corridor across different corridor bandwidths. The performance is compared to the historical and the model-implied baselines. Considered corridors are symmetric (*sym*), upward (*up*), and downward biased (*down*).

and all symmetry alternatives. Figure 2 shows that, as bandwidth increases, effectiveness is higher for the upward-biased corridors, but decreasing for symmetric and downward-biased corridors. Second, increasing the corridor bandwidth achieves higher welfare improvements for the symmetric and upward-biased corridor approaches. Downward-biased corridors exhibit decreasing welfare for wider corridors. Third, cost-efficiency decreases for symmetric and upward-biased corridors, and improves slightly for the downward-biased corridor when increasing the corridor width.

3.2.1. *The incentive structure of (a)symmetric corridors*

The three symmetry scenarios provide distinct financial incentives, causing differences in performance. The upward-biased corridor is by design the most generous one, followed by the symmetric, and then the downward-biased corridor, i.e. $RR^{up}(t) \geq RR^{sym}(t) \geq RR^{down}(t)$ for all bandwidths.[25] Moreover, an increase in the corridor bandwidth (x) impacts the REDD revenues differently, depending on the symmetry assumption. The overall impact of an increase in bandwidth is twofold: (1) a linear impact on the number of REDD credits received for keeping deforestation rates below the upper corridor bound, i.e. on $n = dB^U(t) - d(t)$ and (2) a non-linear impact on the weight ($\omega(t)$) provided by the corridor (see Table 6).

The upward-biased approach achieves increasing welfare at larger corridor widths. With an increase in x, both the number of REDD credits received and the weight provided by the upward corridor increase. As captured in Figure 2, welfare and effectiveness change in the same direction when x increases, but the large increase in welfare obtained at wider corridors is accompanied by only modest improvements in effectiveness that have the tendency to flatten out as x increases. The stronger financial motivation has a diminishing effect on forest protection.

Downward-biased corridors exhibit negative partial derivatives with respect to x, showing that here welfare improvements from BaU are lower for wider corridors. Larger bandwidths decrease welfare and, as expected, effectiveness.

The symmetric-corridor approach achieves higher welfare but lower effectiveness as bandwidth increases. The overall positive impact on welfare follows, as usually, from the fact that its REDD revenues are increasing in the corridor bandwidth. However, although the total impact is positive, the linear and non-linear effects have opposite signs (Table 6).

Table 6. Sensitivity of REDD revenues to corridor bandwidth and deforestation rate in the case of the variable corridor. $RR(t) = P^R(t)\omega(t)n$, with optimal $d(t) \in (dB^L(t), dB)$.

Symmetry	Linear impact on REDD credits $\frac{\partial n}{\partial x}$	Non-linear impact on weight $\frac{\partial \omega(t)}{\partial x}$	Overall impact on REDD revenues $\frac{\partial RR(t)}{\partial x}$	Second order impact on REDD revenues $\frac{\partial^2 RR(t)}{\partial x \partial d(t)}$
Upward biased	+	+	+	−
Symmetric	+	−	+	+
Downward biased	0	−	−	+

Note: The table captures the sign of the partial derivatives of REDD revenues with respect to corridor width (x) and deforestation rate ($d(t)$) across different symmetry scenarios for the variable corridor. The optimal deforestation rate stays within the corridor, i.e. $d(t) \in (dB^L(t), dB(t))$. $n = dB^U(t) - d(t)$ is the number of REDD credits awarded, $\omega(t) = 1 - (d(t) - dB^L(t))/(dB^U(t) - dB^L(t))$ is the weight imposed by the corridor approach, and the lower and upper bounds of the corridor ($dB^L(t)$, $dB^U(t)$) vary across the three corridor symmetry assumptions. The computations are detailed in the Appendix.

As bandwidth increases, the landowner benefits, on one hand, by receiving more REDD credits (higher n), but loses, on the other hand, from stronger discounts imposed by the weighting factor (lower $\omega(t)$). The impact on effectiveness is confirmed when analysing the joint sensitivity of REDD revenues to the deforestation rate and corridor bandwidth (see column (4) in Table 6). The increase in profits due to an increase in x is higher at larger $d(t)$, as indicated by the positive second-order partial derivatives. At larger corridor bandwidths, it benefits the landowner to increase $d(t)$, and therefore reduce effectiveness.

Summing up, with a lack of confidence in the estimates of the BaU deforestation, or with anticipated high seasonality in deforestation rates, wider corridors might need to be accommodated, in a way that forest protection is still incentivised. Our results show that increasing the corridor bandwidth ensures a higher effectiveness of reducing deforestation only in the upward-biased corridor design, and is counter-beneficial for symmetric and downward-biased cases. Both fixed and variable corridors benefit most from having an upward-biased corridor reward system of moderate bandwidth ($x = 0.4, 0.5$), which guarantees strong effectiveness and welfare results, at low efficiency losses.

3.3. Extended criteria for baseline evaluation

Our analysis so far has highlighted three baseline alternatives with strong performance results: the model-implied (MI), the upward-biased fixed corridor (Cf(up)), and the upward-biased variable corridor (Cv(up)), with each baseline alternative performing best in a different area.

Although the three performance indicators considered so far capture the most important economic aspects of the alternative baselines, other factors play an equally important role in the REDD implementation process. In order to achieve a more holistic understanding of the baseline characteristics, we complement the economic evaluation with a multi-tier analysis focusing on the environmental, technical, and social performance of the baselines. Based on the study of Huettner et al. (2009), we select five new criteria whose fulfilment can be easily evaluated for our baselines, namely easiness of implementation, low data requirements, accounting for business cycles, accounting for opportunity costs, and incentivising a reduction in losses from estimation errors.

The fulfilment of these additional qualitative factors cannot, however, be quantified in the same manner as our three initial economic indicators. For this reason, we proceed by giving each baseline type a score[26] representing a rough estimation of how well it is expected to fulfil the performance criteria relative to the other baselines. The scores awarded to each baseline for the three initial indicators and the new qualitative aspects are presented in Figure 3. While the economic analysis (based on E_1, E_2, and E_3) favoured each of the baselines for a different criterion, the integrative analysis sets the four baselines further apart, highlighting stronger differences.

One of the new criteria reveals a strong point of the historical baseline (H). REDD projects, especially in their initial phase, need to be designed as contracts with few and clear requirements in order to encourage the participation of diverse parties and create momentum for the development of such forest protection initiatives worldwide. The historical baseline is likely to benefit from the highest ease of implementation among the considered methodologies. If data availability is not an issue, policy-makers will be required low efforts for baseline computation and landowners will be provided with contract guidelines they can easily relate to. Together with the fact that historical deforestation rates have some predictive power for short- to medium-term deforestation (Angelsen

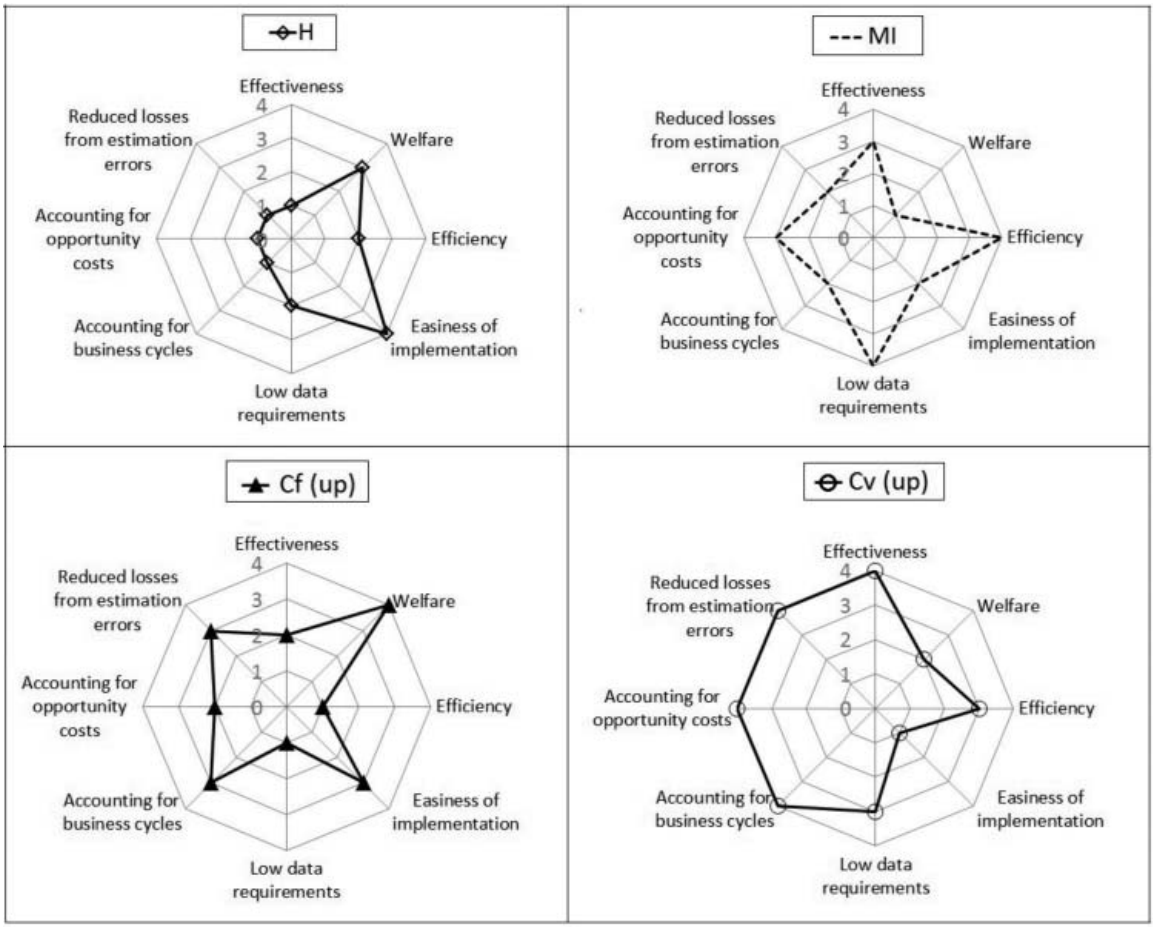

Figure 3. Integrated performance of baseline approaches.

et al. 2009), the ease of implementation explains why current REDD initiatives have opted to rely on the historical baseline for computing reductions in deforestation.

The model-implied (MI) baseline provides rewards for reductions below the estimated counterfactual deforestation, accounting for future opportunity costs. In our model, its computation does not rely on the availability of data records of past deforestation; instead, it requires information regarding current agricultural prices and estimations of the future trend in prices. In this context, we argue that the MI has comparatively less data restrictions than all the other baseline methodologies.[27] Moreover, if the estimation of the BaU deforestation path is truthful, the implementation of REDD with the MI baselines favours additionality. Figure 3 reminds us that this baseline stands out in terms of cost-efficiency, as highlighted in Section 3.1. This can be a strong point in favour of the MI baseline, especially if future REDD rewards will be linked with compliance carbon markets.

The upward-biased fixed corridor (Cf(up)) modifies the historical baseline by replacing the single-threshold with a corridor approach. Section 3.2 showed that selecting an upward-biased corridor can improve its effectiveness and welfare performance. Indeed, the upward-biased corridor approach is the most attractive for the landowner from a welfare perspective. Despite large financial transfers, the effectiveness and efficiency of the Cf(up) remain limited.

Overall, the integrative analysis appears to give highest support to the variable corridor approach. The upward-biased variable corridor (Cv(up)) is the most effective in reducing deforestation below BaU levels (see Section 3.1). Being a prospective method, based on expectations regarding the future movement of timber and agriculture prices, as

well as REDD permit prices, the Cv(up) has a better ability to reflect the opportunity costs faced by the landowner. Additionally, the corridor design brings two advantages. First, the scheme offers REDD compensation also for deforestation rates that come close to the time-varying baseline, even if not strictly below it; this accommodates possible future business cycles and ensures (modest) positive REDD revenues should the economy be expanding (when opportunity costs are high). Second, replacing the single-threshold approach by a corridor approach, and introducing the weighting system for deforestation rates inside the corridor, the baseline has the ability to reduce losses due to misestimation of the BaU baseline (Joanneum Research Institute 2006).

Summing up, designing a baseline methodology that achieves all REDD goals simultaneously proves to be highly challenging. Indeed, the analysed baselines exhibit strong attributes in different areas. For its ability to enhance environmental and economic performance, we consider the upward-biased variable corridor to be the best candidate for achieving the most important REDD goals.

3.3.1. *(Mis)estimation of BaU deforestation*

Two delicate issues require further thought. The first one touches on the issue of additionality. REDD aims to reward reductions in deforestation below BaU levels. One limitation of our analysis is that it is placed in a deterministic setting, where the BaU deforestation path is known. However, in reality many variables of the decision environment are in fact stochastic, such as commodity and REDD prices, and asymmetries in information might lay between REDD promoters (who evaluate emission reductions) and forest owners (who benefit from REDD payments). This surrounds the estimation of the BaU deforestation path with significant uncertainties.

REDD projects implemented based on misspecified BaU deforestation levels can provide undesired incentives to forest owners. Errors in the estimation of the BaU would directly impact the financial incentives of the prospective baselines, i.e. model-implied and variable corridors.[28] We investigate this hypothesis and solve for the optimal deforestation path when the baseline methodology relies on a misspecified BaU path. We define the estimated BaU deforestation as

$$d^{E}_{\mathrm{BaU}}(t) = (1+\epsilon)d_{\mathrm{BaU}}(t) \tag{21}$$

where d_{BaU} is the true deforestation path when no REDD programme is in place, and ε is the percentage misestimation of the BaU deforestation rate, with $\epsilon \in [-0.05, 0.05]$.

Our results are detailed in the Appendix. First, we find that the performance of the variable-corridor methodology is robust if estimation errors stay within [−5%, +5%] from the true BaU deforestation path. As the estimation errors increase, the effectiveness of the variable corridor decreases; however, within the considered range, the variable corridor remains the most effective in reducing deforestation among the four baseline methodologies, despite the performance loss. Our conclusion that the variable corridor should be the preferred baseline methodology is, therefore, robust.

Second, an underestimation of BaU decreases the performance of the model-implied baseline; for estimation errors below −3%, the landowner will opt out of the REDD project and no reductions in deforestation from BaU will be obtained. On the other hand, small underestimations (above −2%) and overestimations in general do not impact the landowner's deforestation reduction decisions, and the MI remains more effective than the historical or fixed-corridor approaches. This analysis reveals the importance of

designing baselines that are in line with the future drivers of deforestation. In particular, for forest-rich regions that have historically very low deforestation rates, like the Congo Basin, significantly underestimating the baseline would lead to ineffective REDD programmes. It appears to be less problematic to provide an overestimated baseline than an underestimated one.

3.3.2. REDD permanence

The second key issue concerns permanence. With REDD, the issue of permanence has a different dimension from that on compliance carbon markets, like the EU ETS. There, being restricted to emit less than a pre-specified cap, regulated companies continue with the same business activity, but are given incentives to switch to a more efficient production process.[29] Being costly, the switch is likely not to be reverted, and emission reductions could remain 'permanent'. The situation is not analogous to REDD, where the landowners cannot continue with their current occupation (deforesting for expanding agriculture), but need to stop the expansion if they want to receive payments (they cannot make the cutting down of trees less emission-intensive). REDD payments are offered on a per-period basis, being linked to deforestation flows instead of the remaining forest stocks. Thus, temporary reductions in deforestation can be reverted in later periods, questioning the long-term success of REDD. Moreover, unlike the current voluntary market for REDD permits, the EU ETS is a capped market, where regulated players face penalty costs if their emissions exceed the allowed level.[30] We argue that REDD payments could be contingent on the emissions of the entire owned land parcel, such that all land uses are covered by the regulation umbrella, and more efficient operations are incentivised, similar to the mechanism of the cap-and-trade systems. However, this takes us away from the original REDD concept, and future research could further investigate this topic.

4. Conclusions

REDD programmes target reductions in emissions from deforestation below BaU levels. A key issue of REDD is the establishment of baselines against which reductions in deforestation are measured. This paper assesses the performance of the most frequently proposed baselines: historical, model-implied, and fixed corridors. Additionally, we introduce a new baseline type − the variable corridor.

We solve for the optimal deforestation path in a dynamic setting where REDD projects are available. One of our main findings is that the baseline choice has a significant impact on land-use behaviour. Landowners choose different deforestation paths when incentivised by distinctive baseline methodologies. We believe this point is key for implementing effective REDD programmes.

We first evaluate the selected baselines according to three economic indicators that describe the effectiveness, welfare increases, and cost-efficiency of reducing deforestation. We find that each indicator points to a different baseline as the best performer. Our analysis shows that a preference for strong effectiveness recommends the variable corridor. The fixed corridor provides the highest increase in landowner's welfare above BaU. Efficiency reasons advocate the model-implied baseline.

We then discuss additional environmental, social, and technical aspects important for REDD implementation and the setting of baselines. This analysis highlights stronger differences among the baselines, and reveals that the prospective variable corridor achieves the best trade-off among the economic and environmental REDD goals. Moreover, this

performance can be boosted by setting the upper bound of the corridor (asymmetrically) high above the estimated BaU deforestation.

We conclude that the current widespread use of the historical baseline may be challenged. Much stronger effectiveness and efficiency could be achieved with the use of a forward-looking baseline, provided that estimation errors do not largely underestimate future deforestation. Additionally, the currently used single-threshold methodology is also not optimal; replacing the single-threshold approach with a corridor formed around the estimated BaU deforestation rate has higher potential of accounting for real opportunity costs and offering continued incentives for reduced deforestation.

Our results offer potential insights for other emission regulation policies, such as the EU ETS. There regulated companies are allocated emission allowances based on their emissions' history, similar to the historical baseline in REDD. Based on our analysis, we expect the EU ETS to benefit also in terms of effectiveness and efficiency from replacing its historical cap with a forward-looking corridor approach. This could potentially address some of the permit overallocation problems, which have persisted since the opening of the EU ETS.

Some additional concerns remain. This paper assumes that REDD funding is achieved through a market-based mechanism. In comparison to voluntary funds, international carbon markets can mobilise much larger amounts of money and favour cost-efficient emission reductions (Angelsen 2008b). However, the weak carbon markets we face nowadays, characterised by low liquidity and permit overallocation, will most probably have difficulties in handling additional amounts of permits coming from the forestry sector. Therefore, when selecting the most appropriate baseline type, one might postpone the implementation of the most effective one in order to avoid drops in permit prices until the stabilisation of the carbon market.

Our analysis has relied on the dynamic setting to check the ability of the different baselines to provide *continued*, not temporary, incentives to reduce deforestation. However, we did not address the issue of resetting reference levels, based on updated information. This would require the setting and solving of the model under conditions of uncertainty, where a decision-maker would readjust the baseline based on newly received information about the deforestation rate of the landowner, and the landowner would subsequently adjust his or her deforestation rate based on the new baseline. This constitutes a very interesting question for future research; it could bring insights into the response of landowners to changes (e.g. tightening) in requirements to reduce deforestation.

Finally, a robust understanding of the deforestation process would require an improved description of the different stakeholders involved in REDD implementation. As Griscom et al. (2009) point out, the selection of reference levels will be based not only on technical and economic considerations, but also on political negotiations among participating countries. REDD projects implemented at the national level will motivate countries to take a strategic position at the negotiation table and try to influence the establishment of crediting levels in their favour. Under these conditions, the adjusted deforestation decision will result in emission reductions of other magnitudes than the ones presented in this study, and might as well reveal a different ranking of baseline approaches. Future research, based on dynamic decision models with multiple players defending contrasting interests, could be relevant for this issue.

Disclosure statement

No potential conflict of interest was reported by the authors.

Notes

1. While REDD gives priority to reducing emissions from deforestation, REDD+ targets additionally the sustainable management of forests and the enhancement of carbon stocks.
2. These emitters could be found among the European polluting companies that are regulated by the EU ETS and need to comply with emission reduction targets.
3. We thank an anonymous referee for the input.
4. We are thankful to an anonymous reviewer for raising this important point.
5. In the paper of Busch et al. (2009, 2011), the owner will 'opt in' if the REDD revenues are higher than the agricultural rental price and 'opt out' otherwise.
6. Reducing the complexity of the harvesting function, which is not central for comparing the reference levels, allows us to focus on the dynamic choice between maintaining the forest cover and harvesting.
7. Using deterministic processes simplifies the solution to the model, but leaves outside of the scope of our analysis the role and influence of risk on the optimal land allocation decision. Under the hypothesis of a risk-neutral landowner, the presence of risk would have no specific effects. However, in the presence of risk aversion, the decision between preservation and deforestation will be significantly impacted by the relative volatility of the two prices and would favour the strategy giving the smallest cash flow variability.
8. We consider this setting to be in line with the reality of many landowners' decision processes in tropical countries. In Latin America, ownership rights tend to be concentrated in the hands of a few proprietors (Brockett 1990; Borras Jr et al. 2012).
9. This time frame is expected to be aligned with the phases of the EU ETS or the successor of the Kyoto protocol.
10. Out of the 6 baseline methodologies reviewed by Griscom et al. (2009), 5 rely partially or totally on historical reference levels.
11. According to Angelsen (2007), 'The FT describes a sequence where a forested region goes through four stages: (1) initially high forest cover and low deforestation, (2) accelerating and high deforestation, (3) slow-down of deforestation and forest cover stabilisation, and (4) a period of reforestation.'
12. According to Huettner et al. (2009), prospective (forward-looking) methods attempt to model land-use change taking into account the various market drivers. The forecasting can be done by using either analytical, regression or simulation models.
13. The *Corridor 1* method proposes that deforestation rates within the corridor accrue credits that would only be eligible for sale once emissions go below the lower boundary of the corridor (Joanneum Research Institute 2006).
14. The analytical results can be provided by the authors upon request.
15. With about 68 million hectares of tropical forest covering nearly 53% of its territory, Peru is fourth in the global ranking, after Brazil, the Democratic Republic of Congo, and Indonesia. About 89% of the total classifies as primary forest (FAO 2010).
16. According to Diaz et al. (2011), the Peruvian and Brazilian Amazon dominate the forest carbon market, with Latin America accountable for about 60% of the 2010 total primary market volume.
17. The annual change in forest area was −0.22% for 2005–2010 (FAO 2010).
18. Hajek et al. (2011) compare 12 local REDD+ projects in south-eastern Peru, 5 of which were at feasibility and 7 at an early implementation stage at the time of writing.
19. Due to the lengthy decision horizon (100 years), we are constrained to select a low value for the discount rate; otherwise, the discounted value of incomes at later periods of time would be very close to zero, rendering irrelevant the decisions further away in the future. This approach is consistent, for instance, with the work of Gollier (2002).
20. Stern (2008) suggests the evaluation of REDD design proposals with the help of three criteria: effectiveness, efficiency, and equity and co-benefits.
21. In the Appendix, we analyse the case of decreasing deforestation paths, where the growth rate of the agricultural composite commodity is low ($\delta = 0$) (see Figure D.9). We find that the ranking of baselines is robust across regions with different trajectories in the deforestation path.
22. For a more detailed illustration of deforestation paths for each period, see Figure B.3 in the Appendix.
23. $d(t)$ is bounded from above by $d_{\mathrm{BaU}}(t)$, due to extraction cost constraints.

24. For the full demonstration, see the Appendix.
25. For a demonstration, see Table E.1 in the Appendix.
26. The score allocated to each baseline takes values from 1 to 4 (4 is the number of baselines considered for comparison: historical, model-implied, upward-biased fixed corridor, and upward-biased variable corridor), such that for each indicator, a score of 4 is awarded to the baseline believed to be most likely to fulfil the criterion, and a score of 1 to the baseline least likely.
27. This might not always be the case; some proposed forward-looking baselines rely on the historical deforestation average as a starting point for predicting future deforestation rates.
28. Misestimations could also occur in the computation of the historical deforestation rate, impacting the financial incentives provided by the historical and fixed-corridor baselines. In this section, we focus only on estimation errors concerning the BaU deforestation path. In our model, this has no impact on the incentives provided by the historical and fixed-corridor methodologies.
29. This refers to relying on less emission intensive sources of energy, such as renewables or the more common switch from coal to gas for the generation of electricity.
30. We thank an anonymous referee for raising this point.
31. We allow for all possible switching points in the range [0, T].
32. Data source is the OSIRIS v.3-4 spreadsheet, available online at http://sp10.conservation.org/osiris/Pages/overview.aspx.
33. Of course, not the entire territory of Peru is covered with forest and eligible for REDD projects. As mentioned in Section 2.3, Peru has about 68 million hectares of tropical forest, covering nearly 53% of its territory.
34. Various international standards have emerged to distinguish between different forest projects, such as the Panda Standard in China.

References

Angelsen, A. 1996. "Deforestation: Population or Market Driven? Different Approaches in Modelling Agricultural Expansion." *Chr. Michelsen Institute Working Paper* 9. http://hdl.handle.net/10202/324

Angelsen, A. 1999. "Agricultural Expansion and Deforestation: Modelling the Impact of Population, Market Forces and Property Rights." *Journal of Development Economics* 58 (1): 185−218.

Angelsen, A. 2007. "Forest Cover Change in Space and Time: Combining the von Thünen and Forest Transition Theories." *The World Bank Policy Research Working Paper*. Washington, DC: World Bank.

Angelsen, A. 2008a. *Moving Ahead with REDD: Issues, Options and Implications*. Bogor: Center for International Forestry Research (CIFOR). http://www.cifor.org/online-library/browse/view-publication/publication/2601.html

Angelsen, A. 2008b. "REDD Models and Baselines." *International Forestry Review* 10 (3): 465−475.

Angelsen, A. 2010. "The 3 REDD I's." *Journal of Forest Economics* 16: 253−256.

Angelsen, A., S. Brown, C. Loisel, L. Peskett, C. Streck, and D. Zarin. 2009. *Reducing Emissions from Deforestation and Forest Degradation (REDD): An Options Assessment Report*. Meridian Institute, Norway. Document prepared for the Government of Norway: http://www.REDD-OAR.org

Assante, P. 2011. "Carbon Sequestration and the Optimal Economic Harvest Decision." PhD thesis, The Faculty of Graduate Studies and Research, Edmonton, Alaberta.

Blom, B., T. Sunderland, and D. Murdiyarso. 2010. "Getting REDD to Work Locally: Lessons Learned from Integrated Conservation and Development Projects." *Environmental Science and Policy* 13 (2): 164−172.

Borras Jr., S.M., J.C. Franco, S. Gomez, C. Kay, and M. Spoor. 2012. "Land Grabbing in Latin America and the Caribbean." *Journal of Peasant Studies* 39: 845−872.

Brockett, C.D. 1990. *Land, Power, and Poverty: Agrarian Transformation and Political Conflict in Central America*. London: Unwin Hyman Publishing House.

Busch, J., F. Godoy, W.R. Turner, and C.A. Harvey. 2011. "Biodiversity Co-Benefits of Reducing Emissions from Deforestation Under Alternative Reference Levels and Levels of Finance." *Conservation Letters* 4 (2): 101−115.

Busch, J., R. Lubowski, F. Godoy, M. Steininger, A. Yusuf, K. Austin, J. Hewson, D. Juhn, M. Farid, and F. Boltz. 2012. "Structuring Economic Incentives to Reduce Emissions from Deforestation within Indonesia". *Proceedings of the National Academy of Sciences* 109 (4): 1062−1067.

Busch, J., B. Strassburg, A. Cattaneo, R. Lubowski, A. Bruner, R. Rice, A. Creed, R. Ashton, and F. Boltz. 2009. "Comparing Climate and Cost Impacts of Reference Levels for Reducing Emissions from Deforestation." *Environmental Research Letters* 4 (October−December 2009): 044006. doi:10.1088/1748−9326/4/4/044006

Cattaneo, A., R. Lubowski, J. Busch, A. Creed, B. Strassburg, F. Boltz, and R. Ashton. 2010. "On International Equity in Reducing Emissions from Deforestation." *Environmental Science & Policy* 13: 742−753.

Chiang, A. 1992. *Elements of Dynamic Optimization*. Singapore: McGraw-Hill International Editions.

Corbera, E., and H. Schroeder. 2011. "Governing and Implementing REDD+." *Environmental Science and Policy* 14: 89−99.

Diaz, D., K. Hamilton, and E. Johnson. 2011. "State of the Forest Carbon Markets 2011: From Canopy to Currency." *Ecosystem Marketplace*. http://www.forest-trends.org/publication_details.php?pub licationID=2963

Doupé, P. 2014. "The Costs of Error in Setting Reference Rates for Reduced Deforestation." *Working paper version* 10 July 2014. http://www.patrickdoupe.net/wp-content/uploads/2014/01/timeSeries.pdf

Entenmann, S., and C. Schmitt. 2013. "Actors' Perceptions of Forest Biodiversity Values and Policy Issues Related to REDD+ Implementation in Peru." *Biodiversity and Conservation* 22: 1229−1254.

FAO (Food and Agriculture Organization). 2005. *Peru Country Profile*. Rome: Forest Area Statistics, FAO Global Forest Resources Assessment 2005.

FAO. 2010. *Global Forest Resources Assessment Main report* (Technical Report). Rome: Food and Agriculture Organization of the United Nations. http://www.fao.org/docrep/013/i1757e/i1757e.pdf

FCPF Carbon Fund. 2013. *FCPF Carbon Fund Methodological Framework* (Technical Report). Forest Carbon Partnership Facility. https://www.forestcarbonpartnership.org/sites/fcp/files/2013/Dec2013/FCFP%20Annual%20Report_2013_0.pdf

Gollier, C. 2002. "Time Horizon and the Discount Rate." *Journal of Economic Theory* 107 (2): 463−473.

Griscom, B., D. Shoch, B. Stanley, R. Cortez, and N. Virgilio. 2009. "Sensitivity of Amounts and Distribution of Tropical Forest Carbon Credits Depending on Baseline Rules." *Environmental Science and Policy* 12: 897−911.

Hajek, F., M. Ventresca, J. Scriven, and A. Castro. 2011. "Regime-Building for REDD+: Evidence from a Cluster of Local Initiatives in South-Eastern Peru." *Environmental Science and Policy* 14: 201−215.

Huettner, M., R. Leemans, K. Kok, and J. Ebeling. 2009. "A Comparison of Baseline Methodologies for 'Reducing Emissions from Deforestation and Degradation'." *Carbon Balance and Management* 4 (4). http://www.cbmjournal.com/content/4/July/2009

Irawan, S., L. Tacconi, and I. Ring. 2013. "Shareholders' Incentives for Land-Use Change and REDD+: The Case of Indonesia." *Ecological Economics* 87: 75−83.

ITTO (International Tropical Timber Organization). 2010. *Annual Review and Assessment of the World Timber Situation 2010*. Yokohama: Division of Economic Information and Market Intelligence, ITTO. http://www.itto.int/annual_review/

Joanneum Research Institute of Energy Research. 2006. *Reducing Emissions from Deforestation in Developing Countries: Potential Policy Approaches and Positive Incentives (Submission to the UNFCCC/SBSTA)* (Technical Report). Joanneum Research Institute of Energy Research, Union of Concerned Scientists, Woods Hole Research Center, Instituto de Pesquisa Ambiental da Amazonia.

Kindermann, G., M. Obersteiner, B. Sohngen, J. Sathaye, K. Andrasko, E. Rametsteiner, B. Schlamadinger, S. Wunder, and R. Beach. 2008. "Global Cost Estimates of Reducing Carbon Emissions Through Avoided Deforestation." *Proceedings of the National Academy of Sciences* 105: 10302−10307.

Lu, H., and G. Liu. 2013. "Distributed Land Use Modeling and Sensitivity Analysis for REDD+." *Land Use Policy* 33: 54−60.

Mosnier, A., P. Havlik, M. Obersteiner, K. Aoki, E. Schmid, S. Fritz, I. McCallum, and S. Leduc. 2014. "Modeling Impact of Development Trajectories and a Global Agreement on Reducing Emissions from Deforestation on Congo Basin Forests by 2030." *Environmental and Resource Economics* 57: 505−525.

NIFCI (Norway's International Forest and Climate Initiative). 2011. *Real-Time Evaluation of Norway's International Forest and Climate Initiative. Contributions to National REDD+ Processes 2007-2010* (Technical Report). NIFCI. http://www.climatefundsupdate.org/listing/norway-s-international-climate-and-forest-initiative

Ollivier, H. 2012. "Growth, Deforestation and the Efficiency of the REDD Mechanism." *Journal of Environmental Economics and Management* 64: 312−327.

Palmer, C. 2010. "Property Right and Liability for Deforestation Under REDD+: Implications for 'Permanence' in Policy Design." *Ecological Economics* 70: 571−576.

Parker, C., A. Mitchell, M. Trivedi, and N. Mardas. 2008. *The Little REDD Book: A Guide to Governmental and Non-Governmental Proposals for Reducing Emissions from Deforestation and Degradation*. Oxford: Global Canopy Programme.

Penman, J., M. Gytarsky, T. Hiraishi, T. Krug, D. Kruger, R. Pipatti, L. Buendia, K. Miwa, T. Ngara, K. Tanabe, and F. Wagner, 2003. *Good Practice Guidance for Land Use, Land Use Change and Forestry*. Geneva: Intergovernmental Panel on Climate Change, Institute for Global Environmental Strategies.

Pfaff, A., G. Amacher, and E. Sills. 2013. "Realistic REDD: Improving the Forest Impacts of Domestic Policies in Different Settings." *Review of Environmental Economics and Policy* 7 (1): 114−135.

Sathaye, J., K. Andrasko, and P. Chan. 2011. "Emissions Scenarios, Costs, and Implementation Considerations of REDD-Plus Programs." *Environment and Development Economics* 16: 361−380.

Schlamadinger, B., L. Ciccarese, M. Dutschlke, P. Fearnside, S. Brown, and D. Mudiyarso. 2005. "Should We Include Avoidance of Deforestation in the International Response to Climate Change?" In *Proceedings of Workshop on Carbon Sequestration and Sustainable Livelihoods*, Bogor, 16−17 February 2005.

Stern, N. 2008. *Key Elements of a Global Deal on Climate Change*. London: London School of Economics and Political Science.

The German REDD Early Movers Program. 2014. http://theredddesk.org/markets-standards/germanys-redd-early-movers-programm e.

von Thünen, J. 1826. *Der isolierte Staat in Beziehung auf Landwirtschaft und Nationalökonomie* [The Isolated State in Relation to Agriculture and National Economics]. Berlin: Akademie Verlag.

UNFCCC (Bonn: United Nations Framework Convention on Climate Change). 2009. *Decision 4/CP.15: Methodological Guidance for Activities Relating to Reducing Emissions from Deforestation and Forest Degradation and the Role of Conservation, Sustainable Management of Forests and Enhancement of Forest Carbon Stocks in Developing Countries* (Technical Report). Bonn: UNFCCC.

Verburg, P.H., P.P. Schot, M.J. Dijst, and A. Veldkamp, 2004. "Land Use Change Modelling: Current Practice and Research Priorities." *GeoJournal* 61: 309−324.

Verissimo, A., P. Barreto, M. Mattos, R. Tarifa, and C. Uhl. 1992. "Logging Impacts and Prospects for Sustainable Forest Management in an Old Amazonian Frontier: The Case of Paragominas." *Forest Ecology and Management* 55: 169−199.

Vitel, C.S.M.N., G.C. Carrero, M.C. Cenamo, M. Leroy, P.M.L.A. Graça, and P.M. Fearnside. 2013. "Land-Use Change Modeling in a Brazilian Indigenous Reserve: Construction of a Reference Scenario for the Suruí REDD Project." *Human Ecology* 41 (6): 807−826.

Wassenaar, T., P. Gerbera, P. Verburg, M. Rosales, M. Ibrahim, and H. Steinfeld. 2007. "Projecting Land Use Changes in the Neotropics: The Geography of Pasture Expansion into Forest." *Global Environmental Change* 17: 86−104.

van der Werf, G.R., D. Morton, R. DeFries, J.G.J. Olivier, P.S. Kasibhatla, R.B. Jackson, G. Collatz, and J.T. Randerson. 2009. "CO_2 Emissions from Forest Loss." *Nature Geoscience* 2: 737−738.

Appendix

A. Optimal deforestation path in the business-as-usual scenario

When no REDD programme is in place, the net revenue of the landowner at time t is given by

$$\pi\Big(d(t)\Big) = P^{cc}(t)d(t) - \Big(a_1 d(t) + a_2 d(t)^2\Big) \tag{A.1}$$

The optimal control problem can be described as follows:

$$\max_{(d(t))_{t\in[0,T]}} \int_0^T e^{-rt}\pi\Big(d(t)\Big)dt \tag{A.2}$$

$$\text{such } \dot{F} = -d(t) \tag{A.3}$$

$$F(0) = F_0 \tag{A.4}$$

We build the current-value Hamiltonian as

$$H^c = \pi\Big(d(t)\Big) - \mu d(t) \tag{A.5}$$

The equations of motion follow immediately:

$$\frac{\partial H^c}{\partial d(t)} : \pi'\Big(d(t)\Big) - \mu = 0 \tag{A.6}$$

$$-\frac{\partial H^c}{\partial F} + r\mu = \dot{\mu} \tag{A.7}$$

$$\dot{F} = -d(t) \tag{A.8}$$

The partial derivative of the Hamiltonian with respect to the forest stock is zero $\left(\frac{\partial H^c}{\partial F} = 0\right)$. We obtain from Equation (A.7) that

$$\dot{\mu} = r\mu \Rightarrow d\mu = \mu r dt \Rightarrow \mu(t) = \mu(0)e^{rt} \tag{A.9}$$

From Equation (A.6) we know that $\pi'(d(t)) = \mu(t)$, which holds for all $t \in [0, T]$. It follows that $\pi'(d(0)) = \mu(0)$. Introducing this result in Equation (A.9), we obtain that

$$\pi'\Big(d(t)\Big) = \pi'\Big(d(0)\Big)e^{rt} \tag{A.10}$$

We explicit Equation (A.10) with the help of the profit function given in Equation (A.1). After some simplifications, the optimal deforestation rate at time t is given by

$$d(t) = d(0)e^{rt} + \frac{P^{cc}(0)(e^{\delta t} - e^{rt}) - a_1(1 - e^{rt})}{2a_2} \tag{A.11}$$

The optimal deforestation at time t depends on the initial deforestation rate ($d(0)$), the discount rate (r), the initial price of the composite commodity ($P^{cc}(0)$) and its growth function (δ), and the parameters of the cost function (a_1, a_2). In order to define the optimal deforestation path, the last element that needs to be defined is the initial deforestation rate ($d(0)$). We iterate over a large grid of possible values and choose the initial deforestation that maximises total profits.

B. Optimal deforestation path under REDD

The simultaneous presence of REDD rewards for lower-than-baseline and absence of penalties for higher-than-baseline deforestation levels brings discontinuities to the profit function. The resulting non-smoothness in the objective function impedes the application of standard optimisation methods. To overcome this difficulty, we develop a solution approach based on regime switches. This method allows for a break in the continuity of the deforestation path, which would otherwise be forced under the standard Hamiltonian procedure. A smooth deforestation path would not be able to guarantee optimality in the context of a non-smooth objective function. Here, we allow the landowner to decide at each moment of time whether to deforest below or above the reference level, i.e. they make their choice between a *REDD regime* (hereafter Regime 1) and a *BaU regime* akin to BaU (hereafter Regime 2).

One observation is key to solving the optimisation problem: in the absence of stochasticities, the decision regarding deforestation levels at each moment of time can be taken from the beginning for all future periods. While it could be possible in theory that the landowner switches between regimes multiple times, in practice the dynamic requirement at equilibrium ensures smooth evolution for the deforestation path within each regime and limited shifts between regimes over the entire horizon. We begin by explaining the solution approach for the historical and the model-implied cases. Since it requires an additional modification, we present the solution to the corridor scenario at the end of this section.

For the historical and the model-implied baselines, the landowner chooses low deforestation rates and stays in Regime 1 as long as the total benefits from REDD and forest exploitation below the reference level remain higher that the total benefits from forest exploitation above the reference level. Depending on the values of the parameters, the regime switch can occur either from the beginning, somewhere during the lifetime of the maximisation period, or never at all. Formally, the optimisation procedure can be described as follows:

$$\max_{d(t)|t\in[0,T]} \left\{ \int_0^{\tau} e^{-rt}\pi^{R_1}\Big(d(t)\Big)dt + \int_{\tau}^{T} e^{-rt}\pi^{R_2}(d(t))dt \right\} \tag{B.1}$$

with R_1 and R_2 standing for Regime 1 and Regime 2, respectively. τ is the switching time from Regime 1 to Regime 2:

$$\tau = \inf\{t \geq 0 | d(t) \geq dB\} \tag{B.2}$$

We adapt the solution method of Chiang (1992) to allow for regime switches. The current-value Hamiltonian is defined as

$$H^c = \begin{cases} H^{R_1} = \pi^{R_1}(d(t)) - \mu_1(t)d(t), & \text{if } t \in [0, \tau) \\ H^{R_2} = \pi^{R_2}(d(t)) - \mu_2(t)d(t), & \text{if } t \in [\tau, T] \end{cases} \tag{B.3}$$

It is important to underline that if Regime 1 occurs in our parametrisation, it will precede Regime 2, due to the different profit dynamics of the two activities. On one hand, the landowner can gain from intensifying forest exploitation, as long as their inflows do not exceed operating costs. In time, their revenues rise due to the increasing price of the composite commodity. On the other hand, even if revenues from REDD increase due to rising permit prices, these profits are limited, since the deforestation rate is bounded from above by the reference level and from below by zero (we do not allow for reforestation). Therefore, even if initially marginal benefits with REDD could be higher than BaU marginal benefits, this advantage would decrease over time. As a consequence, remaining in Regime 1 could become suboptimal at a certain moment of time (τ), after which the landowner will move to Regime 2.

Figure B.1 captures dominant profits of either REDD or BaU regimes at different deforestation rates. The hashed area represents cases where taking part in the REDD project is optimal, while the grey area symbolises regions where the BaU scenario is optimal. Within each section of the graph, lighter colours stand for higher profit values. As long as the deforestation rate is below the fixed baseline, the optimal regime to choose is the REDD one (see Figure B.2). This holds for initial time periods. As time passes, the overall optimum is to be found in the BaU regime. The two figures

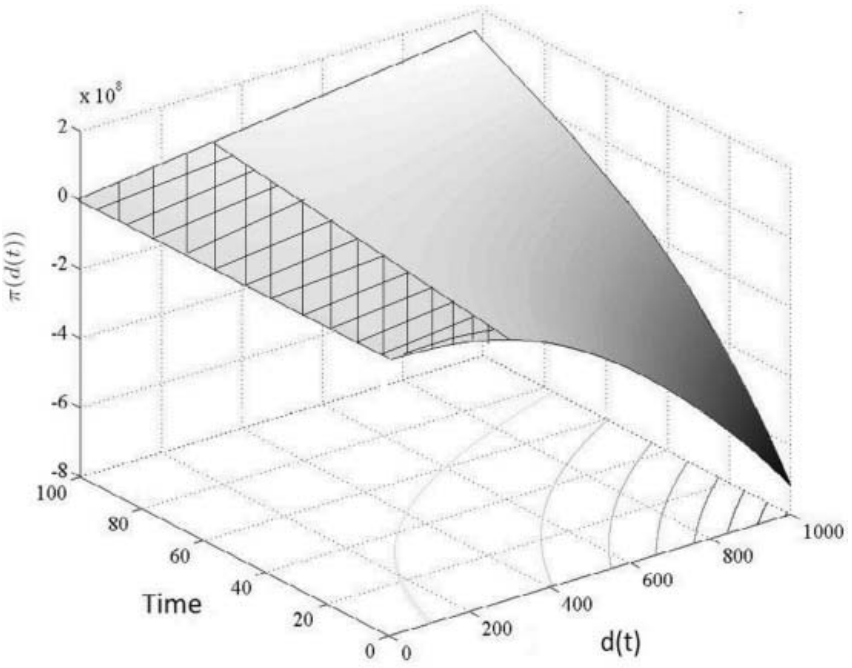

Figure B.1. Land-use revenues.

show that if a regime switch does occur at some moment of time, this switch is expected to take place one time only, as the dominance alternation takes place only once. Moreover, Figure B.1 shows that the REDD regime should precede the BaU regime, since for later periods of time profits are increasing in the deforestation rate and the landowner will be better off opting for the BaU

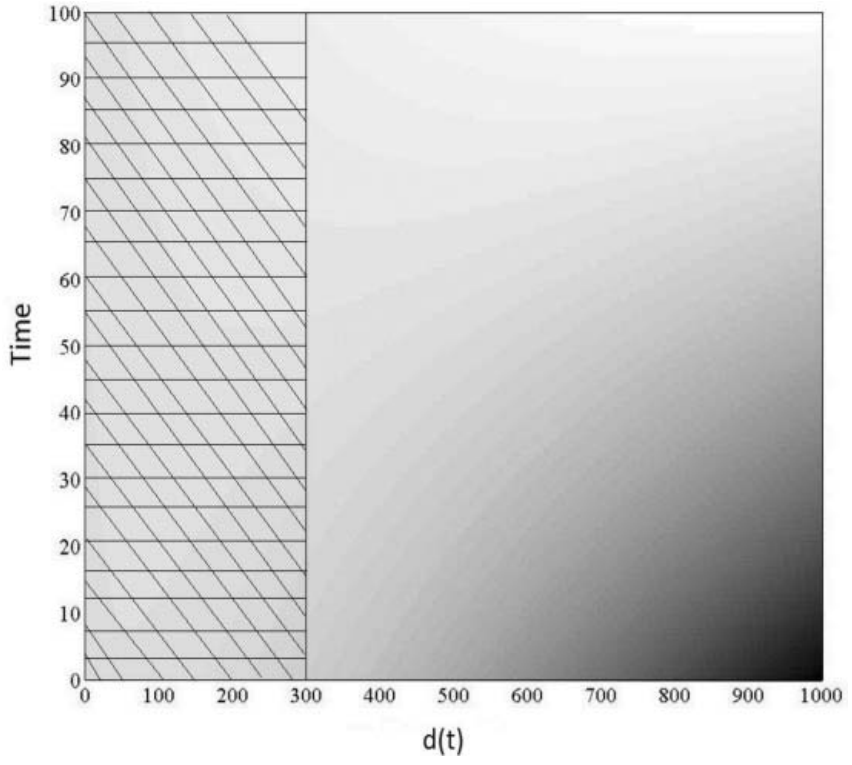

Figure B.2. Land-use revenues (view from top).

regime. The solution for the optimal deforestation path is given by

$$d(t) = \begin{cases} d(0)e^{rt} + \dfrac{P^{cc}(0)(e^{\delta t} - e^{rt}) - a_1(1 - e^{rt}) - P^R(0)(e^{\gamma t} - e^{rt})}{2a_2}, & \text{if } t \in [0, \tau) \\ d(\tau)e^{rt} + \dfrac{P^{cc}(\tau)(e^{\delta t} - e^{rt}) - a_1(1 - e^{rt})}{2a_2}, & \text{if } t \in [\tau, T] \end{cases} \tag{B.4}$$

Considering the lack of continuity at τ, we solve the landowner's maximisation using a numerical search algorithm that combines all possible combinations of Regime 1 and Regime 2 paths at different switching points.[31] We select the combined path that yields the highest profits.

In the case of the corridor scenarios, the profit function is non-smooth at two points, i.e. at the boundaries of the corridor (dB^U and dB^L for the fixed; dB^U and dB^L for the variable); the landowner will be able to switch between three different regimes. Depending on the relationship between initial parameter values, they will choose an optimal deforested area that satisfies

$$d(t) = \begin{cases} d(0)e^{rt} + \dfrac{P^{cc}(0)(e^{\delta t} -, e^{rt}) - a_1(1 - e^{rt}) - P^R(0)(e^{\gamma t} -, e^{rt})}{2a_2}, & \text{if } t \in [0, \tau_1) \\ d(\tau_1)e^{rt}\dfrac{a_2 - \dfrac{P^R(\tau_1)}{dB^U - dB^L}}{a_2 - \dfrac{P^R(\tau_1)e^{\gamma t}}{dB^U - dB^L}} + \dfrac{P^{cc}(\tau_1)(e^{\delta t} -, e^{rt}) - a_1(1 -, e^{rt}) - P^R(\tau_1)(e^{\gamma t} -, e^{rt})\left(1 + \dfrac{dB^U + dB^L}{dB^U - dB^L}\right)}{2\left(a_2 - \dfrac{P^R(\tau_1)e^{\gamma t}}{dB^U - dB^L}\right)}, & \text{if } t \in [\tau_1, \tau_2) \\ d(\tau_2)e^{rt} + \dfrac{P^{cc}(\tau_2)(e^{\delta t} -, e^{rt}) - a_1(1 - e^{rt})}{2a_2}, & \text{if } t \in [\tau_2, T] \end{cases} \tag{B.5}$$

in the fixed-corridor case. For the variable corridor, the optimal deforestation rate will take the same form, with $dB^U(t)$ and $dB^L(t)$ replacing dB^U and dB^L, respectively. In our setting, the order of the switching times ($0 \leq \tau_1 \leq \tau_2 \leq T$) is due to the combination of two characteristics of our model. First, the benefits of taking part in REDD decrease over time: for later periods, net revenues from land exploitation outpace REDD revenues due to higher composite commodity prices and larger deforestation rates. Second, REDD gains get marginally smaller as the deforestation level gets closer to the upper corridor boundary until it eventually fades away for rates above the corridor. Therefore, the motivation to stay in REDD decreases over time, but at different paces within each

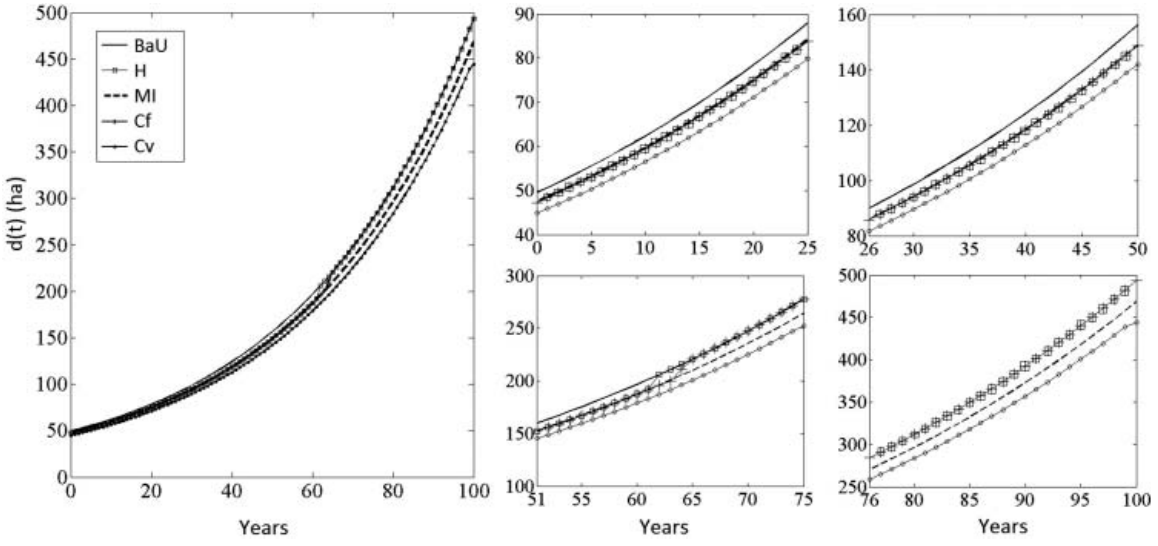

Figure B.3. Optimal deforestation paths under BaU and different REDD baselines, detailed for sub-periods of 25 years.

interval. The landowner's optimisation problem accounts for three possible regimes:

$$\max_{d(t)|t\in[0,T]} \left\{ \int_0^{\tau_1} e^{-rt}, \pi^{R_1}\Big(d(t)\Big)dt + \int_{\tau_1}^{\tau_2}, e^{-rt}, \pi^{R_2}\Big(d(t)\Big)dt + \int_{\tau_2}^{T}, e^{-rt}, \pi^{R_3}\Big(d(t)\Big)dt \right\} \tag{B.5}$$

To determine the optimal regime switching times (τ_1 and τ_2), we first define optimal paths within each regime for all possible combinations of switching times. We then use a numerical search algorithm that selects the combination of the three paths yielding the highest profits.

Figure B.3 captures the optimal deforestation path for the BaU and the four REDD baseline methodologies. The large box on the left-hand side refers to the entire deforestation path, reproducing the results in Figure 1. To better understand the differences in optimal deforestation for each baseline, we detail in the other boxes on the right-hand side the deforestation path for sub-periods of 25 years each.

C. Efficiency of the single-threshold and corridor approaches

Proposition: The single-threshold baseline approach is more efficient than the corresponding corridor approach, that is,

$$E_3^{\mathrm{H}} \leq E_3^{\mathrm{Cf}} \tag{C.1}$$

$$E_3^{\mathrm{MI}} \leq E_3^{\mathrm{Cv}} \tag{C.2}$$

where $E_3^i = \frac{SRR^i}{S_{\mathrm{Tot}}^{\mathrm{BaU}} - S_{\mathrm{Tot}}^i}$, where $SRR^i = \int^T{}_0 RR^i(t)dt$, $S^i{}_{\mathrm{Tot}} = \int_0{}^T d^i(t)dt$, $i \in \{\mathrm{H}, \mathrm{MI}, \mathrm{Cf}, \mathrm{Cv}\}$, and BaU stands for business-as-usual.

Proof: Let *ST* refer to the single-threshold approach and *C* to the corresponding corridor approach. For the proof, we will use three results from Section 3.1. First, relations (15) and (16) in Section 3.1 show that

$$RR^{ST}(t) \leq RR^{C}(t) \tag{C.3}$$

Since relation (C.3) holds $\forall t \in [0; T]$, we can write that

$$\int_0^T RR^{ST}(t)dt \leq \int_0^T RR^{C}(t)dt \Leftrightarrow SRR^{ST} \leq SRR^{C} \tag{C.4}$$

Let us denote then

$$SRR^{ST} = (1-a)SRR^{C} \tag{C.5}$$

with $a \in [0; 1]$ such that relation (C.5) is satisfied.

Second, relations (17) and (18) in Section 3.1 show that

$$E_1^{ST} \leq E_1^{C} \tag{C.6}$$

From the definition of $E^i{}_1$, it follows that

$$\frac{S_{\mathrm{Tot}}^{\mathrm{BaU}} - S_{\mathrm{Tot}}^{ST}}{S_{\mathrm{Tot}}^{\mathrm{BaU}}} \leq \frac{S_{\mathrm{Tot}}^{\mathrm{BaU}} - S_{\mathrm{Tot}}^{C}}{S_{\mathrm{Tot}}^{\mathrm{BaU}}} \Leftrightarrow S_{\mathrm{Tot}}^{\mathrm{BaU}} - S_{\mathrm{Tot}}^{ST} \leq S_{\mathrm{Tot}}^{\mathrm{BaU}} - S_{\mathrm{Tot}}^{C} \tag{C.7}$$

Let us denote then

$$S_{\text{Tot}}^{\text{BaU}} - S_{\text{Tot}}^{ST} = (1-b)\left(S_{\text{Tot}}^{\text{BaU}} - S_{\text{Tot}}^{C}\right) \tag{C.8}$$

where $b \in [0; 1]$ such that relation (C.7) is satisfied.

Third, we observe from Table 4 that $a > b$, i.e. the percentage gain in welfare (a) achieved by the corridor relative to the single-threshold approach is larger than its gain in effectiveness (b). Therefore, accounting for relations (C.5) and (C.8), we can compare the efficiency of the single-threshold and corridor approaches:

$$E_3^{ST} - E_3^{C} = \frac{SRR^{ST}}{S_{\text{Tot}}^{\text{BaU}} - S_{\text{Tot}}^{ST}} - \frac{SRR^{C}}{S_{\text{Tot}}^{\text{BaU}} - S_{\text{Tot}}^{C}} = \frac{(1-a)SRR^{C}}{(1-b)(S_{\text{Tot}}^{\text{BaU}} - S_{\text{Tot}}^{C})} - \frac{SRR^{C}}{S_{\text{Tot}}^{\text{BaU}} - S_{\text{Tot}}^{C}} \tag{C.9}$$

$$E_3^{ST} - E_3^{C} = \frac{SRR^{C}}{S_{\text{Tot}}^{\text{BaU}} - S_{\text{Tot}}^{C}} \frac{b-a}{1-b} \tag{C.10}$$

With $a > b$, we get that

$$E_3^{ST} \leq E_3^{C} \tag{C.11}$$

D. Parameter calibration and sensitivity analysis

This section verifies the robustness of our results to several key calibration parameters, namely the carbon content of the forest, the discount rate, and the growth rates of the composite commodity and REDD permit prices.

D1. Forest carbon content (Ω)

REDD programmes aim to achieve reductions in emissions from deforestation below BaU levels. While deforestation can be measured in terms of hectares of land where forest has been removed, the GHG emissions coming from deforestation depend on the carbon content stored in the trees. The carbon content of one hectare of forest can vary across geographical regions, depending on tree type and forest density.

Across the REDD candidate countries, the average carbon content varies widely. Figure D.1 captures the distribution of the average above and below ground carbon content of 85 REDD countries, grouped according to their deforestation patterns and the geographical region.[32] The variability of the carbon content is very large even within each geographical and forest transition theory (FTT) group.

The forest carbon content varies not only from country to country, but also within countries. Figure D.3 shows the above ground carbon content across the territory of Peru,[33] which takes values from 0 to more than 150 tC/ha. The existence of large differences between the carbon content of different regions brings a strong argument for the need to design REDD projects that take into account regional characteristics.

The success of REDD is likely to depend on its ability to provide payments that correctly reflect the carbon content of each project area. We test the sensitivity of the baseline performance to different levels of carbon content per hectare of forest. This setting depicts a situation where REDD projects are implemented in several regions of a country, with the average carbon content varying from region to region. Holding everything else constant, we assume identical conditions regarding the composite commodity and REDD permit markets across the different regions.

Figure D.2 illustrates the performance of the four REDD baselines across different levels of average carbon content. It demonstrates the robustness of the baseline ranking presented in

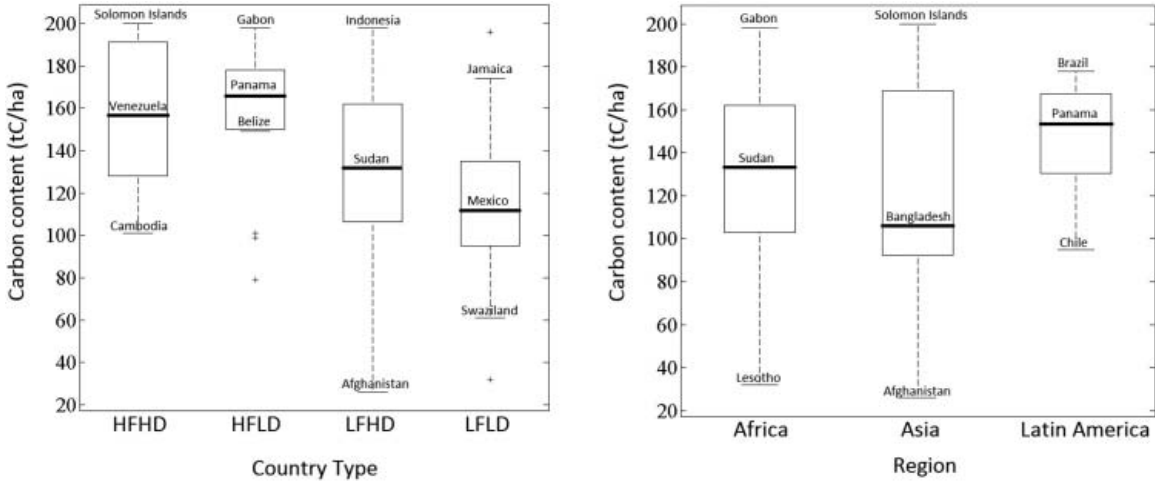

Figure D.1. Distributions of the average above and below ground carbon contents across different stages of FTT and world regions.
Notes: The right-hand panel groups countries according to the geographical region. The left-hand panel groups countries based on their deforestation patterns according to the FTT. HFHD is high forest, high deforestation; HFLD is high forest, low deforestation; LFHD is low forest, high deforestation; LFLD is low forest, low deforestation. *Source*: Authors' own calculations based on OSIRIS v.3-4.

Section 3.1. The variable corridor (Cv) continues to be the most effective in reducing deforestation. The fixed corridor (Cf) offers the highest increase in welfare from BaU. The model-implied baseline (MI) is the most efficient, having the lowest costs per hectare of avoided deforestation.

Additionally, we observe an increase in the difference in performance of the static versus dynamic baselines at higher carbon contents. The results are particularly interesting in terms of effectiveness; it results that REDD projects employing the variable-corridor (Cv) approach will have a high potential in reducing deforestation and the inherent GHG emissions, especially if they target high carbon content (HCC) areas. With the current international fora inclined to direct REDD programmes towards HCC areas, it appears especially important to understand and underline the benefits of the variable-corridor approach.

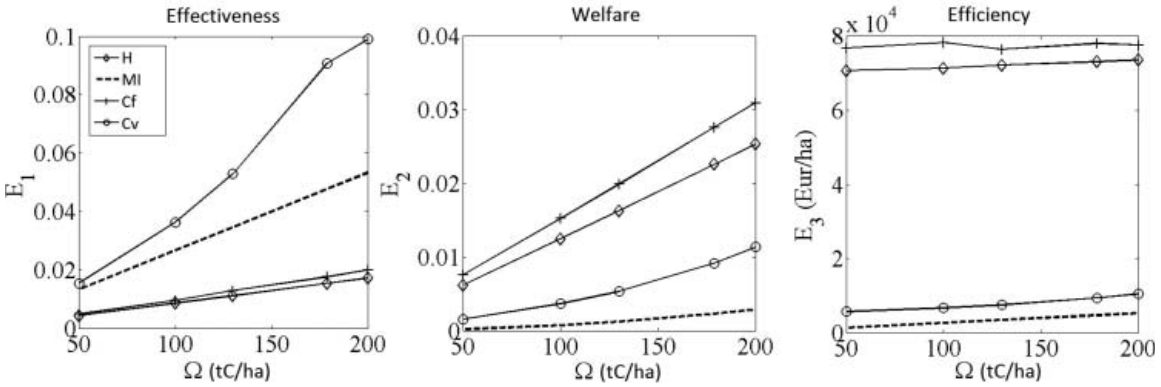

Figure D.2. Baseline performance across different average forest carbon contents (Ω).
Notes: The figure captures the performance of the four baselines for different average carbon contents per hectare of forest. The historical deforestation rate (*dB*) is 200 ha/year. Corridor width is $x = 0.1$.

*D2. Crediting threshold in the static baselines (*dB*)*

In this section, we verify the change in the performance of the static baseline approaches to different crediting levels. The REDD rewards of the historical and fixed-corridor approaches depend on the fixed threshold *dB* (Table 5). As mentioned in the baseline presentation (Section 2.2), the fixed threshold can be set equal to the average past deforestation in the area. Aside from data availability and estimation issues, linking rewards to a single value over a larger horizon can result in payments

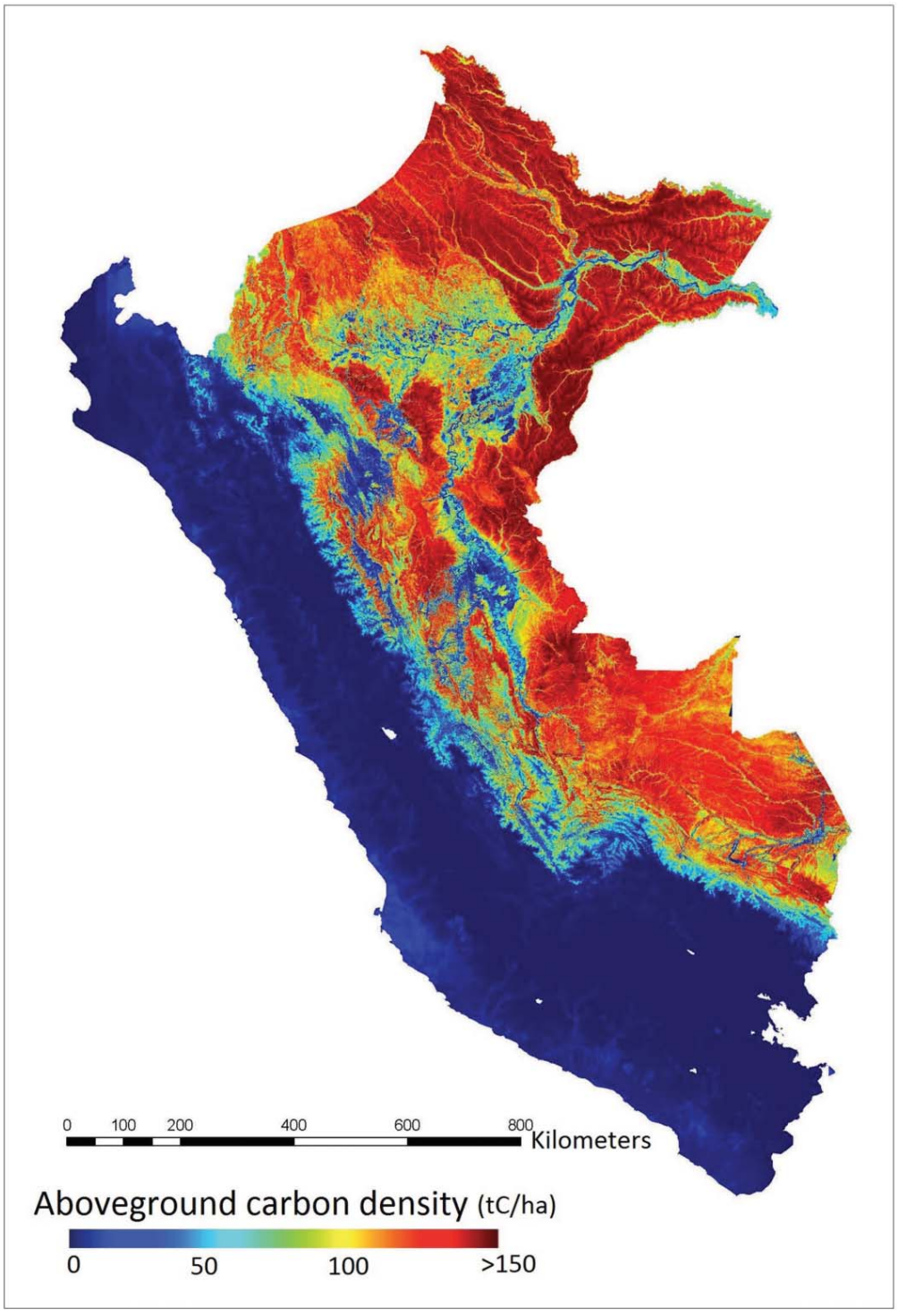

Figure D.3. Above ground carbon content in Peru.
Source: *The High-resolution Carbon Geography of Peru*, Carnegie Institution for Science, 2014, available online at http://carnegiescience.edu/news/per%C3%BA%E2%80%99s_carbon_quantified_economic_and_conservation_boon.

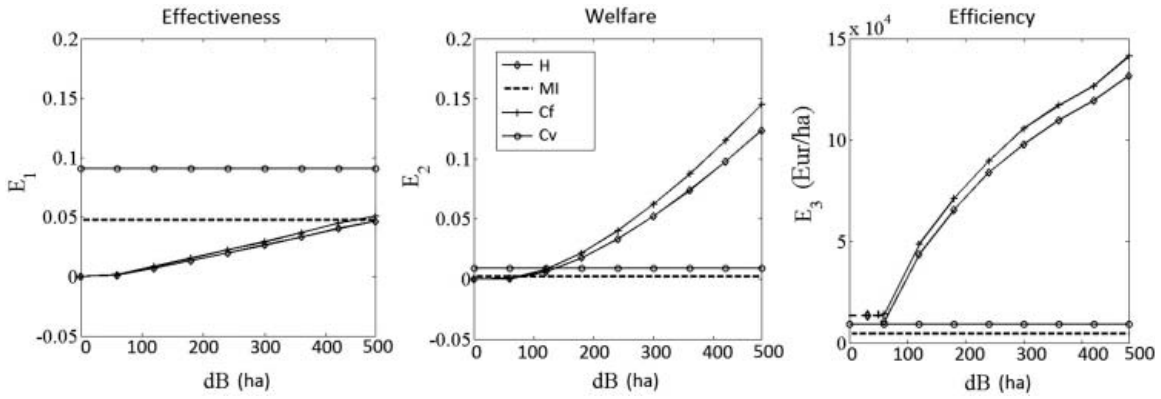

Figure D.4. Baseline performance across different fixed thresholds.
Notes: The ranking of the four baselines changes across different historical deforestation rates. For the historical and fixed-corridor baselines, efficiency is not defined for deforestation averages below 60 ha/year, where deforestation reduction and REDD costs are zero. Corridor width is $x = x_0 = 0.1$.

that reflect only partially actual efforts. There remains a certain level of risk involved in choosing a fixed threshold, and we check now the sensitivity of baseline performance to various levels (*dB*) against which rewards are accrued for the historical and fixed-corridor schemes. The results are displayed in Figure D.4. We find that the ranking of baselines is robust to variations in the fixed threshold level *dB*. The historical and the fixed-corridor baselines gain ground at larger fixed thresholds, in terms of both effectiveness and welfare. However, these improvements come at the high cost of large losses in efficiency.

The increase in welfare at higher *dB* follows from the fact that the REDD revenues of the historical and fixed-corridor schemes are an increasing function of the fixed threshold. This is confirmed by the positive partial derivatives of the REDD revenue functions of the static baselines with respect to *dB*. Moreover, the higher REDD revenues foster increases in effectiveness, but also reductions in efficiency.

Our findings show that, if a static baseline is selected, the fixed threshold should be set above the average predicted deforestation rate in order to achieve stronger effectiveness and welfare results.

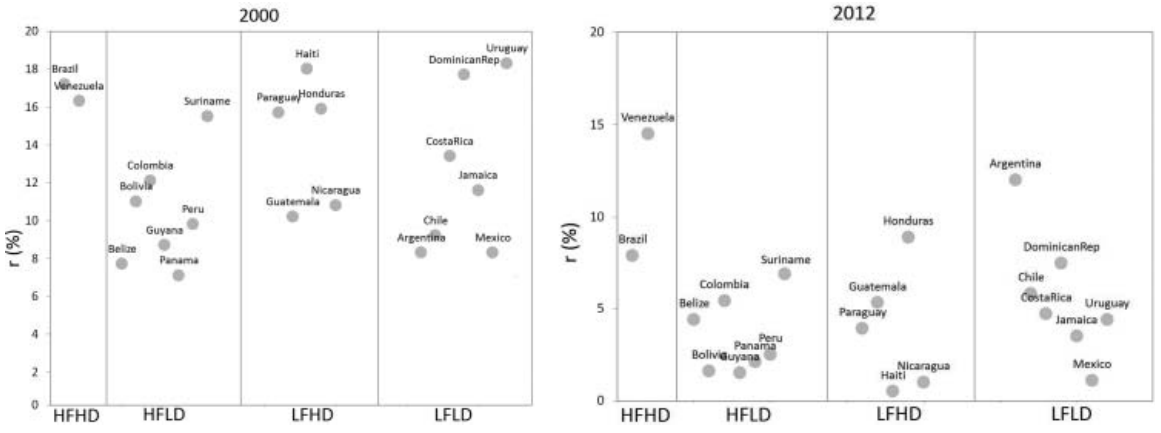

Figure D.5. Deposit rates (*r*) in the Latin America region in the years 2000 and 2012.
Source: Authors' own graphical representation based on the data provided by the World Bank, World Development Indicators, available online at http://wdi.worldbank.org/table/4.15.

D3. Discount rate (r)

In our initial calibration, the discount rate was chosen slightly below the growth rates of the composite commodity and REDD permit prices, depicting a setting in which forest exploitation and REDD bring higher financial benefits than saving at the discount rate. However, the discount rate in many developing countries varies widely from country to country and across time. Figure D.5 shows the discount rates for the years 2000 and 2012 in the Latin America region, with r taking values in the range [0.5%, 19.5%].

We test the sensitivity of our results to changes in the discount rate. Figure D.6 shows the total deforested area under BaU and the four REDD baseline methodologies. The BaU optimal deforestation rate is a decreasing function in r (Equation (A.11)), with higher impacts at later periods of time (as t approaches T). We detail the impact on the static and the dynamic baselines separately:

- Higher discount rates reduce the total deforestation of the static baselines. The landowner switches from REDD to BaU in the second part of the optimisation horizon (see Figure D.7). After the switch, the optimal deforestation follows the BaU path, achieving reductions in deforestation due to higher r.
- For the prospective baselines, whose reference levels depend on the BaU deforestation ($dB(t) = d_{\mathrm{BaU}}(t)$), the impact of an increase in r on total deforestation is non-monotonous. The plots of total deforestation at different r present an inflection point (at $r = 8\%$ for MI and $r = 2\%$ for Cv). For r lower than the inflection point, an increase in r leads to a decrease in total deforestation; for r higher than the inflection point, an increase in r leads to higher deforestation. Below the inflection point, an increase in r results in lower $dB(t)$, requiring stronger reductions in deforestation for obtaining the same REDD profits. Reducing the deforestation rate pays off until some point (the inflection point), above which the time-varying threshold is so low that the opportunity costs of REDD exceed the benefits, and the landowner is better off following the BaU scenario (exiting REDD and increasing deforestation) (see Figure D.7).

Figure D.8 shows that the ranking of baselines across the three performance measures is robust across different discount rates. Additionally, for higher discount rates, the difference in

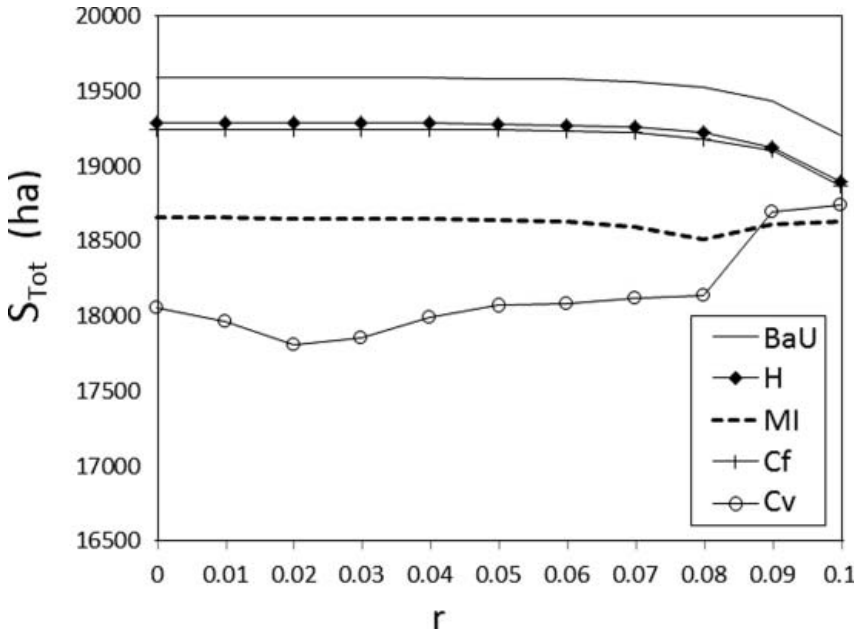

Figure D.6. Total deforestation across different baselines and discount rates (r).

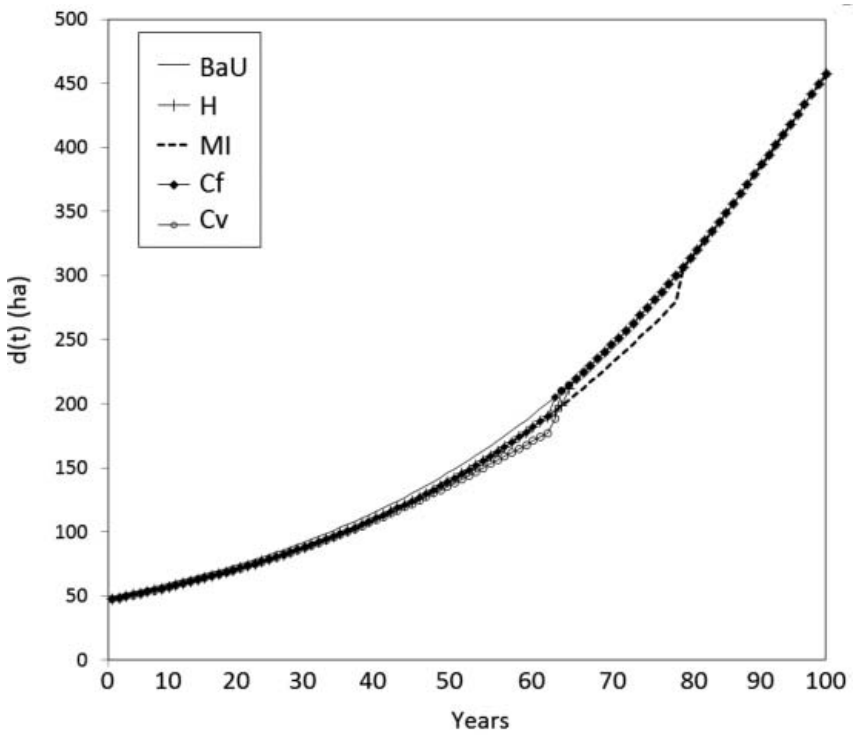

Figure D.7. Optimal deforestation across different baselines ($r = 0.1$).

performance between the static and dynamic baselines decreases in terms of effectiveness and efficiency, but widens considerably in terms of welfare. The results need to be interpreted carefully. Firstly, at higher r, both BaU and static baselines result in lower total welfare. The impact of higher r on the change in welfare from BaU is measured by the E_2 indicator. With the income under the static baselines decreasing less than the BaU income, the percentage change in welfare appears to be increasing, despite the fact that welfare itself is decreasing in r.

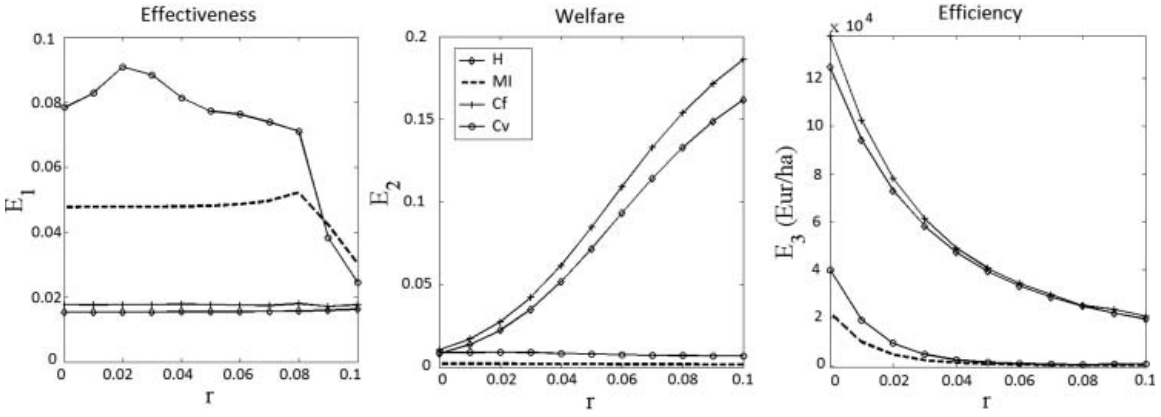

Figure D.8. Baseline performance across different discount rates (r).
Notes: The figure captures the performance of the four baselines for different discount rates. The historical deforestation rate (dB) is at 200 ha/year. Corridor width is $x = 0.1$.

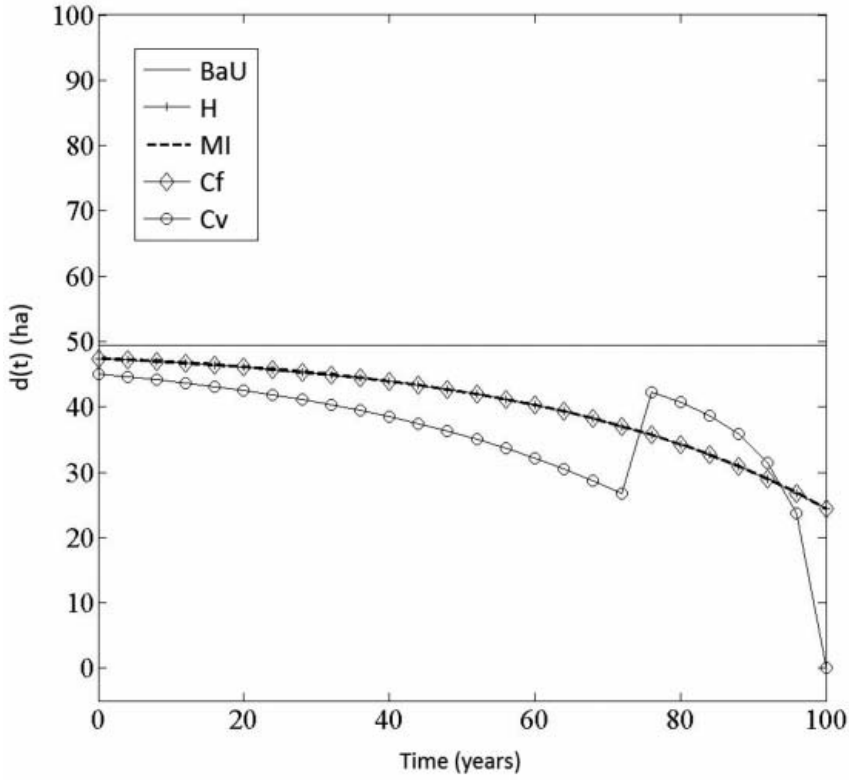

Figure D.9. Optimal deforestation across different baselines ($\delta = 0$).

Second, with efficiency measured as total discounted REDD revenues per hectares of avoided deforestation (the E_3 indicator), an increase in r reduces heavily the nominator (lower total discounted revenues), without increasing the forest area saved (we have seen that effectiveness is constant across different r). The improvement in efficiency at higher r is, therefore, just a discounting effect.

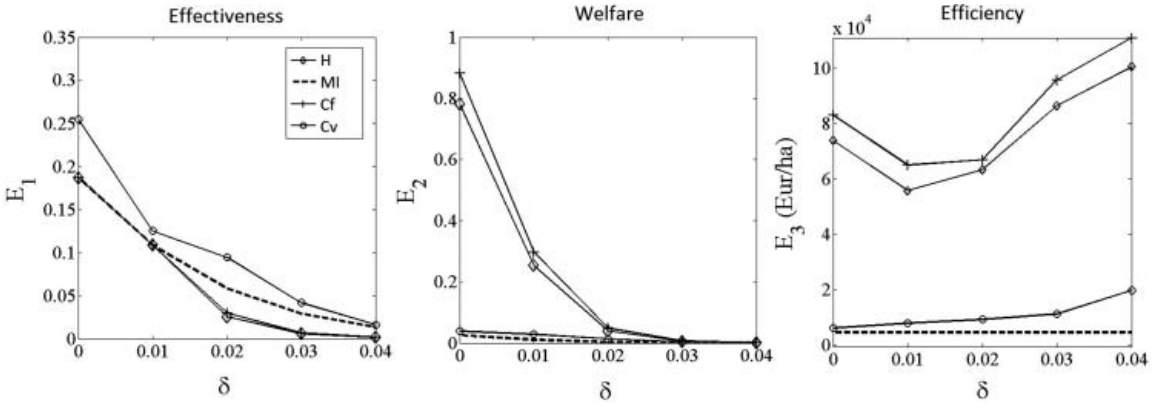

Figure D.10. Baseline performance across different growth rates of the composite commodity price (δ).
Notes: The figure captures the performance of the four baselines for different growth rates of the composite commodity price. The historical deforestation rate (dB) is at 200 ha/year. Corridor width is $x = 0.1$.

Summing up, we find that the ranking of baselines at different discount rates is consistent with the results presented under the initial calibration (Section 3.1). Higher discount rates lower the amount of total deforestation, especially for periods of time that are further away in the future. With lower deforestation also under BaU, there is little room for additionality obtained by REDD, and the effectiveness of the different baselines decreases. We argue that policy-makers interested in achieving high effectiveness might prefer to direct REDD projects to countries of higher political stability, where discount rates are lower.

D4. Growth rate of the composite commodity price (δ)

REDD programmes are currently being designed in many developing countries, and the opportunity costs of avoiding deforestation are likely to vary widely across different regions. The price dynamics of the alternative land use – in our model the growth rate of the composite commodity price (δ) – represents a key parameter influencing the opportunity costs of avoiding deforestation. Intuitively, the higher the growth rate of the composite commodity, the larger the price of the commodity in the future, strengthening the incentives to deforest more at later periods of time. With higher opportunity costs, REDD programmes are expected to be less effective (Irawan et al. 2013).

Figure D.9 shows that when the growth rate of the price of the agricultural composite commodity is low ($\delta = 0$), the deforestation path will be decreasing in time, since the REDD permit price increases and makes REDD participation more attractive. With constant, although different, baselines, the historical, model-implied, and fixed corridors lead to the same deforestation path. With constant agricultural composite commodity prices, it is the variable corridor that achieves again the best results in terms of avoided emissions. Although the H, MI, and Cf baselines obtain the same levels of effectiveness, they differ significantly in terms of welfare change and efficiency (see Figure D.10).

We test the sensitivity of baseline ranking to different levels of opportunity costs, by varying the growth rate of the composite commodity. We observe that, with our calibration, for $\delta > 0.04$ REDD projects are no longer effective in reducing deforestation below BaU.

Figure D.10 shows that the ranking of baselines is consistent with the results presented in Section 3.1 across all values of δ. Higher values of δ increase deforestation under BaU and the four REDD scenarios, reducing the effectiveness of REDD, as expected. As δ gets higher, landowners opt out of REDD and follow BaU, with their welfare converging to the BaU income. At lower effectiveness rates, payments for deforestation reductions under REDD are less cost-efficient.

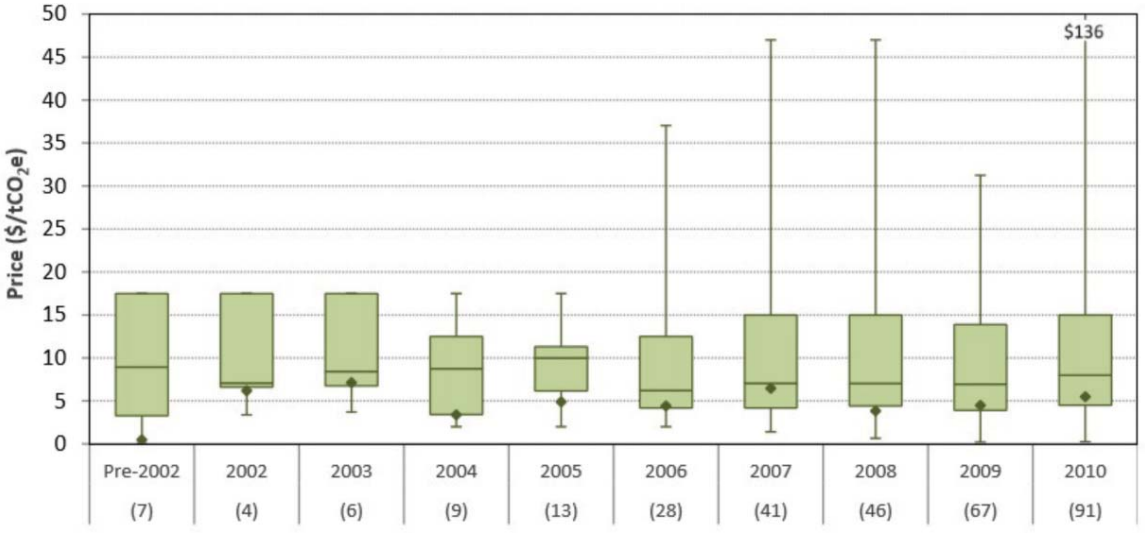

Figure D.11. Historical forest carbon price distributions (primary market).
Source: Diaz et al. (2011), *Ecosystem Marketplace*, available online at http://www.forest-trends.org/documents/files/doc_2963.pdf. Values in parentheses show the number of reported prices included in each year.

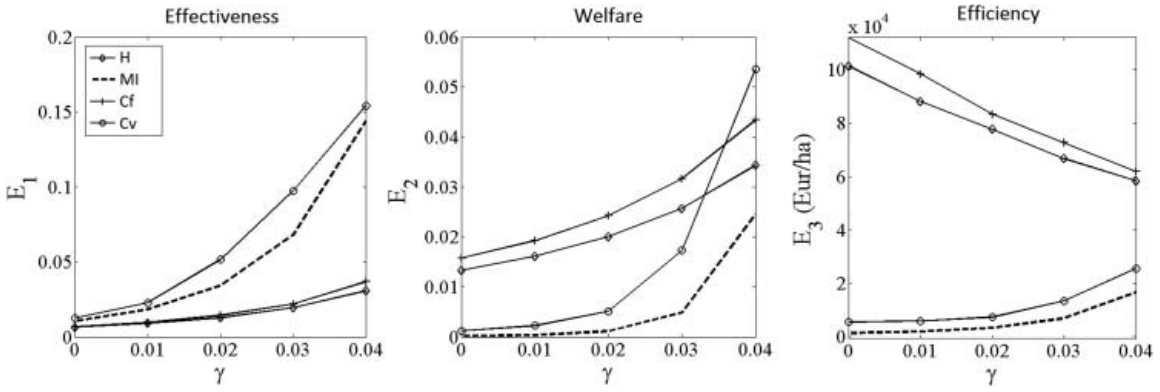

Figure D.12. Baseline performance across different growth rates of the REDD permit (γ).
Notes: The figure captures the performance of the four baselines for different growth rates of the REDD permit price. The historical deforestation rate (dB) is at 200 ha/year. Corridor width is $x = 0.1$.

The policy implication that arises from our analysis is that REDD programmes need to be accompanied by payments that stand up to the specific opportunity costs of the region; otherwise, where opportunity costs are very high, REDD programmes will be ineffective. This result is in line with the of findings of Irawan et al. (2013), who underline that REDD might not be able to compete with some alternative land uses that have prohibitive opportunity costs.

D5. Growth rate of the REDD permit price (γ)

The success of REDD is critically dependent on the incentive structure offered by the scheme. A key element is the amount of money rewarded per hectare of avoided deforestation, given by the REDD permit price (P^R) and its growth rate over time (γ).

Forest carbon projects have started their slow but steady increase at the end of the 1980s, and since then the largest part of demand for forest offsets has come from the voluntary carbon markets. Since 2005, forest carbon markets have experienced a significant boom, clearly marked by the development of REDD projects starting with 2010 (Diaz et al. 2011). REDD projects do not result in unique prices per ton of avoided emissions from deforestation; instead, prices vary according to demand levels, international regulations, and the quality of the specific projects.[34] Figure D.11 captures the historical distribution of forest carbon prices and illustrates two key characteristics of the market: (1) forest carbon prices present large variability; and (2) the trend in average prices after 2008 was increasing.

Motivated by the high price variability observed empirically, and by the fact that only increasing prices can motivate the sustained reduction of deforestation in the long run, we test the robustness of our results to different growth rates of the REDD credits price (γ).

Figure D.12 captures the performance of the four REDD baseline methodologies across different levels of γ. The baseline ranking presented in Section 3.1 is robust to changes in the growth rate of the REDD price. As expected, low future REDD prices diminish the incentives to avoid deforestation, and the modest reductions in deforestation are cost-inefficient. In contrast, if forest owners expect large future increases in REDD prices, they are motivated to keep the deforestation rates significantly lower than the BaU scenario; REDD projects are in this case likely to achieve high effectiveness. Moreover, the higher is the growth rate, the larger becomes the difference in effectiveness between the static and the dynamic baselines.

The policy implication that results from our analysis is that it is not enough to ensure high future REDD payments in order to achieve large reductions in deforestation, but it is necessary to choose carefully the baseline methodology. While static baselines achieve limited effectiveness at high REDD rewards, a dynamic baseline approach, designed as a corridor around the estimated BaU deforestation rate, will strongly increase the effectiveness of REDD.

E Corridor bandwidth and symmetry

E1. Fixed corridor

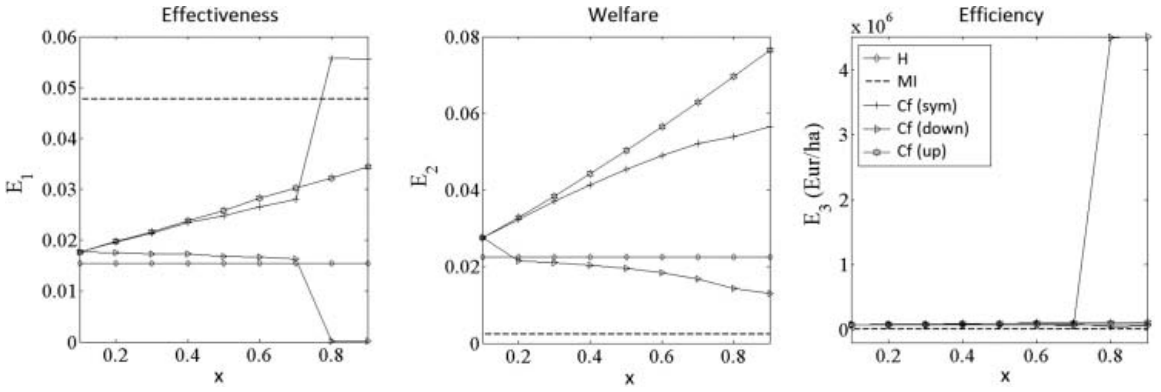

Figure E.1. Performance of the fixed corridor at different corridor bandwidths (x).
Notes: The figure captures the performance of the fixed corridor for different corridor widths and symmetry assumptions. Considered corridors are symmetric (*sym*), upward (*up*), and downward biased (*down*). Bounds in the downward-biased case are set as $dB^U = (1 + x_0)dB$, $dB^L = (1 - x)dB$; in the upward-biased case, $dB^U = (1 + x)dB$, $dB^L = (1 - x_0)dB$, with $x \in [0.1, 0.9]$ and $x_0 = 0.1$

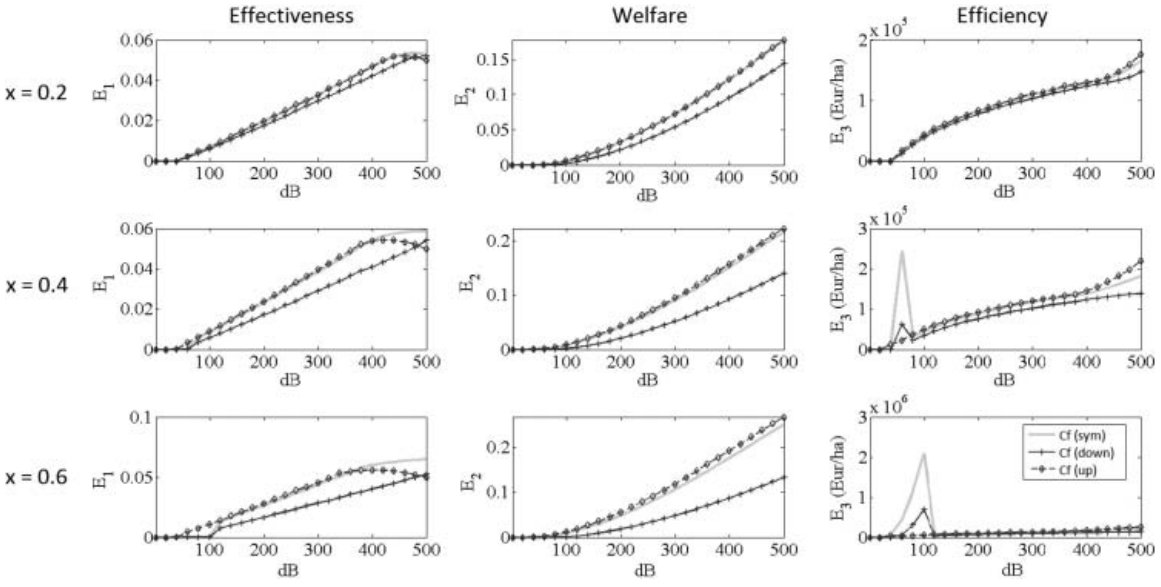

Figure E.2. Performance of the fixed corridor at different fixed thresholds (dB).
Notes: The figure captures performance results of the fixed (symmetric, upward, and downward biased) corridor. Three cases of corridor width are considered ($x \in \{0.2, 0.4, 0.6\}$) for different fixed thresholds ($dB \in [1, 500]$ ha/year).

Table E.1 REDD revenues detailed for different ranges of the deforestation rate.

Deforestation range	Symmetric	Upward biased	Downward biased	Ranking
Cf	$RR(t) = P^R(t)\left(1 - \frac{(d(t)-dB^L)^+}{dB^U - dB^L}\right)\left(dB^U - d(t)\right)^+$			
$d(t) \in [0, (1-x)dB]$	$P^R(t)((1+x)dB - d(t))$	$P^R(t)((1+x)dB - d(t))$	$P^R(t)((1+x_0)dB - d(t))$	$RR(t)^{up} = RR(t)^{sym} \geq RR(t)^{down}$
$d(t) \in ((1-x)dB, (1-x_0)dB]$	$P^R(t)\frac{((1+x)dB-d(t))^2}{2xdB}$	$P^R(t)((1+x)dB - d(t))$	$P^R(t)\frac{((1+x_0)dB-d(t))^2}{(x+x_0)dB}$	$RR(t)^{up} \geq RR(t)^{sym} \geq RR(t)^{down}$
$d(t) \in ((1-x_0)dB, (1+x_0)dB]$	$P^R(t)\frac{((1+x)dB-d(t))^2}{2xdB}$	$P^R(t)\frac{((1+x)dB-d(t))^2}{(x+x_0)dB}$	$P^R(t)\frac{((1+x_0)dB-d(t))^2}{(x+x_0)dB}$	$RR(t)^{up} \geq RR(t)^{sym} \geq RR(t)^{down}$
$d(t) \in ((1+x_0)dB, (1+x)dB]$	$P^R(t)\frac{((1+x)dB-d(t))^2}{2xdB}$	$P^R(t)\frac{((1+x)dB-d(t))^2}{(x+x_0)dB}$	0	$RR(t)^{up} \geq RR(t)^{sym} \geq RR(t)^{down}$
$d(t) \geq (1+x)dB$	0	0	0	$RR(t)^{up} = RR(t)^{sym} = RR(t)^{down}$
Cv	$RR(t) = P^R(t)\left(1 - \frac{(d(t)-dB^L(t))^+}{dB^U(t) - dB^L(t)}\right)(dB^U(t) - d(t))^+$			
$d(t) \in [0, (1-x)dB(t)]$	$P^R(t)((1+x)dB(t) - d(t))$	$P^R(t)((1+x)dB(t) - d(t))$	$P^R(t)((1+x_0)dB(t) - d(t))$	$RR(t)^{up} = RR(t)^{sym} \geq RR(t)^{down}$
$d(t) \in ((1-x)dB(t), (1-x_0)dB(t)]$	$P^R(t)\frac{((1+x)dB(t)-d(t))^2}{2xdB(t)}$	$P^R(t)((1+x)dB(t) - d(t))$	$P^R(t)\frac{((1+x_0)dB(t)-d(t))^2}{(x+x_0)dB(t)}$	$RR(t)^{up} \geq RR(t)^{sym} \geq RR(t)^{down}$
$d(t) \in ((1-x_0)dB(t), (1+x_0)dB(t)]$	$P^R(t)\frac{((1+x)dB(t)-d(t))^2}{2xdB(t)}$	$P^R(t)\frac{((1+x)dB(t)-d(t))^2}{(x+x_0)dB(t)}$	$P^R(t)\frac{((1+x_0)dB(t)-d(t))^2}{(x+x_0)dB(t)}$	$RR(t)^{up} \geq RR(t)^{sym} \geq RR(t)^{down}$
$d(t) \in ((1+x_0)dB(t), (1+x)dB(t)]$	$P^R(t)\frac{((1+x)dB(t)-d(t))^2}{2xdB(t)}$	$P^R(t)\frac{((1+x)dB(t)-d(t))^2}{(x+x_0)dB(t)}$	0	$RR(t)^{up} \geq RR(t)^{sym} \geq RR(t)^{down}$
$d(t) \geq (1+x)dB(t)$	0	0	0	$RR(t)^{up} = RR(t)^{sym} = RR(t)^{down}$

Table E.2 Change in REDD revenues when varying corridor bandwidth and deforestation rate.

Symmetry	Boundaries	$\frac{\partial RR(t)}{\partial x}$	$\frac{\partial RR(t)}{\partial x}$	$\frac{\partial^2 RR(t)}{\partial x \partial d(t)}$	$\frac{\partial^2 RR(t)}{\partial x \partial d(t)}$
Cf		$d(t) \in [0, dB^L]$	$d(t) \in (dB^L, dB^U)$	$d(t) \in [0, dB^L]$	$d(t) \in (dB^L, dB^U)$
Symmetric	$dB^L = (1-x)dB$	$P^R(t)dB > 0$	$P^R(t)\frac{((1+x)dB-d(t))((x-1)dB+d(t))}{2x^2dB} > 0$	0	$P^R(t)\frac{dB-d(t)}{x^2dB} > 0$
	$dB^U = (1+x)dB$				$(\forall d(t) \in (dB^L, dB])$
Upward biased	$dB^L = (1-x_0)dB$	$P^R(t)dB > 0$	$P^R(t)\frac{((1+x)dB-d(t))((x+2x_0-1)dB+d(t))}{(x_0+x)^2dB} > 0$	0	$2P^R(t)\frac{(1-x_0)dB-d(t)}{(x_0+x)^2dB} < 0$
	$dB^U = (1+x)dB$				
Downward biased	$dB^L = (1-x)dB$	0	$-P^R(t)\frac{((1+x_0)dB-d(t))^2}{(x_0+x)^2dB} < 0$	0	$2P^R(t)\frac{(1+x_0)dB-d(t)}{(x_0+x)^2dB} > 0$
	$dB^U = (1+x_0)dB$				
Cv		$d(t) \in [0, dB^L(t)]$	$d(t) \in (dB^L(t), dB^U(t))$	$d(t) \in [0, dB^L(t)]$	$d(t) \in (dB^L(t), dB^U(t))$
Symmetric	$dB^L(t) = (1-x)dB(t)$	$P^R(t)dB(t) > 0$	$P^R(t)\frac{((1+x)dB(t)-d(t))((x-1)dB(t)+d(t))}{2x^2dB(t)} > 0$	0	$P^R(t)\frac{dB(t)-d(t)}{x^2dB(t)} > 0$
	$dB^U(t) = (1+x)dB(t)$				$(\forall d(t) \in (dB^L(t), dB(t)])$
Upward biased	$dB^L(t) = (1-x_0)dB(t)$	$P^R(t)dB(t) > 0$	$P^R(t)\frac{((1+x)dB(t)-d(t))((x+2x_0-1)dB(t)+d(t))}{(x_0+x)^2dB(t)} > 0$	0	$2P^R(t)\frac{(1-x_0)dB(t)-d(t)}{(x_0+x)^2dB(t)} < 0$
	$dB^U(t) = (1+x)dB(t)$				
Downward biased	$dB^L(t) = (1-x)dB(t)$	0	$-P^R(t)\frac{((1+x_0)dB(t)-d(t))^2}{(x_0+x)^2dB(t)} < 0$	0	$2P^R(t)\frac{(1+x_0)dB(t)-d(t)}{(x_0+x)^2dB(t)} > 0$
	$dB^U(t) = (1+x_0)dB(t)$				

Notes: Columns (3) and (4) show results for first partial derivatives of REDD revenues with respect to corridor width across different symmetry scenarios for the fixed- and the variable-corridor methodologies. Columns (5) and (6) display results of the second partial derivative of REDD revenues, first with respect to corridor width and then with respect to deforestation rate. A distinction is made between the case when the deforestation rate is below the lower boundary and the case when it is inside the corridor.

Table E.3 Double impact of varying the corridor width on REDD revenues.

Symmetry	Characteristics	Linear impact on REDD credits (n)	Non-linear impact on weight (ω)
Cf			
Symmetric	$dB^L = (1-x)dB$ $dB^U = (1+x)dB$ $n = (1+x)dB - d(t)$ $\omega = 1 - \frac{d(t)-(1-x)dB}{(1+x)dB-(1-x)dB}$	$\frac{\partial n}{\partial x} = dB > 0$	$\frac{\partial \omega}{\partial x} = \frac{d(t)-dB}{2x^2 dB}$ ($\frac{\partial \omega}{\partial x} < 0$ if $d(t) < dB$) ($\frac{\partial \omega}{\partial x} \geq 0$ if $d(t) \geq dB$)
Upward biased	$dB^L = (1-x_0)dB$ $dB^U = (1+x)dB$ $n = (1+x)dB - d(t)$ $\omega = 1 - \frac{d(t)-(1-x_0)dB}{(1+x)dB-(1-x_0)dB}$	$\frac{\partial n}{\partial x} = dB > 0$	$\frac{\partial \omega}{\partial x} = \frac{d(t)-(1-x_0)dB}{(x+x_0)^2 dB} > 0$
Downward biased	$dB^L = (1-x)dB$ $dB^U = (1+x_0)dB$ $n = (1+x_0)dB - d(t)$ $\omega = 1 - \frac{d(t)-(1-x)dB}{(1+x_0)dB-(1-x)dB}$	$\frac{\partial n}{\partial x} = 0$	$\frac{\partial \omega}{\partial x} = \frac{d(t)-(1+x_0)dB}{(x+x_0)^2 dB} < 0$
Cv			
Symmetric	$dB^L(t) = (1-x)dB(t)$ $dB^U(t) = (1+x)dB(t)$ $n = (1+x)dB(t) - d(t)$ $\omega(t) = 1 - \frac{d(t)-(1-x)dB(t)}{(1+x)dB(t)-(1-x)dB(t)}$	$\frac{\partial n}{\partial x} = dB(t) > 0$	$\frac{\partial \omega(t)}{\partial x} = \frac{d(t)-dB(t)}{2x^2 dB(t)} < 0$ (since optimal $d(t) < dB(t)$)
Upward biased	$dB^L(t) = (1-x_0)dB(t)$ $dB^U(t) = (1+x)dB(t)$ $n = (1+x)dB(t) - d(t)$ $\omega(t) = 1 - \frac{d(t)-(1-x_0)dB(t)}{(1+x)dB(t)-(1-x_0)dB(t)}$	$\frac{\partial n}{\partial x} = dB(t) > 0$	$\frac{\partial \omega(t)}{\partial x} = \frac{d(t)-(1-x_0)dB(t)}{(x+x_0)^2 dB(t)} > 0$
Downward biased	$dB^L(t) = (1-x)dB(t)$ $dB^U(t) = (1+x_0)dB(t)$ $n = (1+x_0)dB(t) - d(t)$ $\omega(t) = 1 - \frac{d(t)-(1-x)dB(t)}{(1+x_0)dB(t)-(1-x)dB(t)}$	$\frac{\partial n}{\partial x} = 0$	$\frac{\partial \omega(t)}{\partial x} = \frac{d(t)-(1+x_0)dB(t)}{(x+x_0)^2 dB(t)} < 0$

F Misestimations in the business-as-usual deforestation path

REDD projects implemented based on misspecified BaU deforestation levels can provide undesired incentives to forest owners and undermine the effectiveness performance of REDD. The two baselines methodologies that could be affected by the errors in the BaU deforestation are the prospective ones, i.e. model-implied or variable corridor. We investigate this hypothesis and solve for the optimal deforestation path when the baseline methodology relies on a misspecified BaU path, such that

$$d^E_{\text{BaU}}(t) = (1+\varepsilon) d_{\text{BaU}}(t) \tag{F.1}$$

where d_{BaU} is the true deforestation path when no REDD programme is in place, and ε is the percentage misestimation of the BaU deforestation rate, with $\varepsilon \in [-0.05, 0.05]$. The corresponding

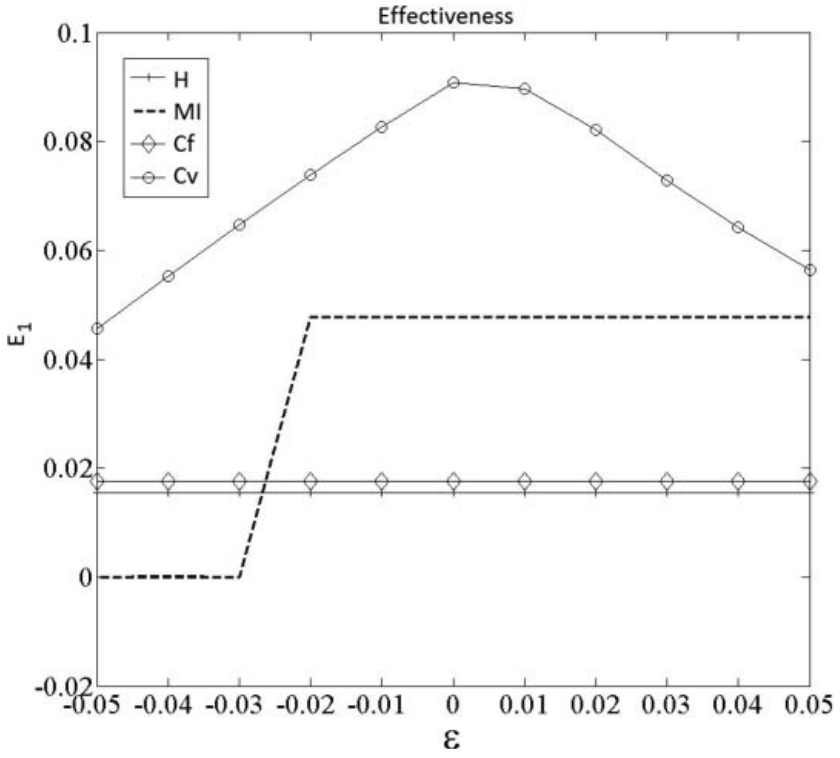

Figure F.1. Realised effectiveness in reducing deforestation when the BaU deforestation is estimated with error ($\varepsilon \in [-0.05, 0.05]$).

REDD revenues ($RR(t)$) take the form

$$RR(t) = \begin{cases} P^R(t)\left(d^E_{\text{BaU}}(t) - d(t)\right)^+, & \text{if MI} \\ P^R(t)\left((1+x)d^E_{\text{BaU}}(t) - d(t)\right)^+ \left(1 - \dfrac{\left(d(t) - (1-x)d^E_{\text{BaU}}(t)\right)^+}{(1+x)d^E_{\text{BaU}}(t) - (1-x)d^E_{\text{BaU}}(t)}\right), & \text{if Cv} \end{cases}$$

where P^R is the price of the carbon permit and x is the corridor wideness, as always.

Figure F.1 captures the effectiveness performance of the four baseline methodologies, when there are estimation errors in the specification of the BaU deforestation. First, for estimation errors that underestimated the BaU deforestation by more than 3%, the landowner will opt out of the REDD project under the model-implied (MI) baseline methodology. Larger estimation errors do not impact their deforestation reduction decisions, and the MI remains more effective than the historical or fixed-corridor approaches.

Second, we find that the variable-corridor methodology is robust if estimation errors stay within $[-5\%, +5\%]$ from the true BaU deforestation path. Our conclusion that the variable corridor should be the preferred baseline methodology is, therefore, robust.

C Anca Claudia Pana - Curriculum Vitae

Nationality	Romanian
Date of birth	14 February 1985

Education	2010 - 2015	**University of Zurich** *Department of Banking and Finance* PhD studies Finance
	2008 - 2010	**University of Lausanne** *Department of Finance* M. Sc. Finance (Financial Engineering and Risk Management)
	2004 - 2008	**Academy of Economic Studies Bucharest** *Department of Finance, Insurance, Banking and Stock Exchanges* B. Sc. Finance (Dissertation July 2008 - awarded 10/10)
	2006 - 2007	**Polytechnic University of Marche, Italy** *Department of Economics* Erasmus Exchange Program
	2005 - 2006	**University of Political and Administrative Studies Bucharest** *Department of Social and Political Sciences* B. A. Political Science (first year)
	2000 - 2004	**Sfantul Sava National College Bucharest** Profile in Mathematics - Informatics, Baccalaureat: 9.41/10
Academic services	2011-2015	Teaching assistant for "Continuous Time Quantitative Finance".
	2010-11, 2014	Teaching assistant for "Environmental Finance".
	2015	Teaching assistant for "Environmental and Financial Sustainability".
	2011-2015	Supervision of Bachelors (7) and Masters (7) theses.

Publications

Bahn, O., Chesney, M., Gheyssens, J., Knutti, R., Pana, A., *Is there room for geoengineering in the optimal climate policy mix?*, Journal of Environmental Science and Policy, 48: 67-76 (2015).
Pana, A. and Gheyssens, J. *Baseline Choice and Performance Implications for REDD*, Journal of Environmental Economics and Policy (2015).
Chesney, M., Gheyssens, J., Pana, A., Taschini L. *Environmental Finance and Investments*, Second Edition, Springer Texts in Business and Economics (forthcoming 2015).

Working papers

Pana, A. and Chesney, M. *Simultaneous CO_2 permit trading and output decisions in a dynamic setting with multiple sources of uncertainty.*
Pana, A. *Who is driving the volatility of the CO_2 permit price? Evidence from EU ETS Phase I.*